

THERMODYNAMIC AND EXERGY ANALYSIS OF THERMAL SYSTEM

by

SHYAM AGARWAL

(Enrolment No.: 2K11 / Ph.D. / ME / 13)

DEPARTMENT OF MECHANICAL ENGINEERING

Submitted

in fulfillment of the requirements for the degree of

DOCTOR OF PHILOSOPHY

to the



DELHI TECHNOLOGICAL UNIVERSITY

April 2019

©DELHI TECHNOLOGICAL UNIVERSITY-2019
ALL RIGHTS RESERVED



DELHI TECHNOLOGICAL UNIVERSITY

BAWANA ROAD, DELHI – 110042

DECLARATION

I hereby declare that the thesis entitled “*Thermodynamic and exergy analysis of thermal System*” submitted by me, for the award of the degree of *Doctor of Philosophy* to the **Delhi Technological University (Formerly Delhi College of Engineering)** is a record of *bona fide* work carried out by me under the guidance of **Prof. B. B. Arora & Dr. Akhilesh Arora.**

I further declare that the work reported in this thesis has not been submitted and will not be submitted, either in part or in full, for the award of any other degree or diploma in this Institute or any other Institute or University.

Shyam Agarwal

Enrollment No. : 2K11/Ph.D./ME/13
Department of Mechanical, Production
Industrial, and Automobile Engineering
Delhi Technological University,
Bawana, Delhi-110042

Signature



DELHI TECHNOLOGICAL UNIVERSITY

BAWANA ROAD, DELHI – 110042

CERTIFICATE

This is to certify that the Ph.D. thesis entitled "*Thermodynamic and exergy analysis of thermal System*" being submitted by **Shyam Agarwal** (Enrolment No.: **2K11/Ph.D./ME/13**) for the award of degree of *Doctor of Philosophy (Ph.D.)* in Mechanical Engineering, Delhi Technological University, is a bona fide record of research work carried out by him. Shyam Agarwal has worked under our supervision and has fulfilled the requirements for the submission of this thesis, which to our knowledge has reached requisite standards.

It is further certified that the work is based on original research and the matter embodied in this thesis has not been submitted earlier for the award of any degree or diploma to the best of our knowledge and belief.

Dr. B. B. Arora
Professor,
Department of Mechanical Engineering,
Delhi Technological University,
Delhi 110042.

Dr. Akhilesh Aroa
Associate Professor,
Department of Mechanical Engineering,
Delhi Technological University,
Delhi 110042.

ACKNOWLEDGEMENTS

First and foremost I am thankful to almighty GOD for keeping me fit, healthy and energetic during entire course of my Ph. D. work.

I would like to express my gratitude to Prof. Yogesh Singh, Vice chancellor, Delhi Technological University, Delhi for providing this opportunity to carry out this work in this prestigious institute.

I would like to thanks Prof. R.S Mishra, DRC Chairman and Prof. Vipin Kumar, Head of the department, Department of Mechanical, Production, Industrial, and Automobile Engineering, for their support to finish this work.

With pleasure, I would like to express my greatest gratitude to my supervisors Prof. B. B. Arora, Professor and Dr. Akhilesh Arora, Associate Professor, Department of Mechanical, Production, Industrial, and Automobile Engineering, Delhi Technological University for their proficient guidance, intelligent approach, constructive critique, whole hearted and ever available help, which has been the primary impetus behind the research. Without the wise advice and able guidance, it would have been impossible to complete the thesis in this manner.

I wish to record my thanks and gratitude to our all External and Internal SRC experts, Prof. Subhashish Maji (IGNOU, Delhi), Prof. J.A. Usmani (Jamia Milia Islamia, Delhi), Prof. Narendra Kumar (DTU, Delhi), Prof. Neeta Pandey (DTU, Delhi) and Prof. S. Maji (DITE, Delhi) for their valuable guidance, critical and constructive discussion during this work.

I also convey my sincere thanks to my seniors Prof. Rajiv Chaudhary, Prof. R.C. Singh and Dr. K. Manjunath for their patience and active support.

I would like to thank my fellow lab mates especially Rajesh Vohra, Sh. Om Prakash, Gugan Ram, Sh. Lakhan, Vipin Kumar, Deepak Tiwari, and all staff members of Mechanical Engineering Department for helping and encouraging me throughout my research.

Thanks are due to the wonderful friends in my life who were always on the stand by to bring me to positivity, hope and smiles when things didn't seem favouring and it seemed a far-fetched journey. Special mention is deserved for all my other peers especially Prof Atul Kumar Agarwal, Prof. Alok Verma and Prof. B. D. Malhotra who have always been my guiding light when I didn't believe in myself.

I am greatly indebted to my parents Sh. R. P. Agarwal & Smt. Veena Agarwal, my younger brother Mr. Robin Agarwal and my younger sister Mrs. Chhavi Agarwal for their love and blessings to see me scaling greater heights of life. One who matters most in my Ph.D work is my wife Dr. Ritu Agarwal without whose motivation and encouragement, pursuit of this Ph.D work would have never been possible. I thank her for her care and relieving me entirely from the domestic work. Last but not the least I am thankful to my sons Gauransh Agarwal and Devashsish Agarwal whose voice imparts impart me immense energy to work.

Above all, I would thanks Almighty for blessing such an affectionate & efficient people who are great asset for me.

April 2019

Shyam Agarwal

ABSTRACT

In the thesis, the refrigeration and air-conditioning systems having low carbon emission and eco-friendly relationship have been examined and evaluated. An attempt has been made to synthesise the vapour compression and absorption cycles for the investigation of energy and exergy performance.

The subcooling methods viz. liquid vapour heat exchanger incorporation to vapour compression refrigeration (VCR) system and dedicated mechanical subcooled VCR system have been investigated using R134a and alternate refrigerants R1234yf and R1234ze. An experimental VCR setup has also compared to simple theoretical VCR system in order to examine the performance and compatibility of alternative refrigerants. The results depict that the subcooling methods improve coefficient of performance (COP) and exergy efficiency of the VCR system. The performance of R1234ze is better than that of R1234yf and it competes with R134a.

The low grade energy (waste heat) available at temperature (i.e. within 60-200⁰C) is utilized as source in the various cascade configurations of vapour compression-absorption refrigeration cycles. The objectives of the present work are reduction in high grade energy (electrical energy) consumed by the compressor consequently, reduction in carbon emission and global warming potential. Simultaneously, the cascading effect produces lower temperature for the deep freezing and chilling applications.

For achieving the dual objectives, the energy and exergy analysis of absorption-compression cascade refrigeration cycles along with wide range of parametric analysis have been carried out by developing engineering equation solver (EES) software based computer programs.

The waste heat available at higher temperature (165-200⁰C) has been utilized in compression-absorption (triple effect series flow H₂O-LiBr) cascade refrigeration cycle while the low temperature (65-95⁰C) waste heat has been utilized in compression-absorption (single and half effect series flow H₂O-LiBr) cascade refrigeration cycle. The low global warming potential (GWP) and zero ozone depleting potential (ODP), hydrofluoroolefin (HFO) refrigerant R1234yf has been proposed as a working fluid for vapour compressor refrigeration system. The various configurations of cascade refrigeration system have been compared to vapour absorption and compression systems separately to examine the thermodynamic performance. The results depict that COP and

exergetic efficiency of single effect H₂O-LiBr absorption-compression cascade refrigeration system (ACCRS) are highest and lowest for half effect ACCRS. The total exergy destruction is lowest for single effect ACCRS and highest for half effect ACCRS. It has also been observed that the energy and exergy performance of R1234ze is better than that of R1234yf in the VCR section of absorption-compression (single effect H₂O-LiBr) cascade refrigeration system. The electricity consumption of half and triple effect cascade refrigeration systems is reduced by 54.29 % and 45.84% than that of conventional vapour compression refrigeration cycle. The enhancement in COP by 85.26% and 118.7% in triple and half effect cascade refrigeration systems respectively. The enhancement in the exergetic efficiency of VCR circuit of triple effect absorption compression cascade refrigeration is 85.28% and the reduction in total exergy destruction is 70.8% and in half effect absorption compression cascade refrigeration system, enhancement in the exergetic efficiency of VCR circuit is 118.74% and the reduction in total exergy destruction is 80.66% .

For simultaneous production of power, heat and refrigeration, tri-generation power plants having absorption compression cascade refrigeration system are examined and analysed for their performance improvement using energy and exergy principles. The results depict that the COP and exergetic efficiency of the cascade refrigeration system powered by micro-gas turbine improve over conventional VCR and vapour absorption refrigeration (VAR) system along with reduction in consumption of high grade energy (electricity).

Additionally, retrofitted technologies viz. evaporative cooling (EVC) of inlet air to compressor and steam injection to gas turbine (STIG) are also investigated for performance improvement of gas turbine. The results highlight that the use of retrofitted techniques enhances power output by 60.79% and generation efficiency by 28.4% of simple gas turbine cycle.

The current work is worthwhile to develop and design the energy efficient, eco-friendly advanced cooling cycles and thermal power plants.

CONTENTS

Declaration	
Certificate	
Acknowledgements	(i)
Abstract	(iii)
Contents	(v)
List of Figures	(xi)
List of Tables	(xix)
Nomenclature	(xxi)

CHAPTER 1: INTRODUCTION

1.1. Background.....	1
1.2. Objective and scope of the thesis	5
1.3. Organization of the thesis	5

CHAPTER 2 : LITERATURE REVIEW

2.1. Introduction.....	11
2.2. Vapour compression refrigeration (VCR) systems and alternative refrigerants.....	11
2.3. Vapour absorption refrigeration (VAR) systems.....	14
2.3.1 Triple effect, double effect, single effect and half effect VAR systems.....	14
2.4 Cascade refrigeration systems.....	15
2.4.1 VCR cascade refrigeration systems	15
2.4.2 Absorption-compression cascade refrigeration systems.....	16
2.5 Power, heat and refrigeration combined trigeneration systems	17
2.6 Conclusions of literature review	21
2.7 Research gaps	21
2.8 Objectives of the proposed research	22

CHAPTER 3 : THERMODYNAMIC PERFORMANCE (ENERGY AND EXERGY) ANALYSIS OF MECHANICALLY SUBCOOLED VCR SYSTEM USING ALTERNATIVE REFRIGERANTS R1234yf AND R1234ze AS REPLACEMENTS OF R134a

3.1. Introduction.....	23
3.2. Description of system	24
3.3 Mathematical modelling	27

3.3.1	Assumptions.....	27
3.3.2	Energy and exergy analysis	27
3.3.2.1	Energy analysis	27
3.3.2.2	Exergy analysis	28
3.3.2.2.1	Exergy destruction in the components of liquid vapour heat exchanger incorporated vapour compression refrigeration cycle.....	29
3.3.2.2.2	Total exergy destruction	30
3.3.2.2.3	Exergetic efficiency	30
3.3.2.2.4	Exergy destruction ratio (EDR)	31
3.4	Results and discussion	32
3.4.1	Results of energy, exergy and parametric analysis.....	32
3.4.1.1	Effect of subcooling	33
3.4.1.2	Effect of evaporator temperature	36
3.4.1.3	Effect of liquid vapour heat exchanger effectiveness.....	39
3.4.1.4	Effect of compressor efficiency	41
3.4.1.5	Effect of subcooling, evaporator temperature, effectiveness of LVHE and compressor efficiency on total exergy destruction and exergy destruction ratio	43
3.4.1.6	Results of exergy analysis.....	49
3.5	Conclusions.....	49

CHAPTER 4 : THERMODYNAMIC PERFORMANCE ANALYSIS OF DEDICATED MECHANICALLY SUB-COOLED VAPOUR COMPRESSION REFRIGERTION SYSTEM

4.1	Introduction.....	51
4.2	Description of system	52
4.3	Thermodynamic & mathematical modelling	54
4.3.1	Assumptions.....	54
4.3.2	Energy analysis	54
4.3.3	Exergy analysis	55
4.3.3.1	Exergy destruction in the components of dedicated mechanically subcooled vapour compression refrigeration cycle (DSC)	55
4.3.3.2	Total exergy destruction (TEXD)	57
4.3.3.3	Exergetic efficiency (EXE).....	58

4.3.3.4	Exergy destruction ratio (EDR)	60
4.3.4	Model validation	61
4.3.5	Input parameters.....	62
4.4	Results and discussion	63
4.4.1	Results of energy, exergy and parametric analysis	63
4.4.1.1	Effect of subcooling	67
4.4.1.2	Effect of evaporator temperature	71
4.4.1.3	Effect of temperature of condenser	74
4.4.1.4	Effect of compressor efficiency	78
4.4.1.5	Effect of subcooler effectiveness	82
4.4.1.6	Exergetic efficiency and exergy destruction rate of system components	88
4.5	Conclusions.....	89
4.6	Comparison between LVHE incorporated VCR system and Dedicated Mechanically subcooled VCR system	91

CHAPTER 5: PERFORMANCE ANALYSIS (ENERGY AND EXERGY) OF EXPERIMENTAL VAPOUR COMPRESSION REFRIGERATION CYCLE

5.1	Introduction.....	92
5.2	Description of system	93
5.3	Mathematical formulation.....	95
5.3.1	Energy analysis	95
5.3.2	Exergy analysis	95
5.3.2.1	Exergy destruction in the components of experimental vapour compression refrigeration system	96
5.3.2.2	Total exergy destruction (TEXD)	96
5.3.2.3	Exergetic efficiency (EXE).....	96
5.3.2.4	Exergy destruction ratio (EDR)	97
5.3.2.5	Assumptions.....	98
5.3.2.6	Experimental data	98
5.4	Results and discussion	98
5.4.1	Results of energy, exergy and parametric analysis	99
5.4.1.1	Effect of pressure ratio	100
5.4.1.2	Effect of evaporator temperature	104

5.4.1.3	Effect of condenser temperature	107
5.5	Conclusions.....	111

CHAPTER 6: ENERGY AND EXERGY ANALYSIS OF VAPOUR COMPRESSION-ABSORPTION (H₂O-LiBr) CASCADE REFRIGERATION SYSTEM

6.1	Introduction.....	113
6.2	Description of vapour compression-absorption (triple effect series flow H ₂ O-LiBr) cascade refrigeration system	114
6.3	Mathematical modelling	117
6.3.1	Assumptions.....	117
6.3.2	Energy analysis	117
6.3.3	Exergy analysis	118
6.3.3.1	Total exergy destruction	119
6.3.3.2	Exergetic efficiency	119
6.3.3.3	Exergy destruction ratio (EDR)	120
6.3.4	Model validation	123
6.3.5	Input parameters.....	125
6.4	Results and discussion	126
6.4.1	Results of energy analysis.....	126
6.4.2	Results of exergy analysis.....	128
6.4.3	Parametric analysis	128
6.4.3.1	Effect of high pressure generator temperature.....	129
6.4.3.2	Effect of evaporator 1 temperature	137
6.4.3.3	Exergy destruction rate and EDR of system components.....	140
6.5	Conclusions.....	141
6.6	Description of vapour compression-absorption (double effect series flow H ₂ O/LiBr) cascade refrigeration system.....	142
6.7	Description of vapour compression-absorption (single effect H ₂ O/LiBr) cascade refrigeration system	145
6.8	Mathematical modelling	148
6.8.1	Assumptions.....	148
6.8.2	Energy analysis	149

6.8.3	Exergy analysis	149
6.8.3.1	Total exergy destruction	149
6.8.3.2	Exergetic efficiency	149
6.8.3.3	Exergy destruction ratio (EDR)	150
6.8.4	Input parameters.....	150
6.9	Results and discussion	151
6.9.1	Results of energy, exergy and parametric analysis	151
6.9.1.1	Effect of variation in effectiveness of solution heat exchanger.....	151
6.9.1.2	Effect of variation in evaporator1 temperature.....	153
6.10	Conclusions.....	156
6.11	Description of vapour compression-absorption (half effect series flow H ₂ O-LiBr) cascade refrigeration system	157
6.12	Thermodynamic and mathematical modelling.....	160
6.12.1	Assumptions.....	160
6.12.2	Energy analysis	161
6.12.3	Exergy analysis	161
6.12.3.1	Total exergy destruction	161
6.12.3.2	Exergetic efficiency	162
6.12.3.3	Exergy destruction ratio (EDR)	162
6.12.4	Model validation	168
6.13	Results and discussion	171
6.13.1	Results of energy analysis.....	171
6.13.2	Results of exergy analysis.....	172
6.13.3	Parametric analysis	173
6.13.3.1	Effect of generator temperature	173
6.13.3.2	Effect of evaporator temperature	178
6.13.3.3	Exergy destruction rate and EDR of system components.....	181
6.14	Conclusions.....	182
6.15	Performance comparison of compression-absorption (triple, double, single and half effect H ₂ O-LiBr) cascade refrigeration systems	184

CHAPTER 7: THERMODYNAMIC PERFORMANCE ANALYSIS OF TRIGENERATION SYSTEM (POWER, HEAT AND REFRIGERATION) FOR PERFORMANCE IMPROVEMENT USING RETROFITTED TECHNIQUES AND ALTERNATE REFRIGERANTS

7.1	Introduction.....	187
7.2	Description of vapour compression absorption (H ₂ O-LiBr) cascade refrigeration system powered by a micro-gas turbine.....	188
7.3	Mathematical formulation.....	190
7.4	Results and discussion	192
7.4.1	Effect of ambient temperature	193
7.4.2	Effect of generator temperature	195
7.4.3	Effect of refrigerated air temperature	196
7.5	Conclusions.....	197
7.6	Description of a retrofitted tri-generation power plant	199
7.7	Modelling of system	201
7.8	Conclusions.....	206

CHAPTER 8: OVERALL CONCLUSIONS AND RECOMMENDATIONS

References

Publications List

Author's Bio-data

LIST OF FIGURES

Figure No.	Title of Figures	Page No.
Figure 3.1	Schematic diagram of Liquid vapour heat exchanger (LVHE) incorporated Vapour compression refrigeration cycle	25
Figure 3.2	P-h diagram of LVHE incorporated vapour compression refrigeration cycle	25
Figure 3.3	Pressure-enthalpy (P-h) and temperature-entropy (T-s) state diagrams of R134a, R1234yf and R1234ze	26
Figure 3.4	Exergy balance in evaporator and the space to be cooled	31
Figure 3.5	Effect of degree of subcooling $(\Delta T)_{SC}$ in LVHE on degree of superheating $(\Delta T)_{SH}$ and compressor work (\dot{W}_{comp}) ($T_e = -10^0C$)	33
Figure 3.6	Effect of degree of subcooling $(\Delta T)_{SC}$ in LVHE on COP ($T_e = -10^0C$)	34
Figure 3.7	Effect of degree of subcooling $(\Delta T)_{SC}$ in LVHE on exergetic efficiency (η_{ex}) ($T_e = -10^0C$)	35
Figure 3.8	Variation in degree of subcooling $(\Delta T)_{SC}$ with evaporator temperature (T_e)	36
Figure 3.9	Temperature of evaporator temperature (T_e) Vs compressor work (\dot{W}_{comp})	37
Figure 3.10	COP Vs evaporator temperature (T_e) on VCR cycle with and without LVHE	37
Figure 3.11	Exergetic efficiency (η_{ex}) Vs evaporator temperature (T_e)	38
Figure 3.12	Degree of subcooling $(\Delta T)_{SC}$ Vs Effectiveness of liquid vapour heat exchanger (ϵ_{LVHE}) ($T_e = -10^0C$)	39
Figure 3.13	Compressor work (\dot{W}_{comp}) Vs Effectiveness of liquid vapour heat exchanger (ϵ_{LVHE}) ($T_e = -10^0C$)	39
Figure 3.14	Coefficient of performance (COP) Vs Effectiveness of LVHE (ϵ_{LVHE}) ($T_e = -10^0C$)	40
Figure 3.15	Exergetic efficiency (η_{ex}) Vs LVHE effectiveness (ϵ_{LVHE}) ($T_e = -10^0C$)	41
Figure 3.16	Coefficient of performance (COP) & Compressor work (\dot{W}_{comp})	42

	Vs Isentropic compressor efficiency (η_{comp}) ($T_e = -10^0\text{C}$)	
Figure 3.17	Exergetic efficiency (η_{ex}) Vs isentropic compressor efficiency (η_{comp}) ($T_e = -10^0\text{C}$)	43
Figure 3.18	The total exergy destruction and exergy destruction ratio Vs degree of subcooling (ΔT) _{SC} , evaporator temperature (T_e), effectiveness of LVHE (ϵ_{LVHE}) and isentropic efficiency of compressor (η_{comp})	41
Figure 3.18(a)	The total exergy destruction and EDR Vs. degree of subcooling (Δ) _{SC}	44
Figure 3.18(b)	Total exergy destruction and EDR Vs. evaporator temperature (T_e)	44
Figure 3.18(c)	Total exergy destruction and EDR Vs. effectiveness of LVHE (ϵ_{LVHE})	45
Figure 3.18(d)	Total exergy destruction and EDR Vs. isentropic efficiency of compressor (comp)	45
Figure 3.19(a)	Exergy destruction (D) in different components of LVHE incorporated VCR system ($T_e = -100\text{C}$)	46
Figure 3.19(b)	Percentage EDR in different components of LVHE incorporated VCR system ($T_e = -100\text{C}$)	47
Figure 3.19(c)	Percentage exergetic efficiency () in different components of LVHE incorporated VCR system ($T_e = -100\text{C}$)	48
Figure 4.1	Schematic diagram of dedicated mechanically subcooled VCR system	52
Figure 4.2	P-h diagram of dedicated mechanically subcooled VCR system	52
Figure 4.3 (a)	Temperature-entropy (T-s) state diagram of dedicated mechanically subcooled (DSC), subcooler (SC) VCR systems using R1234ze	64
Figure 4.3 (b)	Pressure-enthalpy (P-h) state diagram of dedicated mechanically subcooled (DSC), subcooler (SC) VCR systems using R1234ze	64
Figure 4.3 (c)	Temperature-entropy (T-s) state diagram of dedicated mechanically subcooled (DSC), subcooler (SC) VCR systems using R1234yf	65

Figure 4.3 (d)	Pressure-enthalpy (P-h) state diagram of dedicated mechanically subcooled (DSC), subcooler (SC) VCR systems using R1234yf	65
Figure 4.3 (e)	Temperature-entropy (T-s) state diagram of dedicated mechanically subcooled (DSC), subcooler (SC) VCR systems using R134a	66
Figure 4.3 (f)	Pressure-enthalpy (P-h) state diagram of dedicated mechanically subcooled (DSC), subcooler (SC) VCR systems using R134a	66
Figure 4.4	Variation in compressor work (\dot{W}_C) with degree of subcooling (ΔT_{sc})	67
Figure 4.5	Effect of degree of subcooling (ΔT_{sc}) on COP	68
Figure 4.6	Effect of degree of subcooling (ΔT_{sc}) on exergetic efficiency (η_{ex})	69
Figure 4.7	Variation in total exergy destruction rate ($\dot{E}_{D, Total}$) and exergetic efficiency (η_{ex}) with subcooling (ΔT_{sc}) of OC	70
Figure 4.8	Variation in compressor work (\dot{W}_C) with evaporator1 temperature ($T_{e,DSC}$)	71
Figure 4.9	Effect of evaporator1 temperature ($T_{e, DSC}$) on degree of subcooling (ΔT_{sc}) and COP	72
Figure 4.10	Variation in exergy efficiency (η_{ex}) with evaporator1 temperature ($T_{e, DSC}$) of overall cycle (OC)	73
Figure 4.11	Variation in total exergy destruction rate ($\dot{E}_{D, Total}$) and exergy destruction ratio (EDR) with evaporator1 temperature ($T_{e, DSC}$) of overall cycle (OC)	73
Figure 4.12	Variation in compressor work of simple vapour compression refrigeration cycle (SVCR), DSC, SC and OC ($\dot{W}_{C,SVCR}, \dot{W}_{Comp1}, \dot{W}_{Comp2}$ and $(\dot{W}_{Comp1} + \dot{W}_{Comp2})$) with condenser1,2 temperature ($T_{c, DSC} = T_{c, SC}$)	75
Figure 4.13	Effect of condenser1,2 temperature on ($T_{c, DSC} = T_{c, SC}$) on COP of DSC, OC, SC and SVCR cycle	75
Figure 4.14	Effect of condenser temperature (T_c) on exergetic efficiency (η_{ex})	77
Figure 4.15	Variation in total exergy destruction rate ($\dot{E}_{D, Total}$) and exergy destruction ratio (EDR) with condenser temperature (T_c)	77

Figure 4.16	Variation in compressor(\dot{W}_C) work of DSC, OC, SC and SVCR system with isentropic efficiency of compressor ($\eta_{comp.}$)	78
Figure 4.17	Effect of isentropic efficiency of compressor ($\eta_{comp.}$) on $COP_{max.}$	79
Figure 4.18	Variation in exergetic efficiency (η_{ex})with isentropic efficiency of compressor($\eta_{comp.}$)	80
Figure 4.19	Effect of isentropic efficiency of compressor ($\eta_{comp.}$) on total exergy destruction rate ($\dot{E}_{D, Total}$)	81
Figure 4.20	Effect of isentropic efficiency of compressor ($\eta_{comp.}$) on EDR	81
Figure 4.21	Effect of effectiveness of subcooler (ϵ_{SC}) on degree of subcooling ($\Delta T)_{sc}$	82
Figure 4.22	Variation in compressor work (\dot{W}_C) with effectiveness of subcooler (ϵ_{SC})	83
Figure 4.23	Variation in $COP_{max.}$ with effectiveness of subcooler (ϵ_{SC})	84
Figure 4.24	Effect of effectiveness of subcooler (ϵ_{SC}) on exergetic efficiency (η_{ex})	85
Figure 4.25	Effect of effectiveness of subcooler (ϵ_{SC}) on $\dot{E}_{D, Total}$	86
Figure 4.26	Variation in exergy destruction ratio (EDR) with effectiveness of subcooler (ϵ_{SC})	87
Figure 4.27	Exergetic efficiency of system components of simple VCR cycle and DSC	88
Figure 4.28	Exergy destruction rate of system components in simple VCR system and DSC	89
Figure 5.1	Block diagram of experimental VCR unit	93
Figure 5.2	P-h diagram of experimental VCR unit	93
Figure 5.3	Experimental setup of vapour compression refrigeration unit	99
Figure 5.4	Variation in theoretical refrigeration effect ($\dot{Q}_{e,Theo.}$), compressor work ($\dot{W}_{c,Theo.}$) and COP with pressure ratio (P_{ratio})	100
Figure 5.5	Effect of pressure ratio (P_{ratio}) on experimental refrigeration effect($\dot{Q}_{e,Exp.}$), and $COP_{Exp.}$	101
Figure 5.6	Effect of pressure ratio (P_{ratio}) on theoretical and experimental exergetic efficiency ($\eta_{ex,Theo.}$, $\eta_{ex,Exp.}$)	101

Figure 5.7	Impact of pressure ratio (P_{ratio}) on theoretical TEXD ($\dot{E}_{D,Total,Theo.}$) and EDR ($EDR_{Theo.}$)	102
Figure 5.8	Impact of pressure ratio (P_{ratio}) on experimental TEXD ($\dot{E}_{D,Total,Prac.}$) and EDR ($EDR_{Prac.}$)	103
Figure 5.9	Variation in refrigeration effect ($\dot{Q}_{e,Theo.}$), compressor work ($\dot{W}_{c,Theo.}$) and COP with temperature of evaporator (T_e) for theoretical VCR system	104
Figure 5.10	Effect of evaporator temperature (T_e) on experimental refrigeration effect ($\dot{Q}_{e,Exp.}$), and $COP_{Exp.}$	105
Figure 5.11	Effect of evaporator temperature (T_e) on theoretical and experimental exergetic efficiency ($\eta_{ex,Theo.}, \eta_{ex,Exp.}$)	105
Figure 5.12	Impact of temperature of evaporator (T_e) on TEXD rate ($\dot{E}_{D,Total,Theo.}$) and EDR ($EDR_{Theo.}$) for theoretical VCR setup	106
Figure 5.13	Impact of temperature of evaporator (T_e) on TEXD rate ($\dot{E}_{D,Total,Prac.}$) and EDR ($EDR_{Prac.}$) for experimental VCR setup	107
Figure 5.14	Variation in refrigeration effect ($\dot{Q}_{e,Theo.}$), COP and compressor work ($\dot{W}_{c,Theo.}$) with condenser temperature (T_c) for theoretical VCR system	108
Figure 5.15	Impact of temperature of condenser (T_c) on refrigeration effect ($\dot{Q}_{e,Exp.}$), and $COP_{Exp.}$ for experimental VCR system	108
Figure 5.16	Impact of temperature of condenser (T_c) on $COP_{Theo.}$ and $COP_{Exp.}$	109
Figure 5.17	Impact of temperature of condenser (T_c) on EXE ($\eta_{ex,Theo.}, \eta_{ex,Exp.}$) for theoretical and experimental VCR setup	110
Figure 5.18	Impact of T_c on TEXD rate ($\dot{E}_{D,Total,Theo.}$) and EDR ($EDR_{Theo.}$) for theoretical VCR setup	110
Figure 5.19	Impact of T_c on TEXD rate ($\dot{E}_{D,Total,Exp.}$) and EDR ($EDR_{Exp.}$) for experimental VCR setup	111
Figure 6.1	Schematic diagram of absorption-compression (triple effect $H_2O/LiBr$ series flow) cascade refrigeration system (ACCRS)	116
Figure 6.2	Variation of COP with T_{Hpg} ($T_{eVA} = 7.20C$, $T_a = T_{cVA}$, $T_{eVC} = -400C$, $\epsilon_{she(s)} = 0.7$)	124

Figure 6.3	Variation in exergetic efficiency with T_{HPg} ($T_{\text{eVA}} = 7.2^{\circ}\text{C}$, $T_{\text{a}} = T_{\text{cVA}}$, $T_{\text{eVC}} = -40^{\circ}\text{C}$, $\varepsilon_{\text{she}}(s) = 0.7$)	124
Figure 6.4	Effect of HP generator temperature (T_{HPg}) on various parameters ($T_{\text{eVA}} = 7.2^{\circ}\text{C}$, $T_{\text{a}} = T_{\text{cVA}} = 37.8^{\circ}\text{C}$, $T_{\text{a}} = T_{\text{cVA}}$, $T_{\text{eVC}} = -40^{\circ}\text{C}$, $\varepsilon_{\text{she}}(s) = 0.7$)	129
Figure 6.5	Effect of absorber temperature (T_{a}) on various parameters ($T_{\text{eVA}} = 7.2^{\circ}\text{C}$, $T_{\text{HPg}} = 185^{\circ}\text{C}$, $T_{\text{a}} = T_{\text{cVA}}$, $T_{\text{eVC}} = -40^{\circ}\text{C}$, $\varepsilon_{\text{she}}(s) = 0.7$)	131
Figure 6.6	Variation of solution circulation ratio (SCR), with HP generator temperature (T_{HPg}) at different absorber temperatures ($T_{\text{eVA}} = 7.2^{\circ}\text{C}$, $T_{\text{a}} = T_{\text{cVA}}$, $T_{\text{eVC}} = -40^{\circ}\text{C}$, $\varepsilon_{\text{she}}(s) = 0.7$)	132
Figure 6.7	Variation of COP with HP generator temperature (T_{HPg}) at different absorber temperatures ($T_{\text{eVA}} = 7.2^{\circ}\text{C}$, $T_{\text{a}} = T_{\text{cVA}}$, $T_{\text{eVC}} = -40^{\circ}\text{C}$, $\varepsilon_{\text{she}}(s) = 0.7$)	133
Figure 6.8	Variation of exergetic efficiency (η_{ex}) with HP generator temperature (T_{HPg}) at different absorber temperatures ($T_{\text{eVA}} = 7.2^{\circ}\text{C}$, $T_{\text{a}} = T_{\text{cVA}}$, $T_{\text{eVC}} = -40^{\circ}\text{C}$, $\varepsilon_{\text{she}}(s) = 0.7$)	135
Figure 6.9	Variation of total exergy destruction ($\dot{E}_{\text{D, total}}$) and EDR with HP generator temperature (T_{HPg}) at different absorber temperatures ($T_{\text{eVA}} = 7.2^{\circ}\text{C}$, $T_{\text{a}} = T_{\text{cVA}}$, $T_{\text{eVC}} = -40^{\circ}\text{C}$, $\varepsilon_{\text{she}}(s) = 0.7$)	136
Figure 6.10	Effect of evaporator 1 temperature (T_{eVC}) on COP at different generator temperatures ($T_{\text{eVA}} = 7.2^{\circ}\text{C}$, $T_{\text{a}} = T_{\text{cVA}} = 37.8^{\circ}\text{C}$, $\varepsilon_{\text{she}}(s) = 0.7$)	137
Figure 6.11	Effect of evaporator 1 temperature (T_{eVC}) on exergetic efficiency (η_{ex}) at different generator temperatures ($T_{\text{eVA}} = 7.2^{\circ}\text{C}$, $T_{\text{a}} = T_{\text{cVA}} = 37.8^{\circ}\text{C}$, $\varepsilon_{\text{she}}(s) = 0.7$)	138
Figure 6.12	Variation of total exergy destruction rate ($\dot{E}_{\text{D, total}}$) and exergy destruction ratio (EDR) with evaporator 1 temperature (T_{eVC}) at different generator temperatures ($T_{\text{eVA}} = 7.2^{\circ}\text{C}$, $T_{\text{a}} = T_{\text{cVA}} = 37.8^{\circ}\text{C}$, $\varepsilon_{\text{she}}(s) = 0.7$)	139
Figure 6.13	Exergy destruction rate (\dot{E}_{D}) in various components of ACCRC	140
Figure 6.14	%Exergy destruction ratio (% EDR) of various components of ACCRC	141
Figure 6.15	Schematic diagram of absorption-compression (double effect)	145

	H ₂ O/LiBr series flow) cascade refrigeration system (ACCRS)	
Figure 6.16	Schematic diagram of absorption-compression (single effect H ₂ O/LiBr series flow) cascade vapour refrigeration cycle (ACCVRC)	146
Figure 6.17	Variation in COP _{ACCVRC} and exergetic efficiency ($\eta_{ex, ACCVRC}$) with effectiveness of solution heat exchanger ($\epsilon_{She.}$)	152
Figure 6.18	Variation in total exergy destruction rate ($\dot{E}_{E, total, ACCVRC}$) and exergy destruction ratio (EDR _{ACCVRC}) with effectiveness of solution heat exchanger ($\epsilon_{She.}$)	153
Figure 6.19	Effect of evaporator1 temperature (T_{eVC}) on COP _{ACCVRC} and exergetic efficiency ($\eta_{ex, ACCVRC}$)	154
Figure 6.20	Variation in total exergy destruction rate ($\dot{E}_{E, total, ACCVRC}$) and exergy destruction ratio (EDR _{ACCVRC}) with evaporator1 temperature (T_{eVC})	155
Figure 6.21	Schematic diagram of absorption-compression (half effect H ₂ O/LiBr series flow) cascade refrigeration system (ACCRS)	157
Figure 6.22	Pictorial representation of general exergy balance in a thermal system	163
Figure 6.23	Variation in optimum pressure (P _{OPT.}) of LP generator with generator temperature (T_{Hpg}, T_{Lpg})	168
Figure 6.24	Effect of generator temperature (T_{Hpg} & T_{Lpg}) on maximum value of COP (COP _{MAX.})	169
Figure 6.25	Variation in maximum thermal efficiency ($\eta_{ex}(MAX.)$) with generator temperature ($T_{Hpg},$ & T_{Lpg})	169
Figure 6.26	Variation in solution circulation ratio (SCR) with generator temperature (T_{Hpg}, T_{Lpg})	174
Figure 6.27	Effect of generator temperature (T_{Hpg}, T_{Lpg}) on COP	174
Figure 6.28	Effect of generator temperature (T_{Hpg}, T_{Lpg}) on exergetic efficiency (η_{ex})	176
Figure 6.29	Variation in total exergy destruction ($\dot{E}_{D, total}$) and exergy destruction ratio (EDR) with (T_{Hpg}, T_{Lpg})	176
Figure 6.30	Effect of evaporator1 temperature ($T_{e, vc}$) on COP	178

Figure 6.31	Variation in exergetic efficiency (η_{ex}) with evaporator1 temperature ($T_{e,vc}$)	179
Figure 6.32	Effect of evaporator1 temperature on total exergy destruction rate ($\dot{E}_{D,total}$) and exergy destruction ratio (EDR)	179
Figure 6.33	Exergy destruction rate (\dot{E}_D) of system components of ACCRS	181
Figure 6.34	Exergy destruction ratio (EDR) of system components of ACCRS	182
Figure 7.1	Schematic diagram of micro-gas turbine based cascade refrigeration system	189
Figure 7.2	Effect of ambient temperature on performance of micro-gas turbine	192
Figure 7.3	Effect of ambient temperature on thermal efficiency of micro-gas turbine ($\eta_{ThermalMGT}$) and COP of the cascade refrigeration cycle	193
Figure 7.4	Variation in exergetic efficiency of the cascade refrigeration cycle with ambient temperature	194
Figure 7.5	Variation in COP and waste heat with generator temperature	195
Figure 7.6	Effect of generator temperature on exergetic efficiency	196
Figure 7.7	Effect of refrigerated air temperature on COP	196
Figure 7.8	Effect of refrigerated air temperature on exergetic efficiency	197
Figure 7.9	Schematic diagram of a retrofitted tri-generation power system	199
Figure 7.10	Net power difference of retrofitted tri-generation power system with respect to simple gas turbine cycle	203
Figure 7.11	Comparison of generation efficiency of various cycles using retrofitted techniques	203
Figure 7.12	Effect of ambient temperature on net power output, thermal efficiency and generation efficiency of gas turbine cycle and steam turbine cycle	204
Figure 7.13	Effect of ambient temperature on first law efficiency of gas turbine cycle and steam turbine cycle	205
Figure 7.14	Effect of ambient temperature on second law efficiency of gas turbine cycle and steam turbine cycle	205
Figure 7.15	Effect of generator temperature on COP of absorption-compression cascade refrigeration cycle	206

LIST OF TABLES

Table No.	Title of Table	Page No.
Table 1.1	Thermodynamic and environmental characteristics of refrigerants R134a, R1234yf and R1234ze	2
Table 3.1	The results of exergy analysis of LVHE incorporated VCR system ($T_e = -10^{\circ}\text{C}$, $(\Delta T)_{SC} = 5^{\circ}\text{C}$)	49
Table 4.1	Comparison of results of (Qureshi and Zubair [12]) and current work	62
Table 4.2	Input variable considered except where the variation of these system variables involved (Arora and Kaushik [18])	62
Table 5.1	Experimental data recorded on experimental VCR set up	98
Table 6.1	Mass balance, Energy balance and Exergy balance relations in individual component of compression-absorption (triple effect $\text{H}_2\text{O}/\text{LiBr}$ series flow) cascade refrigeration system	120-123
Table 6.2	Heat rate (\dot{Q}_1) or work rate (\dot{W}_1) of components of ACCRS. Comparison of present work with Arora et al.[4] for $\text{H}_2\text{O}/\text{LiBr}$ TESFVARS ($T_a = T_{cVA} = 37.8^{\circ}\text{C}$, $T_{\text{Hpg}} = 185^{\circ}\text{C}$, $\epsilon_{\text{she}(s)} = 0.7$ and $\dot{m}_{rVA} = 1\text{kg/s}$)	125
Table 6.3	Input parameters considered except where the variation of physical parameters involved (Arora et al., 2015)	126
Table 6.4	The thermodynamic properties (temperature (T_k), pressure (P_k), concentration of solution (X_k), mass flow rate (\dot{m}_k), enthalpy (h_k) and entropy (s_k)) of ACCRS at state points ($T_{eVA} = 7.2^{\circ}\text{C}$, $T_a = T_{cVA} = 37.8^{\circ}\text{C}$, $T_{\text{Hpg}} = 185^{\circ}\text{C}$, $T_{eVC} = -40^{\circ}\text{C}$, $\epsilon_{\text{she}(s)} = 0.7$)	126-127
Table 6.5	Exergy results of ACCRS. ($T_a = T_{cVA} = 37.8^{\circ}\text{C}$, $T_{\text{Hpg}} = 185^{\circ}\text{C}$, $\epsilon_{\text{she}(s)} = 0.7$ and $\dot{m}_{rVA} = 1\text{kg/s}$)	128
Table 6.6	Input parameters considered except where the variation of physical parameters involved (Kaushik and Arora, 2009)	150
Table 6.7	Energy, exergy and mass balance formulations of individual system component of absorption compression (half effect $\text{H}_2\text{O}/\text{LiBr}$) cascade refrigeration system	163-167
Table 6.8	.Heat rate (\dot{Q}_1) or work rate (\dot{W}_1),) of components of ACCRS. Comparison of present work with (Arora et al., 2016) for $\text{H}_2\text{O}/\text{LiBr}$ HEVARS ($T_{e, VA} = 7$, $T_{a, L} = T_{a, H} = T_{\text{cond}, VA} = 37.8^{\circ}\text{C}$, $T_{\text{Lpg}} = T_{\text{Hpg}} = 67^{\circ}\text{C}$, $\epsilon_{\text{She, L}} = \epsilon_{\text{She, H}} = 0.7$, $\dot{m}_{r,VA} = 1\text{kg/s}$ and $T_{e, VC} = -25^{\circ}\text{C}$)	170

Table 6.9	The thermodynamic properties (temperature (T_j), pressure (P_j), concentration of solution (X_j), mass flow rate (\dot{m}_j), enthalpy (h_j) and entropy (s_j)) of ACCRS at state points ($T_{e,VA} = 7, T_{a,L} = T_{a,H} = T_{cond,VA} = 37.8^{\circ}C, T_{Lpg} = T_{Hpg} = 67^{\circ}C, \epsilon_{She,L} = \epsilon_{She,H} = 0.7, \dot{m}_{r,VA}=1\text{kg/s}$ and $T_{e,VC} = -25^{\circ}C$)	171- 172
Table 6.10	The input and output exergy in each system component of ACCRS ($T_{e,VA} = 7, T_{a,L} = T_{a,H} = T_{cond,VA} = 37.8^{\circ}C, T_{Lpg} = T_{Hpg} = 67^{\circ}C, \epsilon_{She,L} = \epsilon_{She,H} = 0.7, \dot{m}_{r,VA}=1\text{kg/s}$ and $T_{e,VC} = -25^{\circ}C$)	172- 173
Table 6.11	Thermodynamic performance comparison of absorption-compression cascade, absorption and compression refrigeration cycles	185- 186

NOMENCLATURE

SYMBOLS AND ABBREVIATIONS

A	Absorption system
ACCRS	Absorption compression cascade refrigeration system
C	Cascade system
COP	Coefficient of performance
CW	Net compressor work (kW)
DESF	Double effect series flow
$(\Delta T)_{sc}$	Degree of subcooling
\dot{E}	Rate of exergy (kW)
\dot{E}_D	Exergy destruction rate (kW)
ED	Exergy destruction
EDR	Exergy destruction ratio
EES	Energy equation solver
EXE	Exergetic efficiency
GWP	Global warming potential
h	Specific enthalpy (kJ/kg)
HFC	Hydrofluorocarbon
HFO	Hydrofluoroolefin
HP	High pressure
Hpg	High pressure generator
LiBr	Lithium bromide
Lpg	Low pressure generator
MP	Medium pressure
Mpg	Medium pressure generator
\dot{m}	Mass flow rate (kg/s)
\dot{m}_{rVA}	Mass flow rate of refrigerant H ₂ O in VARS
\dot{m}_{rVC}	Mass flow rate of refrigerant R1234yf in VCRS
ODP	Ozone depleting potential
P	Pressure (kPa)
\dot{Q}_e	Rate of net refrigerating effect (kW)
\dot{Q}_{eVC}	Net refrigerating effect of cascade cycle (kW)
\dot{Q}_{Hpg}	Input heat rate of high pressure generator (kW)
s	Specific entropy (kJ/kg ⁰ C)
SCR	circulation ratio

SH	Superheating
T	Temperature ($^{\circ}\text{C}$)
T_b	Boundary temperature ($^{\circ}\text{C}$)
T_e	Evaporator temperature ($^{\circ}\text{C}$)
TESF	Triple effect series flow
T_0	Dead state temperature ($^{\circ}\text{C}$)
VARs	Vapour absorption refrigeration system
VCRs	Vapour compression refrigeration system
\dot{W}	Work rate (kW)
X	mass fraction of Lithium bromide in solution (kg/kg)

Greek symbols

ε	Effectiveness
η	Efficiency
Σ	represents summation

Subscripts

0	Dead state
a, Abs	Absorber
b	Boundary
C, Cond	Condenser
Comp	Compressor
Che	Cascade heat exchanger
cVC	Condenser of vapour compression cycle
D	Destruction
eVA	Evaporator of vapour absorption cycle
eVC	Evaporator of vapour compression cycle
EVP	Evaporator
Ex.	Expansion
ex	Exergetic
i	Inlet, any component of the system
in	Input

INTRODUCTION

1.1 BACKGROUND

The demand of refrigeration and air-conditioning is going on increase day by day in our daily life. The applications of refrigeration and air-conditioning touch every domain of our social life as well as society. These range from food preservation, water chilling, medical preservation and diagnostics, frozen milk to semiconductor cooling. These also involve residential, office and automobile air-conditioning.

A number of refrigeration and air-conditioning applications include automotive & super markets air-conditioning, walk-in coolers, residential refrigerators and chillers are using low GWP refrigerant R1234yf (Honeywell, 2014) and some other include air-dryers, beverage dispenser, vending machines, refrigerators and chillers for supermarkets & commercial buildings are using R1234ze (Honeywell, 2015). Moreover, the European Union has approved a regulation (Regulation (EU) No 517/2014). According to that, the fluorinated gases having global warming potential (GWP) more than 150 can't be used in freezers and domestic refrigerators w.e.f.1st Jan, 2015. The same regulation has been implemented for modern types of mobile air-conditioning systems from January 1, 2017. Therefore the low GWP and zero ODP Table 1.1 alternative refrigerants R1234yf and R1234ze may propose to investigate as replacements of R134a however, the thermodynamic and exergetic performance should match with the existing refrigerants. Additionally, a refrigeration system with simple modifications reduces the energy consumption and running cost.

In recent years, the fourth generation Hydrofluoro-olefins (HFOs)-R1234yf and R1234ze are being considered as alternative to R134a. Although, R134a is a wide spread used refrigerant due to its commercial availability, similar properties to R12, less ODP value, excellent thermal stability, non-toxic and non-flammability etc., it is a HFCs and has high GWP value (Table 1.1). The European Union (EU) regulation is phasing out the current generation HFCs like R134a due to its high GWP and environment consequences.

The alternate refrigerants R1234yf and R1234ze are established refrigerants due to their remarkable thermodynamic and environmental characteristics which have been illustrated in Table 1.1.

Table 1.1 Thermodynamic and environmental characteristics of refrigerants R134a, R1234yf and R1234ze (^PHoneywell [1], ^qHoneywell [2], ^rNIST REFPROP version 9.0 [59], ^sBitzer [51], ^tANSI/ASHRAE standard 34 [49], ^uEES [53])

Refrigerant	R134a ^{p,q,r}	R1234yf ^p	R1234ze ^q
Chemical Name ^r	1,1,1,2-Tetrafluoroethane	2,3,3,3-Tetrafluoropropene	trans-1,3,3,3-Tetrafluoroprop-1-ene
Molecular formula ^r	CH ₂ CF ₄ (CF ₃ -CH ₂ F)	C ₃ H ₂ F ₄ (CH ₂ =CFCF ₃)	C ₃ H ₂ F ₄ (CF ₃ CH=CHF)
Molecular mass (kg/kmol) ^r	102.03	114.04	114.04
Boiling Point (°C) ^r at 1 atm	-26.07	-29.45	-18.95
Freezing Point (°C) ^{p,q} at 1 atm	-103.3	-150	-156
GWP Rating ^{p,q,s}	1430	4	<1
ODP Rating ^{p,q,s}	0	0	0
Critical Temperature(°C) ^r	101.06	94.69	109.37
Critical Pressure (MPa) ^r	4.0593	3.3822	3.6363
Safety group ^t	A1	A2L	A2L
Purity (wt.%)	100%	100%	100%
Appearance ^{p,q}	Colourless	Colourless	Colourless
Combustibility ^{p,q}	No	Yes (Low)	No
Corrosiveness	No	--	--
Toxicity ^{p,q}	No	No	No
Thermal stability	Excellent	Very good	--
Flammability ^s	Non flammable	Mild flammable	Mild flammable
Specific heat (kJ/kg°C) ^u	(C _{pv}) at -10°C	0.8543	0.8849
	(C _{pl}) at 50°C	1.566	1.478
Heat of vaporization (kJ/kg) ^u	(h _{fg}) at -10°C	206.7	170.0
	(h _{fg}) at 50°C	151.8	123.4

The studies to determine the performance improvement, energy efficient and cost effective vapour compression refrigeration systems have been carried out by some researchers associated to subcooling techniques i.e. wire-on-tube condenser, heat exchanger as a subcooler, expansion power recovery through an expander, coupled vapour compression refrigeration cycle, multistate compression, ejector and liquid vapour heat exchanger etc. (Azzouzi et al., 2017, Yang and Yeh, 2015, She et al. 2014,

Koeln and Alleyne, 2014, Maurizio et al., 2015, Khan and Zubair, 2000, Staicovici, 2011, Xing et al., 2015, Yu et al., 2007). The performance improvement of VCR cycle through LVHE is also a suggested technique of subcooling. Arora et al. (2007, 2016) have explored an actual vapour compression refrigeration system for its energy, exergy and parametric analysis. They have examined the refrigerants R22, R407C and R410A. They have also performed the exergy analysis of various component of actual VCR cycle. They concluded that the exergetic efficiency and COP are more for refrigerants R22 than that of R407C and R410A. For minimum exergy destruction, the optimum evaporator temperature has been explored for various condenser temperature. The efficient and eco-sustainable refrigeration systems are in current demand. The developing countries like India have hunger demand of electricity especially in summer season due to increasing refrigeration and air-conditioning load. In order to fulfil the need of high grade energy during peak load, efficient refrigeration systems are required. The price of high grade energy is also growing continuously. The protection of environment from high GWP HFCs which are used in refrigeration and air-conditioning systems is a current issue. A large number of researchers have been explored the mechanical subcooling techniques viz. liquid vapour internal heat exchanger between evaporator and compressor, dedicated mechanical subcooling and integrated mechanical subcooling etc. Thornton et al. (1992) have developed design strategies for dedicated mechanical subcooling cycles. A small vapour compression refrigeration cycle was utilized to subcool the main refrigeration cycle. They predicted that the optimum subcooling temperature was strongly dependent on the sink and refrigerated space temperatures and weakly dependent on the subcooler heat exchange parameters. Qureshi and Zubair (2012, 2013), Qureshi et al. (2013) observed the effect of refrigerant combination on the performance of dedicated mechanically subcool vapour compression refrigeration cycle. They also reviewed the future aspects of mechanical subcooling in vapour compression refrigeration cycle. They analysed that the load carrying capacity of the evaporator increased by approximately 0.5kW when R22 was subcooled in the main cycle by 5-8°C. They noted that using the subcooling, the second-law efficiency of the cycle increased by an average 21% and this percentage increase is directly proportional to the ambient temperature. Zubair (1990, 1994) and Zubair et al. (1996) have performed thermodynamic analysis of an integrated and a dedicated mechanical subcooling system. The results of these analysis show that the

performance of the system improves for the larger difference in condenser and evaporator temperature.

In the current scenario, the energy, exergy, economy, environment and safety strategies are the major issues which are being considered to evaluate refrigeration cycles both high as well as low evaporator temperatures. The low temperatures for cryogenics approaching 0 K, airconditioning around 0°C, industrial refrigeration are -35 to -50°C and its applications such as freeze drying, pharmaceuticals, chemical and petroleum industry use cascade refrigeration cycles (ASHRAE_R02_39SI.pdf). Tassou et al. (2010) suggested to slowdown the growth and microbiological, physical and chemical activities that spoil or rancid the food, refrigeration is necessary. The food is frozen between -18 to -35°C. Generally, mechanical refrigeration technologies are invariably employed in these processes which either contribute electricity consumption and environmental impact or low performance. These processes include vapour compression refrigeration, half, single, double and triple effect vapour absorption refrigeration. Although the performance of vapour compression refrigeration cycle supersedes the others yet its electricity consumption is higher. The vapour absorption refrigeration (VAR) cycles which utilize either waste heat or renewable source of energy prove more significant electrical energy saving technologies. In order to utilize the heat available at low temperature half effect vapour absorption refrigeration cycle has been explored by some researchers. Kaushik and Arora (2009), Arora et al. (2016) have analyzed half, single and double effect series and parallel flow vapour absorption cycles. They reported that the generator temperature and COP for half, single and double effect series flow refrigeration cycles were (65°C, 0.41), (87.8°C, 0.7609) and (140.6°C, 1.26) respectively. They deduced that the COP of double effect system was about twice that of single effect. The use of waste heat and renewable source of energy in absorption cycle not only enhances the performance of the cascade system but also a cost saving scheme. Han et al. (2013) have suggested an absorption-compression hybrid refrigerator powered by waste heat. They declared that the system COP was 41.9% higher than that of a simple NH₃ absorption refrigerator and have confirmed performance improvement by exergy analysis.

From the fundamental thermodynamic point of view, the reason for low thermal efficiency of simple gas turbine are high back work ratio (more amount of turbine work is utilized to compress the inlet air through compressor) and substantial amount of available energy loss due to high temperature exhaust (often above 500°C) caused by

rotation of shaft of turbine at a high back pressure relatively. This waste heat recovery from the gas turbine exhaust can be utilized to improve generation efficiency through some alterations to conventional cycle such as chemical recuperation, inlet air cooling, gas to gas recuperation steam injection, and combined cycle etc. The combined power cycle is rated as one of the most innovative and efficient technique to extract the high grade energy from the exhaust gases for enhancing the efficiency and capacity of the power generation plant among from the present well established techniques. However, the combined cycle technology is unsuitable for daily on-off operation pattern units due to low mobility (start-up time). The fossil fuel consumption is increasing world-wide due to demand of high grade energy. The fossil fuels viz. coal, crude oil and natural gas have been used to produce high grade energy i.e. electricity. The waste heat of electricity generation power plants can be utilized either to increase the efficiency of existing power plants and to run a separate power generation plant of lower capacity or to produce the refrigeration. The combination of power generation and production of refrigeration along production of steam or hot water can also be carried out using the waste heat of a power plant. The utilization of waste heat in the exhaust gases of power plant not only conserves the fossil fuels, it also reduces the environmental pollution.

1.2 OBJECTIVES AND SCOPE OF THE THESIS

The specific objectives of the present thesis are as follows:

- Reduction in fossil fuel consumption used in various thermal systems.
- Waste heat recovery of various thermal power plants.
- Energy efficient thermal systems design and development through waste heat recovery.
- Protection of environment from Global warming and Ozone Depletion.
- Replacement of HFOs (R1234yf and R1234ze) to HFCs (R134a) to reduce GWP and ODP.

1.3 ORGANIZATION OF THE THESIS

The thesis consists of seven chapters which are summarized below:

CHAPTER 1: INTRODUCTION

This chapter represents the background of the vapour compression refrigeration and vapour absorption refrigeration systems. The energy, exergy and environmental issues of conventional vapour compression and absorption refrigeration cycles have been discussed. A novel approach of analysing the refrigeration system has been discussed. The cascading of vapour compression refrigeration cycle and compression absorption vapour refrigeration cycles has been discussed. The alternate refrigerants of HFCs have been proposed and their performance for liquid vapour heat exchanger associated VCR cycle, dedicated mechanically subcooled VCR cycle and an experimental VCR cycle has been discussed in detail. The energy and exergy performance improvement of a tri-generation (power, heat and refrigeration) system have also been highlighted. Further the objectives of the thesis along with the organization of the thesis in chapters have also been represented in the chapter.

CHAPTER 2: LITERATURE REVIEW

This chapter includes the complete literature survey up to current date on vapour compression and absorption refrigeration systems, subcooling techniques of VCR system, Alternate refrigerants to HFCs, cascade and non-cascade VCR and absorption compression refrigeration systems. Absorption compression combined and integrated systems and their configurations. Gas power plants, cogeneration, tri-generation plants and retrofitted techniques used in the gas power plant. The research gap has been identified for the investigation of present work.

CHAPTER 3: THERMODYNAMIC PERFORMANCE (ENERGY AND EXERGY) ANALYSIS OF MECHANICALLY SUBCOOLED VCR SYSTEM USING ALTERNATIVE REFRIGERANTS R1234yf AND R1234ze AS REPLACEMENTS OF R134a

The energy and exergy analysis of a simple VCR cycle incorporated to a liquid vapour heat exchanger (LVHE) has been performed using low GWP and zero ODP refrigerants R1234yf and R1234ze for the replacement of HFC-R134a. The effect of degree of sub-cooling (5 to 30⁰C), evaporator temperature (-30⁰C to 15⁰C), effectiveness of liquid vapour heat exchanger (0.2 to 1.0) and compressor efficiency (0.4 to 1.0) has been investigated on the performance parameters viz. exergy destruction, exergy destruction ratio (EDR) and exergetic efficiency of the system components. It is

observed that the COP and exergetic efficiency of R1234ze are 1.87% and 1.88% more than that of R134a for 30⁰C of subcooling. However, R1234yf offers lower performance than R134a. The components condenser and evaporator are the sites of highest and lowest exergy destruction respectively for the refrigerants considered.

CHAPTER 4: THERMODYNAMIC PERFORMANCE ANALYSIS OF DEDICATED MECHANICALLY SUB-COOLED VAPOUR COMPRESSION REFRIGERATION SYSTEM

Thermodynamic performance analysis of dedicated mechanically sub-cooled vapour compression refrigeration cycle using refrigerants R1234ze, R1234yf and R134a has been done. The effect of variation of degree of subcooling (5-30⁰C), evaporator temperature (-20 to 10⁰C) and condenser temperature (30-50⁰C) has been investigated for energetic and exergetic performance of the system. It has been observed that the COP and exergetic efficiency of dedicated subcooled VCR cycle are better than that of simple VCR cycle. Refrigerant R1234ze performs better than R1234yf and comparable to R134a

CHAPTER 5: PERFORMANCE ANALYSIS (ENERGY AND EXERGY) OF EXPERIMENTAL VAPOUR COMPRESSION REFRIGERATION CYCLE

The energy and exergy analysis of an experimental vapour compression cycle has been carried out using R134a, R1234yf and R1234ze. The drop in replacement has been done for R1234yf and R1234ze. The theoretical and experimental VCR cycles have been compared. The performance parameters viz. COP, exergetic efficiency, exergy destruction rate and exergy destruction ratio have been computed. The effect of pressure ratio, evaporator temperature and condenser temperature has been observed.

It has been observed that the COP and exergetic efficiency of the theoretical and experimental VCR cycle decrease with increase in pressure ratio and condenser temperature. On the other hand, the COP increases and exergetic efficiency decreases with increase in evaporator temperature. It has also been observed that performance of R1234ze is better than that of R1234yf.

CHAPTER 6: ENERGY AND EXERGY ANALYSIS OF VAPOUR COMPRESSION-ABSORPTION (H₂O-LiBr) CASCADE REFRIGERATION SYSTEM

An absorption-compression (series flow triple effect H₂O-LiBr) cascade refrigeration system (ACCRS) has been analysed for low cooling applications. It comprises of a triple effect H₂O-LiBr series flow vapour absorption refrigeration cycle associated to simple vapour compression refrigeration (VCR) cycle using R1234yf refrigerant. Energetic and exergetic analysis have been performed for the parametric investigation of the system. The analysis determines the effect of generator temperature (175-200⁰C), absorber temperature (25-40⁰C) and evaporator temperature (-50 to -10⁰C) on the energetic (COP) and exergetic (exergetic- efficiency, exergy destruction rate and exergy destruction ratio (EDR)) performance of the system. It has been observed that the electricity savings of triple effect cascade vapor refrigeration cycle are 45.84% than that of conventional VCR cycle. The COP and exergetic-efficiency of VCR circuit in the cascade system boost up by 85.26% and 85.28% respectively

An absorption-compression (series flow double effect H₂O-LiBr) cascade refrigeration system (ACCRS) has been analyzed for low cooling applications. It comprises of a double effect H₂O-LiBr series flow vapor absorption refrigeration cycle cascaded to a vapor compression refrigeration (VCR) cycle using R1234yf and R1234ze as refrigerants. Energy and exergy performance analysis have been carried out by Colorado and Rivera (2015). It has been observed that the double effect cascade vapor refrigeration cycle consumes less electricity than that of conventional VCR cycle as well as the COP and exergetic efficiency of VCR circuit in the cascade cycle are higher than that of simple VCR cycle.

Exergy and energy analysis of single effect H₂O-LiBr VAR cycle cascaded to a simple VCR cycle (R1234ze and R1234yf) has been carried out. In which, energy performance (COP) and exergy performance (exergy efficiency), total exergy destruction rate and exergy destruction ratio (EDR) have been investigated with the variation in effectiveness of solution heat exchanger (0-1) and evaporator temperature of VCR cycle (-25⁰C to -5⁰C). It has been observed that the cascading of absorption and compression vapour refrigeration cycles improves the thermodynamic performance for the low temperature production as well as reduces the consumption of high grade energy i.e. electricity. Refrigerant R1234ze performs better than that of R1234yf.

An absorption-compression (half effect H₂O-LiBr) cascade refrigeration system (ACCRS) has been analyzed for high grade energy savings. It comprises of a half effect water lithium bromide vapor absorption refrigeration (VAR) cycle and an R1234yf vapor compression refrigeration (VCR) cycle. The energy and exergy investigation

have been carried out for COP, exergetic efficiency, exergy destruction rate and exergy destruction ratio. The effect of generator temperature, absorber temperature and evaporator temperature has been observed on performance parameters. The COP and exergetic efficiency of VCR circuit of cascade cycle are about twice and 2.19 times respectively than that of simple VCR cycle. The cascade cycle saves the high grade energy than that of simple VCR cycle.

CHAPTER 7: THERMODYNAMIC PERFORMANCE ANALYSIS OF TRIGENERATION SYSTEM (POWER, HEAT AND REFRIGERATION) FOR PERFORMANCE IMPROVEMENT USING RETROFITTED TECHNIQUES AND ALTERNATE REFRIGERANTS

Thermodynamic analysis of vapor absorption (single effect H₂O- LiBr)-compression (R1234yf) cascade refrigeration system energized by a gas turbine (micro) has been carried out. In which vapor compression refrigeration cycle using R1234yf and a single effect H₂O- LiBr vapour absorption refrigeration cycle coupled to each other through cascade heat exchanger. The cascade cycle is energized by a gas turbine (micro). The high grade energy (electrical energy) generated by the gas turbine (micro) is used to run the compressor of vapour compression refrigeration cycle. The generator of vapour absorption refrigeration cycle receives heat energy from the waste heat of flue gases of gas turbine (micro). The evaporator of VCR system produces lower temperature as compared to VAR system. The cascade refrigeration system performs better energy efficient than that of conventional VCR system.

Thermodynamic analysis of a tri-generation system (power, heat and refrigeration) for performance improvement using retrofitted techniques and alternative refrigerants (R1234yf and R1234ze) has been carried out. The system comprises a gas turbine cycle, a steam turbine cycle, heat recovery steam generator (HRSG) and a cascade refrigeration cycle. The retrofitted techniques viz. steam injection to gas turbine (STIG) and evaporative cooling (EVC) and have been considered to enhance the performance of gas turbine cycle. Various performance parameters viz. thermal efficiency, generation efficiency, overall cycle efficiency and exergetic efficiency have been computed and the effect of ambient temperature and relative humidity have been analysed on performance parameters. It has been observed that the retrofitted techniques improve the power output and generation efficiency of the gas turbine cycle.

The waste heat recovered from the exhaust gases has been utilized to improve performance of gas turbine as well as in heat and refrigeration production.

CHAPTER 8: OVERALL CONCLUSIONS AND RECOMMENDATIONS

In this chapter, overall conclusions of the present work are presented. The appropriate recommendations and suggestions for the further work are proposed in the chapter.

LITERATURE REVIEW

2.1 INTRODUCTION

This chapter illustrates the comprehensive literature survey gathered from esteemed database sources. It comprises of simple vapour compression refrigeration systems and investigation of alternate refrigerants in mechanically subcooled VCR systems, vapour absorption refrigeration systems, compression-absorption combined/integrated or cascade systems and combined power, heat and refrigeration systems.

2.2 VAPOUR COMPRESSION REFRIGERATION (VCR) SYSTEMS AND ALTERNATE REFRIGERANTS

Arora et al. (2007, 2016) have investigated vapour absorption and vapour compression refrigeration systems for performance improvement using liquid vapour heat exchanger subcooling techniques energetically and exergetically. They observed that subcooling of vapour compression refrigeration cycle enhances the COP and exergetic efficiency of the cycle. They have also analysed half effect water lithium bromide, double effect parallel flow vapour absorption refrigeration system on the basis of energy and exergy.

The exergy is a universal measure of work potential or quality of different forms of energy in relation to a given environment. The loss of exergy or irreversibility provides a generally applicable quantitative measure of process inefficiency. Analysing a multi-component system indicates the total system irreversibility distribution among the components of system (Kotas, 1995). Thus the first law based energy analysis as well as first law and second law based exergy analysis is essential to evaluate the performance of a system. A number of researchers have suggested the exergy analysis and energy and exergy analysis both. Zubair et al. (1996) carried out first and second law analysis of both two stage and mechanical subcooling refrigeration cycles with HFC-134a and predicted that most of the losses were due to the low compressor efficiency. Llopis et al. (2015) analysed theoretically a simplified model of CO₂ transcritical refrigeration system using a dedicated mechanical subcooling cycle. It was reported that cooling capacity and COP increased by 28.8% and 20% respectively.

They have presented the five simplified two stage refrigeration system models and analysed these system for energy performance and total environmental warming impact (TEWI) analysis with low-GWP HFC, HFO and naturals refrigerants. It is reported that the future solutions might be based on low-GWP refrigerants. Numerical and experimental approach for different refrigerant combinations in mechanical sub-cooling system, vapour compressor cycle using integrated mechanical sub-cooling, simple vapour compression cycle with dedicated mechanical subcooling cycle and employing a subcooler in two stage refrigeration cycle considered by Qureshi et al. (2013). She et al. (2014) proposed an energy efficient refrigeration system subcooled by liquid desiccant dehumidification and evaporation process. It was predicted that COP of the hybrid system was 16.3% higher than that of conventional vapour compression refrigeration system. Mota-Babiloni et al. (2014, 2015) reviewed the recent developments in commercial refrigeration and focused on system modifications dedicated subcooling/implementation of ejectors, tri-generation technologies (electrical, heating and cooling demand) and better evaporation conditions control. It was reported that the hydrocarbon, HFO and CO₂ were HFC replacements. Additionally, analysed and proposed various mixtures (HFCs: R32, R125, R152a and R134a and HFOs: R1234yf and R1234ze (E)) to phase out the refrigerants R134a, R404A and R410A as per EU Regulation No 517/2014. Ansari et al. (2013) carried out theoretical exergy analysis of a simple vapour compression refrigeration system with a liquid vapour heat exchanger using alternative refrigerants R1234yf and R1234ze as replacements of R134a. It is highlighted that the refrigerants R1234yf and R1234ze can be good replacements of R134a. The liquid vapour heat exchanger shows lower efficiency defect value while condenser shows highest efficiency defect value. Dixit et al. (2016, 2017) carried out energy and exergy analysis of absorption-compression cascade and waste heat driven triple effect refrigeration cycles. Topal et al. (2017) presented case studies of poultry industry and power plant in turkey based on application of tri-generation and exergy analysis of plant. Taner (2015); Taner and Sivrioglu (2015, 2017) have carried out optimization, energy-exergy analysis and techno-economic & cost analysis of a drying plant, model of sugar factory and turbine power plant of sugar in turkey respectively. Moreover, the energy efficient and cost saving refrigeration cycles studies include (Cecchinato and Minetto, 2010; CEATI, 2010) presented the energy efficient and cost saving configurations of small, medium and large sized refrigeration and air-conditioning systems.

A number of studies have been carried out using R1234yf and R1234ze. In the notable studies, Yataganbaba et al. (2015) performed exergy analysis on a two evaporator vapour compression refrigeration system using R1234yf, R1234ze and R134a as refrigerants. The two refrigerants R1234yf and R1234ze were good alternatives to R134a regarding their environment friendly properties. Sethi et al. (2016) carried out tests in a representative vending machine system (cassette) at two representative outdoor ambient temperatures of 32.2°C (efficiency test), and 40.5°C (capacity test) for return air temperatures of 2°C, 20°C and 38°C using refrigerants R1234yf and R1234ze(E) as a replacement to R134a. It is predicted that the performance of R1234yf is similar to R134a while R1234ze (E) requires minor changes in the system design. Zheng and Zhao (2015) proposed a two-stage heat pump (TSHP) based on the combination of vapour expander and compressor i.e. TSHP-E. Thermodynamic and economic performance comparison have been carried out for wet refrigerants R152a, R134a, R161 and R290, and dry fluids including R227ea, R1234yf and R1234ze and concluded that the COP and exergetic efficiency of TSHP-E is higher than that of single-stage heat pump (SSHP) when temperature lift was large. Devecioglu and Oruc (2015) investigated properties of low GWP refrigerants R450A, R513A, R1234yf and R1234ze (E) replaced to R134a; DR-33, L40, DR-7; R448A replaced to R404A; DR-5; R447A replaced to R410A; and N20 and R444B replaced to R22. The study highlighted that all the new refrigerants are better regarding their low GWP values and R1234yf, L40, DR-5 and R444B refrigerants can be good alternatives to R134a, R404A, R410A and R22, respectively. Pigania et al. (2016) examined the safety, efficiency, volumetric capacity and total environmental warming impact for a marine refrigeration system using low GWP refrigerants ammonia (NH₃), carbon dioxide (CO₂), and the HFOs R1234yf and R1234ze (E) and predicted that the Low-GWP refrigerants may increase the system total environmental warming impact (TEWI). Five low GWP refrigerants R152a, R1234yf, R1234ze (E), R290 and R600a have been compared by Sanchez et al. (2017) for the replacement of R134a on the same refrigerating test bench equipped with a hermetic compressor designed for R134a. It was predicted that R1234yf and R152a can be considered suitable drop-in alternative to R134a considering the energy consumption and the cooling capacity of refrigerating facility. On the other hand, R1234ze (E), R600a and R290 were not suitable drop-ins because these required different displacement compared to R134a. Jankovic et al. (2015) analysed R1234yf and R1234ze (E) as drop-in replacement for R134a in a small

power refrigeration system considering equal evaporation and condensation temperatures before and after the refrigerant replacement and for equal cooling medium conditions in the condenser. It was announced that the R1234yf was an adequate drop-in refrigerant for R134a but R1234ze might perform better when an overridden compressor can be used to match the refrigerating system cooling power. Fang et al. (2017) carried out numerical and thermodynamic analysis of ejector heat driven refrigeration cycle (EHDRC) for the drop-in replacement of refrigerant R134a with R1234yf and R1234ze (E). It was reported that R1234yf appeared good drop-in replacement of R134a in a real EHDRC with decrease of 5.2% for the entrainment ratio, 9.6% for the COP and 19.8% for the cooling power in average. On the other hand using R1234ze(E) would induced some modifications due to its thermodynamic properties with reduced coefficient of performance (COP) and cooling power by 4.2% and 26.6% in average with better entrainment ratio. Kalla et al. (2018) reviewed vapour compression refrigeration system for alternative refrigerants and investigated the performance of R22 and its substitutes in air-conditioners. Esen et al. (2006, 2007) performed techno-economic appraisal of a ground source heat pump system for a heating season in eastern Turkey and energy and exergy analysis of a ground coupled heat pump system with two horizontal ground heat exchangers. Poachaiyapoom et al. investigated a miniature vapour compression refrigeration system for electronic cooling using R134a. The speed of compressor considered between 3000 and 6000RPM. They predicted that the highest value of COP observed 9.069 at 3000RPM and 200W. They added that the proposed system was not suitable for electronic cooling at heating power of 100W and 150W.

2.3 VAPOUR ABSORPTION REFRIGERATION (VAR) SYSTEMS

2.3.1 Triple effect, Double effect, Single effect and Half effect VAR Systems

Some research studies are available in the literature on the triple effect vapour absorption cycle i.e. Arora et. al. (2015) utilized the waste heat of I.C. engine exhaust available in the temperature range of 350-400⁰C in the triple effect series flow water-lithium bromide vapour absorption system. The COP of triple effect system was higher than the double effect vapour absorption system. Similarly, Alvarez et al. (2015) analysed a alkali-titrate triple-effect (single effect lithium, potassium, sodium nitrate cycle coupled to a double effect H₂O/LiBr cycle) absorption cycle for high temperature heat source. The alkitrates triple effect cycle was feasible efficient with slight higher

COP than H₂O/LiBr triple effect cycle at generator temperature over 180⁰C. The comparison of half effect to triple effect absorption refrigeration system has been carried out by Maryami and Dehghan (2017). Azhar and Siddiqui (2019) analysed H₂O-LiBr single to triple effect cycle. They concluded that the COP of the triple effect cycle was 132% higher than the single effect. They added that the triple effect series flow VAR cycle was performing best among all. However, it required input heat energy at the higher temperature range 175 to 200⁰C.

Kaushik and Arora (2009), Arora et al. (2007, 2016) analysed half, single, double effect series and parallel flow vapour absorption cycles. They reported that the generator temperature and COP for half, single and double effect series flow refrigeration cycles were (65⁰C, 0.41), (87.8⁰C, 0.7609) and (140.6⁰C, 1.26) respectively. They deduced that the COP of double effect system was about twice that of single effect. Gomri and Hakimi (2008) carried out the exergy analysis of double effect H₂O-LiBr vapour absorption refrigeration system. Kim and Ferreira (2008) have performed the first law analysis of double and single effect VAR systems. Bellos et al. (2016) performed Engineering Equation Solver (EES) based steady state analysis of water-lithium bromide single effect 100kW solar driven absorption chiller.

Berhane et al. (2010) carried out exergy analysis of multi-effect water-LiBr absorption refrigeration systems from half to triple effect. They predicted that the COP increased significantly from double effect to triple effect cycles. Maryami and Dehghan (2017) studied an exergy based comparison between LiBr/water absorption refrigeration systems from half effect to triple effect. They investigated the effect of various operating parameters on COP, exergetic efficiency, thermal load of the system components and total change in the energy of the system along with the energy and exergy analysis of system components. They depicted that the COP and exergetic efficiency increased from half to single, double and triple effect. However total exergy change decreased slightly.

2.4 CASCADE REFRIGERATION SYSTEMS

2.4.1 VCR Cascade Refrigeration Systems

Generally, the vapour compression refrigeration cycle and its configurations viz. double stage, triple stage or multistage cascade are employed for the production of lower evaporation temperature with very high cooling capacity. Messineo (2012) analysed a two stage cascade refrigeration system using carbon dioxide (CO₂) in low

temperature section and ammonia (NH_3) in high temperature section. He reported that CO_2 - NH_3 cascade refrigeration system was an interesting alternative to R404A for low evaporation temperatures (-30 to -50°C). Mosaffa et al. (2016) investigated two stages CO_2 - NH_3 cascade refrigeration system for exergetic and environmental view of analysis. Mafi et al. (2009) have performed exergy analysis of multistage cascade low temperature cascade refrigeration system. They reported that the exergetic efficiency of the system was 30.88%.

2.4.2 Absorption-Compression Cascade Refrigeration Systems

A large number of studies are available in the literature on compression-absorption (combined) or cascade refrigeration cycles. The considered studies (Shahhosseini et al., 2016; Colorado and Rivera, 2015; Cimsit and Ozturk, 2012; Garimella et al., 2011; Wang et al., 2012; Ayala et al., 1997; Kairouani and Nehdi, 2006; Jain, 2013; Pratihari, 2010; Sun and Guo, 2006; Chinnappa et al., 1993; Dixit et al., 2017) fall under two categories viz. single stage and double stage cycle. The first configuration is the combination of single effect VAR cycle coupled to a VCR cycle and the second configuration comprises of a double effect VAR cycle coupled to a VCR cycle. It has been observed that the double effect VAR performs better than the single effect VAR. Colorado and Rivera (2015) compared single stage and double stage compression-absorption system. They reported that the COP of compression-absorption double stage (CADS) could be 50% higher than the compression-absorption single stage (CASS) system. Thus the cascading of double effect VAR to VCR could be a right strategy for energy as well as exergetic performance improvement.

The use of waste heat and renewable source of energy in absorption cycle not only enhances the performance of the cascade system but also a cost saving scheme. Han et al. (2013) have proposed a hybrid absorption-compression refrigerator powered by waste heat. They declared that the system COP was 41.9% higher than that of a simple NH_3 absorption refrigerator and have confirmed performance improvement by exergy analysis.

Thus, the COP of compression-absorption combined cycle was higher than VCR or vapour absorption refrigeration (VAR) cycle. Ayala et al. (1997) explored ammonium/lithium nitrate absorption/compression refrigeration cycle. Kairouani and Nehdi (2006) carried out cooling performance and energy saving of a compression-absorption refrigeration system assisted by geothermal energy. Jain et al. (2018)

analysed a novel configuration of vapour compression-absorption integrated refrigeration system (VCAIRS). They reported that the electrical energy consumption in VCAIRS was 21.4% more as compared to VCACRS. However it was 63% lower than equivalent VCRS. They further investigated the VCAIRS on the basis of coefficient of structural bonds (CBS) and advanced exergy analysis methods. The researchers (Colorado and Rivera, 2015; Cimsit and Ozturk, 2012; Garimella et al., 2011; Wang et al., 2012) investigated that the electricity consumption in the cascade refrigeration cycle was lower than that of conventional vapour compression refrigeration cycle.

2.5 POWER, HEAT AND REFRIGERATION COMBINED TRIGENERATION SYSTEMS

Pilavachi (2002) introduced mini and micro gas turbines for combined heat and power. He emphasized number of advantages and potentials of mini and micro gas turbines compared to other technologies. He predicted about the uncertainty about their market potential but they could be used for power generation in the industrial, commercial and residential sectors. Wang et al. (2007) have studied economic feasibility of waste heat to power-conversion. The simple cycle gas-turbine generation system usually has a low generation-efficiency with high back-work ratio and high exhaust-temperature especially when the ambient weather is hot. Among many technologies to improve the efficiency of a simple cycle gas turbine, inlet air cooling and steam re-injection are considered the best way to modify an existing simple cycle unit without major destruction to its original integrity. To evaluate the individual effects after system modifications, a computer code for the simulation of the power-generation system was developed and validated in this study. They concluded that the system with steam re-injection feature has the highest generation efficiency and thus the most potential profit on investment, while the system with both inlet air-cooling and steam re-injection features can generate the highest power-output and release the least exergy via the flue gases. Bruno et al. (2005) analysed various integrated configurations of several types of commercially available absorption cooling chillers and micro-gas turbine cogeneration systems driven by biogas. Micro-gas turbines are fuelled with biogas and their waste heat is used to drive absorption chillers and other thermal energy users. They conducted a case study for the existing sewage treatment plant. They have investigated tri-generation system that uses biogas and micro gas turbine. They

predicted that the tri-generation plant used all available biogas may replace the existing conventional plant. Tsatsaronis (2006) presented application of thermoeconomics to the design and synthesis of energy plants. He presented thermo-economics, as an exergy-aided cost-reduction method, provides important information for the design of cost-effective energy-conversion plants. The exergy costing principle is used to assign monetary values to all material and energy streams within a plant as well as to the exergy destruction within each plant component. The design evaluation and optimization is based on the trade-offs between exergy destruction (exergetic efficiency) and investment cost for the most important plant components. He concluded that exergoeconomic approaches apply the principle of exergy costing to enable the objective costing of energy carries and to provide effective assistance in the decision making process and the optimization or improvement of energy-intensive plants. In addition, exergoeconomics demonstrates that the exergy destruction plays a positive role in the design of energy-conversion plants by helping engineers to keep the investment costs associated with the plant components at a acceptable level. Misra et al. (2003) analysed thermo-economic optimization of a single effect water/LiBr vapour absorption refrigeration system. The thermo-economic theory is applied to the economic optimization of a single effect water/LiBr vapour absorption refrigeration system for air-conditioning application, aimed at minimizing its overall operation and amortization cost. A simplified cost minimization methodology is applied to evaluate the economic costs of all internal flows and products of the system by formulating exergoeconomic cost equations. Once these costs are determined, the system is thermodynamically evaluated to identify the effects of design variables on costs and enables to suggest values of design variables that would make the overall system cost effective. They concluded that the thermo-economic analysis of a system is able to provide suggestions about potential cost-effective improvements achievable by means of changes in the structure of the system, which is not possible through the mathematical or numerical techniques. Bilgen (2000) presented exergetic and engineering analysis as well as a simulation of gas turbine based cogeneration plants consisting of a gas turbine, heat recovery steam generator and steam turbine. The exergy analysis is based on the first law and second laws of thermodynamics. The engineering analysis is based on both the methodology of levelized cost and pay-back period. He observed that by changing various relevant parameters, parametric studies can be carried out to determine thermodynamic and engineering parameters as well as

suitable operational conditions. Khaliq (2008) performed the exergy analysis of gas turbine trigeneration system for combined production of power heat and refrigeration. In this paper, a conceptual trigeneration system is proposed based on the conventional gas turbine cycle for the high temperature heat addition while adopting the heat recovery steam generator for process heat and vapour absorption refrigeration for cold production. Combined first and second law approach is applied and computational analysis is performed to investigate the effects of overall pressure ratio, turbine inlet temperature, pressure drop in combustor and heat recovery steam generator, and evaporator temperature on the exergy destruction in each component, first law efficiency, electrical to thermal energy ratio, and second law efficiency of the system. Khaliq & Kumar (2008) analysed the thermodynamic performance assessment of gas turbine trigeneration system for combined heat, cold and power production. The thermodynamic performance of the combustion gas turbine tri-generation system has been studied based on first law as well as second law analysis. The effects of overall pressure ratio and process heat pressure fuel utilization efficiency, electrical to thermal energy ratio, second law efficiency, and exergy destruction in each component are examined. Results for gas turbine cycle, cogeneration cycle, and tri-generation cycle are compared. They concluded that performance evaluation of the tri-generation system based on first law analysis alone is not adequate and hence more meaningful evaluation must include second law analysis. Bastos et al. (2005) worked out the simulation of cogeneration system. A dynamic model of mid-capacity system is developed, including gas turbine and HRSG. The simulation for different demands cases are performed. In this work solution to how a cogeneration system can be controlled to satisfy transient power, heating and cooling demands. Temporal simulation of the cogeneration system shows that it's possible to meet all the demand with conventional equipments and controls. Minciuc et al. (2003) presented thermodynamic analysis of tri-generation with absorption chilling machine. They focused on solutions of tri-generation plants based on gas turbine or internal combustion engine with absorption chilling machine. There have been established the limits for the best exergetic performance of tri-generation. The dependence of different technical criteria on each other has also been analyzed. They concluded that the present method can be used for analyzing and sizing a tri-generation plant and choosing the equipment. Sinha and Bansode (2010) studied a thermodynamic analysis for gas turbine power optimization by fog cooling system. Gas turbine output is a strong function of the ambient air temperature with power output

dropping by 0.5% to 0.9% for every 1⁰C rise in ambient temperature (0.3%-0.5% for every 1⁰F). One way to counter this drop in output is to cool the inlet air. An approach becoming increasingly popular is that of the high pressure inlet fogging. Unlike conventional media type evaporative cooling, fogging, can achieve 100% saturation of the air so that air can be cooled up to the wet bulb temperature. A thermodynamic analysis has been carried out for evaluating the gains from increased power and reduced heat rate of a gas turbine that results from pre cooling the turbine inlet air by inlet evaporative cooling and fogging. They concluded that performance parameters indicative of inlet fogging effects have a definite correlation with the climate condition (humidity and temperature). They predicted improvement in turbine power and heat rate with inlet fogging. Bouam et al. (2008) studied combustion chamber steam injection for gas turbine performance improvement during high ambient temperature operations. Their work is to improve the principal characteristics of gas turbine used under hard condition of temperature in Algerian Sahara by injecting steam in the combustion chamber. The suggested method has been studied and compared to a simple cycle efficiency, however is held constant when the ambient temperature increases from ISO conditions to 50⁰C. The comparison predicted to test data is in good agreement. Srinivas et al. (2007) worked out on sensitivity analysis of STIG based combined cycle with dual pressure HRSG. Thermodynamic evaluation has been carried out for a combined cycle with Steam Injected Gas Turbine (STIG) having dual pressure heat recovery steam generator (HRSG). Steam from high-pressure steam turbine is injected into the combustion chamber at a pressure higher than the combustion pressure to improve the exergy efficiency of combined cycle. The effect of steam injection mass ratio, de-aerators pressure (or temperature ratio), steam reheat pressure ratio, HP steam turbine pressure, compressor ratio and combustion temperature on combined cycle exergy efficiency has been investigated. They concluded that steam injection decreases combustion chamber and gas re-heater exergetic loss from 38.5 to 37.4% compared to the case without steam injection in the combustion chamber. Nishida et al. (2005) analyzed the performance characteristics of two types of regenerative steam-injection gas-turbine (RSTIG) systems. These are compared with the performances of the simple, regenerative, water injected and steam injected gas-turbine (STIG) cycles. They concluded that the thermal efficiencies of the RSTIG systems are higher than those of regenerative, water injected and STIG systems and the specific power is larger than that of regenerative cycle. The optimum pressure-ratio for maximum efficiency of the

RSTIG systems is relatively low. The RSTIG system can be applied to the flexible heat-and-power generation system. The total efficiency of the electric power generation reaches more than 70% (HHV) when the heat output is maximized.

2.6 CONCLUSIONS OF LITERATURE REVIEW

A vast variety of research work has been done by the researchers in the field of refrigeration and tri-generation which includes VCR systems, subcooling techniques, VAR systems, VCR cascade systems, vapour compression-absorption combined/cascade refrigeration systems and the coupling of cascade system to the power generation plant. The main conclusions are highlighted below:

- The performance of simple VCR cycle has been investigated using different refrigerants.
- VCR cycle has been investigated for performance improvement using subcooling techniques i.e. wire-on-tube condenser, heat exchanger as a sub-cooler, expansion power recovery through an expander, integrated vapour compression refrigeration cycle, multistate compression, ejector and internal heat exchanger etc.
- VAR cycle has been investigated with its half, single, double and triple effect versions for waste heat recovery.
- VCR-VAR (single and double effect H₂O-LiBr) cascade cycle has been investigated for performance improvement.
- Performance of co-generation and tri-generation cycles has been explored using performance improvement techniques.

2.7 RESEARCH GAPS

The following research gaps have been identified from the vast literature review.

- A simple vapour compression refrigeration (VCR) system has investigated scantily on an experimental setup to investigate energy-exergy performance using alternate refrigerants R1234yf and R1234ze.
- The energy and exergy performance analysis of liquid vapour heat exchanger (LVHE) incorporated VCR system has not been explored using alternative refrigerants viz. HFOs: R1234yf and R1234ze.

- A dedicated mechanically sub-cooled VCR cycle has been scantily investigated for performance improvement using R1234yf and R1234ze.
- The energy and exergy performance of vapour absorption refrigeration (VAR) (half, single, double and triple effect series flow and parallel flow)-VCR (R1234yf and R1234ze) cascade cycles has not been investigated.
- A tri-generation (power, heat and refrigeration) cycle comprises gas turbine, steam turbine, heat recovery steam generator and VAR-VCR cascade refrigeration cycle has been scantily analysed for its performance improvement using retrofitted techniques viz. inlet air cooling (IAC) and steam injection to gas turbine (STIG).

2.8 OBJECTIVES OF THE PROPOSED RESEARCH WORK

With the reference to the literature survey constituted from the different established database sources. The main objectives of the present research are pointed below:

- To compare R134a, R1234yf and R1234ze on the basis of COP and exergy efficiency for experimental vapor compression refrigeration unit to explore alternative refrigerants.
- To explore the performance of alternate refrigerants viz. hydrofluoroolefins (HFOs) R1234yf and R1234ze for the replacement of hydrofluorocarbons (HFCs) viz. R134a in conventional and modified refrigeration cycles.
- To investigate cascading of vapour compression system with single, double and triple -effect absorption system using R1234yf to find better performance.
- To examine the performance improvement of tri-generation system coupled with half, single, double and triple effect vapour absorption system and vapour compression refrigeration system (R1234yf and R1234ze) using retrofitting techniques.
- To investigate performance analysis for various performance parameters of a tri-generation system (power, heat and refrigeration) using R1234yf.

THERMODYNAMIC PERFORMANCE (ENERGY AND EXERGY) ANALYSIS OF MECHANICALLY SUBCOOLED VCR SYSTEM USING ALTERNATIVE REFRIGERANTS R1234yf AND R1234ze AS REPLACEMENTS OF R134a

3.1 INTRODUCTION:

Energy consumption in refrigeration systems, environmental issues and cost effectiveness are essential considerations in the recent scenario in order to meet the current demand of energy, conserve energy resources, protection of the environment and in access to the large number of consumers. A number of refrigeration and air-conditioning applications include automotive & super markets air-conditioning, walk-in coolers, residential refrigerators and chillers are using low GWP refrigerant R1234yf (Honeywell, 2014) and some other include air-dryers, beverage dispenser, vending machines, refrigerators and chillers for supermarkets & commercial buildings are using R1234ze (Honeywell, 2015). Moreover, the European Union has approved a regulation (Regulation (EU) No 517/2014). According to that, the fluorinated gases having global warming potential (GWP) more than 150 can't be used in freezers and domestic refrigerators w.e.f.1st Jan, 2015. The same regulation has been implemented for modern types of mobile air-conditioning systems from January 1, 2017. Therefore the low GWP and zero ODP alternative refrigerants R1234yf and R1234ze (Table1.1) may be proposed to investigate as replacements of R134a. However, the thermodynamic and exergetic performance of alternative refrigerants should match with the existing refrigerants. Additionally, a refrigeration system with simple modifications consumes lesser energy and having lower running cost. Although, the modified simple VCR systems have been investigated earlier using conventional refrigerants, may be investigated for alternative refrigerants.

The objective of current work is to investigate the performance of alternate refrigerants in a modified simple VCR system. The energy and exergy analysis of a simple VCR system having a liquid vapour heat exchanger (LVHE) has been carried out using low GWP and zero ODP refrigerants R1234yf and R1234ze for the replacement of HFC-R134a. The LVHE is coupled to simple VCR system between evaporator and condenser such that the refrigerant vapour leaving the evaporator and

the liquid refrigerant leaving the condenser exchanges heat within it. The energy and exergy analysis of LVHE incorporated VCR system is followed by parametric analysis for the refrigerants R134a, R1234yf and R1234ze. The effect of operating variables viz. degree of sub-cooling (5 to 30⁰C), evaporator temperature (-30⁰C to 15⁰C), effectiveness of liquid vapour heat exchanger (0.2 to 1.0) and compressor efficiency (0.4 to 1.0) has been investigated on the performance of the system.

3.2 DESCRIPTION OF SYSTEM

Fig.s 3.1 and 3.2 illustrate the schematic and P-h diagrams liquid vapour heat exchanger (LVHE) incorporated simple vapour compression cycle respectively. The system comprises a compressor, a condenser, a throttle valve, an evaporator and a liquid vapour heat exchanger.

Generally, commercial refrigerating units are incorporated with liquid vapour heat exchanger (LVHE) for making the advantage of mechanical subcooling to enhance the cooling capacity of the system. Mechanical subcooling is a process to subcool the saturated liquid at the exit of condenser and superheat the saturated vapour at the exit of evaporator. Moreover, refrigeration involves the phase change of refrigerants i.e. from vapour to liquid or liquid to vapour to absorb the heat from a colder region, temperature and pressure of refrigerant rises and finally rejected heat to a hotter region. The cold fluid (superheated vapour) is received by the compressor at state point 1a which is compressed the fluid to the high pressure at state point 2a. The high pressure and temperature superheated fluid rejects its heat in the condenser from state 2a to 3 and saturated liquid is obtained at state point 3. The saturated liquid refrigerant leaving the condenser (state point 3) enters into LVHE where it loses the heat to the saturated vapour refrigerant coming from evaporator. The heat exchanger subcools the saturated liquid (state point 3a, from where the subcooled liquid is expanded through a throttle valve to state 4a) and saturated vapour gets superheated (state point 1a) before entering into the compressor.

In the compressor the superheated refrigerant is compressed to state 2a. The refrigeration effect is produced in the evaporator from state 4a to state 1. The effect of incorporating the LVHE in the cycle is to increase the specific refrigeration effect as well as specific compressor work. The change in COP depends upon the rate of increase of cooling capacity and compressor power.

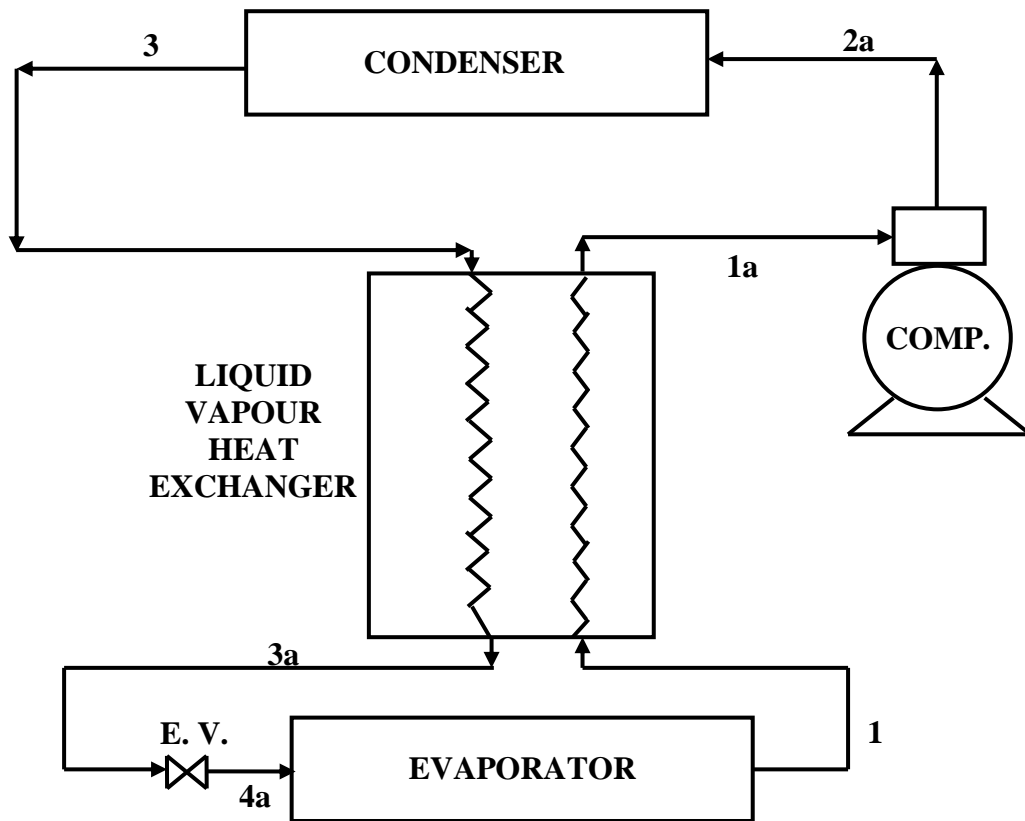


Fig. 3.1 Schematic diagram of liquid vapour heat exchanger (LVHE) incorporated simple vapour compression refrigeration cycle (Arora et al., 2009)

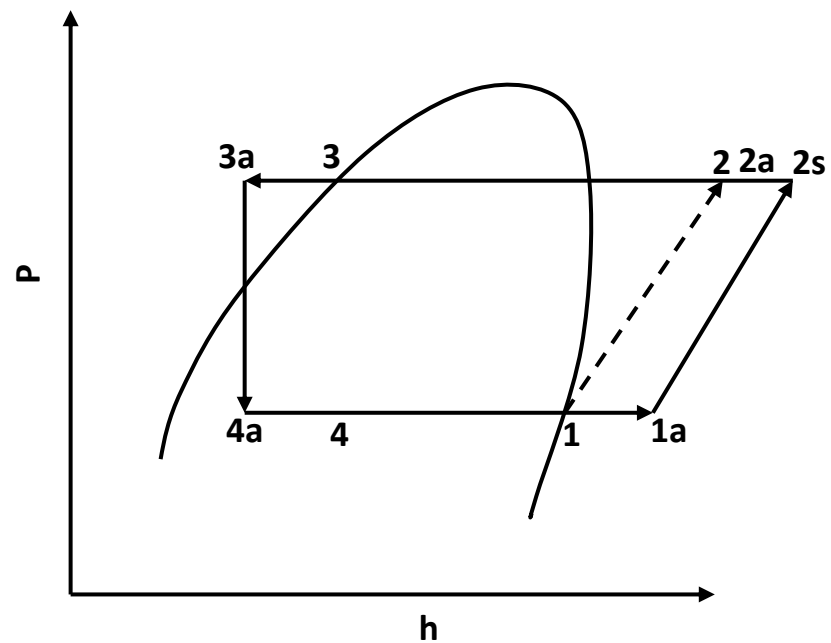


Fig. 3.2 P-h diagram of LVHE incorporated simple vapour compression refrigeration cycle

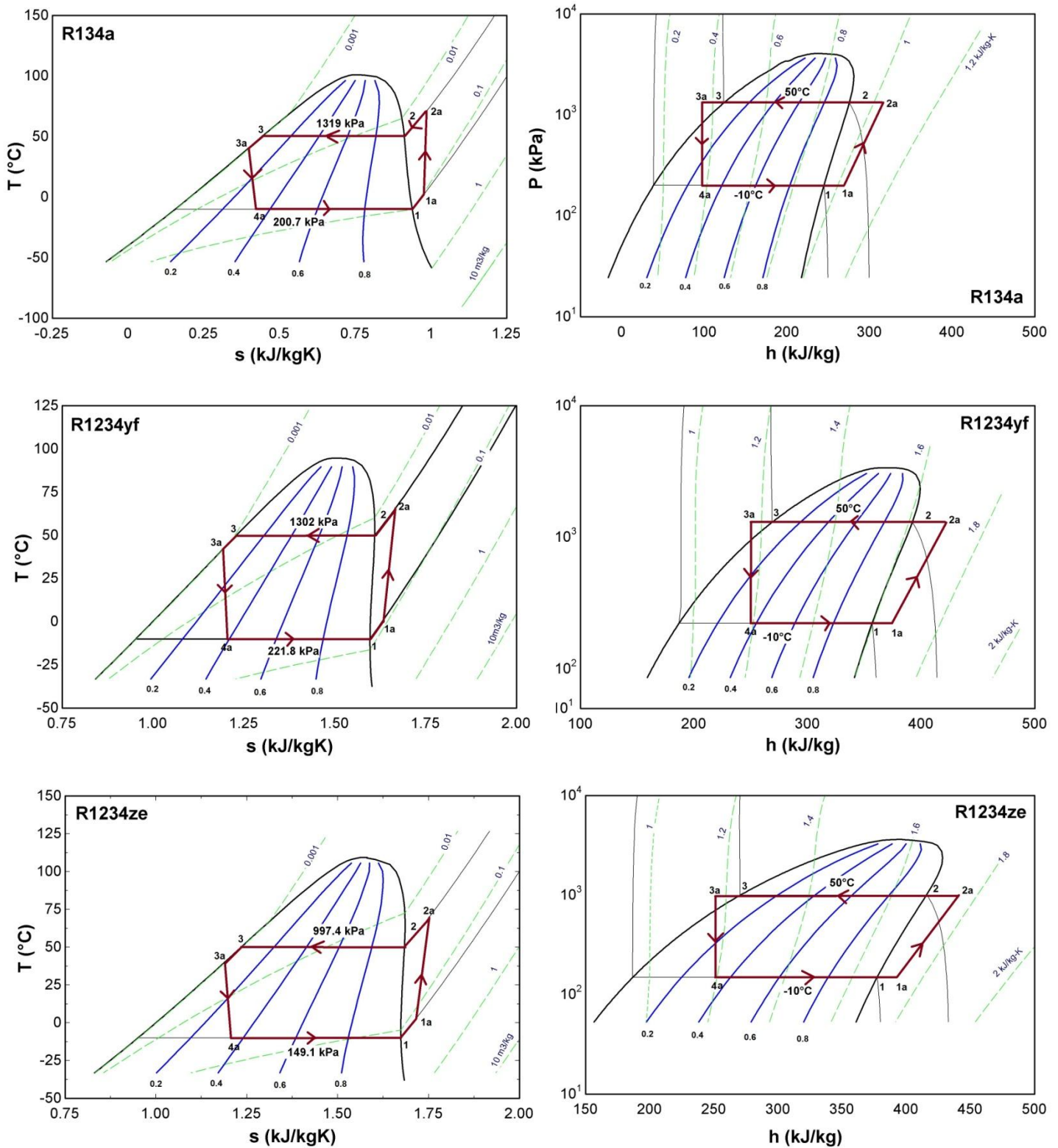


Fig. 3.3 Pressure-enthalpy (P-h) and temperature-entropy (T-s) state diagrams of R134a, R1234yf and R1234ze

The pressure-enthalpy and temperature-entropy diagrams of considered refrigerants R134a, R1234yf and R1234ze have been shown in Fig. 3.3 with the evaporator (-10°C) and condenser temperature (50°C). The evaporator pressure (200.7, 221.8 and 149.1 kPa) and condenser pressure (1319, 1302, 997.4 kPa) corresponding to evaporator (-10°C) and condenser temperature evaporator (50°C) have been notified to

compare the applicability of the refrigerants R134a, R1234yf and R1234ze respectively.

3.3 MATHEMATICAL MODELLING

3.3.1 Assumptions

For the energy and exergy analysis of mechanically subcooled vapour compression refrigeration cycle, following assumption have been considered.

- The steady state is considered for the operation of each component of the system.
- The refrigerant entering in the compressor is dry and saturated for simple VCR system (state point1).
- The pressure drop in evaporator (δ_e), condenser (δ_c), LVHE , other system ocmponents and connecting pipelines is neglected.
- Heat losses in LVHE and connected pipelines are neglected.
- The chemical, kinetic and potential exergies are neglected.

3.3.2 Energy and Exergy Analysis

3.3.2.1 Energy Analysis

The first law based work, energy and mass conservation principles are presented in equations (3.1) and (3.2).

$$\sum \dot{Q} - \sum \dot{W} = \sum \dot{m}_o h_o - \sum \dot{m}_i h_i \quad (3.1)$$

$$\sum \dot{m}_i - \sum \dot{m}_o = 0 \quad (3.2)$$

Where \dot{Q} , \dot{W} and \dot{m} are the rate of heat, work and mass transfer crossing the boundary of the system respectively.

The coefficient of performance (COP) of LVHE incorporated to VCR cycle is given by the equation (3.3) to (3.5).

$$\text{COP} = \frac{\dot{Q}_e}{\dot{W}_{\text{comp}}} \quad (3.3)$$

Where \dot{Q}_e is the net refrigeration effect produced and \dot{W}_{comp} is the actual work of the compressor.

$$\dot{Q}_e = \dot{m}_r (h_1 - h_{4a}) \quad (3.4)$$

$$\dot{W}_{\text{comp}} = \dot{m}_r (h_{2a} - h_{1a}) \quad (3.5)$$

The effectiveness of liquid-vapour heat exchanger is the ratio of minimum amount of heat transfer to the maximum amount of heat transfer.

$$\varepsilon = \frac{\dot{m}_r (c_p)_{\min} (T_3 - T_{3a})}{\dot{m}_r (c_p)_{\min} (T_3 - T_1)} \quad (3.6)$$

Where ε is the effectiveness of LVHE and C_p is the specific heat capacity of flowing refrigerant.

The energy balance in the LVHE is given by equation (3.7)

$$\dot{m}_r (h_3 - h_{3a}) = \dot{m}_r (h_{1a} - h_1) \quad (3.7)$$

3.3.2.2 Exergy Analysis

The exergy is defined as an effective measure of the potential of substance to impact the environment or the maximum useful work which can be extracted from a system as it reversibly comes into equilibrium with its environment. The concept of exergy is derived from the second law of thermodynamics and it is the degree measure of usefulness and quality of matter in response to the environment (Bejan et al., 1996, Arora and Kaushik, 2008).

The total exergy (E) of a system is the sum of potential exergy (E_{PT}), kinetic exergy (E_{KN}), physical exergy (E_{PH}) and chemical exergy (E_{CH}) (Bejan et al., 1996).

$$E = (E_{PH}) + (E_{KN}) + (E_{PT}) + (E_{CH}) \quad (3.8)$$

However, due to minute speed changes and elevation, the kinetic and potential exergy are assumed to be insignificant. The chemical exergy is significant with the departure of the chemical composition of a system from its chemical equilibrium (Ahmadi et al., 2013; Srinivas and Deb, 1994). Therefore the physical exergy is considered in the system and the chemical exergy is supposed to be neglected as the considered refrigeration system is free from chemical reactions (i.e. combustion) or mixture of chemical substances.

For the refrigerant flowing in a refrigerating system, the exergy is defined as follows (Bejan et al., 1996):

$$\dot{E} = \dot{m}_r [(h - h_0) - T_0 (s - s_0)] \quad (3.9)$$

Where s_0 and h_0 are the entropy and enthalpy values of the refrigerant at dead state (pressure P_0 and temperature T_0).

Exergy destruction (\dot{E}_D) or internal exergy destruction losses which are caused by irreversibilities of the system is the algebraic sum of total exergy at the inlet and outlet of the system. General exergy balance is given by (Dincer and Kanoglu 2010):

$$\dot{E}_D = \dot{E}_{in} - \dot{E}_{out} \quad (3.10)$$

Where \dot{E}_D is the rate of exergy destruction, \dot{E}_{in} and \dot{E}_{out} are the total exergy input and out by heat, work and mass respectively.

The steady flow process is occurring in a control volume, the exergy balance for the system is given by (Bejan et al., 1996):

$$\dot{E}_D = \left[\sum \dot{Q} \left(1 - \frac{T_0}{T_b} \right)_{in} - \sum \dot{Q} \left(1 - \frac{T_0}{T_b} \right)_{out} \right] \pm \dot{W} + [\sum (me_x)_{in} - \sum (me_x)_{out}] \quad (3.11)$$

Where \dot{E}_D is the rate of exergy destruction. The first bracket on the right side of Equation (3.11) is equal to the maximum reverseible work obtained from heat transfer \dot{Q} by the Carnot engine operating between T_b and T_0 . Where T_0 is the dead state temperature which is the exergy transfer from the source maintaing constant boundary temperature T_b associated with the transfer of energy by heat \dot{Q} . The second bracket represents the exergy transfer rates at control volume inlets and outlets and the \dot{W} represents the time rate of exergy transfer by work other than the flow work (mechanical work) to or from the control volume.

3.3.2.2.1 Exergy Destruction (\dot{E}_D) in the Components of LVHE Incorporated Simple VCR System

The exergy destruction and exergy efficiency in each component of the LVHE VCR system is given by the following equations:

EVAPORATOR

$$(\dot{E}_D)_{evp} = \dot{E}_{X_{4a}} + \dot{Q}_e \left(1 - \frac{T_0}{T_b} \right) - \dot{E}_{X_1} = \dot{m}_r(h_{4a} - T_0 s_{4a}) + \dot{Q}_e \left(1 - \frac{T_0}{T_b} \right) - \dot{m}_r(h_1 - T_0 s_1) \quad (3.12)$$

$$\eta_{ex, evp} = 1 - \frac{(\dot{E}_D)_{evp}}{\dot{E}_{X_{4a}}} \quad (3.13)$$

COMPRESSOR

$$(\dot{E}_D)_{comp} = \dot{E}_{X_{1a}} + \dot{W}_{comp} - \dot{E}_{X_{2a}} = \dot{m}_r(h_{1a} - T_0 s_{1a}) + \dot{W}_{comp} - \dot{m}_r(h_{2a} - T_0 s_{2a}) \quad (3.14)$$

$$\eta_{ex, comp} = 1 - \frac{(\dot{E}_D)_{comp}}{\dot{W}_{comp}} \quad (3.15)$$

CONDENSER

$$(\dot{E}_D)_{\text{cond}} = \dot{E}_{X_{2a}} - \dot{E}_{X_3} = \dot{m}_r(h_{2a} - T_0 s_{2a}) - \dot{m}_r(h_3 - T_0 s_3) \quad (3.16)$$

$$\eta_{\text{ex,cond}} = 1 - \frac{(\dot{E}_D)_{\text{cond}}}{\dot{E}_{X_{2a}} - \dot{E}_{X_3}} \quad (3.17)$$

THROTTLE VALVE

$$(\dot{E}_D)_{\text{thv}} = \dot{E}_{X_{3a}} - \dot{E}_{X_{4a}} = \dot{m}_r(h_{3a} - T_0 s_{3a}) - \dot{m}_r(h_{4a} - T_0 s_{4a}) = \dot{m}_r T_0 (s_{4a} - s_{3a}) \quad (3.18)$$

$$\eta_{\text{ex,thv}} = \frac{\dot{E}_{X_{4a}}}{\dot{E}_{X_{3a}}} \quad (3.19)$$

LIQUID VAPOUR HEAT EXCHANGER (LVHE)

$$\begin{aligned} (\dot{E}_D)_{\text{LVHE}} &= (\dot{E}_{X_1} - \dot{E}_{X_{1a}}) + (\dot{E}_{X_3} - \dot{E}_{X_{3a}}) \\ &= \dot{m}_r(h_1 - h_{1a} + h_3 - h_{3a}) - \dot{m}_r T_0 (s_1 - s_{1a} + s_3 - s_{3a}) \end{aligned} \quad (3.20)$$

$$\eta_{\text{ex,LVHE}} = 1 - \frac{(\dot{E}_D)_{\text{LVHE}}}{(\dot{E}_{X_1} + \dot{E}_{X_3}) - (\dot{E}_{X_{3a}} + \dot{E}_{X_{1a}})} \quad (3.21)$$

3.3.2.2.2 Total Exergy Destruction Rate

Total exergy destruction rate of the system is the sum of destruction of exergy in each component of the system.

The total exergy destruction rate in LVHE incorporated VCR system is given by:

$$\Sigma(\dot{E}_D) = (\dot{E}_D)_{\text{evp}} + (\dot{E}_D)_{\text{comp}} + (\dot{E}_D)_{\text{cond}} + (\dot{E}_D)_{\text{thv}} + (\dot{E}_D)_{\text{LVHE}} \quad (3.22)$$

3.3.2.2.3 Exergetic Efficiency

Exergetic efficiency is an important parameter for evaluating thermodynamic performance of a system or a system component. In general exergetic efficiency is defined as (Dincer and Kanoglu, 2010):

$$\eta_{\text{ex}} = \frac{\Sigma \dot{E}_{\text{out}}}{\Sigma \dot{E}_{\text{in}}} = 1 - \frac{\Sigma \dot{E}_D}{\Sigma \dot{E}_{\text{in}}} \quad (3.23)$$

Where η_{ex} is the exergetic efficiency of the cycle. $\Sigma \dot{E}_{\text{out}}$, $\Sigma \dot{E}_{\text{in}}$ and $\Sigma \dot{E}_D$ are the total exergy recovered, supplied and destructed respectively.

The exergetic efficiency is the ratio of exergy in products to the exergy of fuel. The exergetic efficiency of VCR system is defined as the ratio of the exergy of

evaporator heat absorbed at temperature T_b from the space to be cooled to the actual compressor work input (\dot{W}_{comp}) (Arora and Kaushik, 2008).

$$\eta_{ex} = \frac{|\dot{Q}_e \left(1 - \frac{T_0}{T_b}\right)|}{\dot{W}_{comp}} \quad (3.24)$$

$$\eta_{ex} = COP \times \left| \left(1 - \frac{T_0}{T_b}\right) \right| \quad (3.25)$$

where T_0 is the ambient or dead state temperature

3.3.2.2.4 Exergy Destruction Ratio (EDR)

The exergy destruction ratio (EDR) is the ratio of total destruction of exergy of the system to the exergy of the products (Arora and Kaushik, 2008) which is represented by Eq. (3.26).

The exergy balance in the evaporator of LVHE incorporated VCR system has been depicted in Fig. 3.4. \dot{E}_{X4a} is the exergy entering in to the evaporator and \dot{E}_{X1} is the exergy leaving from the evaporator.

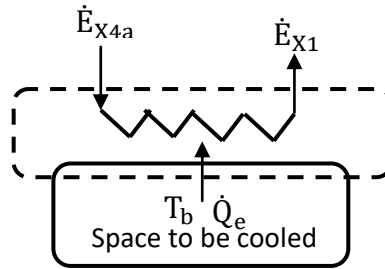


Fig. 3.4 Exergy balance in evaporator and the space to be cooled (Kotas, 1995)

$$EDR = \frac{\dot{E}_{D,total}}{\dot{E}_p} = \frac{1}{\eta_{ex}} - 1 \quad (3.26)$$

The exergy destruction ratio is the rate of exergy destruction in a system component ($\dot{E}_{D,i}$) to the exergy rate of the fuel provided to the overall system ($\dot{E}_{E,tot}$) or the total exergy destruction rate within the system ($\dot{E}_{D,total}$) (Bejan et al., 1996).

$$EDR = \frac{\dot{E}_{D,i}}{\dot{E}_{E,tot}} = \frac{\dot{E}_{D,i}}{\dot{E}_{D,total}} \quad (3.27)$$

The exergy destruction ratio in each component of the liquid vapour heat exchanger (LVHE) vapour compression cycle is given by the following equations:

EVAPORATOR

$$\text{EDR}_{\text{evp}} = \frac{(\dot{E}_D)_{\text{evp}}}{\dot{E}_{D,\text{total}}} \quad (3.28)$$

COMPRESSOR

$$\text{EDR}_{\text{comp}} = \frac{(\dot{E}_D)_{\text{comp}}}{\dot{E}_{D,\text{total}}} \quad (3.29)$$

CONDENSER

$$\text{EDR}_{\text{cond}} = \frac{(\dot{E}_D)_{\text{cond}}}{\dot{E}_{D,\text{total}}} \quad (3.30)$$

THROTTLE VALVE

$$\text{EDR}_{\text{thv}} = \frac{(\dot{E}_D)_{\text{thv}}}{\dot{E}_{D,\text{total}}} \quad (3.31)$$

LIQUID VAPOUR HEAT EXCHANGER (LVHE)

$$\text{EDR}_{\text{thv}} = \frac{(\dot{E}_D)_{\text{LVHE}}}{\dot{E}_{D,\text{total}}} \quad (3.32)$$

3.4 RESULT AND DISCUSSION

An EES (Klein and Alvarado, 2012) software based program has been compiled for the model described in section 3 above, to analyse LVHE incorporated to simple VCR system using R134a, R1234yf and R1234ze considering the principles of thermodynamics. The property codes for various properties are inbuilt in function directory of the EES and are called for computation of various properties such as specific enthalpy, specific entropy, specific volume, pressures and temperatures etc. The results from the present analysis have been compared with the results of Arora and Kaushik (2008). It is observed that the difference in the value of COP and exergy efficiency is within a range of $\pm 1\%$. The difference in results may be due to the pressure drop in evaporator and condenser is assumed to be zero.

3.4.1 Results of Energy, Exergy and Parameteric Analysis

The performance LVHE associated vapour compression refrigeration cycle depends on various operating variables. The selection of operating variables plays

significant role in the exergy and energy performance analysis of LVHE associated VCR system. The effect of significant operating variables viz. degree of subcooling, evaporator temperature, effectiveness of LVHE and isentropic efficiency of compressor on performance parameters viz. compressor work, COP, exergy efficiency, total exergy destruction of the system and EDR has been evaluated. The exergy efficiency, EDR and exergy destruction in each component of system are also examined. The energy and exergy analysis is followed by parametric analysis of LVHE incorporated VCR system for refrigerants considered.

3.4.1.1 EFFECT OF SUBCOOLING

The effect of degree of subcooling ($(\Delta T)_{SC}$) on degree of superheating ($(\Delta T)_{SH}$), compressor work, COP and exergetic efficiency is shown in Figs 3.5 to 3.7.

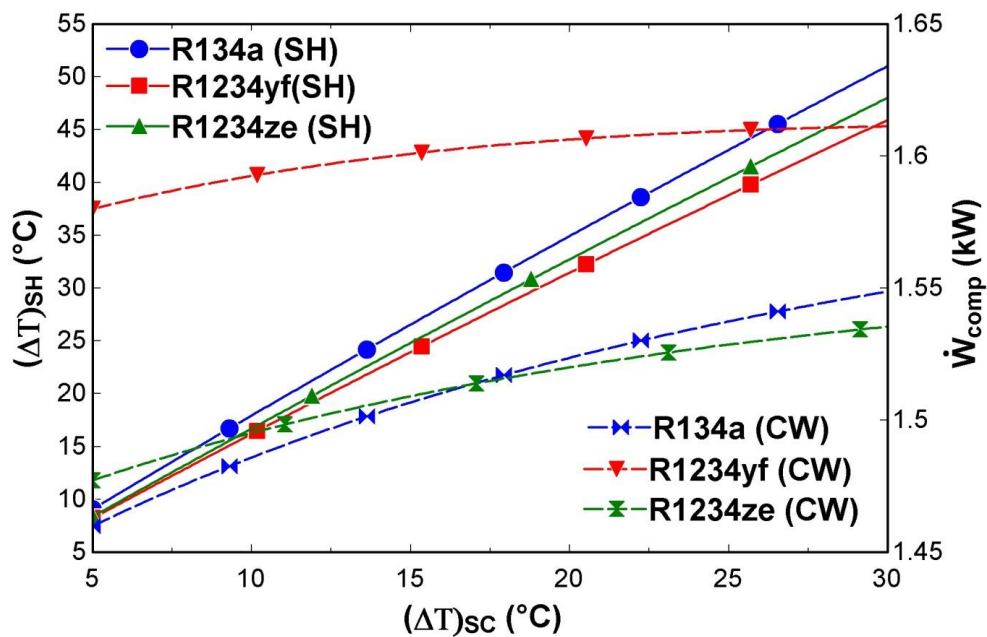


Fig. 3.5 Variation in degree of superheating $(\Delta T)_{SH}$ and compressor work (\dot{W}_{comp}) with degree of subcooling $(\Delta T)_{SC}$ ($T_e = -10^0C$)

CW: Net compressor work in kW, SH: Superheating

Fig. 3.5 presents the effect of mechanical subcooling on superheating and compressor work. The degree of superheating increases for considered refrigerants with the increase in degree of subcooling due to exchange of heat in the LVHE. Thus the compressor work also increases with the increase in degree of superheating. Since the specific heat of liquid refrigerant is higher than the vapour, refer to equation (3.6), the

degree of superheating $(\Delta T)_{SH}$ is more than the degree of subcooling $(\Delta T)_{SC}$. It is observed that for R134a, the superheating achieved in LVHE is higher compared to other refrigerants. Since the ratio of specific heat of liquid to specific heat of vapour is maximum in its case. The average value of C_{Pl} / C_{Pv} for R134a is 1.833 and the corresponding value for R1234yf and R1234ze are 1.670 and 1.739 at the temperature 50°C and -10°C (Table 1.1).

Fig. 3.6 shows the variation in COP with degree of subcooling for the refrigerants R134a, R1234yf and R1234ze. As the degree of subcooling increases, the compressor work also increases, however the rate of increase in specific refrigerating effect is observed to be more than the rate of increase of specific compressor work. Thus the COP of vapour compression cycle with LVHE for all the three refrigerants is observed to increase with increase in degree of subcooling. The COP of simple saturated VCR cycle (i.e. in absence of LVHE) is 2.464, 2.255 and 2.420 for R134a, R1234yf and R1234ze respectively.

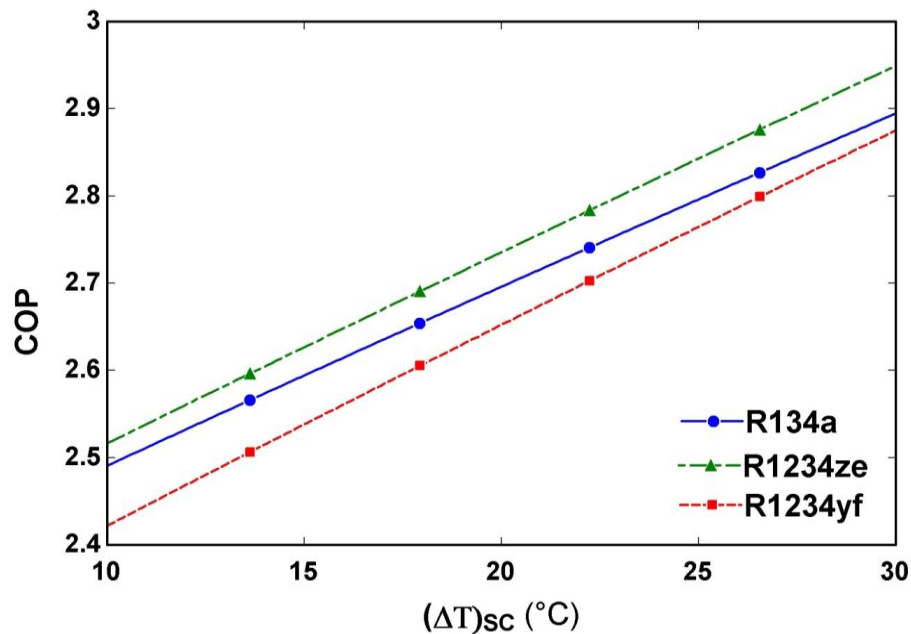


Fig. 3.6 Variation in COP with degree of subcooling $(\Delta T)_{SC}$ ($T_e = -10^{\circ}\text{C}$)

The refrigerant R1234ze outperforms the other two refrigerants with regard to COP. R134a shows better COP than the R1234yf for both the lower end and higher end values of subcooling. The difference in the COP for R134a and R1234ze is 1.04% at 10°C of subcooling while 1.87% at 30°C of subcooling. The percentage difference in COP for R134a and R1234yf are 2.73% at 10°C and 0.69% at 30°C of subcooling. The

difference for R1234ze and R1234yf are 3.77% at 10⁰C and 2.56% at 30⁰C of subcooling.

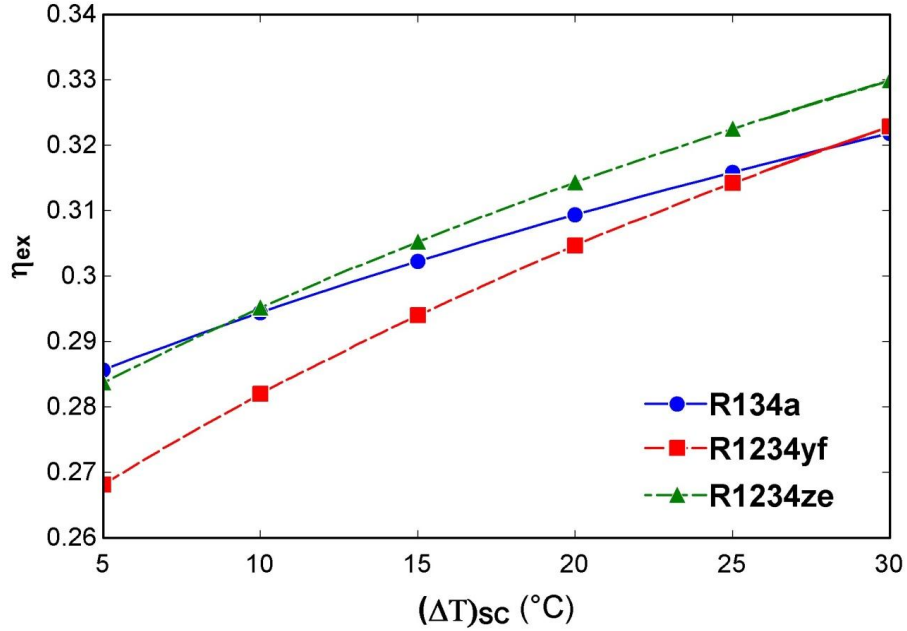


Fig. 3.7 Effect of degree of subcooling $(\Delta T)_{sc}$ in LVHE on exergetic efficiency (η_{ex}) ($T_e = -10^0C$).

The effect of subcooling on exergy efficiency is shown in Fig. 3.7 The η_{ex} is observed to increase with increase in degree of subcooling. For simple vapour compression cycle without subcooling, the exergetic efficiencies are for R134a = 0.2757, R1234yf = 0.2523 and R1234ze = 0.2707. The η_{ex} is given by the formula $\eta_{ex} = COP \times \left(1 - \frac{T_0}{T_b}\right)$. Since the COP increases with increase in degree of subcooling whereas the term $\left(1 - \frac{T_0}{T_b}\right)$ remains constant hence with increase in degree of subcooling, the value of η_{ex} increases. Refer to Fig. 3.5, with the increase in DOS, the compressor work increases, however the rate of increase in specific refrigerating effect is observed to be more than the rate of increase of compressor work. Thus the exergetic efficiency of vapour compression cycle with LVHE is observed to increase with increase in degree of subcooling for all the three refrigerants. The exergetic efficiency for R134a and R1234ze is more than the R1234yf. It is observed that the slope of curve for R134a is less than that of R1234yf and R1234ze. The percentage difference in exergetic efficiency for R1234ze and R134a are 0.82% at 10⁰C and 1.88% at 30⁰C of subcooling. The difference for R1234yf and R134a are 3.53% at 10⁰C and 0.68% at

30⁰C of subcooling. Similarly the difference for R1234ze and R1234yf are 4.38% at 10⁰C and 2.58% at 30⁰C.

3.4.1.2 EFFECT OF TEMPERATURE OF EVAPORATOR (T_e)

The effect of temperature of evaporator (T_e) on various performance parameters viz. DOS, compressor work (\dot{W}_{comp}), COP and exergy efficiency (η_{ex}) of mechanically subcooled LVHE incorporated VCR system is shown in Fig.s 3.8 to 3.11.

The variation in degree of subcooling with temperature of evaporator is depicted in Fig. 3.8. As the evaporator temperature increases, the degree of subcooling is observed to decrease.

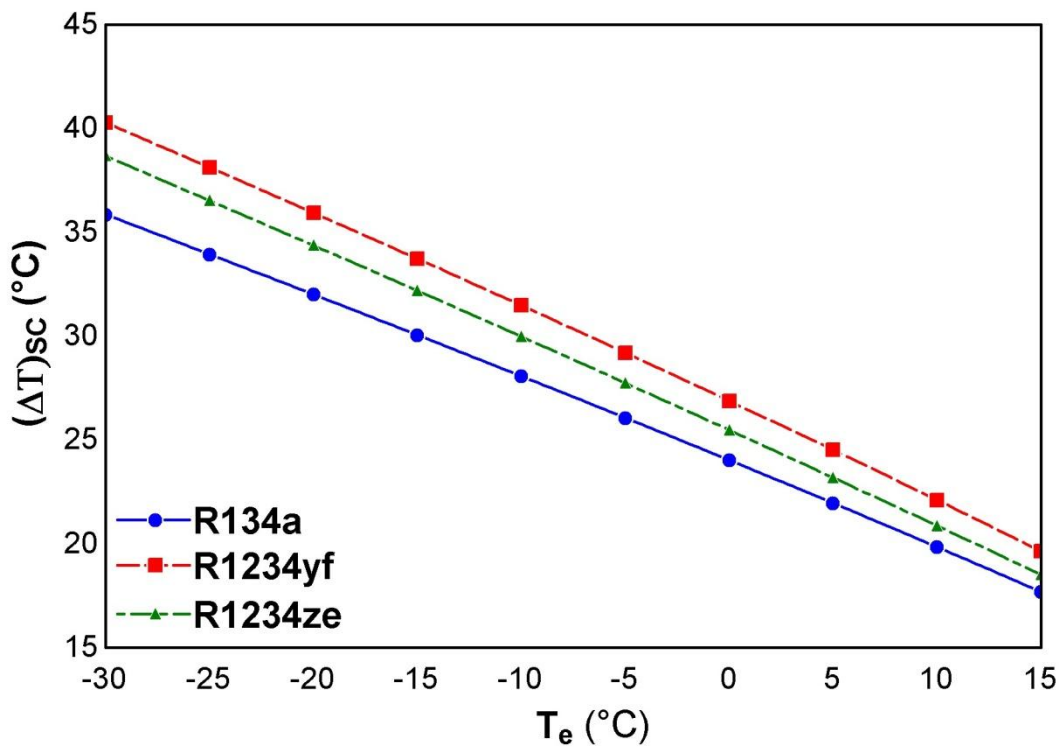


Fig. 3.8 Variation in degree of subcooling $(\Delta T)_{sc}$ evaporator temperature (T_e)

At higher evaporator temperature the rate of heat transfer from high refrigerant to low temperature refrigerant decreases and hence degree of subcooling decreases. The observed value of degree of subcooling is minimum for R134a and maximum for R1234yf.

The effect of evaporator temperature on compressor work is shown in Fig. 3.9. As the evaporator temperature increases, the compressor work is observed to decrease. The pressure ratio between evaporator and compressor and degree of subcooling

decrease with increase in evaporator temperature (Refer Fig. 3.8) consequently decrease in degree of superheating. Hence the compressor work decreases.

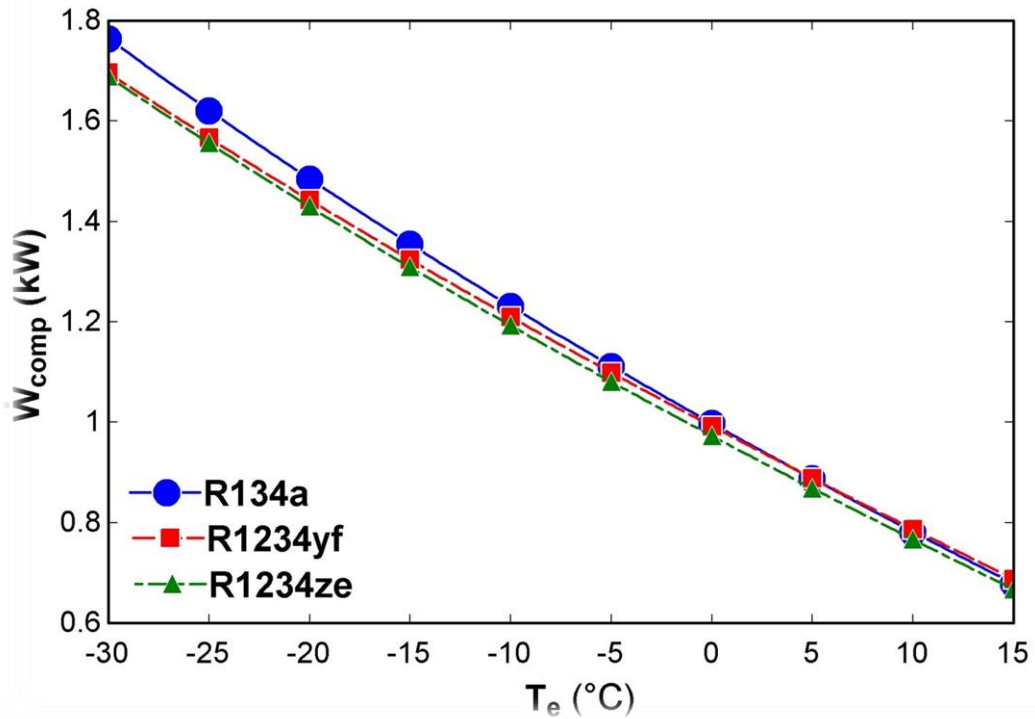


Fig. 3.9 Temperature of evaporator Vs. (T_e) on compressor work (\dot{W}_{comp})

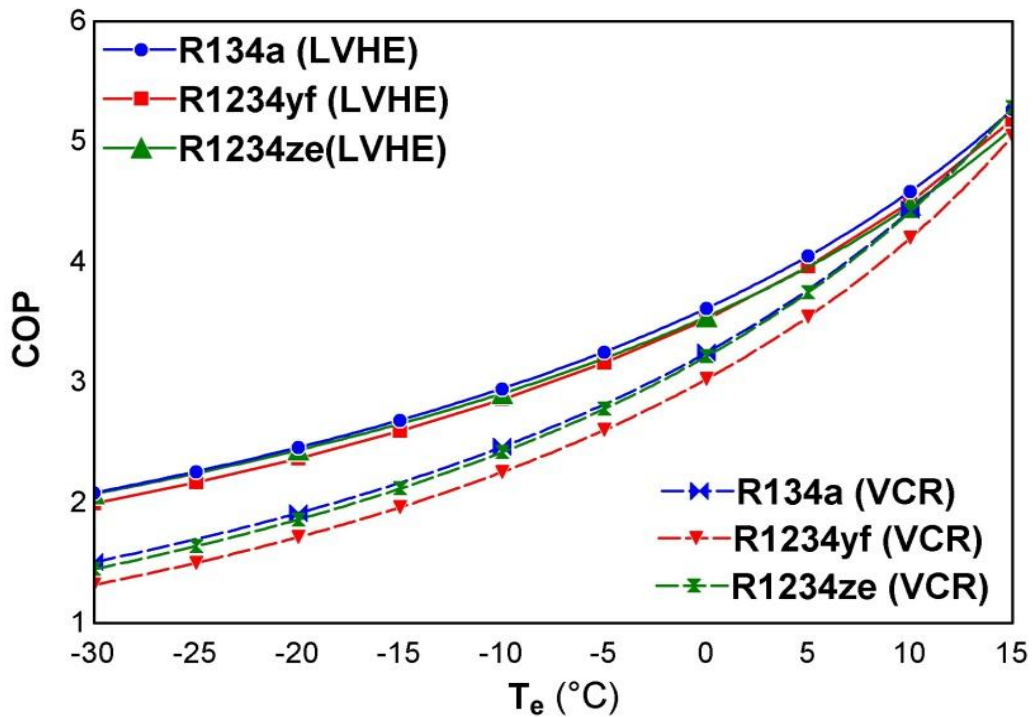


Fig. 3.10 COP Vs. evaporator temperature (T_e) of VCR cycle with and without LVHE

It is observed that the compressor work is least for R1234ze.

The variation in COP with temperature of evaporator is shown in Fig. 3.10. The COP of VCR cycle with or without LVHE increases with increase in temperature of evaporator. With the increase in temperature of evaporator, the compressor work decreases (refer Fig. 3.9) and the specific refrigerating effect increases. Thus the COP of the cycle increases. It has been found that the COP of LVHE incorporated VCR system is higher than that of simple VCR cycle without LVHE for the considered refrigerants. At lower evaporator temperature (between -30°C to 0°C), the VCR cycle with LVHE performs better for the refrigerants considered.

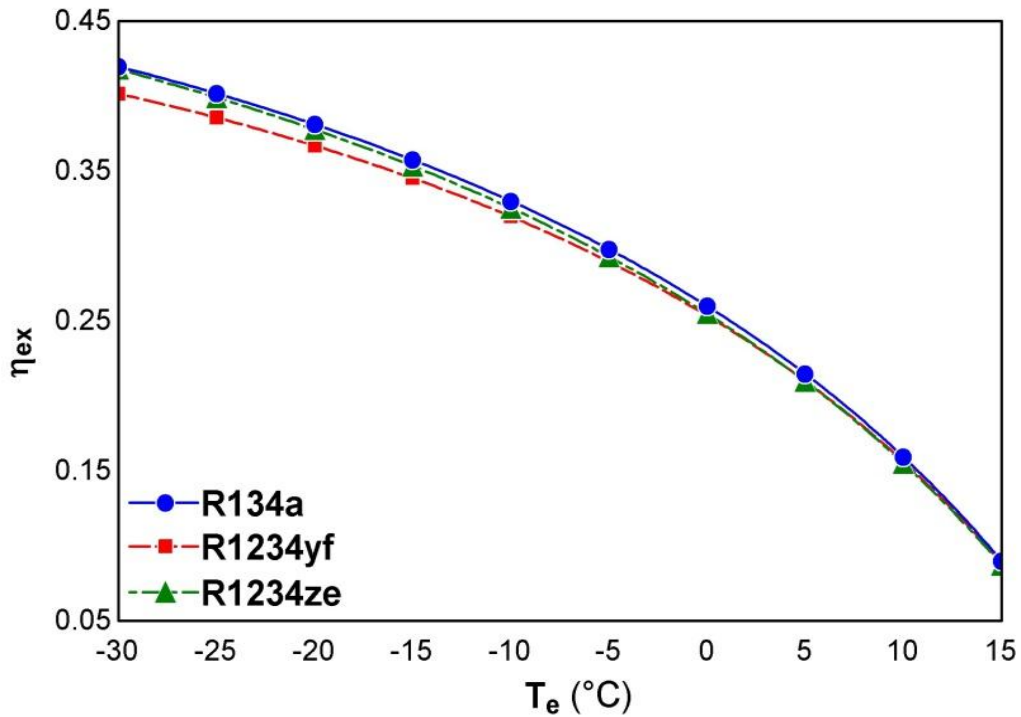


Fig. 3.11 Exergetic efficiency (η_{ex}) Vs. temperature of evaporator (T_e)

The variation in exergy efficiency with temperature of evaporator is shown in Fig. 3.11. With increase in temperature of evaporator, exergy efficiency decreases. Exergy efficiency is given by formula $\eta_{ex} = \text{COP} \times \left| \left(1 - \frac{T_0}{T_b} \right) \right|$, the term COP increases (Refer Fig. 3.10) on the other hand, the term $\left| \left(1 - \frac{T_0}{T_b} \right) \right|$ decreases with increase in temperature of evaporator (i.e. $(T_b - T_e) = 5^{\circ}\text{C}$). Thus the result of two is that the exergetic efficiency decreases. It has been seen that the exergetic efficiency is least for R134a and highest for R1234ze.

3.4.1.3 EFFECT OF LIQUID VAPOUR HEAT EXCHANGER EFFECTIVENESS

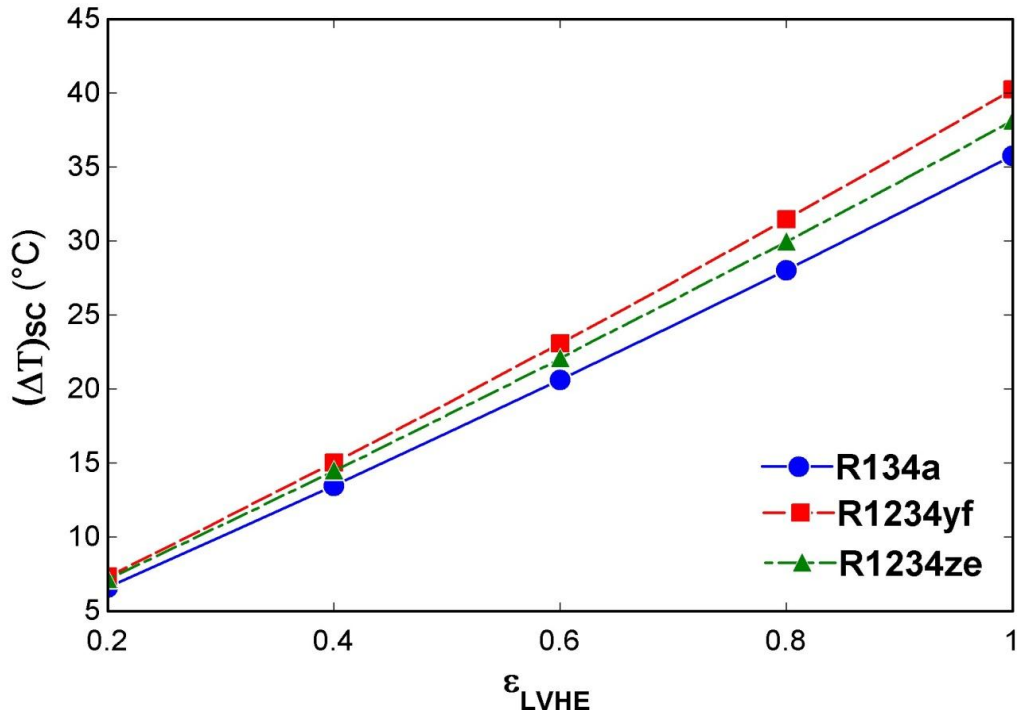


Fig. 3.12 Degree of subcooling ($\Delta T)_{sc}$ Vs. Effectiveness of LVHE (ϵ_{LVHE}) ($T_e = -10^0C$)

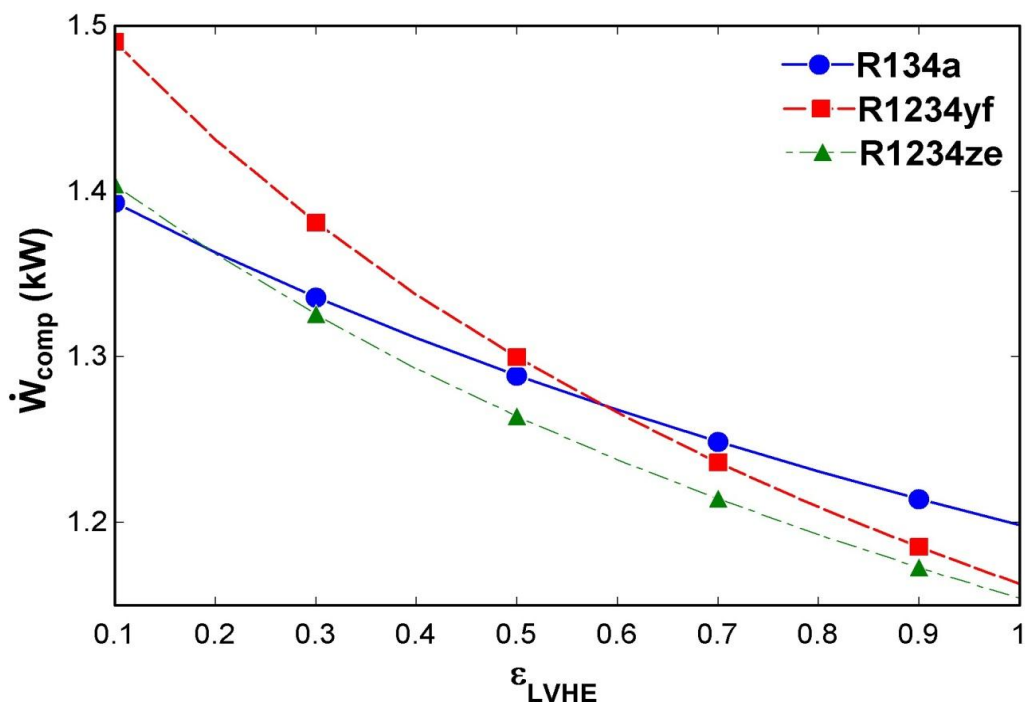


Fig. 3.13 Compressor work (\dot{W}_{comp}) Vs. Effectiveness of LVHE (ϵ_{LVHE}) ($T_e = -10^0C$)

The variation in effectiveness of LVHE on various performance parameters viz. DOS, compressor work (\dot{W}_{comp}), COP and exergy efficiency (η_{ex}) of mechanically subcooled LVHE incorporated VCR system is shown in Figs. 3.12 to 3.15.

Fig. 3.12 shows the effect of effectiveness of LVHE on degree of subcooling. As the effectiveness of LVHE increases, the degree of subcooling of the LVHE incorporated VCR system increases due to increasing rate of heat extraction from the liquid refrigerant. It has been observed that R1234yf registers more increase in degree of subcooling in comparison to R134a and R1234ze.

Fig. 3.13 shows variation in compressor work with LVHE effectiveness. The compressor work decreases with increase in LVHE effectiveness. For the considered operating conditions with increase in effectiveness of LVHE, the mass flow rate of the refrigerant decreases and hence the compressor work also decreases. It has been perceived that the compressor work decreases more for refrigerant R1234yf than the other two refrigerants. For R134a the decrease in compressor work is least.

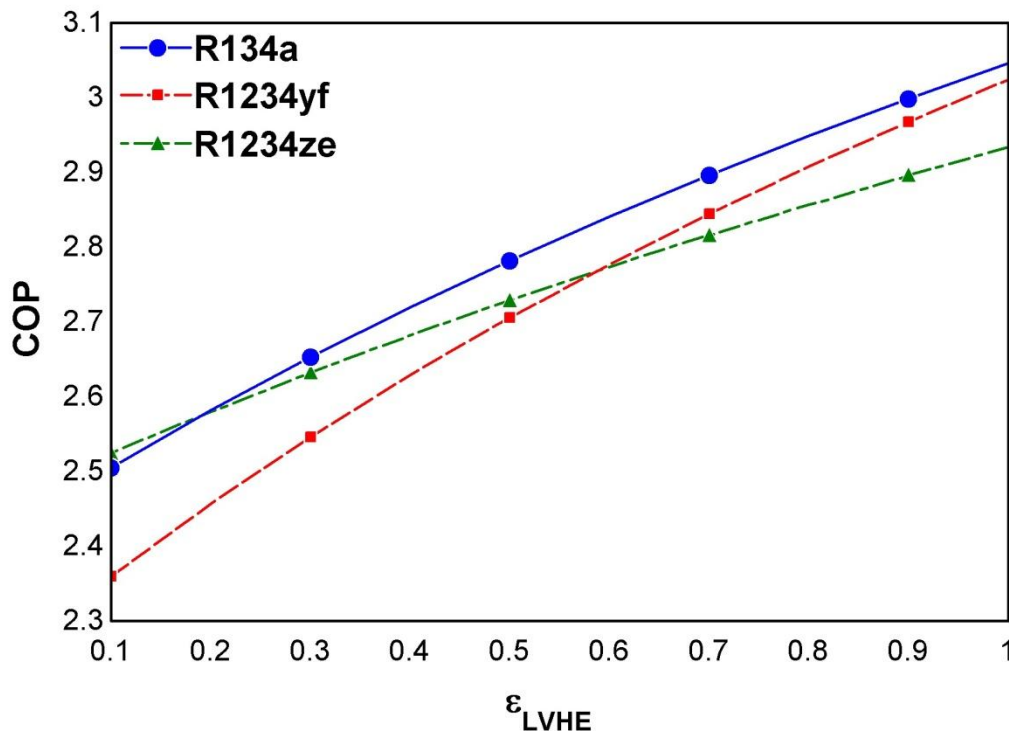


Fig. 3.14 Coefficient of performance (COP) Vs. effectiveness of LVHE (ϵ_{LVHE}) ($T_c = -10^{\circ}\text{C}$)

Fig.3.14 shows the variation in COP with effectiveness of LVHE. The COP of the cycle increases with increase in values of LVHE effectiveness. Fig. 3.12 and 3.13

show that the degree of subcooling increases and refrigerating effect increases while the compressor work decreases with increase in values of LVHE effectiveness. Hence the COP of LVHE incorporated VCR system increases. It has been seen that the rate of increase in COP of the cycle for refrigerant R1234yf is more than the other two refrigerants. The increase in COP is least for R1234ze.

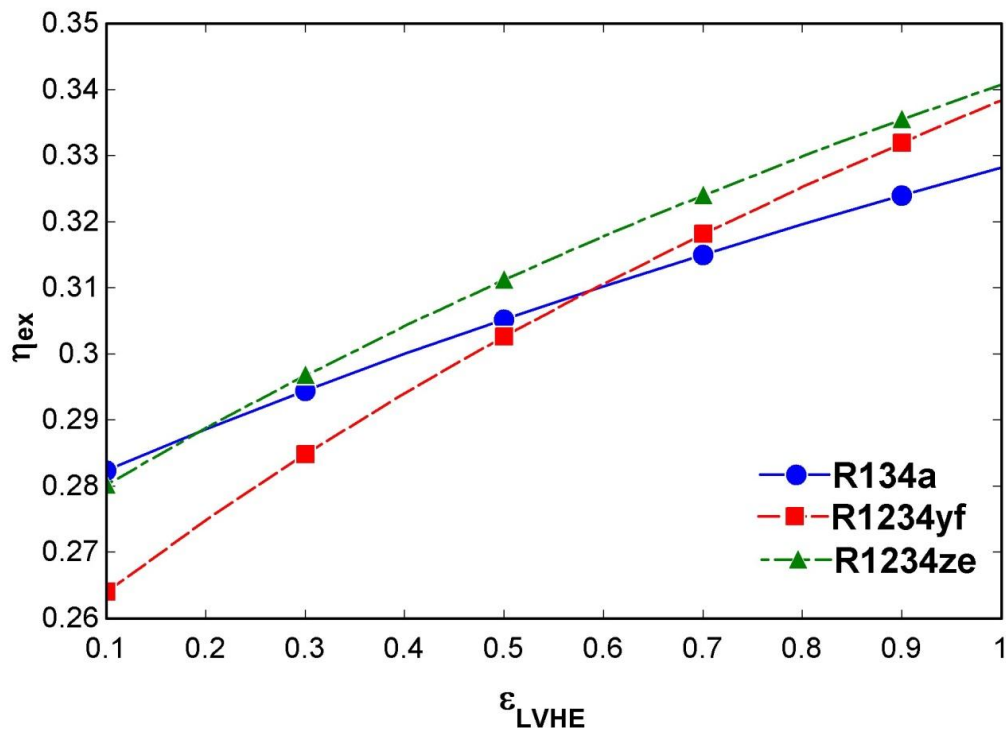


Fig. 3.15 Exergetic efficiency (η_{ex}) Vs. LVHE effectiveness (ϵ_{LVHE}) for ($T_e = -10^0C$)

Fig. 3.15 shows the variation in exergetic efficiency with LVHE effectiveness. The exergetic efficiency of the cycle increases with increase in effectiveness of LVHE. Due to increase in refrigeration effect and decrease in compressor work with increase in LVHE effectiveness (Fig. 3.13 and 3.15), the exergetic efficiency increases. It has been noticed that the increase in exergetic efficiency is maximum for R1234yf and is minimum for refrigerant R134a.

3.4.1.4 EFFECT OF COMPRESSOR EFFICIENCY

The variation of compressor efficiency on different performance parameter viz. compressor work (\dot{W}_{comp}), COP and exergy efficiency (η_{ex}) is shown in Figs. 3.16 and 3.17.

Fig. 3.16 shows the variation in COP and compressor work with isentropic efficiency of compressor of LVHE incorporated VCR system. It has been noticed that

the COP of the system increases with increase in compressor isentropic efficiency for the refrigerants considered. The reason for increase in COP of the cycle is reduction in compressor work with increase in isentropic η of compressor. It has been perceived that the increment in the COP is maximum for refrigerant R1234yf and minimum for R134a while the decrease in compressor work is maximum for R1234yf and minimum for R134a.

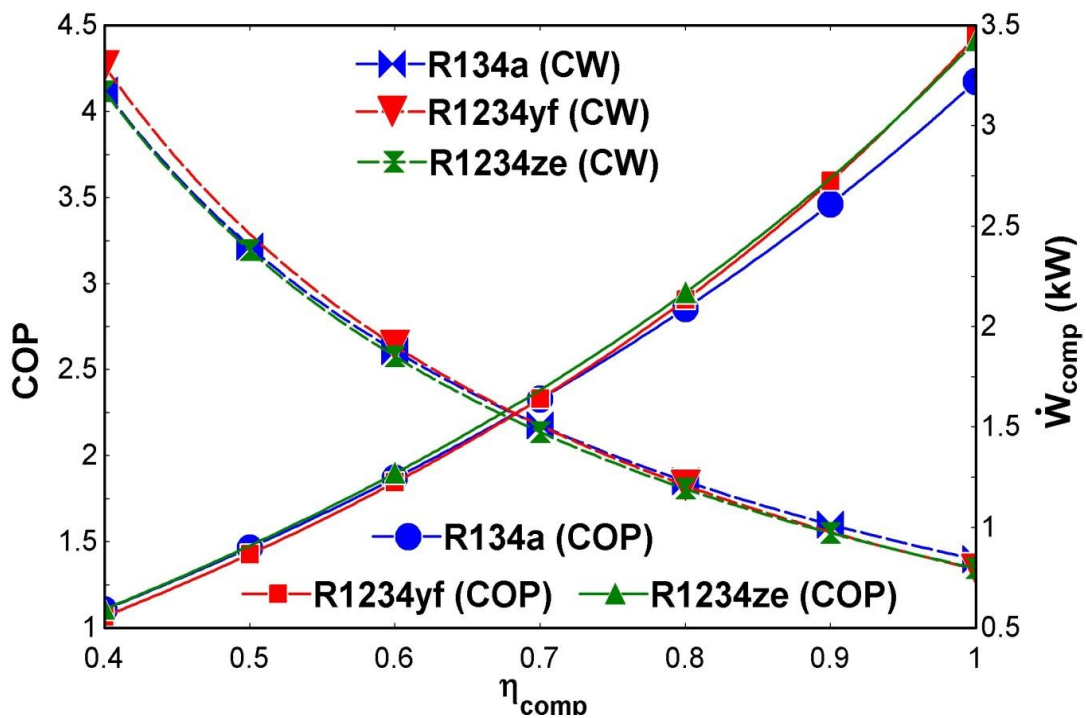


Fig. 3.16 Coefficient of performance (COP) & compressor work (\dot{W}_{comp}) Vs. isentropic compressor efficiency (η_{comp}) ($T_e = -10^0C$)

Fig. 3.17 shows the effect of compressor efficiency (isentropic) on the exergy efficiency LVHE incorporated VCR system. The exergy efficiency of the system increases with increase in compressor isentropic efficiency for the considered refrigerants. As the compressor work decreases (Fig. 3.16) with increase in compressor isentropic efficiency, the exergetic efficiency of the LVHE incorporated VCR system increases with increase in compressor efficiency. It has been seen that the increment in the exergetic efficiency is maximum for refrigerant R1234ze and minimum for refrigerant R134a.

Thus, the COP and exergy efficiency of LVHE incorporated VCR system enhance with increase in DOS, LVHE effectiveness and compressor efficiency.

However, the COP of the system increases and exergy efficiency decreases with increase in temperature of evaporator. It is also noticed that the thermodynamic performance of R1234ze is better than that of R1234yf.

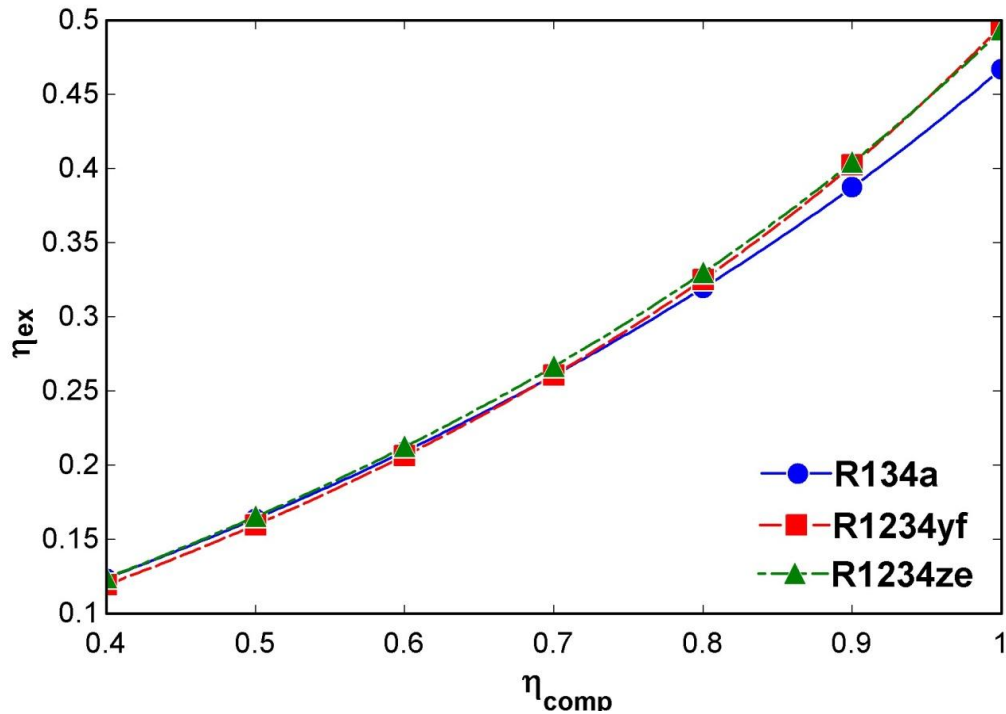


Fig. 3.17 Exergetic efficiency (η_{ex}) Vs. isentropic compressor efficiency (η_{comp}) ($T_e = -10^{\circ}\text{C}$)

3.4.1.5 EFFECT OF SUBCOOLING, EVAPORATOR TEMPERATURE, EFFECTIVENESS OF LVHE AND COMPRESSOR EFFICIENCY ON TOTAL EXERGY DESTRUCTION AND EXERGY DESTRUCTION RATIO (EDR)

The effect of subcooling (ΔT_{SC}), evaporator temperature (T_e), effectiveness of LVHE (ϵ_{LVHE}) and compressor isentropic efficiency (η_{comp}) on performance parameters viz. total exergy destruction and EDR is shown in Fig. 3.18 (a) to (d).

The value of total exergy destruction and EDR decreases with increase in degree of subcooling (ΔT_{SC}), effectiveness of LVHE (ϵ_{LVHE}) and isentropic efficiency (η_{comp}) of compressor. However, the value of total exergy destruction decreases and EDR increases with increase in temperature of evaporator. Figs. 3.7, 3.15 and 3.17, predict that the exergetic efficiency increases with increase in degree of subcooling, effectiveness of LVHE and isentropic efficiency of compressor. As the rate of exergy

extracted from the system increases, consequently, the value of the total exergy destruction and EDR decreases.

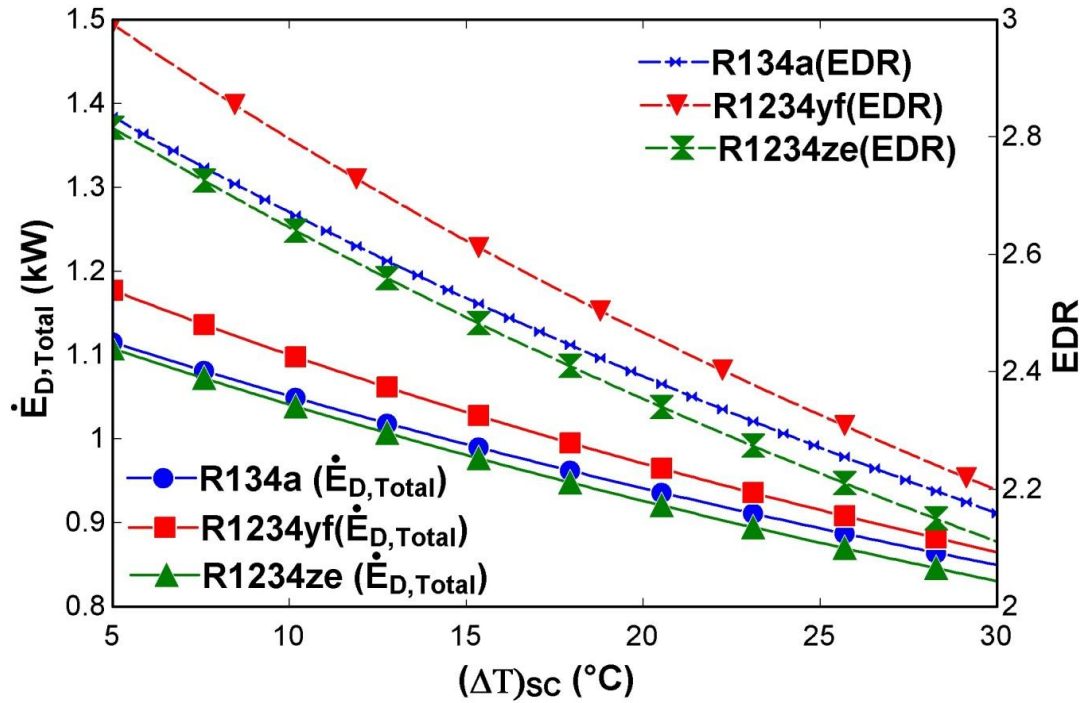


Fig. 3.18 (a) The total exergy destruction and EDR Vs. degree of subcooling $(\Delta T)_{sc}$

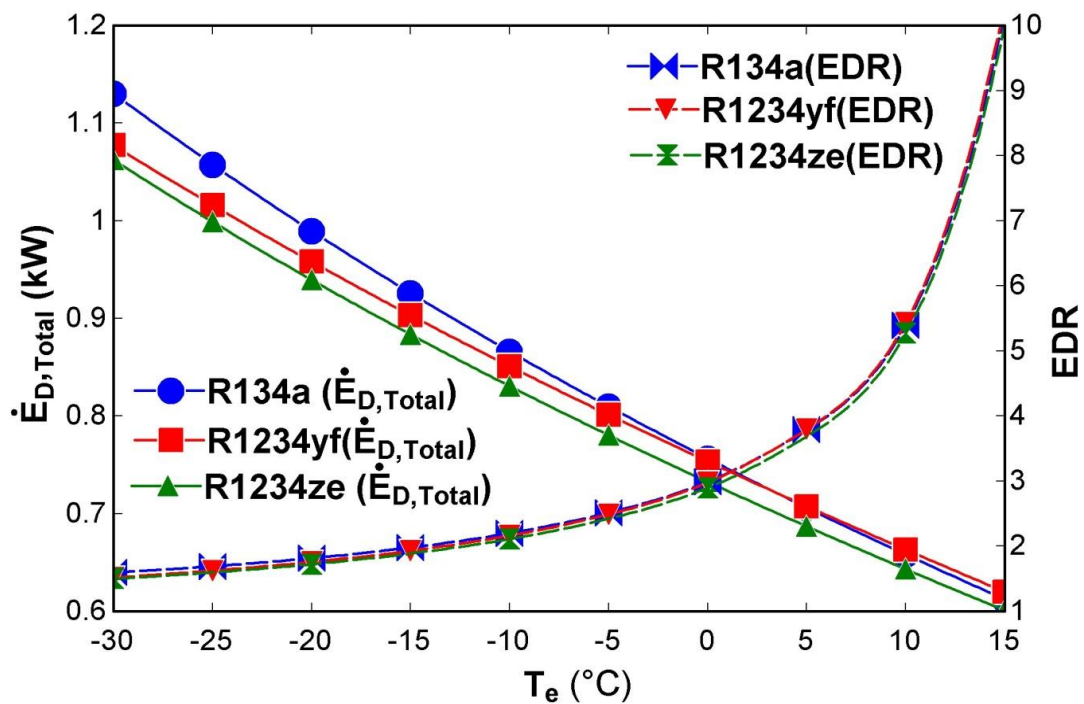


Fig. 3.18 (b) Total exergy destruction and EDR Vs. evaporator temperature (T_e)

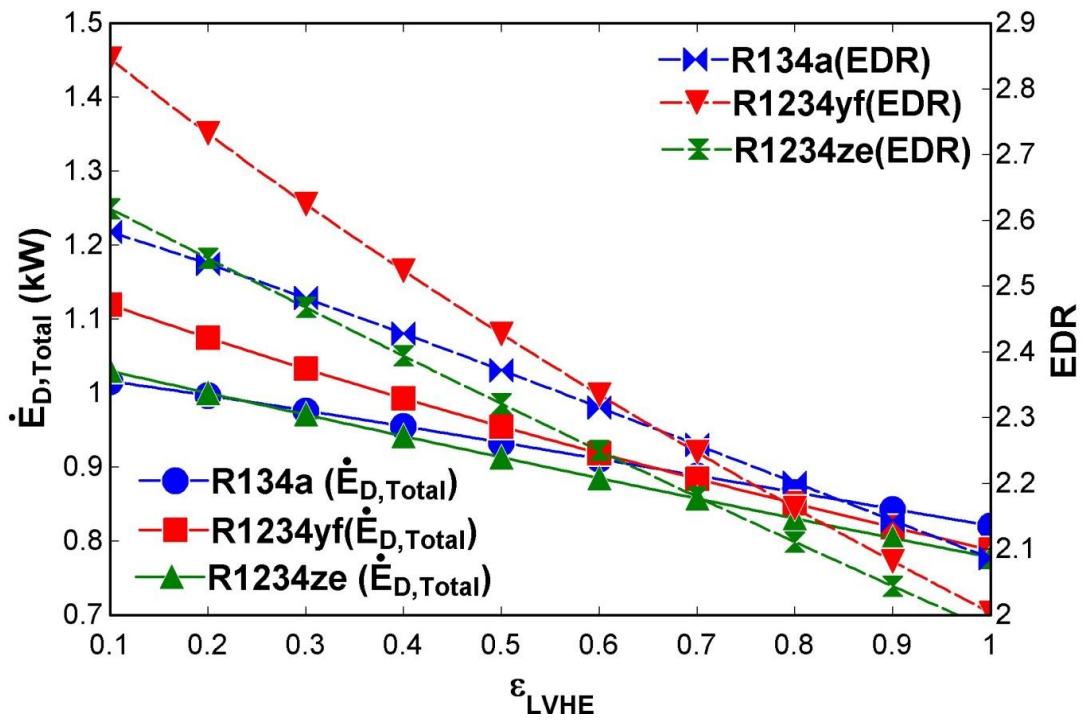


Fig. 3.18 (c) Total exergy destruction and EDR Vs. effectiveness of LVHE (ϵ_{LVHE})

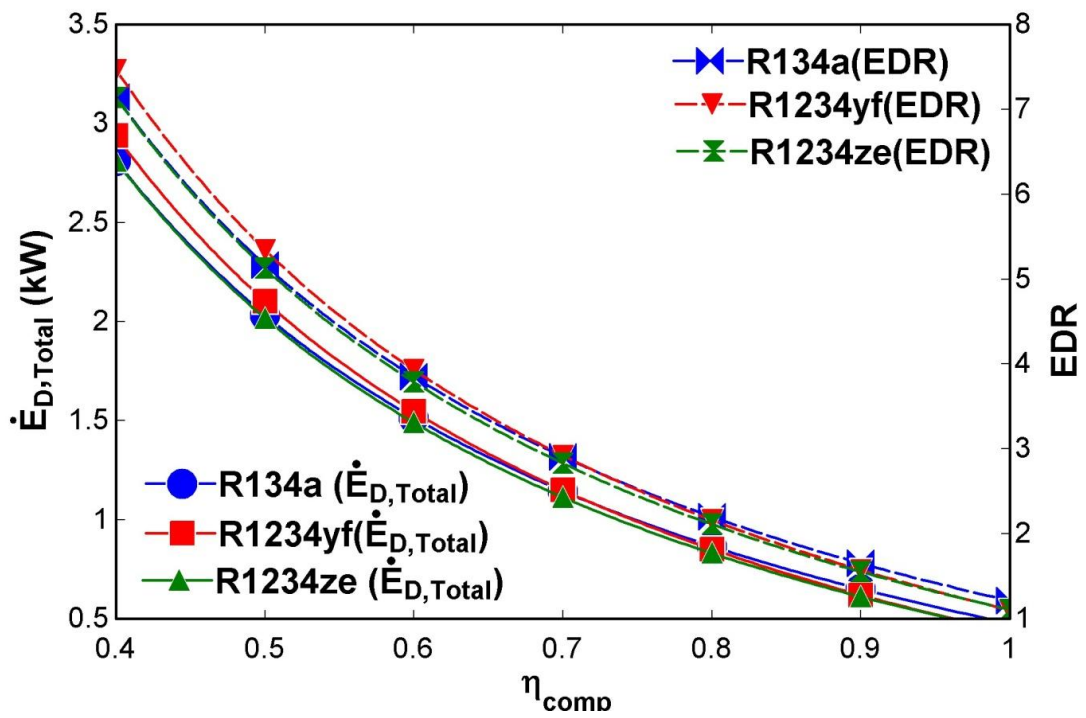


Fig. 3.18 (d) Total exergy destruction and EDR Vs. isentropic efficiency of compressor (η_{comp})

The EDR is given by the relation $EDR = \frac{\dot{E}_{D,total}}{\dot{E}_P} = \frac{1}{\eta_{ex}} - 1$ in which, the value of $\dot{E}_{D,total}$ decreases and the exergy in product (\dot{E}_P) also decreases with increase in temperature of evaporator. Hence, the value of EDR increases with increase in temperature of evaporator.

It has also been noticed that the value of total exergy destruction and EDR is minimum for R1234ze and maximum for R1234yf with increase in DOS, LVHE effectiveness and compressor isentropic efficiency. However, the value of total exergy destruction is minimum for R1234ze and maximum for R134a and the value of EDR is minimum for R1234ze and maximum for R1234yf with increase in evaporator temperature.

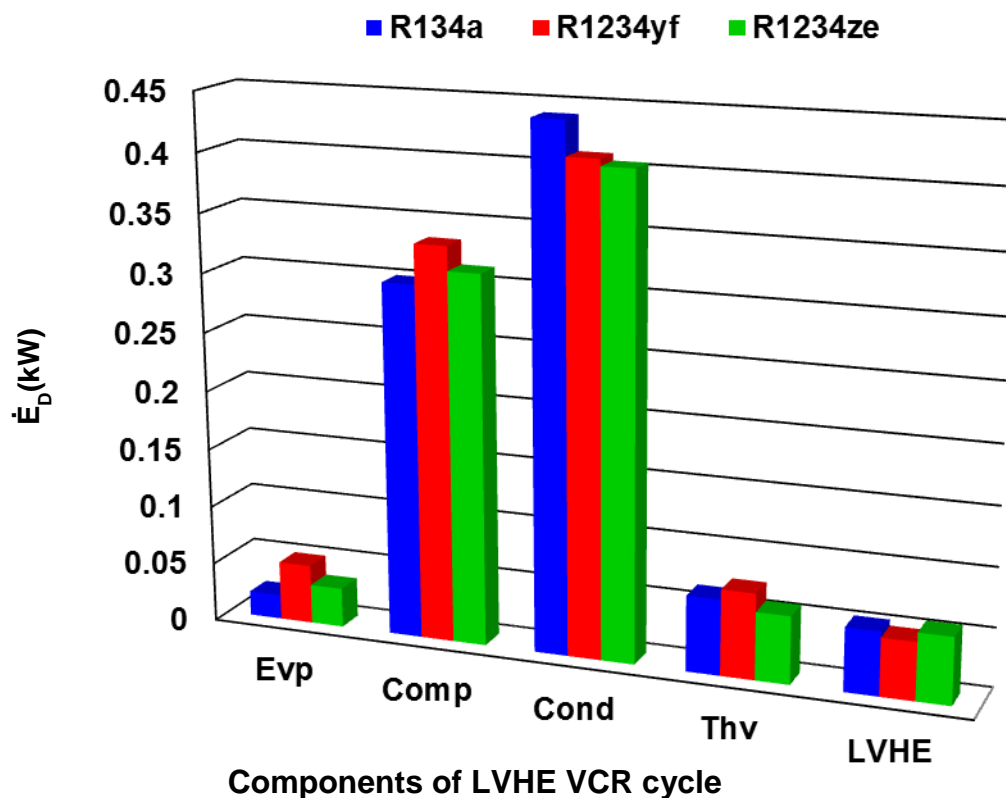


Fig. 3.19 (a) Exergy destruction (\dot{E}_D) in different components of LVHE incorporated VCR system ($T_e = -10^\circ\text{C}$)

The variation in exergy destruction, % EDR and % exergetic efficiency (η_{ex}) in different components of LVHE incorporated VCR system is illustrated in Figs. 3.19 (a)-(c) for the considered refrigerants. The value of \dot{E}_D and % EDR are highest in condenser and lowest in evaporator as compared to other system components viz. compressor, throttle valve and LVHE. Hence, the system components condenser and evaporator are the sites of highest and lowest value of \dot{E}_D respectively. However, the system component evaporator is the site of highest exergy recovery as the exergetic efficiency of evaporator is observed to be highest.

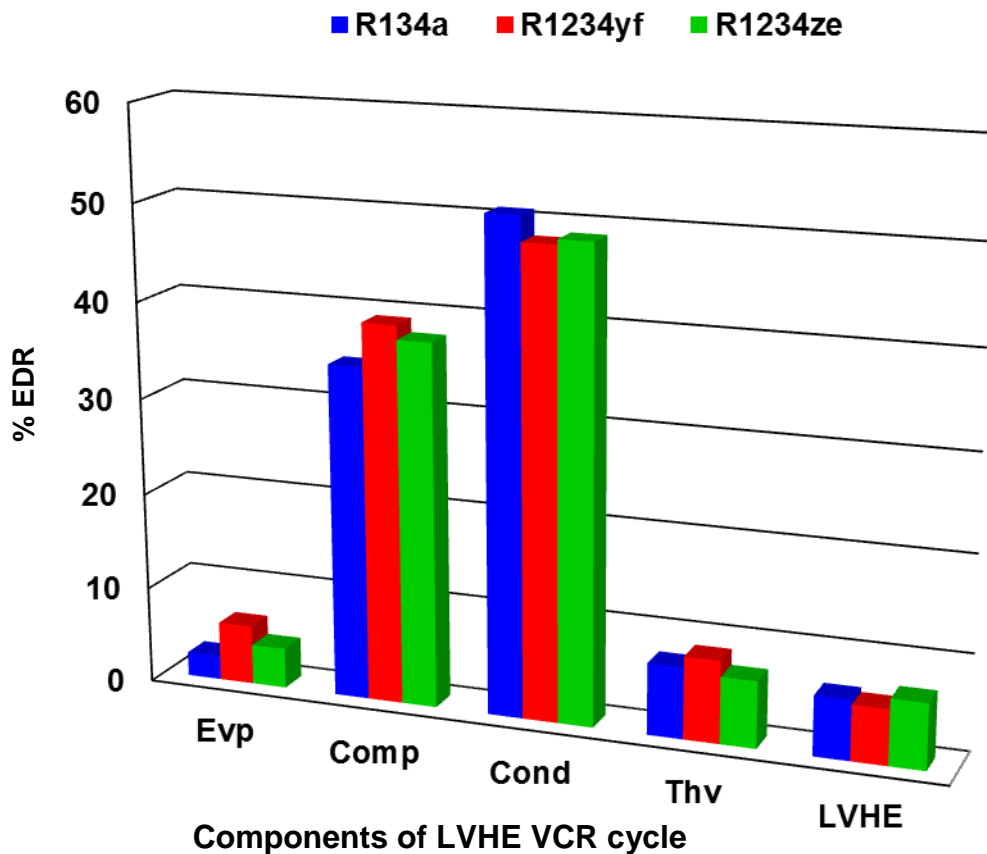


Fig. 3.19 (b) Percentage EDR in different components of LVHE incorporated VCR system ($T_e = -10^0\text{C}$)

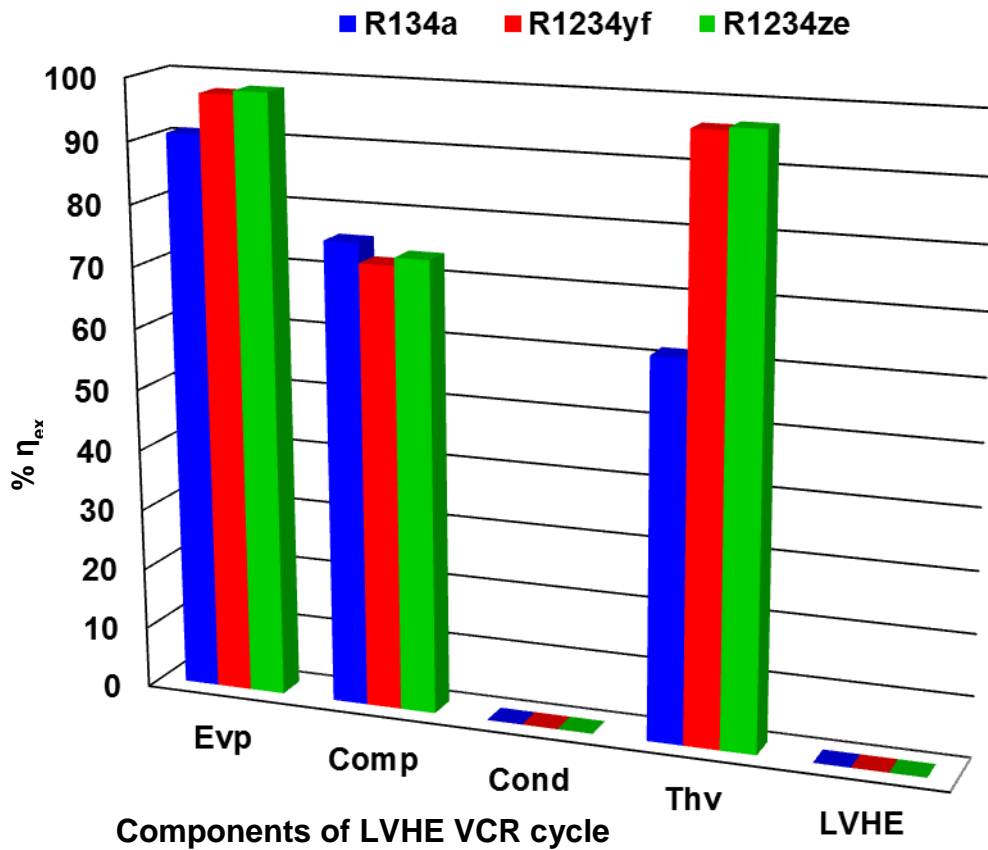


Fig. 3.19 (c) Percentage exergetic efficiency (η_{ex}) in different components of LVHE incorporated VCR system ($T_e = -10^0\text{C}$)

The exergetic efficiency (η_{ex}) of condenser and LVHE is observed to be zero. Thus the system components condenser and LVHE are the sites of lowest exergy recovery. However exergetic efficiency of throttle valve and compressor is observed higher than that of condenser and LVHE and lower than evaporator for the considered refrigerants. It has been noticed that the value of \dot{E}_D and percentage EDR are lowest for R134a in the evaporator and highest for R134a in the condenser. The exergetic efficiency of evaporator is highest for R1234ze. The recovery of exergy in the throttle valve and compressor carried out by R1234ze is higher than that of other refrigerants.

3.4.1.6 Results of Exergy Analysis

Table 3.1 Results of exergy analysis of LVHE incorporated VCR system ($T_e = -10^0\text{C}$, $(\Delta T)_{sc} = 5^0\text{C}$)

Refrigerants	System components of LVHE VCR cycle					
		Evap	Comp	Cond	Thv	LVHE
R134a (HFC)	\dot{E}_{in} (kW)	-0.6257	-0.6334	0.2976	-0.1679	-0.7473
	\dot{E}_{out} (kW)	-0.6048	0.2976	-0.1425	-0.2323	-0.8013
	\dot{E}_D (kW)	0.0772	0.3000	0.4401	0.0644	0.0540
	EDR	0.0089	0.3463	0.5081	0.0743	0.0624
	η_{ex}	0.9100	0.7563	0	0.6168	0
R1234yf (HFO)	\dot{E}_{in} (kW)	-2.4400	-0.2424	-1.5480	-1.9730	-4.3490
	\dot{E}_{out} (kW)	-2.3890	-1.5480	-1.9590	-2.4060	-4.3980
	\dot{E}_D (kW)	-0.0154	0.3335	0.4109	0.0729	0.0491
	EDR	-0.0181	0.3919	0.4828	0.0857	0.0577
	η_{ex}	0.9754	0.7243	0	0.9631	0
R1234ze (HFO)	\dot{E}_{in} (kW)	-2.2550	-2.2530	-1.3740	-1.8040	-4.0010
	\dot{E}_{out} (kW)	-2.2222	-1.3740	-1.7790	-1.8620	-4.0580
	\dot{E}_D (kW)	-0.0019	0.3130	0.4051	0.0576	0.0569
	EDR	-0.0023	0.3768	0.4876	0.0693	0.0686
	η_{ex}	0.9820	0.7375	0	0.9681	0

3.5 CONCLUSIONS

The present work compares thermodynamic performance of alternative low GWP alternative refrigerants (R1234yf & R1234ze) to R134a in a simple VCR system which is mechanically subcooled by a heat exchanger (LVHE). The energy and exergy analysis have been carried out for a theoretical model of LVHE incorporated to VCR cycle using R134a, R1234yf and R1234ze. The effect of DOS, evaporator temperature, LVHE effectiveness and compressor isentropic efficiency have been observed on compressor work, degree of superheating, COP, exergy efficiency, exergy destruction (total) and EDR of the LVHE incorporated VCR system. The exergetic efficiency, exerg destruction and exergy destruction ratio of components of system have also been evaluated. The results have been compared for simple VCR system and subcooled LVHE incorporated VCR system and are presented for three different refrigerants R134a, R1234yf and R1234ze. The summary of main conclusions of the present analysis is communicated below:

- The COP of the LVHE incorporated VCR system is higher for HFO-R1234ze than R134a and R1234yf. The COP of the system enhances with the increase in different variables i.e. degree of subcooling, evaporator temperature, effectiveness of LVHE and isentropic efficiency of compressor. Similarly the cycle achieves highest value of exergetic efficiency for R1234ze.
- The difference in the COP for R134a and R1234ze is 1.04% at 10⁰C of subcooling while 1.87% at 30⁰C of subcooling.
- The percentage difference in exergetic efficiency for R1234ze and R134a are 0.82% at 10⁰C and 1.88% at 30⁰C of subcooling.
- The values of performance parameters are lower for R1234yf than the HFC-R134a. However the difference is comparable small and it has eco-loving characteristics, so it can be a considerable replacement of R134a.
- The greater amount of exergy destruction takes place with the R1234yf and R134a.
- The condenser is the site of major portion of destruction of exergy.
- The destruction of exergy in the evaporator takes place lower than the other components.
- The highest exergetic efficiency is obtained by the evaporator.
- The exergetic efficiencies of condenser and LVHE are lower as compared to other system components.

In the light of above conclusions, it is inferred that HFO-R1234ze is the best among the refrigerants considered and can replace the traditional HFC-R134a with minor modifications in design. Although the performance of HFO-R1234yf is lower than that of HFC-R134a, having eco-loving characteristics and small deviation in the values of performance parameters, it might be a better alternative to HFC-134a. It is also predicted that the condenser and evaporator are most sensitive system components in context to the recovery of exergy criteria. These systems have utility in house hold and offices.

THERMODYNAMIC PERFORMANCE ANALYSIS OF DEDICATED MECHANICALLY SUB-COOLED VAPOUR COMPRESSION REFRIGERTION SYSTEM

4.1 INTRODUCTION:

The efficient and eco-sustainable refrigeration systems are in current demand. The developing countries like India have huge demand of electricity especially in summer season due to increasing refrigeration and air-conditioning load. In order to fulfil the need of high grade energy during peak load, efficient refrigeration systems are required. The hike in price of high grade energy and the protection of environment from high GWP HFCs which are used in refrigeration and air-conditioning systems are major current issues. Moreover, the high GWP HFCs have to be phased out as per the European Union (EU) regulation (Regulation (EU) No 517/2014).

Therefore, energy efficient and eco-friendly refrigeration and air-conditioning systems are in current demand.

In the present work, thermodynamic performance analysis of dedicated mechanically sub-cooled VCR system using R1234ze, R1234yf and R134a has been executed. The system comprises of two VCR systems operating simultaneously and having same refrigerant at a time. One is dedicated mechanically subcooled system (DSC) and other is subcooler system (SC). The refrigeration effect of subcooler VCR system is utilized to subcool the condensate of dedicated mechanically subcooled VCR system. Thus, the subcooler VCR system is dedicated to DSC VCR system as the title suggests. The two systems are coupled in such a way that the evaporator of one VCR system acts as subcooler for other VCR system. In which, the liquid condensate is subcooled.

The current work has been carried out for energy and exergy performance analysis followed by parametric analysis. The effect of various operating variables viz. degree of subcooling (DOS), temperature of evaporator, condenser temperature, isentropic efficiency of compressor and subcooler effectiveness has been examined on various performance parameter viz. total exergy destruction of the sytem, COP, EDR and exergetic efficiency. The EDR and exergy destrction rate in each component of system has also been computed and preseted. An EES software based program has been

compiled to compute the results of exergy and energy analysis of dedicated mechanically subcooled VCR system.

4.2 DESCRIPTION OF SYSTEM

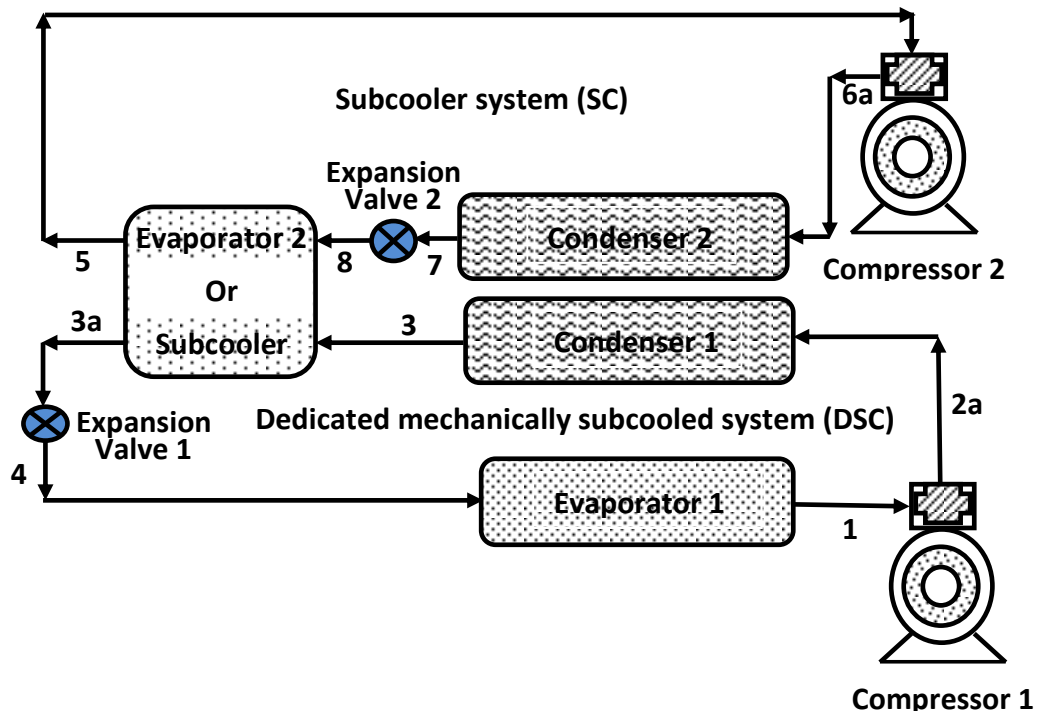


Fig. 4.1 Schematic diagram of dedicated mechanically subcooled VCR system

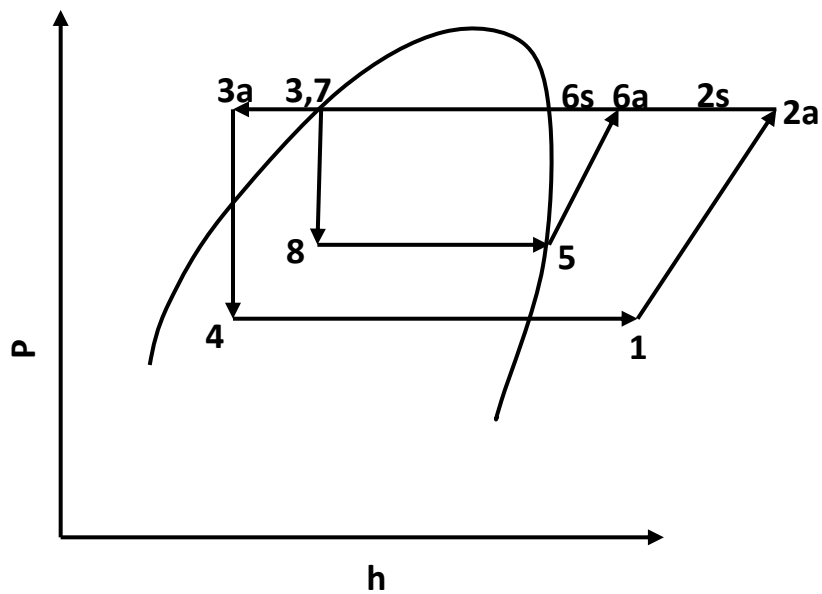


Fig. 4.2 Pressure-Enthalpy diagram of dedicated mechanically subcooled VCR system

Control volume approach has been considered for each components of the system during the formation of steady state governing equations.

Fig. 4.1 & 4.2 illustrate the schematic and P-h diagrams of dedicated mechanically subcooled vapour compression refrigeration system respectively. It comprises of two sections i.e. subcooled and subcooler vapour compression refrigeration cycles. The evaporator of subcooler VCR cycle receives the heat rejected by the condensate liquid refrigerant of subcooled VCR cycle and acts as subcooler. In this way, the two cycles are coupled together through subcooler or evaporator 2 in order to achieve low temperature in evaporator1. The refrigerants considered for the thermodynamic (exergy and energy) analysis of the VCR systems are R134a, R1234yf and R1234ze. The same refrigerant has been considered in the two sections simultaneously.

The subcooled VCR cycle is in lower section which consists of compressor1, evaporator1, expansion valve1, subcooler and condenser1 and the subcooler VCR cycle is upper section which consists of compressor2, condenser2, expansion valve2 and evaporator2 or subcooler. The vapour refrigerant leaving the evaporator1 of subcooled VCR cycle at state point1 enters into the compressor1 and is being compressed. The refrigerant at high pressure and temperature leaving the compressor1 at state point 2 and enters in to the condenser1. The liquid condensate has been subcooled from state point 3-3a by the evaporator2 of the subcooler cycle. The subcooled liquid refrigerant is throttled by the expansion valve1 from state point 3a-4. The low temperature liquid-vapour mixture of refrigerant enters in to the evaporator1 and low temperature is achieved in the evaporator1.

Similarly, the saturated vapour of the refrigerant leaving the evaporator2 or subcooler at state point 5 enters in to the compressor2. The compressed high pressure, high temperature vapour refrigerant enters into the condenser2 at state point 6. The vapour phase of the refrigerant is converted in to liquid in the condenser2. The liquid condensate refrigerant leaving the condenser2 at state point7 is expanded freely by the expansion valve2 from state 7-8. The low temperature liquid-vapour mixture of refrigerant enters into the evaporator2 or subcooler and absorbs heat from the condensate of condenser1 from state 8-5 and transformed into saturated vapour.

In this way, the mechanical sub-cooling is produced by the subcooler VCR cycle in the subcooler from states 3-3a. The evaporator temperature ($T_{e,SC}$) of the

subcooler cycle is more than the evaporator temperature of subcooled cycle. The sub-cooling of liquid condensate refrigerant of subcooled cycle enhances the net specific refrigerating effect as shown in Fig.5.2 from states 4-1. The increase in refrigerating effect enhances the coefficient of performance (COP) of the subcooled VCR system. However, the compressor work of the subcooler VCR system reduces the COP of the overall cycle.

4.3 THERMODYNAMIC & MATHEMATICAL MODELLING

4.3.1 Assumptions

The undermentioned assumptions have been considered to formulate the complex thermodynamic model of dedicated mechanically subcooled vapour compression refrigeration system (DMS) and subcooler VCR system except where the variation of physical parameters involved.

- It is assumed that the state of refrigerant is dry and saturated while entering to the compressor at state points 1 and 5.
- The heat losses and pressure losses from the system and system components are negligible. The whole system operates in steady state and homogeneous condition with control volume approach for each system component.
- The pressure drop in evaporator (δ_e) and condenser (δ_c) is assumed to be zero.
- Control volume approach has been considered during the formation of steady state governing equations for each component of system.

4.3.2 Energy analysis

The first law based work, energy and mass conservation principles are presented in equations (4.1)-(4.2).

$$\sum \dot{Q} - \sum \dot{W} = \sum \dot{m}_o h_o - \sum \dot{m}_i h_i \quad (4.1)$$

$$\sum \dot{m}_i - \sum \dot{m}_o = 0 \quad (4.2)$$

Where \dot{Q} , \dot{W} and \dot{m} are the rate of transfer of heat, work and mass respectively crossing the boundary of the system.

The COP of simple, dedicated mechanically subcooled (DSC), subcooler (SC) and overall (OC) VCR systems are given by the equation (4.3)-(4.9).

$$\text{COP}_{\text{SVCR}} = \frac{\dot{Q}_e}{\dot{W}_{\text{comp}}} \quad (4.3)$$

Where \dot{Q}_e is the net refrigeration effect produced and \dot{W}_{comp} is the actual work of the compressor.

$$\text{COP}_{\text{DSC}} = \frac{\dot{Q}_{e,\text{DSC}}}{\dot{W}_{\text{comp1}}} \quad (4.4)$$

$$\dot{Q}_{e,\text{DSC}} = \dot{m}_{r,\text{DSC}}(h_1 - h_4) \quad (4.5)$$

$$\dot{W}_{\text{comp1}} = \dot{m}_{r,\text{DSC}}(h_2 - h_1) \quad (4.6)$$

$$\text{COP}_{\text{SC}} = \frac{\dot{Q}_{e,\text{SC}}}{\dot{W}_{\text{comp2}}} \quad (4.7)$$

$$\dot{W}_{\text{comp2}} = \dot{m}_{r,\text{SC}}(h_6 - h_5) \quad (4.8)$$

$$\text{COP}_{\text{OC}} = \frac{\dot{Q}_{e,\text{DSC}}}{\dot{W}_{\text{comp1}} + \dot{W}_{\text{comp2}}} \quad (4.9)$$

Where $\dot{Q}_{e,\text{DSC}}$, $\dot{Q}_{e,\text{SC}}$, \dot{W}_{comp1} , \dot{W}_{comp2} , $\dot{m}_{r,\text{DSC}}$ and $\dot{m}_{r,\text{SC}}$ are net refrigerant effect, net compressor work and mass flow rate of dedicated mechanically subcooled and subcooler VCR cycles respectively.

The effectiveness of subcooler ε_{SC} is the ratio of minimum rate of transfer of heat to the maximum rate of transfer of heat.

$$\varepsilon_{\text{SC}} = \frac{T_3 - T_{3a}}{T_3 - T_8} \quad (4.10)$$

Where ε_{SC} is the effectiveness of subcooler and T_3, T_5 and T_8 are temperatures at respective state points.

The energy balance in the subcooler is given by equation (4.11).

$$\dot{m}_{r,\text{DSC}}(h_3 - h_{3a}) = \dot{m}_{r,\text{SC}}(h_5 - h_8) \quad (4.11)$$

4.3.3 Exergy Analysis

The exergy is defined as an effective measure of the potential of substance to impact the environment or the maximum useful work which can be extracted from a system as it reversibly comes into equilibrium with its environment. The concept of exergy is derived from the second law of thermodynamics and it is the degree measure of usefulness and quality of matter in response to the environment (Bejan et al., 1996, Arora and Kaushik, 2008)

For the refrigerant flowing in a refrigerating system, the exergy is defined as follows (Bejan et al., 1996):

$$\dot{E} = \dot{m}_r[(h - h_0) - T_0(s - s_0)] \quad (4.12)$$

Where s_0 and h_0 are the entropy and enthalpy values of the refrigerant at dead state (pressure P_0 and temperature T_0).

Exergy destruction (\dot{E}_D) or internal exergy destruction losses which are caused by irreversibilities of the system is the algebraic sum of total exergy at the inlet and outlet of the system. General exergy balance is given by (Dincer and Kanoglu 2010):

$$\dot{E}_D = \dot{E}_{in} - \dot{E}_{out} \quad (4.13)$$

Where \dot{E}_D is the rate of exergy destruction, \dot{E}_{in} and \dot{E}_{out} are the total exergy input and out by heat, work and mass respectively.

4.3.3.1 Exergy destruction (\dot{E}_D) in the components of dedicated mechanically subcooled vapour compression refrigeration cycle (DSC)

The destruction of exergy in each component of the dedicated mechanically subcooled VCR system is given by the following equations:

Evaporator1

$$(\dot{E}_D)_{e,DSC} = \dot{E}_{X_4} + \dot{Q}_{e,DSC} \left(1 - \frac{T_0}{T_{b,DSC}}\right) - \dot{E}_{X_1} = \dot{m}_{r,DSC}(h_4 - T_0s_4) + \dot{Q}_{e,DSC} \left(1 - \frac{T_0}{T_b}\right) - \dot{m}_{r,DSC}(h_1 - T_0s_1) \quad (4.14)$$

Compressor1

$$(\dot{E}_D)_{comp1} = \dot{E}_{X_1} + \dot{W}_{comp1} - \dot{E}_{X_2} = \dot{m}_{r,DSC}(h_1 - T_0s_1) + \dot{W}_{comp1} - \dot{m}_{r,DSC}(h_2 - T_0s_2) \quad (4.15)$$

Condenser1

$$(\dot{E}_D)_{cond1} = \dot{E}_{X_2} - \dot{E}_{X_3} = \dot{m}_{r,DSC}(h_2 - T_0s_2) - \dot{m}_{r,DSC}(h_3 - T_0s_3) \quad (4.16)$$

Expansion valve1

$$(\dot{E}_D)_{Ex. valve1} = \dot{E}_{X_3} - \dot{E}_{X_{3a}} = \dot{m}_{r,DSC}(h_{3a} - T_0s_{3a}) - \dot{m}_{r,DSC}(h_4 - T_0s_4) = \dot{m}_{r,DSC}T_0(s_4 - s_{3a}) \quad (4.17)$$

Subcooler

$$\begin{aligned}(\dot{E}_D)_{SC} &= (\dot{E}_{X_8} - \dot{E}_{X_5}) + (\dot{E}_{X_3} - \dot{E}_{X_{3a}}) \\ &= \dot{m}_{r,SC}\{(h_8 - h_5) - T_0(s_8 - s_5)\} + \dot{m}_{r,DSC}\{(h_3 - h_{3a}) - T_0(s_3 - s_{3a})\}\end{aligned}\quad (4.18)$$

Compressor2

$$(\dot{E}_D)_{comp2} = \dot{E}_{X_5} + \dot{W}_{comp2} - \dot{E}_{X_6} = \dot{m}_{r,SC}(h_5 - T_0s_5) + \dot{W}_{comp2} - \dot{m}_{r,SC}(h_6 - T_0s_6)\quad (4.19)$$

Condenser2

$$(\dot{E}_D)_{cond2} = \dot{E}_{X_6} - \dot{E}_{X_7} = \dot{m}_{r,SC}(h_6 - T_0s_6) - \dot{m}_{r,SC}(h_7 - T_0s_7)\quad (4.20)$$

Expansion valve2

$$(\dot{E}_D)_{Ex. valve2} = \dot{E}_{X_7} - \dot{E}_{X_8} = \dot{m}_{r,SC}(h_7 - T_0s_7) - \dot{m}_{r,SC}(h_8 - T_0s_8) = \dot{m}_{r,SC}T_0(s_8 - s_7)\quad (4.21)$$

Evaporator2

$$\begin{aligned}(\dot{E}_D)_{e,SC} &= \dot{E}_{X_8} + \dot{Q}_{e,SC}\left(1 - \frac{T_0}{T_{b,SC}}\right) - \dot{E}_{X_5} = \dot{m}_{r,SC}(h_8 - T_0s_8) + \dot{Q}_{e,SC}\left(1 - \frac{T_0}{T_{b,SC}}\right) - \\ &\dot{m}_{r,SC}(h_5 - T_0s_5)\end{aligned}\quad (4.22)$$

where \dot{E}_D , \dot{E}_X , \dot{m}_r and T_b are the rate of destruction of exergy, rate of exergy, mass flow rate and temperature of space to be cooled for the dedicated mechanically subcooled and subcooler cycle respectively. T_0 , h_0 and s_0 are the temperature, enthalpy and entropy at dead state.

4.3.3.2 Total exergy destruction (TEXD)

TEXD of the system is the sum of exergy destruction in each component of the system.

The TEXD in the dedicated mechanically subcooled VCR system (DSC) is given by:

$$\Sigma(\dot{E}_D)_{DSC} = (\dot{E}_D)_{e,DSC} + (\dot{E}_D)_{comp1} + (\dot{E}_D)_{cond1} + (\dot{E}_D)_{Ex. valve1}\quad (4.23)$$

$$\Sigma(\dot{E}_D)_{SC} = (\dot{E}_D)_{e,SC} + (\dot{E}_D)_{comp2} + (\dot{E}_D)_{cond2} + (\dot{E}_D)_{Ex. valve2} \quad (4.24)$$

$$\Sigma(\dot{E}_D)_{OC} = (\dot{E}_D)_{e,DSC} + (\dot{E}_D)_{comp1} + (\dot{E}_D)_{cond1} + (\dot{E}_D)_{Ex. valve1} + (\dot{E}_D)_{SC} + (\dot{E}_D)_{comp2} + (\dot{E}_D)_{cond2} + (\dot{E}_D)_{Ex. valve2} \quad (4.25)$$

4.3.3.3 Exergetic efficiency (EXE)

The EXE is the ratio of total exergy recovered to the total exergy supplied which is given by the equation (4.26) (Dincer and Kanoglu, 2010):

$$\eta_{ex} = \frac{\Sigma \dot{E}_{out}}{\Sigma \dot{E}_{in}} = 1 - \frac{\Sigma \dot{E}_D}{\Sigma \dot{E}_{in}} \quad (4.26)$$

Where η_{ex} is the exergetic efficiency of the cycle. $\Sigma \dot{E}_{out}$, $\Sigma \dot{E}_{in}$ and $\Sigma \dot{E}_D$ are the total exergy recovered, supplied and destructed respectively.

The EXE can also be defined as it is the ratio of exergy in products to the exergy of fuel. The exergetic efficiency of dedicated mechanically subcooled, subcooler and overall VCR systems are given by the equations (4.27)-(4.29) (Arora and Kaushik, 2008).

$$\eta_{ex(DSC)} = \frac{|\dot{Q}_{e,DSC} \left(1 - \frac{T_0}{T_{b,DSC}}\right)|}{\dot{W}_{comp1}} \quad (4.27)$$

$$\eta_{ex(SC)} = \frac{|\dot{Q}_{e,SC} \left(1 - \frac{T_0}{T_{b,SC}}\right)|}{\dot{W}_{comp2}} \quad (4.28)$$

$$\eta_{ex(OC)} = \frac{|\dot{Q}_{e,DSC} \left(1 - \frac{T_0}{T_{b,DSC}}\right)|}{\dot{W}_{comp1} + \dot{W}_{comp2}} \quad (4.29)$$

where T_0 is the ambient or dead state temperature.

The exergetic efficiency (EXE) of each component of the dedicated mechanically subcooled VCR system is given by the following equations:

Evaporator1

$$\eta_{ex(e,DSC)} = 1 - \frac{(\dot{E}_D)_{e,DSC}}{\dot{E}_{X4} + |\dot{Q}_{e,DSC} \left(1 - \frac{T_0}{T_{b,DSC}}\right)|} \quad (4.30)$$

Compressor1

$$\eta_{\text{ex (comp1)}} = 1 - \frac{(\dot{E}_D)_{\text{comp1}}}{\dot{E}_{X_1} + W_{\text{comp1}}} \quad (4.31)$$

Condenser1

$$\eta_{\text{ex (cond1)}} = 1 - \frac{(\dot{E}_D)_{\text{cond1}}}{\dot{E}_{X_2} - \dot{E}_{X_3}} \quad (4.32)$$

Expansion valve1

$$\eta_{\text{ex (Ex. valve1)}} = 1 - \frac{(\dot{E}_D)_{\text{Ex. valve1}}}{\dot{E}_{X_3}} \quad (4.33)$$

Subcooler

$$\eta_{\text{ex (SC)}} = 1 - \frac{(\dot{E}_D)_{\text{SC}}}{(\dot{E}_{X_3} + \dot{E}_{X_8})} \quad (4.34)$$

Compressor2

$$\eta_{\text{ex (comp2)}} = 1 - \frac{(\dot{E}_D)_{\text{comp2}}}{(\dot{E}_{X_5} + W_{\text{comp2}})} \quad (4.35)$$

Condenser2

$$\eta_{\text{ex (cond2)}} = 1 - \frac{(\dot{E}_D)_{\text{cond2}}}{(\dot{E}_{X_6} - \dot{E}_{X_7})} \quad (4.36)$$

Expansion valve2

$$\eta_{\text{ex (Ex. valve2)}} = 1 - \frac{(\dot{E}_D)_{\text{Ex. valve2}}}{\dot{E}_{X_7}} \quad (4.37)$$

Evaporator2

$$\eta_{\text{ex (SC)}} = 1 - \frac{(\dot{E}_D)_{\text{SC}}}{(\dot{E}_{X_3} + \dot{E}_{X_8})} \quad (4.38)$$

Where \dot{m}_r , η_{ex} , \dot{E}_D , \dot{E}_X and T_b are mass flow rate, the exergetic efficiency, exergy destruction rate, exergy rate and temperature of space to be cooled respectively.

4.3.3.4 Exergy destruction ratio (EDR)

The exergy destruction ratio (EDR) is the ratio of total destruction of exergy of the system to the exergy of the products (Arora and Kaushik, 2008) which is represented by equation (4.39):

$$EDR = \frac{\dot{E}_{D,total}}{\dot{E}_P} = \frac{1}{\eta_{ex}} - 1 \quad (4.39)$$

The exergy destruction ratio for the dedicated mechanically subcooled, subcooler and overall VCR cycles are given in following (4.40)-(4.42).

$$EDR_{DSC} = \frac{\Sigma(\dot{E}_D)_{DSC}}{\dot{E}_{P,DSC}} = \frac{\Sigma(\dot{E}_D)_{DSC}}{\left| \dot{Q}_{e,DSC} \left(1 - \frac{T_0}{T_{b,DSC}} \right) \right|} \quad (4.40)$$

$$EDR_{SC} = \frac{\Sigma(\dot{E}_D)_{SC}}{\dot{E}_{P,SC}} = \frac{\Sigma(\dot{E}_D)_{SC}}{\left| \dot{Q}_{e,SC} \left(1 - \frac{T_0}{T_{b,SC}} \right) \right|} \quad (4.41)$$

$$EDR_{OC} = \frac{\Sigma(\dot{E}_D)_{OC}}{\dot{E}_{P,DSC}} = \frac{\Sigma(\dot{E}_D)_{OC}}{\left| \dot{Q}_{e,DSC} \left(1 - \frac{T_0}{T_{b,DSC}} \right) \right|} \quad (4.42)$$

The exergy destruction ratio (EDR) is the ratio of the rate of exergy destruction in a system component ($\dot{E}_{D,i}$) to the exergy rate of the fuel provided to the overall system ($\dot{E}_{E,tot}$) or the total exergy destruction rate within the system ($\dot{E}_{D,total}$) (Bejan et al., 1996).

$$EDR = \frac{\dot{E}_{D,i}}{\dot{E}_{E,tot}} = \frac{\dot{E}_{D,i}}{\dot{E}_{D,total}} \quad (4.43)$$

The EDR in each component of the dedicated mechanically subcooled (DSC), subcooler (SC) and overall (OC) VCR systems is given by the following equations:

Evaporator1

$$EDR_{(e,DSc)} = \frac{(\dot{E}_D)_{e,DSc}}{\Sigma(\dot{E}_D)_{OC}} \quad (4.44)$$

Compressor1

$$EDR_{(comp1)} = \frac{(\dot{E}_D)_{comp1}}{\Sigma(\dot{E}_D)_{OC}} \quad (4.45)$$

Condenser1

$$\text{EDR}_{(\text{cond1})} = \frac{(\dot{E}_D)_{\text{cond1}}}{\Sigma(\dot{E}_D)_{\text{OC}}} \quad (4.46)$$

Expansion valve1

$$\text{EDR}_{(\text{Ex. valve1})} = \frac{(\dot{E}_D)_{\text{Ex. valve1}}}{\Sigma(\dot{E}_D)_{\text{OC}}} \quad (4.47)$$

Subcooler

$$\text{EDR}_{(\text{SC})} = \frac{(\dot{E}_D)_{\text{SC}}}{\Sigma(\dot{E}_D)_{\text{OC}}} \quad (4.48)$$

Compressor2

$$\text{EDR}_{(\text{comp2})} = \frac{(\dot{E}_D)_{\text{comp2}}}{\Sigma(\dot{E}_D)_{\text{OC}}} \quad (4.49)$$

Condenser2

$$\text{EDR}_{(\text{cond2})} = \frac{(\dot{E}_D)_{\text{cond2}}}{\Sigma(\dot{E}_D)_{\text{OC}}} \quad (4.50)$$

Expansion valve2

$$\text{EDR}_{(\text{Ex. valve2})} = \frac{(\dot{E}_D)_{\text{Ex. valve2}}}{\Sigma(\dot{E}_D)_{\text{OC}}} \quad (4.51)$$

Evaporator2

$$\text{EDR}_{(\text{SC})} = \frac{(\dot{E}_D)_{\text{SC}}}{\Sigma(\dot{E}_D)_{\text{OC}}} \quad (4.52)$$

4.3.4 Model Validation

The results of the present analysis have been compared with the results of Qureshi and Zubair (2012) in Table 4.1. The maximum value of COP_N which is the ratio of COP_{DSC} and COP of simple VCR cycle is reduced to -6.2% at the optimum value of normalized sub-cooler saturation temperature (θ) which gets enhanced by 1.3% for the compressor efficiencies of DSC and SC cycles i.e. $\eta_{c,\text{DSC}} = \eta_{c,\text{SC}} = 0.65$, heat exchanger effectiveness (ϵ_{sc}) = 0.8, evaporator temperature of DSC cycle ($T_{e,\text{DSC}} = 0^\circ\text{C}$) and condenser temperature ($T_{\text{cond,DSC}} = 45^\circ\text{C}$).

Table 4.1 Comparison of results of (Qureshi and Zubair, 2012) and current work

S.No.	Parameters	Qureshi and Zubair ¹²	Current work	% Difference
1.	Optimum value of normalized Sub-cooler saturation temperature (θ), $\theta = \frac{T_{e,sc} - T_{ev,DSC}}{T_{cond.,DSC} - T_{e,DSC}}$	0.5	0.5066	1.3%
2.	Maximum value of COP _N	1.28	1.2	-6.2%
3.	Main cycle refrigerant	R134a	R134a	-
4.	Subcooler cycle refrigerant	R134a	R134a	-
5.	Refrigeration load ($\dot{Q}_{e,DSC}$)	100kW	100kW	0

4.3.5 Input Parameters

The current work explores the performance improvement of dedicated mechanically subcooled vapour compression refrigeration cycle (DSC) exergetically. The mathematical formulation of thermodynamic relations have been carried out considering mass, energy and work conservation principles for system and system components.

Table 4.2 Input variable considered except where the variation of these system variables involved (Arora and Kaushik, 2008)

S.No.	Input variables	Values
1.	Evaporator 1 temperature ($T_{e,DSC}$)	-10°C
2.	Degree of subcooling ($(\Delta T)_{sc}$) (3-3a)	5°C
3.	Condenser 1,2 temperature ($T_{c,DSC}$ & $T_{c,SC}$), assuming summer conditions in a country near the equator line.	50°C
4.	Isentropic efficiency of compressor ($\eta_{comp1}, \eta_{comp2}$)	80%
5.	Effectiveness of subcooler (ϵ_{SC})	0.8
6.	Net refrigerating effect ($\dot{Q}_{e,DSC}$)	3.5167 kW
7.	Ambient or dead state temperature (T_0) and pressure (P_0)	25°C & 101.325 kPa
8.	Difference between evaporator temperature and the temperature of space to be cooled ($T_{b,DSC} - T_{e,DSC}, T_{b,SC} -$	5°C

	$T_{e,SC}$	
9.	The range of degree of subcooling $(\Delta T)_{SC}$	5°C-30°C
10.	The range of variation of isentropic efficiency of compressor $(\eta_{comp.})$	0.1-1.0
11.	The range of variation of effectiveness of subcooler (ϵ_{SC})	0.3-1.0

4.4 RESULTS AND DISCUSSION

Thermodynamic (exergy and energy) analysis of dedicated mechanically subcooled VCR system (DSC) has been performed using a computer software based program in Engineering Equation Solver (EES) (Klein and Alvarado, 2012) as shown in Fig.4.1. The considered refrigerants for the analysis are R134a, R1234yf and R1234ze. The computation of the various performance parameters viz. compressor work, COP, EDR, total exergy destruction rate and exergetic efficiency have been done by calling builtin functions (i.e. specific entropy, specific enthalpy, temperature and pressure etc.) of the EES library.

4.4.1 Results of Energy, Exergy and Parametric Analysis

The present work investigates the thermodynamic performance of dedicated mechanically subcooled (DSC), subcooler (SC), overall (OC) and simple VCR systems using R1234yf, R1234ze and R134a. The comparison of considered refrigerant has also been examined for drop-in replacement of R134a to R1234ze and R1234yf. The first and second law based performance parameters viz. COP and exergetic efficiency have been computed and the parametric analysis has been carried out with the variation in degree of subcooling (DOS), temperature of evaporator, condenser temperature, isentropic efficiency of compressor and subcooler effectiveness followed by the thermodynamic analysis.

Fig. 4.3 (a)-(f) illustrate the T-s and P-h state diagrams of dedicated mechanically subcooled (DSC) and subcooler (SC) VCR system for the refrigerants R1234ze, R1234yf and R134a respectively. The operating conditions -10°C (evaporator) and 50°C (condenser) temperature and 149.1, 221.8 and 200.7 kPa (evaporator) and 997.4, 1302 and 1319 kPa (condenser) pressure for DSC and 848.3, 1119 and 1123 kPa (evaporator pressure) and 43.75°C (evaporator temperature) for SC

have been notified to compare the applicability of the refrigerants R1234ze, R1234yf and R134a respectively.

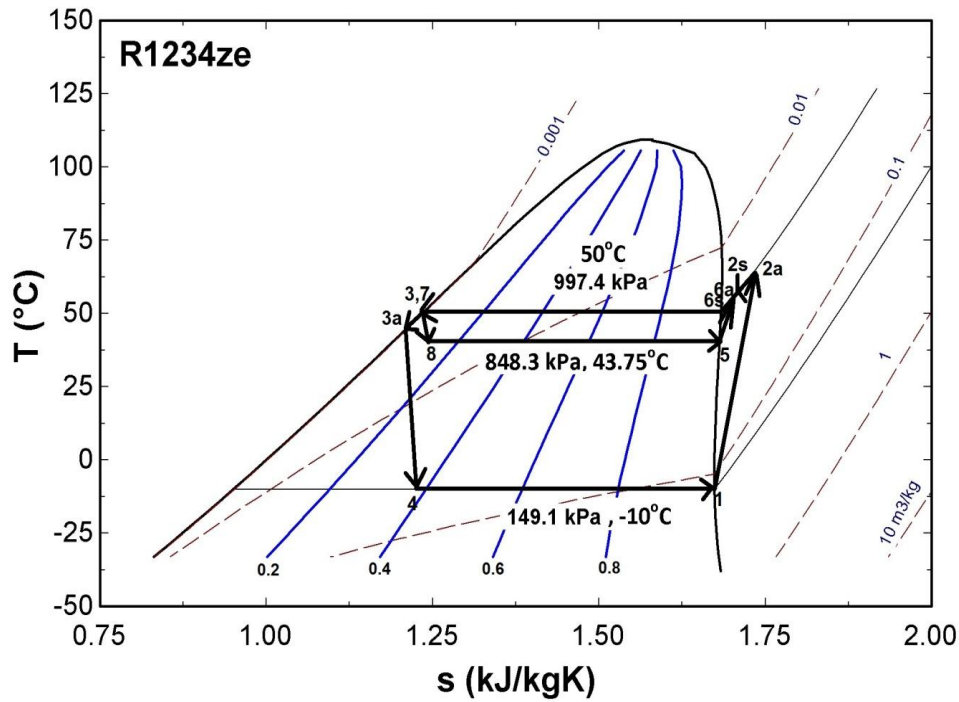


Fig. 4.3 (a) Temperature-entropy (T-s) state diagrams of dedicated mechanically subcooled (DSC), subcooler (SC) VCR systems using R1234ze

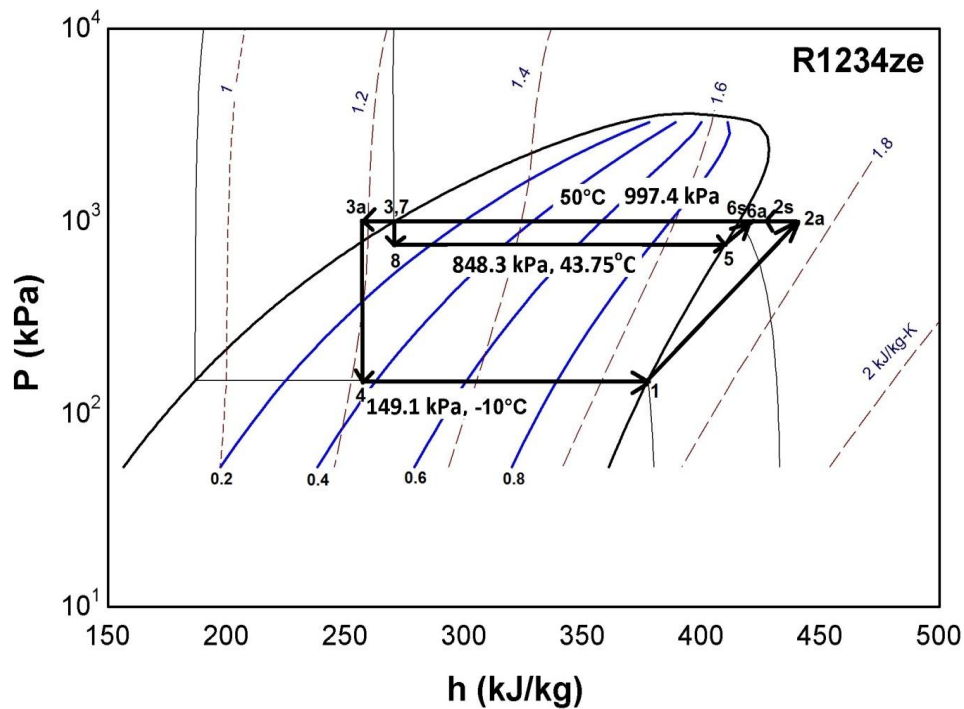


Fig. 4.3 (b) Pressure-enthalpy (P-h) state diagrams of dedicated mechanically subcooled (DSC), subcooler (SC) VCR systems using R1234ze

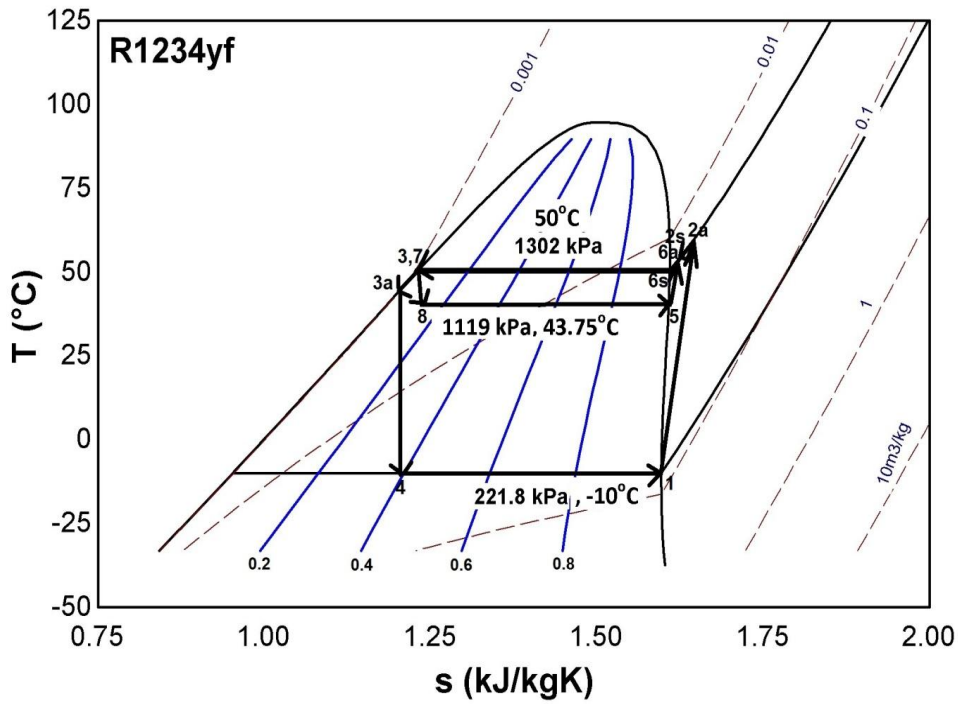


Fig. 4.3 (c) Temperature-entropy (T - s) state diagrams of dedicated mechanically subcooled (DSC), subcooler (SC) VCR systems using R1234yf

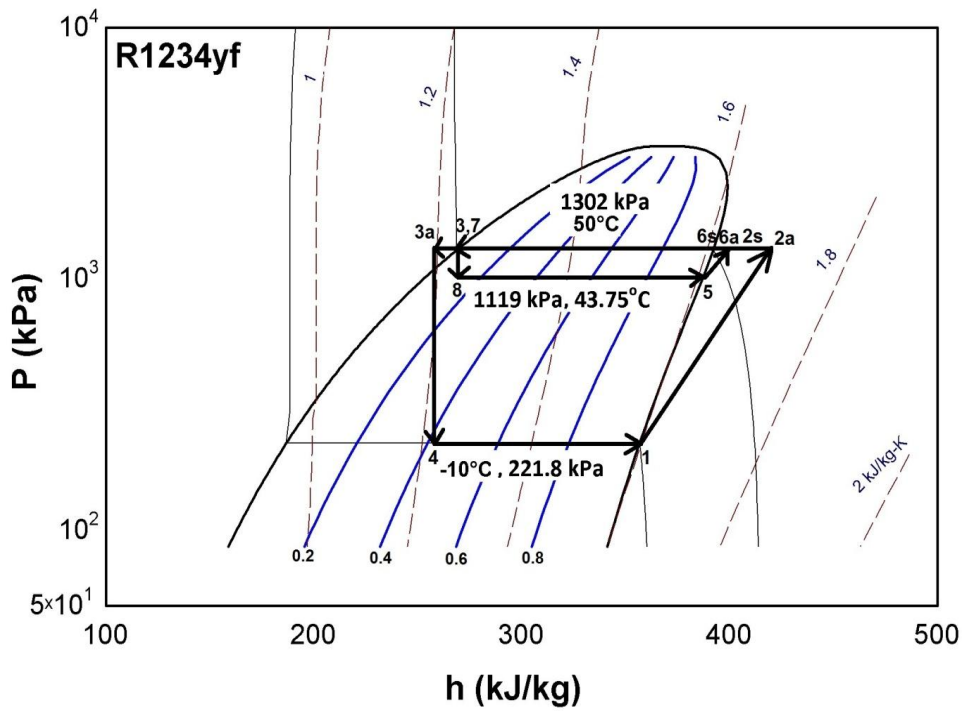


Fig. 4.3 (d) Pressure-enthalpy (P - h) state diagrams of dedicated mechanically subcooled (DSC), subcooler (SC) VCR systems using R1234yf

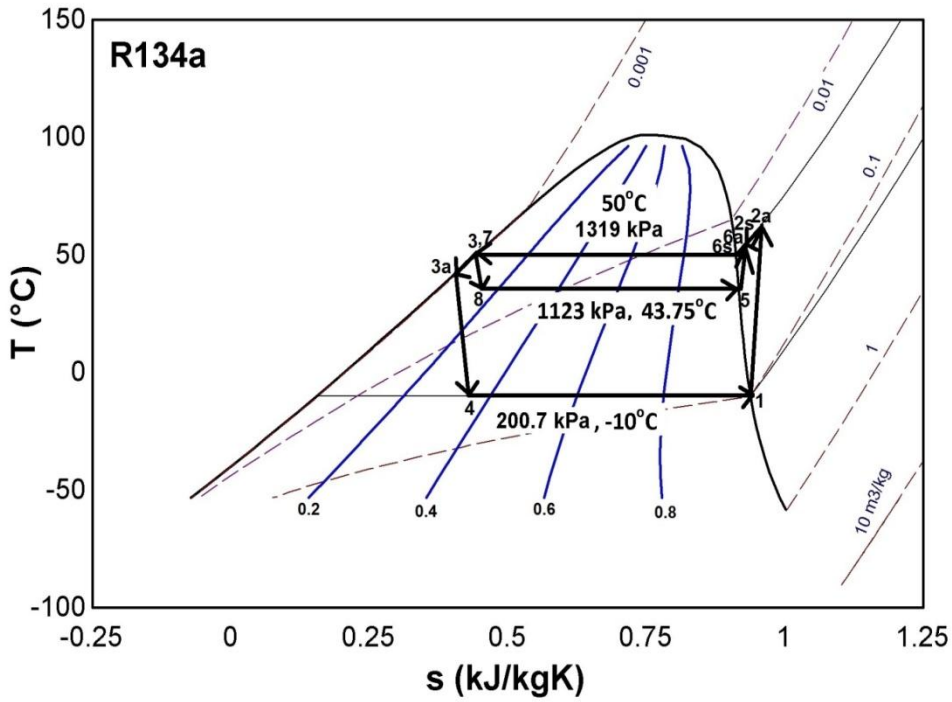


Fig. 4.3 (e) Temperature-entropy (T - s) state diagrams of dedicated mechanically subcooled (DSC), subcooler (SC) VCR systems using R134a

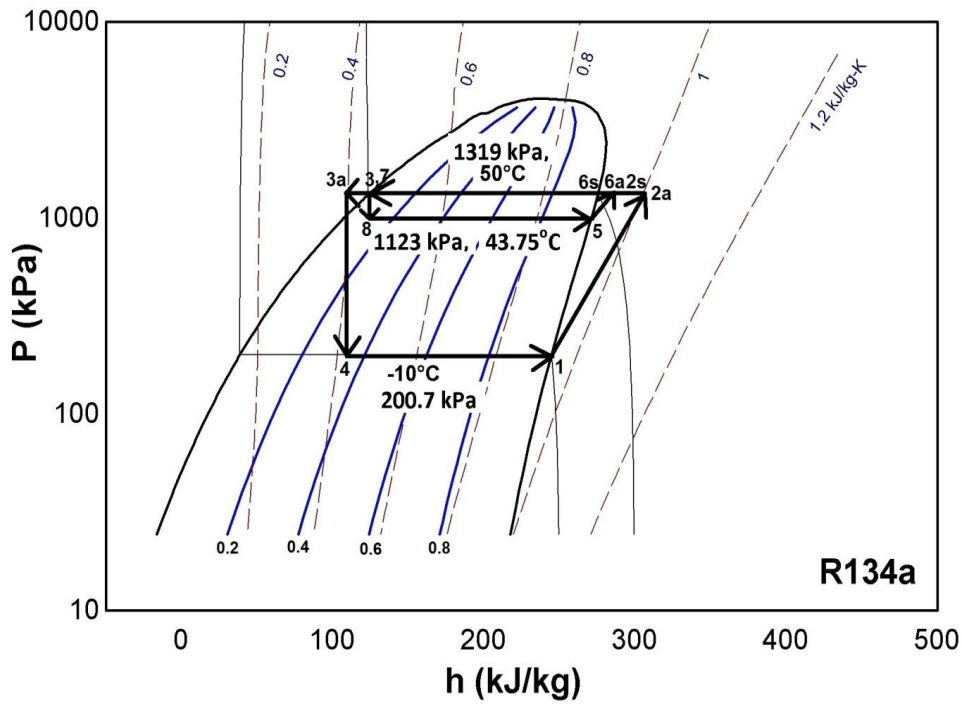


Fig. 4.3 (f) Pressure-enthalpy (P - h) state diagrams of dedicated mechanically subcooled (DSC), subcooler (SC) VCR systems using R1234yf

4.4.1.1 EFFECT OF SUBCOOLING

The effect of degree of sub-cooling (ΔT_{sc}) on various performance parameters viz. compressor work (\dot{W}_C), COP, exergetic efficiency (η_{ex}), total exergy destruction rate ($\dot{E}_{D, Total}$) and EDR has been illustrated in Fig. 4.4 to 4.7.

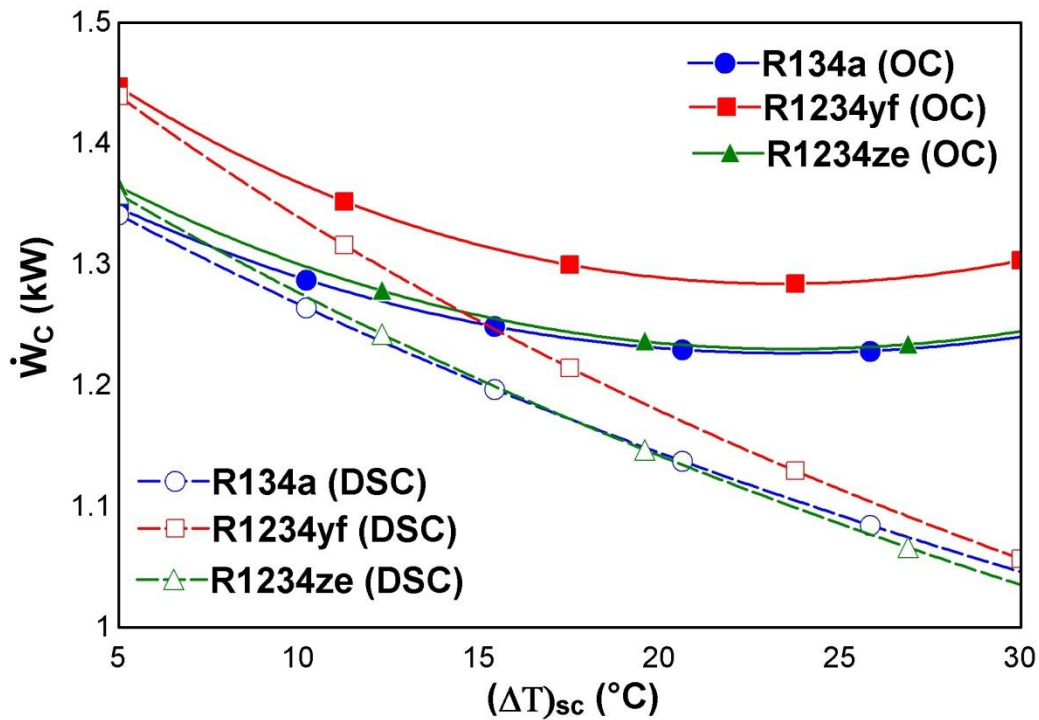


Fig. 4.4 Variation in compressor work (\dot{W}_C) with degree of subcooling (ΔT_{sc})

Fig. 4.4 represents the effect of sub-cooling (ΔT_{sc}) on compressor work (\dot{W}_C). For 1 Ton refrigeration, compressor work of dedicated mechanically subcooled (DSC) (\dot{W}_{Comp1}) decreases with increase in degree of subcooling (DOS) because the rate of mass flow of refrigerant decreases with increase in degree of subcooling for constant refrigeration load of 3.5167 kW. However, the compressor work first decreases and then increases for overall cycle (OC) with increase in degree of sub-cooling for the considered refrigerants. This is due to that the compressor work of OC ($\dot{W}_{Comp1} + \dot{W}_{Comp2}$) decreases for low values of DOS as the value of \dot{W}_{Comp1} decreases and the values of \dot{W}_{Comp2} are very small. For the higher values of DOS, the compressor work of subcooler cycle (\dot{W}_{Comp2}) increases while \dot{W}_{Comp1} decreases. However the compressor work for the simple VCR cycle is higher than that of the DSC. The optimize value of degree of sub-cooling lies within 20-25°C for overall cycle. It has

been observed that the compressor work is minimum for R1234ze and maximum for R1234yf for DSC and OC.

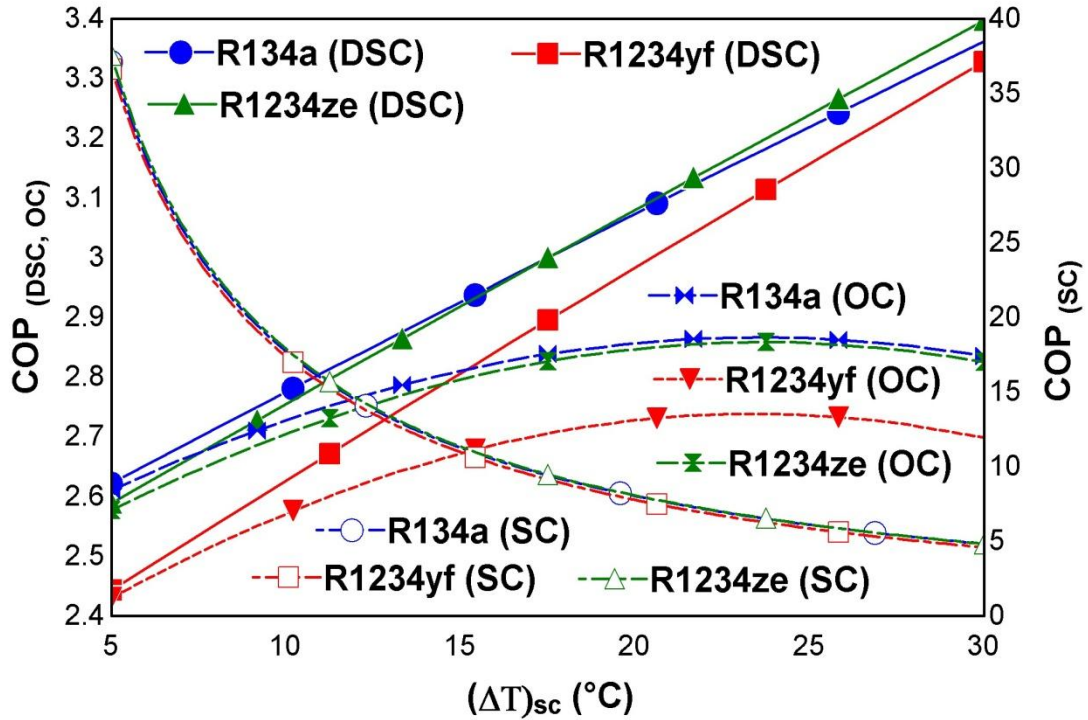


Fig. 4.5 Effect of degree of subcooling (ΔT_{sc}) on COP

Fig. 4.5 shows the variation of COP with degree of sub-cooling for the considered refrigerants R134a, R1234yf and R1234ze. The COP of the dedicated mechanically subcooled cycle increases and the COP of subcooler cycle decreases with increase in DOS for the refrigerants considered. However, the COP of the overall cycle first increases, maximise for optimum value of DOS which lies within 20-25⁰C and then decreases with increase in DOS. In order to increase DOS, The temperature and pressure of evaporator of subcooler cycle has to achieved lower values which reduces the COP of the subcooler cycle while for the constant refrigerating load of $\dot{Q}_{e,DSC} = 3.5167\text{kW}$, the compressor work (\dot{W}_{Comp1}) of DSC decreases linearly and the COP of DSC is $\frac{\dot{Q}_{e,DSC}}{W_{comp1}}$ (Eq.(4.5)). Thus the COP of the DSC increases linearly with increase in DOS. The COP of OC is $\frac{\dot{Q}_{e,DSC}}{W_{comp1} + \dot{W}_{comp2}}$ (Eq.(4.9)) which increases with increase in COP of DSC and decreases with decrease in COP of subcooler cycle due to increase in compressor work of SC with increase in DOS. Thus the COP of OC first increases (as

COP of DSC increases faster) reaches to maximum value and then decreases (as COP of SC cycle decreases faster) for the refrigerant considered. It is seen that the COP is maximum for R1234ze and minimum for R1234yf. The COP of simple VCR cycle is lower than the DSC and OC. It has been noticed that the optimum value of degree of subcooling for maximum COP are 23.55, 23.39 and 23.65 for R134a, R1234yf and R1234ze respectively.

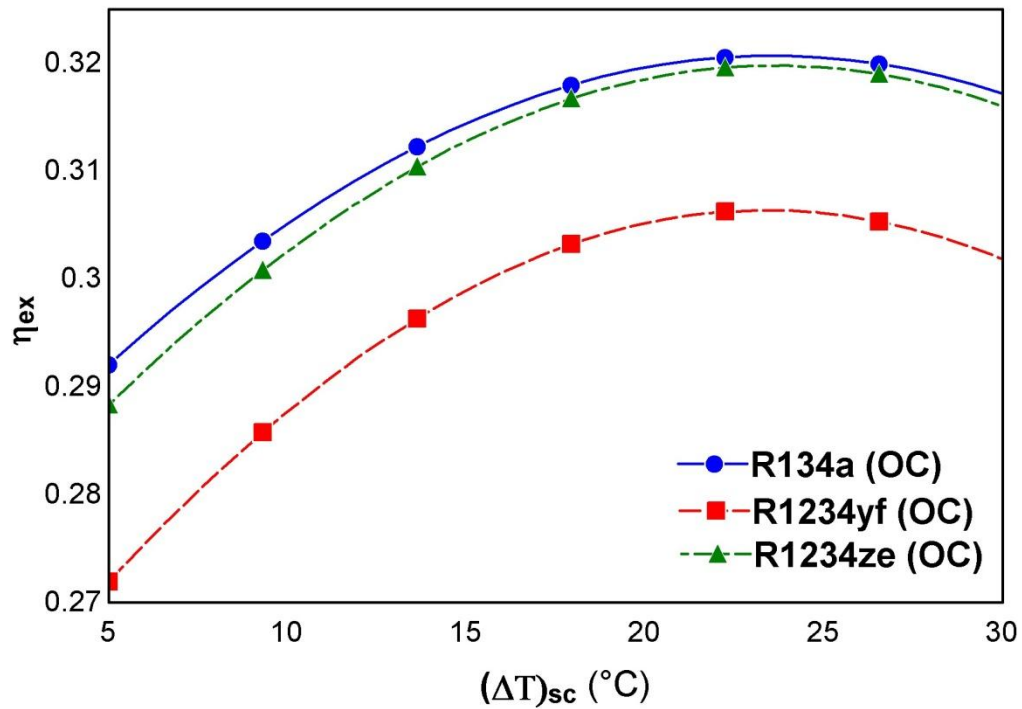


Fig. 4.6 Effect of degree of subcooling (ΔT_{sc}) on exergetic efficiency (η_{ex})

Fig. 4.6 illustrates the effect of DOS (ΔT_{sc}) on exergetic efficiency ($\eta_{ex(OC)}$) of overall cycle. The exergetic efficiency of the overall cycle increases to a maximum value afterwards decreases with increase in DOS for the considered refrigerants. The optimum value of degree of sub-cooling lies between 20 to 25⁰C for which the value of exergetic efficiency is maximum. The exergetic efficiency of overall cycle is given by

$$\eta_{ex(OC)} = \frac{|\dot{Q}_{e,OC} \left(1 - \frac{T_0}{T_{b,DSC}}\right)|}{\dot{W}_{comp1} + \dot{W}_{comp2}} \quad (\text{Eq. 4.29}).$$

In which the term $\frac{|\dot{Q}_{e,OC}|}{\dot{W}_{comp1} + \dot{W}_{comp2}}$ is the $COP_{(OC)}$

which increases to a maximum value afterwards decreases with increase in DOS (Fig. 4.4) and the term $\left| \left(1 - \frac{T_0}{T_{b,DSC}}\right) \right|$ remains constant with increase in DOS because the value of T_0 and $T_{b,DSC}$ remains constant with increase in DOS. Hence the value of

$\eta_{ex(OC)}$ increases to a maximum value afterwards decreases. The optimum value of DOS lies between 20 to 25°C for the considered refrigerants. Hence the exergetic efficiency of the OC follows the trend of COP. It can be noticed that $\eta_{ex(OC)}$ is maximum for R134a and minimum for R1234yf.

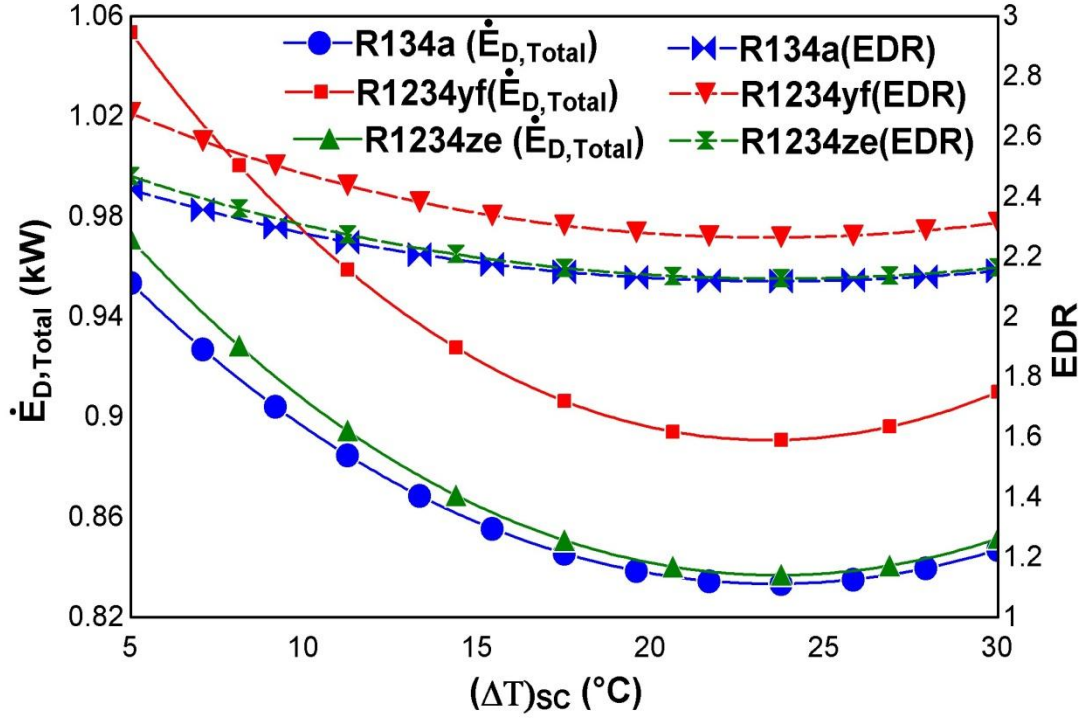


Fig. 4.7 Variation in total exergy destruction rate ($\dot{E}_{D, Total}$) and exergy destruction ratio (EDR) with degree of subcooling (ΔT_{sc}) for OC

Fig. 4.7 shows the variation in total exergy destruction rate ($\dot{E}_{D, Total}$) and EDR with degree of subcooling (ΔT_{sc}) for overall cycle. The value of $\dot{E}_{D, Total}$ and EDR first decreases, reaches to a minimum value and then increases with increase in DOS for the refrigerants considered. The value of $\dot{Q}_{e,OC}$ increases to a maximum value afterwards decreases with increase in DOS (Fig. 4.5). Therefore, the exergy recovered from the system and system components increases to a maximum value afterwards decreases with increase in DOS. Consequently, the $\dot{E}_{D, Total}$ decreases, attaining a minimum value afterwards increases. EDR is given by $\frac{\Sigma(\dot{E}_D)_{OC}}{\left| \dot{Q}_{e,DSC} \left(1 - \frac{T_0}{T_{b,DSC}} \right) \right|}$ (eq. (4.33)) which is proportional to $\dot{E}_{D, Total}$ and reciprocal to $\left| \dot{Q}_{e,DSC} \left(1 - \frac{T_0}{T_{b,DSC}} \right) \right|$. Hence EDR decreases, attaining a minimum value afterwards increases with increase in DOS

(ΔT_{sc}). It can also be noticed that the values of $\dot{E}_{D, Total}$ and EDR are minimum for R134a and maximum for R1234yf.

4.4.1.2 EFFECT OF EVAPORATOR TEMPERATURE

The effect of evaporator1 temperature ($T_{e, DSC}$) on various performance parameters viz. compressor work (\dot{W}_C), DOS (ΔT_{sc}), COP, exergetic efficiency (η_{ex}), total exergy destruction rate ($\dot{E}_{D, Total}$) and EDR has been shown in Fig. 4.8 to 4.11.

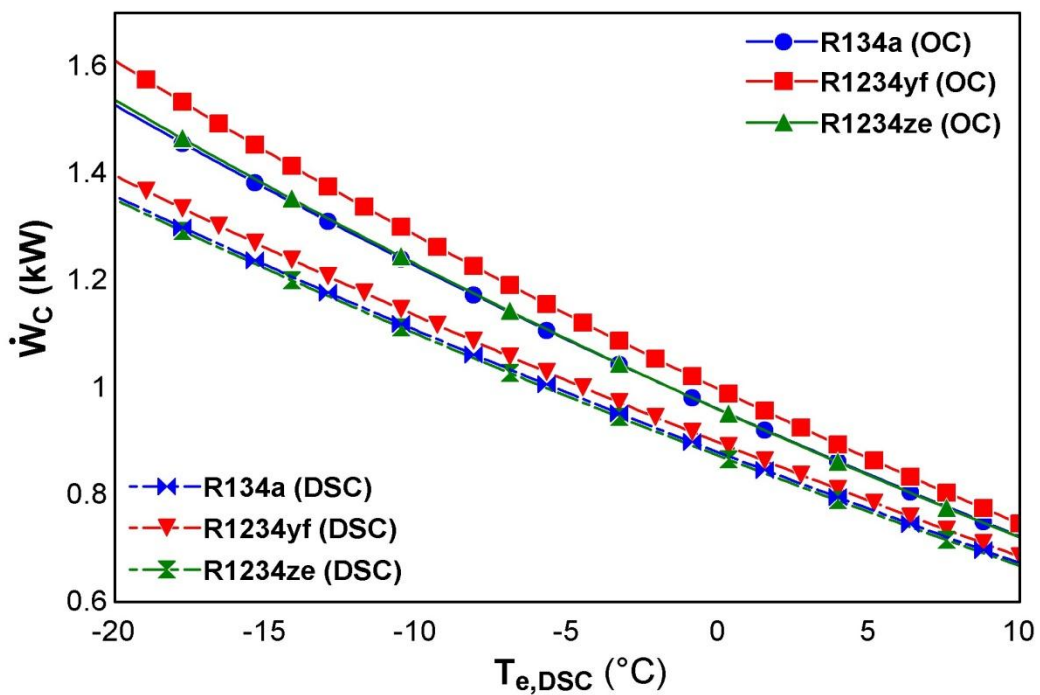


Fig. 4.8 Variation in compressor work (\dot{W}_C) with evaporator1 temperature ($T_{e, DSC}$)

Fig.4.8 shows the variation in compressor work (\dot{W}_C) with evaporator1 temperature ($T_{e, DSC}$) for dedicated mechanically subcooled and overall VCR system. The compressor work of DSC (\dot{W}_{Comp1}) and OC ($\dot{W}_{Comp1} + \dot{W}_{Comp2}$) decreases with increase in evaporator1 temperature ($T_{e, DSC}$) for refrigerants considered. As the evaporator1 temperature increases, the pressure ratio between evaporator and condenser decreases and for constant refrigeration load of 3.5167 kW, the mass flow rate of refrigerant also decreases. Moreover, the evaporator2 temperature of sub-cooler cycle also increases. Hence the compressor work of DSC and OC decreases with increase in

evaporator1 temperature. It has been noticed that the value of compressor work is minimum for R1234ze and maximum for R1234yf.

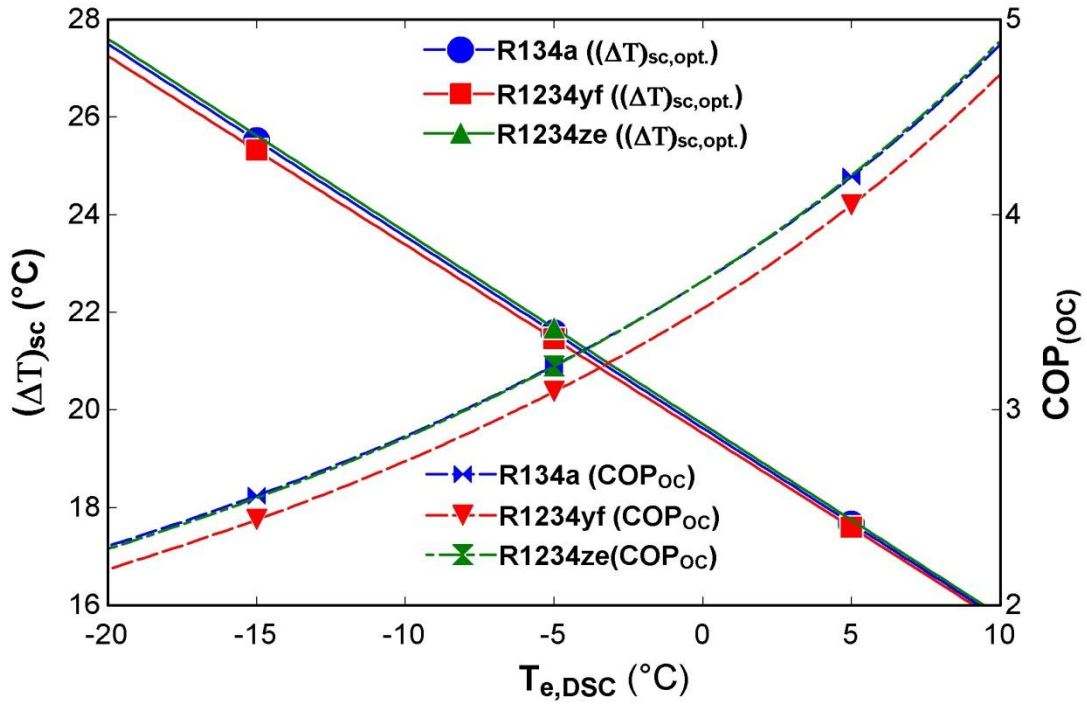


Fig. 4.9 Effect of evaporator1 temperature ($T_{e,DSC}$) on degree of subcooling (ΔT_{sc}) and COP

Fig. 4.9 illustrates the effect of evaporator1 temperature ($T_{e,DSC}$) on DOS (ΔT_{sc}) and COP for OC. The value of DOS decreases and COP increases with increase in evaporator1 temperature for the refrigerant considered. For the constant refrigeration load of 3.5167kW, lower amount of sub-cooling is required in the sub-cooler to the refrigerant of DSC. Thus, the value of DOS decreases with increase in $T_{e,DSC}$. However, the compressor work decreases as shown in Fig. 4.8, the value of COP increases. It has been observed that the value of DOS and COP are maximum for R1234ze and minimum for R1234yf.

Fig. 4.10 depicts the effect of evaporator1 temperature ($T_{e,DSC}$) on exergetic efficiency (η_{ex}) of OC for considered refrigerants. The exergetic efficiency is given by $COP_{(OC)} \times \left| \left(1 - \frac{T_0}{T_{b,DSC}} \right) \right|$ in which the value of $COP_{(OC)}$ increases (Fig. 4.9) and the value of term $\left| \left(1 - \frac{T_0}{T_{b,DSC}} \right) \right|$ decreases with increase in evaporator1 temperature as (T_b ,

DSC $-T_{e, DSC} = 5^{\circ}\text{C}$). Hence, the value of $\eta_{ex(OC)}$ decreases with increase in evaporator1 temperature. It has been noticed that the value of $\eta_{ex(OC)}$ is maximum for R134a and minimum for R1234yf.

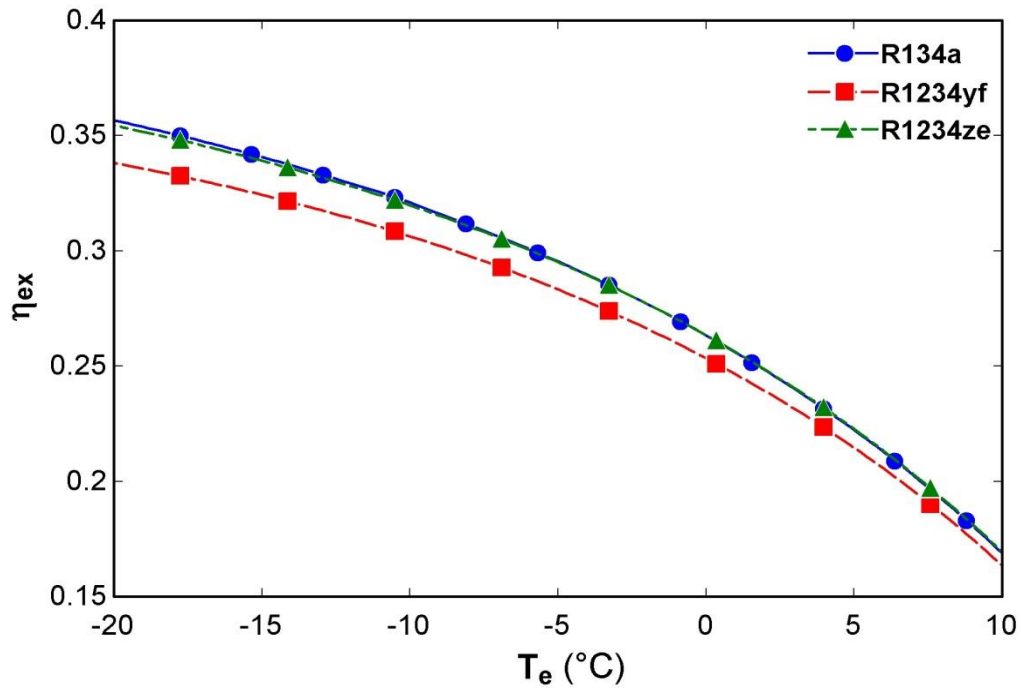


Fig. 4.10 Variation in exergy efficiency (η_{ex}) with evaporator1 temperature ($T_{e, DSC}$) of overall cycle (OC)

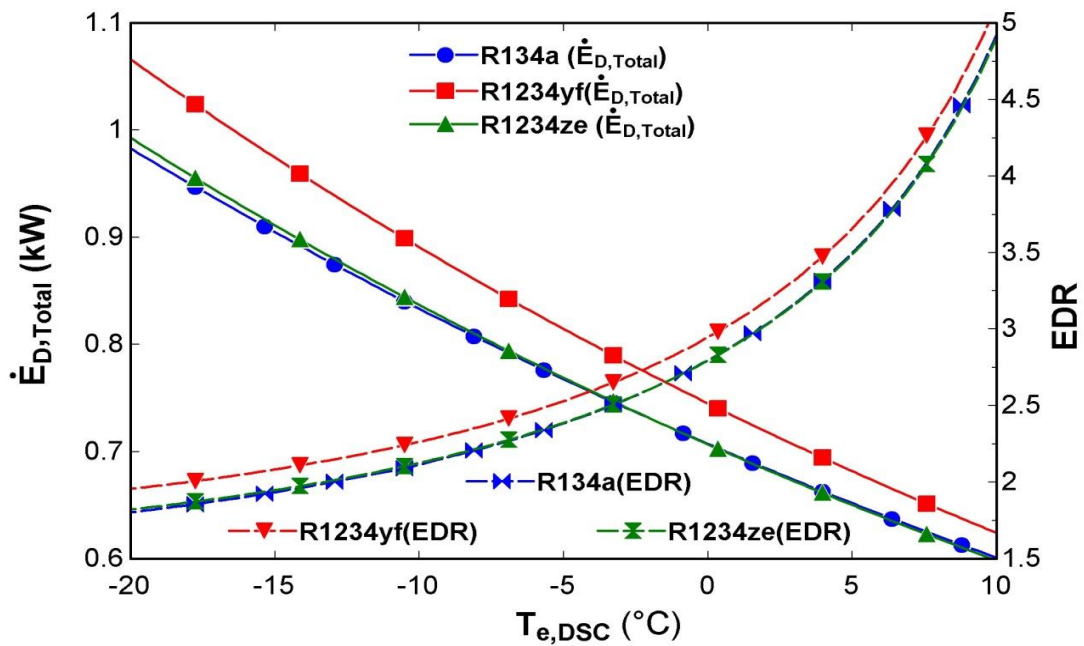


Fig. 4.11 Variation in total exergy destruction rate ($\dot{E}_{D, Total}$) and exergy destruction ratio (EDR) with evaporator1 temperature ($T_{e, DSC}$) of overall cycle (OC)

Fig. 4.11 illustrates the variation in total exergy destruction rate ($\dot{E}_{D, Total}$) and exergy destruction ratio (EDR) with evaporator1 temperature ($T_{e, DSC}$) of OC. The value of $\dot{E}_{D, Total}$ and EDR decreases with increase in $T_{e, DSC}$ for refrigerant considered. It has been noticed that the value of $\dot{E}_{D, Total}$ and EDR are minimum for R1234ze and maximum for R1234yf. As the exergetic efficiency decreases with increase in evaporator1 temperature (Fig. 4.10), the rate of exergy recovered of system component decreases. By which the $\dot{E}_{D, Total}$ decreases with increase in $T_{e, DSC}$. However, the exergy of product decreases with increase in $T_{e, DSC}$ because the term $\left| \left(1 - \frac{T_0}{T_{b,DSC}} \right) \right|$ decreases due to which the EDR of the overall cycle.

4.4.1.3 EFFECT OF TEMPERATURE OF CONDENSER

The effect of condenser1,2 temperature ($T_{c, DSC} = T_{c, SC}$) on various performance parameters viz. compressor work (\dot{W}_C), COP, exergetic efficiency (η_{ex}), exergy destruction ratio (EDR) and total exergy destruction rate ($\dot{E}_{D, Total}$) has been depicted in Fig. 4.12 to 4.15.

Fig. 4.12 illustrates the effect of condenser1,2 temperature ($T_{c, DSC} = T_{c, SC}$) on compressor work ($\dot{W}_{C,SVCR}, \dot{W}_{Comp1}, \dot{W}_{Comp2}$ and $(\dot{W}_{Comp1} + \dot{W}_{Comp2})$) of simple vapour compression refrigeration cycle (SVCR), DSC, SC and OC for refrigerants considered.

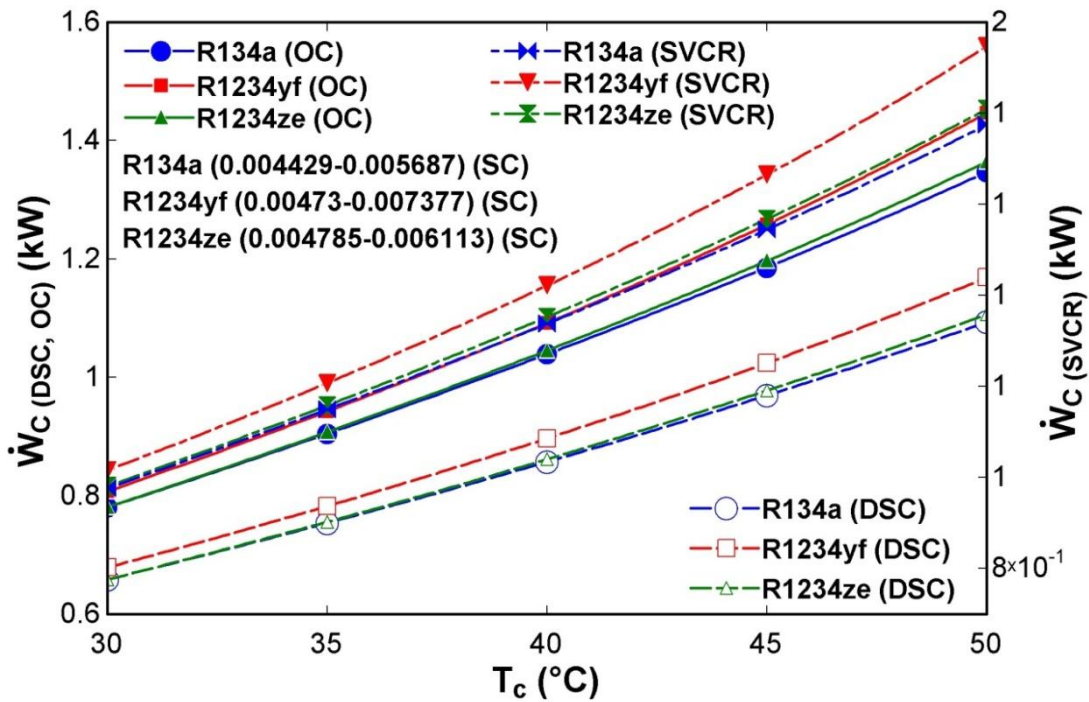


Fig. 4.12 Variation in compressor work of simple vapour compression refrigeration cycle (SVCR), DSC, SC and OC ($\dot{W}_{C,SVCR}$, \dot{W}_{Comp1} , \dot{W}_{Comp2} and $(\dot{W}_{Comp1} + \dot{W}_{Comp2})$) with condenser1,2 temperature ($T_{c,DSC} = T_{c,SC}$)

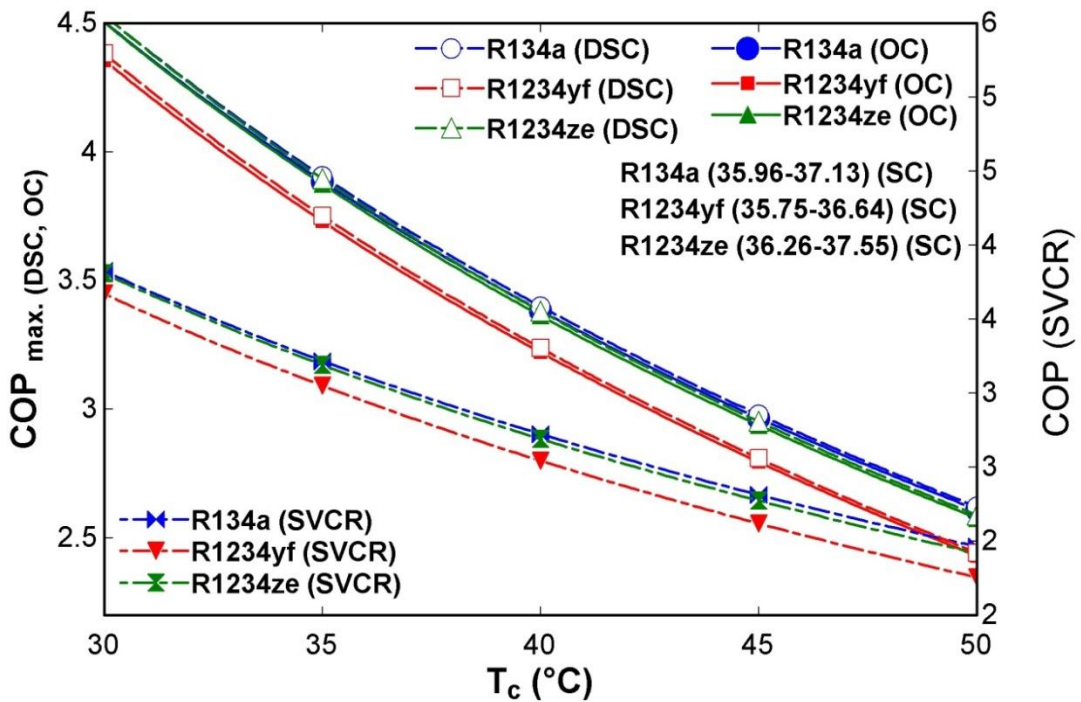


Fig. 4.13 Effect of condenser1,2 temperature on COP of DSC, OC, SC and SVCR cycle ($T_{c,DSC} = T_{c,SC}$)

The values of compressor work increases with increase in temperature of condenser. As the temperature of condenser increases, the pressure ratio between evaporator and condenser increases for which more work has been done by the compressor. Therefore, the value of \dot{W}_C increases with increase in T_c . It has been noticed that the value of \dot{W}_C is minimum for R1234ze and maximum for R1234yf in DSC, OC and SVCR.

Fig. 4.13 shows the effect of condenser1,2 temperature ($T_{c, DSC} = T_{c, SC}$) on COP of DSC, OC, SC and SVCR for considered refrigerants. The COP of DSC, OC and SVCR decreases with increase in $T_{c, DSC} = T_{c, SC}$. This is due to that for constant refrigeration load of 3.5167kW, the compressor work increases with increase in temperature of condenser. Thus the COP of DSC, OC and SVCR decreases with increase in temperature of condenser. However, the COP of sub-cooler VCR cycle (SC) increases with increase in temperature of condenser. The rate of heat of heat transfer to evaporator2 increases in the sub-cooler, consequently the refrigeration load of sub-cooler cycle increases and hence COP of sub-cooler cycle increases with increase in temperature of condenser. It has also been seen that the COP is maximum for R1234ze and minimum for R1234yf.

Fig. 4.14 presents the variation in exergy efficiency (η_{ex}) with temperature of condenser ($T_{c, DSC} = T_{c, SC}$) of DSC, OC and SVCR cycles for considered refrigerants. The value of η_{ex} decreases with increase in $T_{c, DSC} = T_{c, SC}$. Exergetic efficiency is given by the relation, $\eta_{ex} = COP \times \left| \left(1 - \frac{T_0}{T_b} \right) \right|$ in which the term $\left| \left(1 - \frac{T_0}{T_b} \right) \right|$ remains constant and the value of COP decreases with increase in temperature of condenser. Hence the value of η_{ex} decreases with increase in $T_{c, DSC} = T_{c, SC}$. It can also be noticed that the value of η_{ex} is maximum for R1234ze and minimum for R1234yf.

Fig. 4.15 depicts the effect of temperature of condenser ($T_{c, DSC} = T_{c, SC}$) on total exergy destruction rate ($\dot{E}_{D, Total}$) and EDR of DSC, OC and SVCR cycles. The value of $\dot{E}_{D, Total}$ and EDR increases with increase in $T_{c, DSC} = T_{c, SC}$. As the temperature of condenser increases, the exergy destruction rate in system components increases as well as the exergy of products $\left(\left| \dot{Q}_{e, DSC} \left(1 - \frac{T_0}{T_{b, DSC}} \right) \right| \right)$ decreases because the value of COP decreases (Fig. 4.13).

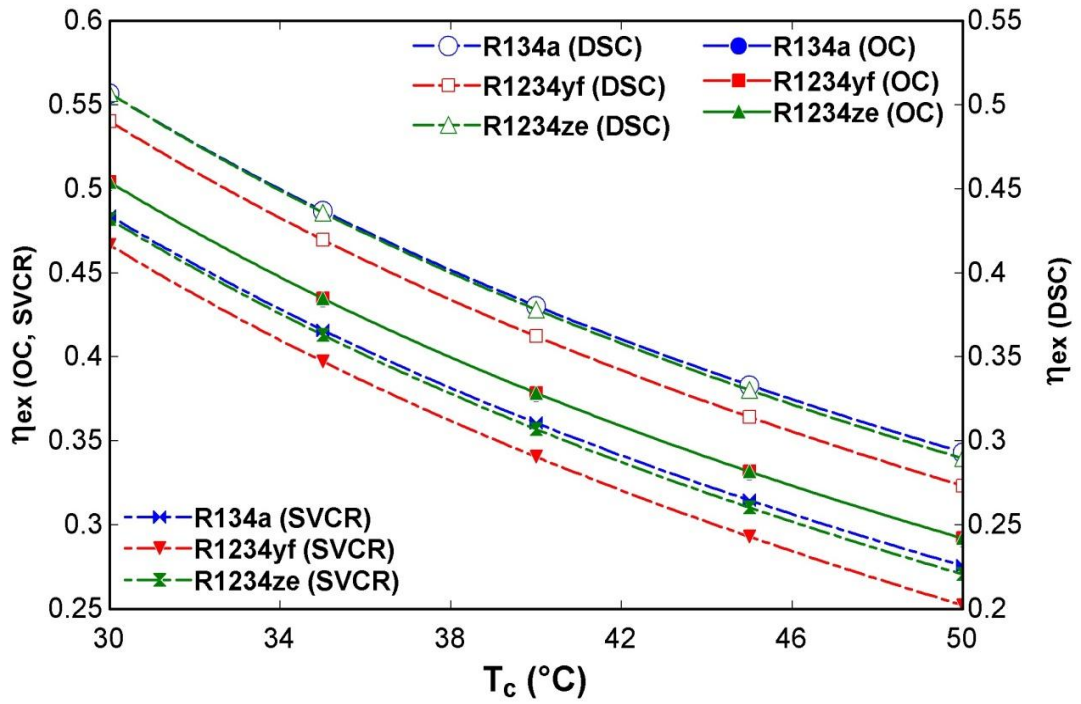


Fig. 4.14 Effect of temperature of condenser (T_c) on exergetic efficiency (η_{ex})

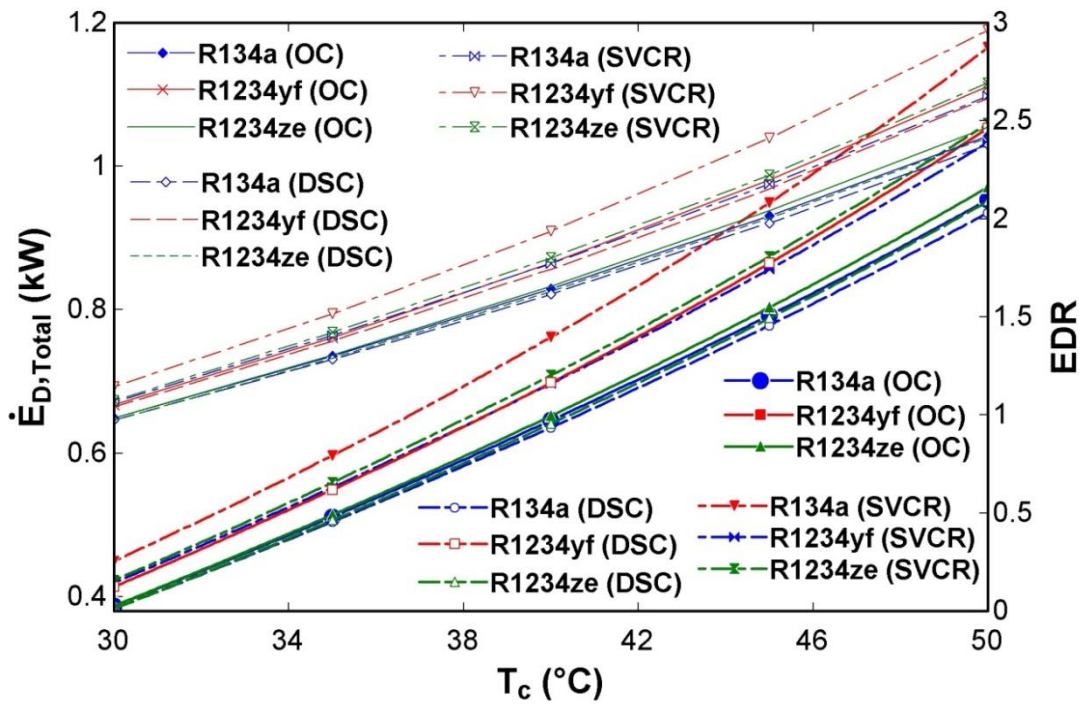


Fig. 4.15 Variation in total exergy destruction rate ($\dot{E}_{D, Total}$) and exergy destruction ratio (EDR) with condenser temperature (T_c)

Hence, the total exergy destruction rate and EDR increases with increase in T_c , $DSC = T_c, SC$. It has been seen that the value of $\dot{E}_{D, Total}$ and EDR is minimum for R134a and maximum for R1234yf.

4.4.1.4 EFFECT OF COMPRESSOR EFFICIENCY

The effect of isentropic efficiency of compressor_{1,2} ($\eta_{comp,1}, \eta_{comp,2}$) on various performance parameters viz. compressor work (\dot{W}_C), COP_{max} , exergetic efficiency (η_{ex}), total exergy destruction rate ($\dot{E}_{D, Total}$) and exergy destruction ratio (EDR) for the considered refrigerants R1234ze, R1234yf and R134a has been shown in Fig. 4.16 to 4.20.

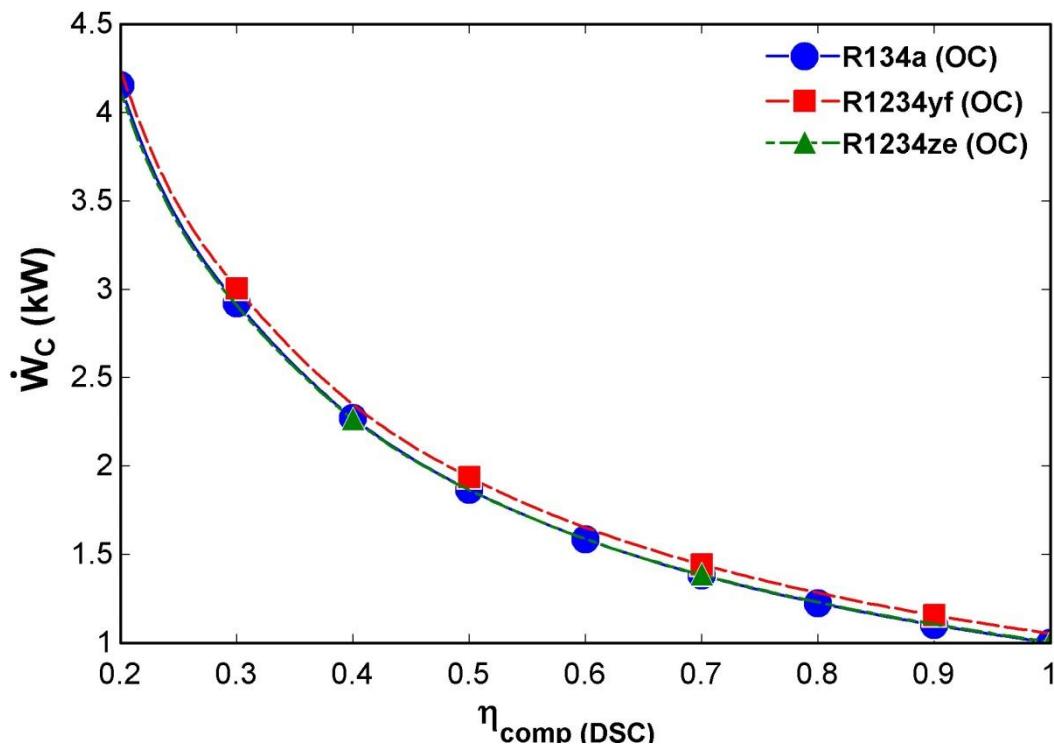


Fig. 4.16 Variation in compressor work (\dot{W}_C) of DSC, OC, SC and SVCR system with isentropic efficiency of compressor (η_{comp})

Fig. 4.16 shows that the effect of isentropic efficiency of compressor_{1,2} ($\eta_{comp,1}$ & $\eta_{comp,2}$) on compressor work (\dot{W}_C) of DSC, OC, SC and SVCR system for the refrigerants considered. The values of \dot{W}_C decreases with increase in $\eta_{comp,1}$, $\eta_{comp,2}$ for DSC, OC, SC and SVCR cycle. The isentropic efficiency of the compressor is isentropic work done divided by the actual work done. The actual work done of compressor decreases with

increase in isentropic efficiency operating between same evaporator and condenser lines. Hence, The actual work done of DSC, OC, SC and SVCR cycles (\dot{W}_{comp1} , $\dot{W}_{comp1}+\dot{W}_{comp2}$, \dot{W}_{comp2} and \dot{W}_{comp}) decreases with increase in isentropic efficiency of compressor1, 2 ($\eta_{comp,1}$, $\eta_{comp,2}$). It has been noticed that the value of \dot{W}_C is minimum for R1234ze and maximum for R1234yf.

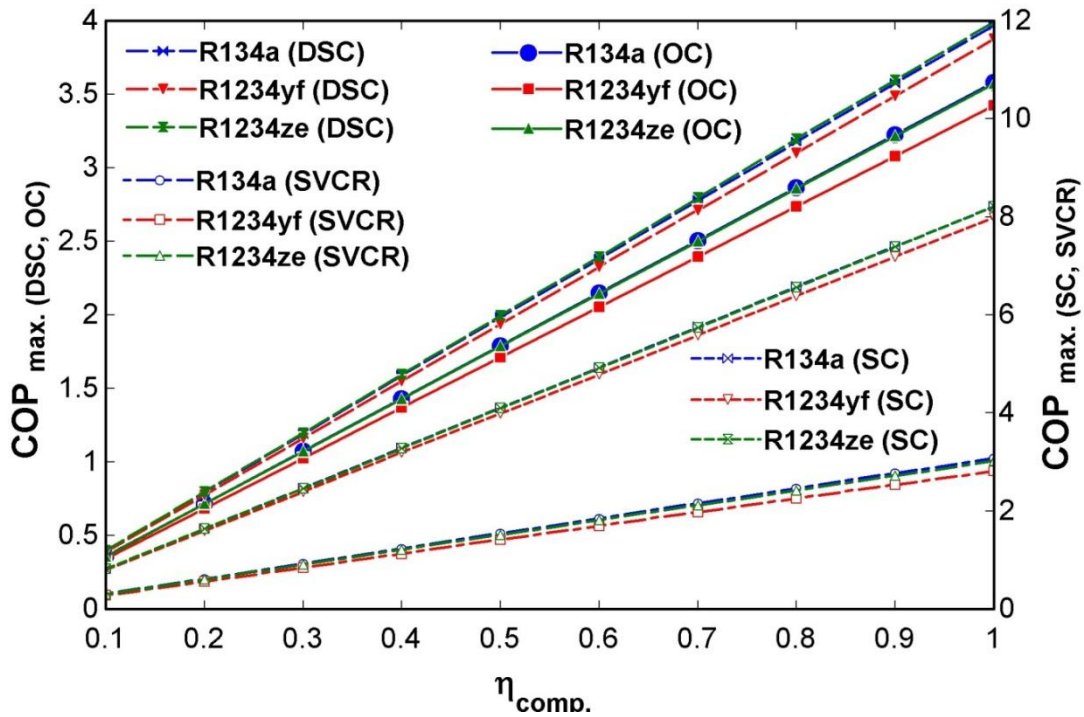


Fig. 4.17 Effect of isentropic efficiency of compressor (η_{comp}) on COP_{max} .

Fig. 4.17 shows the effect of isentropic efficiency of compressor1, 2 ($\eta_{comp,1}, \eta_{comp,2}$) on maximum COP (COP_{max}) for OC, DSC, SC and SVCR cycle. The value of COP_{max} increases with increase in $\eta_{comp,1}, \eta_{comp,2}$. For the constant refrigerating load $\dot{Q}_{e,DSC} = 3.5167kW$, the compressor work of compressor1, 2 decreases with increase in $\eta_{comp,1}, \eta_{comp,2}$ (Fig. 4.16). Hence the value of COP_{max} increases with increase in $\eta_{comp,1}, \eta_{comp,2}$.

It has also been noticed that the value of COP_{max} for OC, DSC and SC is higher than that of SVCR cycle. The maximum and minimum value of COP_{max} is for R1234ze and R1234yf.

Fig. 4.18 shows the effect of isentropic efficiency of compressor1, 2 ($\eta_{comp,1}, \eta_{comp,2}$) on exergetic efficiency (η_{ex}) for OC, DSC and SVCR cycle. The

exergetic efficiency increases with increase in $\eta_{\text{comp},1}, \eta_{\text{comp},2}$. The exergetic efficiency of OC and DSC are given by $\eta_{\text{ex}}(\text{OC}) = \frac{|\dot{Q}_{e,\text{DSC}}(1 - \frac{T_0}{T_{b,\text{DSC}}})|}{\dot{W}_{\text{comp},1} + \dot{W}_{\text{comp},2}}$ (Eq. 4.29) and $\eta_{\text{ex}}(\text{DSC}) = \frac{|\dot{Q}_{e,\text{DSC}}(1 - \frac{T_0}{T_{b,\text{DSC}}})|}{\dot{W}_{\text{comp},1}}$ (Eq. 4.27). In which, the term $|\dot{Q}_{e,\text{DSC}}(1 - \frac{T_0}{T_{b,\text{DSC}}})|$ remains constant and the compressor work $\dot{W}_{\text{comp},1}$ and $\dot{W}_{\text{comp},2}$ decrease with increase in $\eta_{\text{comp},1}, \eta_{\text{comp},2}$. Thus the value of η_{ex} increases with increase in $\eta_{\text{comp},1}, \eta_{\text{comp},2}$ for refrigerants considered. It has also been noticed that the exergetic efficiency of DSC and OC are higher than that of SVCR cycle. The maximum and minimum value of η_{ex} is for R1234ze and R1234yf respectively.

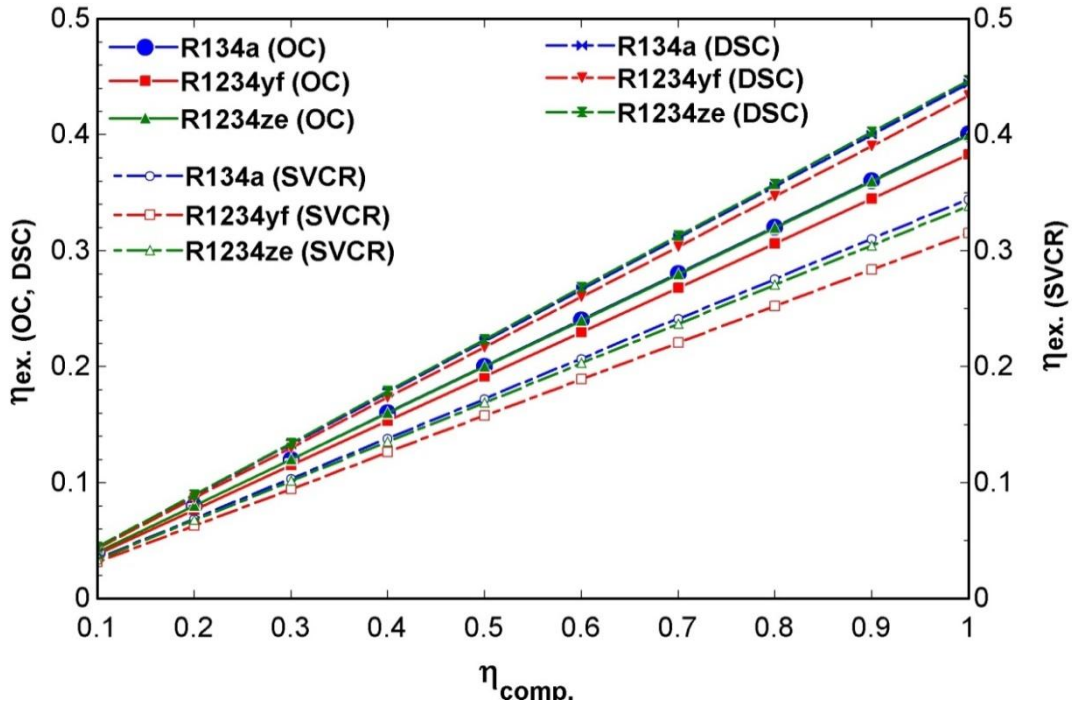


Fig. 4.18 Variation in exergetic efficiency (η_{ex}) with isentropic efficiency of compressor (η_{comp})

Fig. 4.19 illustrates the variation in total exergy destruction rate ($\dot{E}_{D, \text{Total}}$) with isentropic efficiency of compressor1, 2 ($\eta_{\text{comp},1}, \eta_{\text{comp},2}$). The value of $\dot{E}_{D, \text{Total}}$ decreases with increase in $\eta_{\text{comp},1}, \eta_{\text{comp},2}$ for OC, DSC, SC and SVCR cycle. The exergy recovered from the system components increases with increase in $\eta_{\text{comp},1}, \eta_{\text{comp},2}$ (Fig. 4.18).

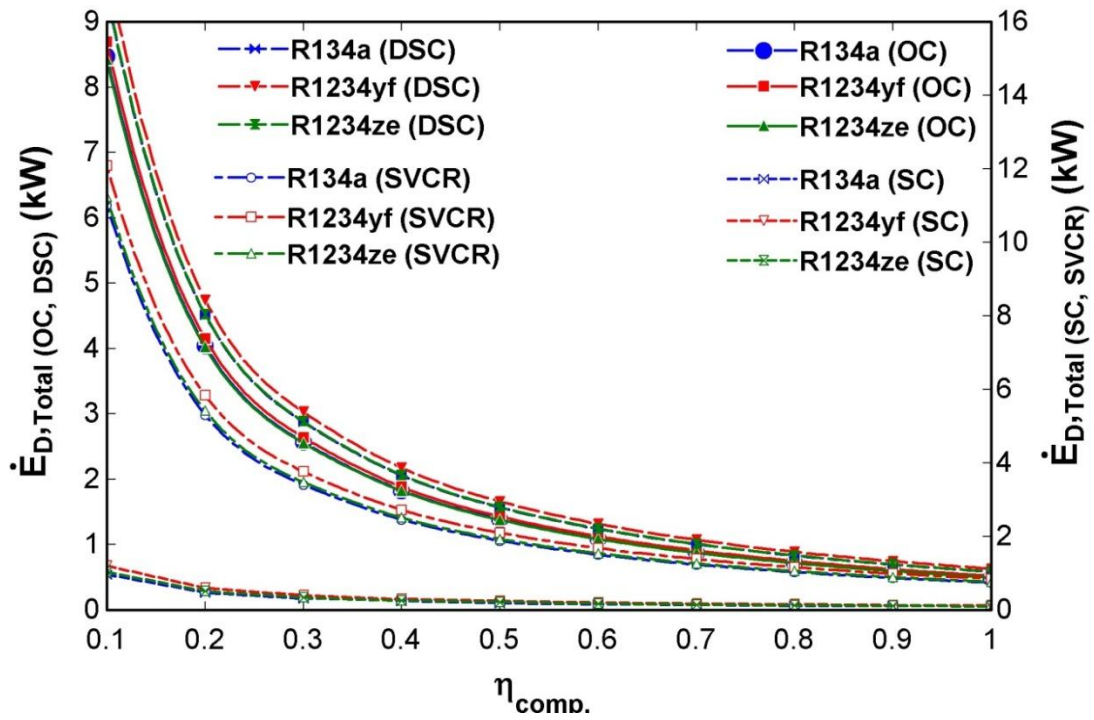


Fig. 4.19 Effect of isentropic efficiency of compressor ($\eta_{comp.}$) on total exergy destruction rate ($\dot{E}_{D, Total}$)

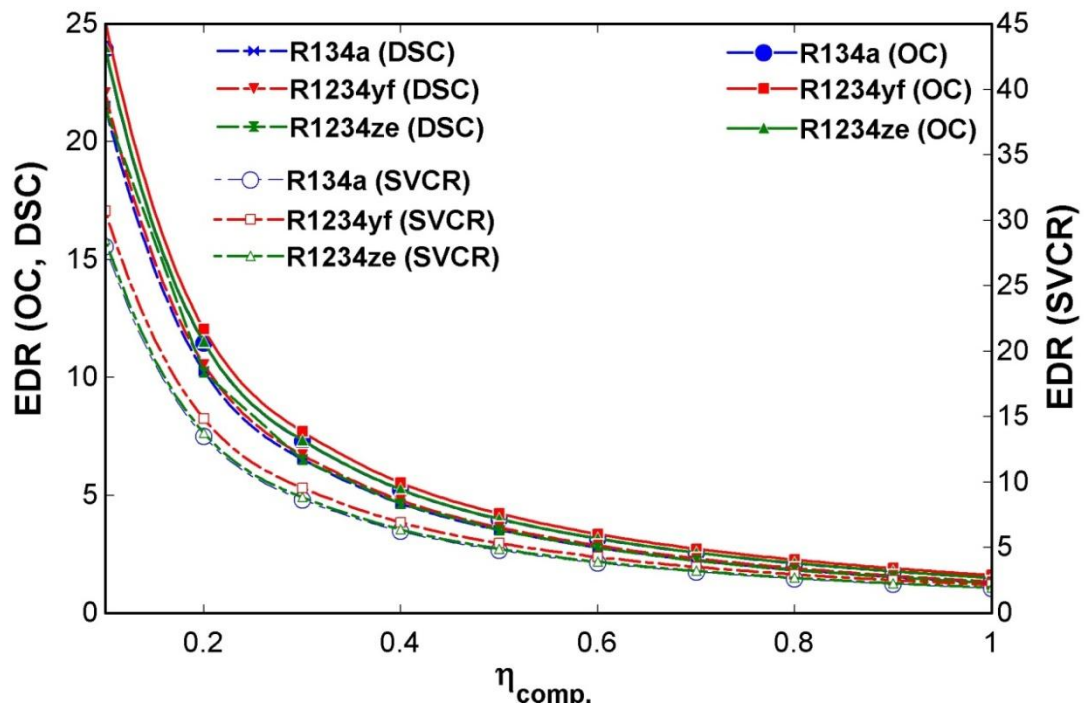


Fig. 4.20 Effect of isentropic efficiency of compressor ($\eta_{comp.}$) on EDR

The exergy destruction rate of components of the system decreases with increase in $\eta_{\text{comp.1}}, \eta_{\text{comp.2}}$. Therefore, the $\dot{E}_{D, \text{Total}}$ decreases with increase in $\eta_{\text{comp.1}}, \eta_{\text{comp.2}}$. It has been noticed that the value of $\dot{E}_{D, \text{Total}}$ of OC and DSC is lower than that of SVCR cycle. The minimum and maximum value of $\dot{E}_{D, \text{Total}}$ is for R1234yf and R1234ze respectively.

Fig. 4.20 depicts the effect of isentropic efficiency of compressor1,2 ($\eta_{\text{comp.1}}, \eta_{\text{comp.2}}$) on exergy destruction ratio (EDR) for refrigerants considered. The EDR of OC, DSC and SVCR cycle decreases with increase in $\eta_{\text{comp.1}}, \eta_{\text{comp.2}}$. EDR is given by $\frac{\Sigma(\dot{E}_D)_{\text{OC}}}{\left| \dot{Q}_{e,\text{DSC}} \left(1 - \frac{T_0}{T_{b,\text{DSC}}} \right) \right|}$ (Eq.(4.42)) which is proportional to $\dot{E}_{D, \text{Total}}$. The value of $\dot{E}_{D, \text{Total}}$ increases and the term $\left| \dot{Q}_{e,\text{DSC}} \left(1 - \frac{T_0}{T_{b,\text{DSC}}} \right) \right|$ remains constant with increase in $\eta_{\text{comp.1}}, \eta_{\text{comp.2}}$ (Fig. (4.18)). Hence, the value of EDR decreases with increase in $\eta_{\text{comp.1}}, \eta_{\text{comp.2}}$ for refrigerants considered. It has also been noticed that the EDR of OC and DSC is lower than that of SVCR cycle. The minimum and maximum value of EDR is for R1234ze and R1234yf.

4.4.1.5 EFFECT OF SUBCOOLER EFFECTIVENESS

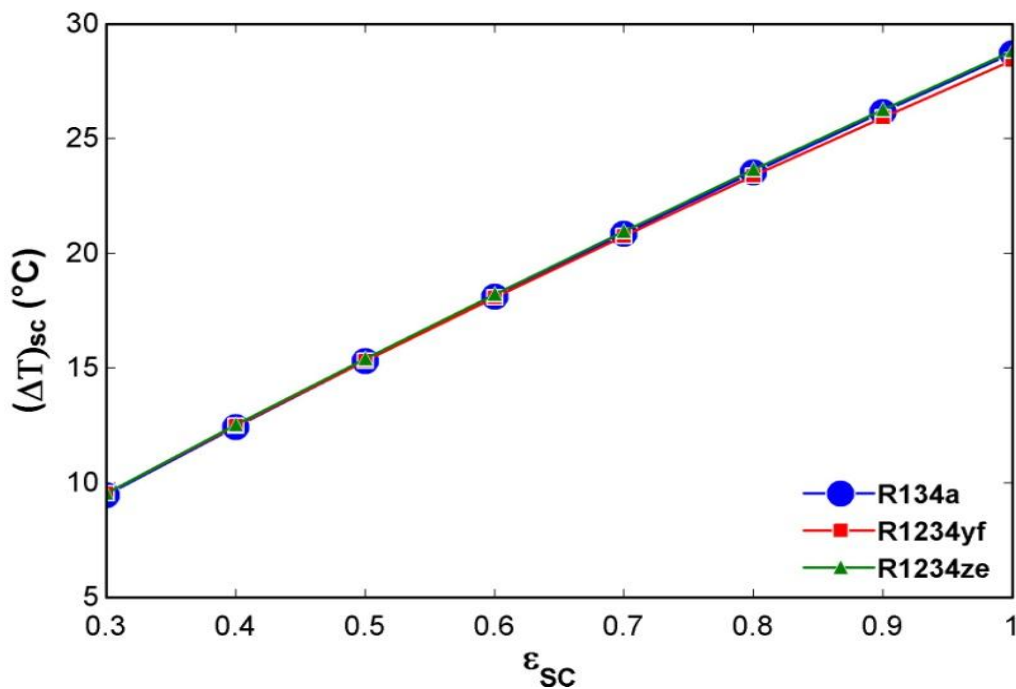


Fig. 4.21 Effect of effectiveness of subcooler (ϵ_{sc}) on degree of subcooling $(\Delta T)_{sc}$

Fig. 4.21 to 4.25 depict the variation in various performance parameters viz. degree of subcooling (ΔT_{sc}), compressor work (\dot{W}_C), $COP_{max.}$, EDR, total exergy destruction rate ($\dot{E}_{D, Total}$) and exergetic efficiency (η_{ex}) with subcooler effectiveness for the refrigerants considered R1234ze, R1234yf and R134a.

Fig. 4.21 shows that the effect of effectiveness of subcooler (ϵ_{SC}) on degree of subcooling (ΔT_{sc}). The degree of subcooling increases with increase in effectiveness of subcooler. The effectiveness is given by $\epsilon_{SC} = \frac{T_3 - T_{3a}}{T_3 - T_8}$ (Eq. 4.10). Where degree of subcooling is $T_3 - T_{3a}$. Which is directly proportional to the ϵ_{SC} . Hence the value of (ΔT_{sc}) increases with increase in subcooler effectiveness. It has also been noticed that the maximum value of DOS (28.84) is for R1234ze However, the minimum value (9.48) is for R134a.

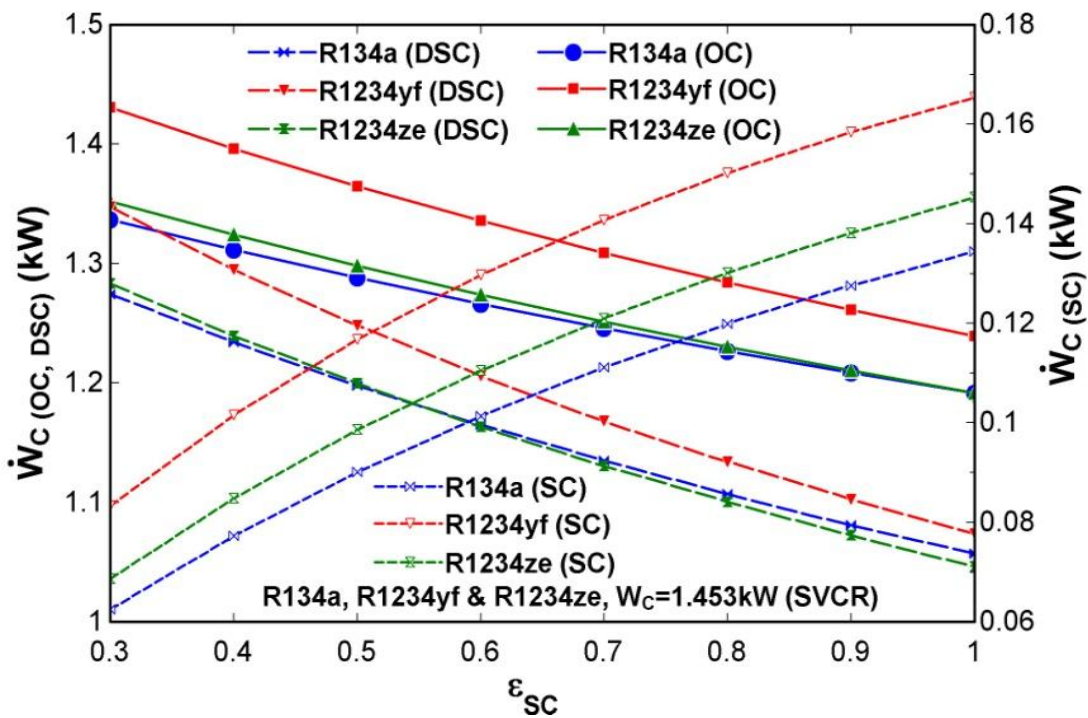


Fig. 4.22 Variation in compressor work (\dot{W}_C) with effectiveness of subcooler (ϵ_{SC})

Fig. 4.22 illustrates the variation of compressor work (\dot{W}_C) with effectiveness of subcooler (ϵ_{SC}) for DSC, OC, SC and SVCR. The value of (\dot{W}_C) decreases with increase in effectiveness of subcooler for DSC and OC. However, compressor work increases with increase in (ϵ_{SC}) for subcooler cycle. For the refrigerating load $\dot{Q}_{e,DSC} =$

3.5167kW, the rate of mass flow of refrigerant decreases with increase in $(\Delta T)_{sc}$ and the value of $(\Delta T)_{sc}$ increases with increase in (ϵ_{SC}) . Therefore the compressor work of DSC and OC decreases for constant value of $T_{e,DSC}$ and $T_{c,DSC}$ with increase in effectiveness of subcooler. However, the cooling load of subcooler cycle increases with increase in DOS $((\Delta T)_{sc})$. By which the rate of mass flow of refrigerant increases with increase in effectiveness of subcooler. Hence, the compressor work of subcooler cycle (SC) increases with increase in ϵ_{SC} . It has been noticed that the maximum compressor work of DSC and OC is less than that of simple VCR (SVCR). The maximum value compressor work is for R1234yf and minimum for R1234ze in DSC and OC.

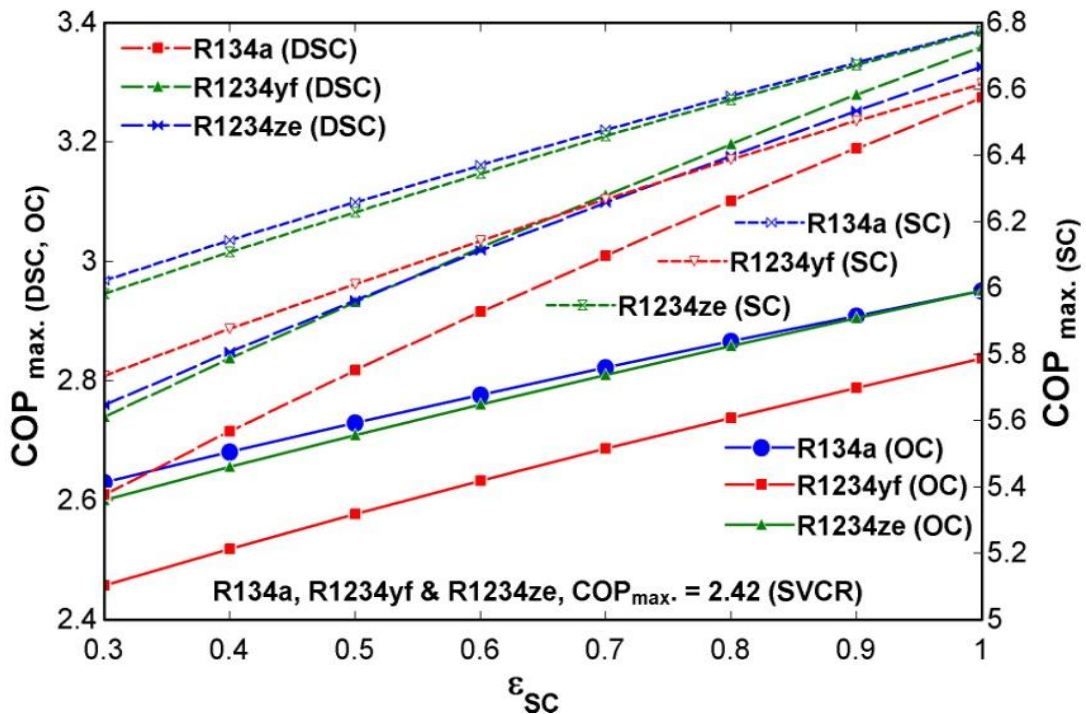


Fig. 4.23 Variation in $COP_{max.}$ with effectiveness of subcooler (ϵ_{SC})

Fig. 4.23 depicts the variation of maximum COP ($COP_{max.}$) with effectiveness of subcooler (ϵ_{SC}). The value of $COP_{max.}$ increases with increase in effectiveness of subcooler. For the constant refrigerant load $\dot{Q}_{e,DSC} = 3.5167kW$, the compressor work decreases with increase in ϵ_{SC} (Fig. 4.21, 4.22). Thus, the maximum value of COP increases with increase in ϵ_{SC} for DSC and OC. However, the cooling load of SC increases with increase in ϵ_{SC} . Thus the value of $COP_{max.}$ of SC increases with increase

in ϵ_{SC} . It has been noticed that the value of COP_{max} is higher for DSC, OC and SC than that of SVCR. The value of COP_{max} is maximum for R1234ze and minimum for R1234yf.

Fig. 4.24 depicts the effect of effectiveness of subcooler (ϵ_{SC}) on exergetic efficiency (η_{ex}). The value of η_{ex} increases with increase in ϵ_{SC} for DSC and OC and remains constant in SVCR for the refrigerants considered.

The exergetic efficiency of OC and DSC are given by $\eta_{ex(OC)} = \frac{|\dot{Q}_{e,DSC}(1 - \frac{T_0}{T_{b,DSC}})|}{\dot{W}_{comp1} + \dot{W}_{comp2}}$ (Eq. 4.29) and $\eta_{ex(DSC)} = \frac{|\dot{Q}_{e,DSC}(1 - \frac{T_0}{T_{b,DSC}})|}{\dot{W}_{comp1}}$ (Eq. 4.27). In which the term $|\dot{Q}_{e,DSC}(1 - \frac{T_0}{T_{b,DSC}})|$ is constant and compressor works \dot{W}_{comp1} decreases and \dot{W}_{comp2} increases with increase in effectiveness of subcooler (Fig. 4.21). However, the increase in \dot{W}_{comp2} is very less as compared to the values of \dot{W}_{comp1} . Thus the exergetic efficiency of DSC and OC increases with increase in ϵ_{SC} . It has been noticed that the value of η_{ex} of DSC and OC is more than that of simple VCR cycle. The maximum and minimum value of η_{ex} is for R1234ze and R1234yf.

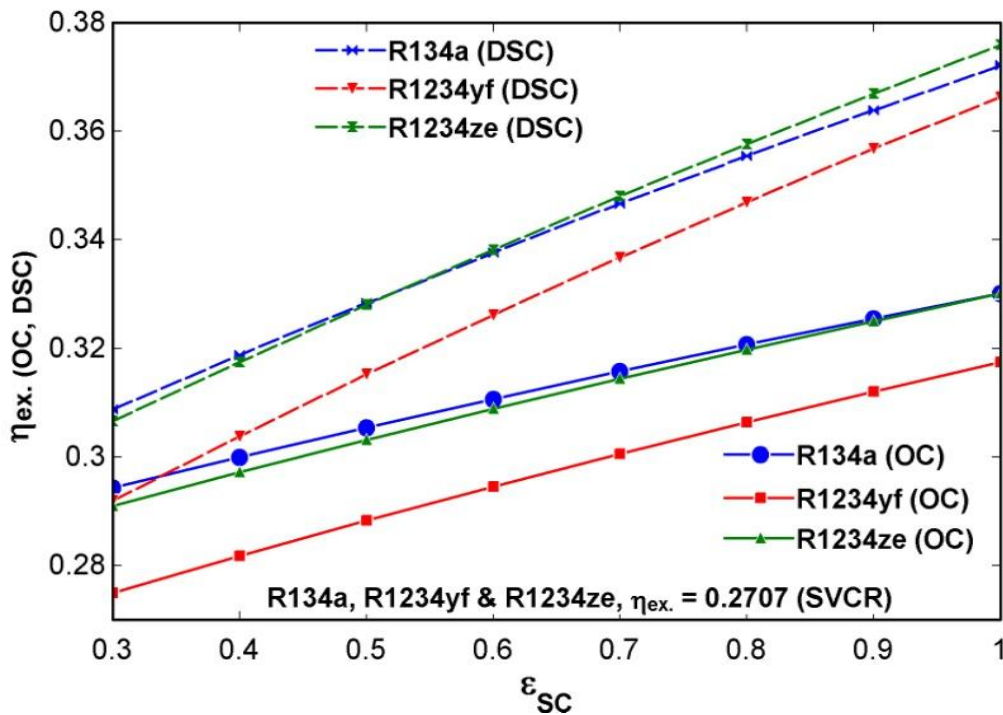


Fig. 4.24 Effect of effectiveness of subcooler (ϵ_{SC}) on exergetic efficiency (η_{ex})

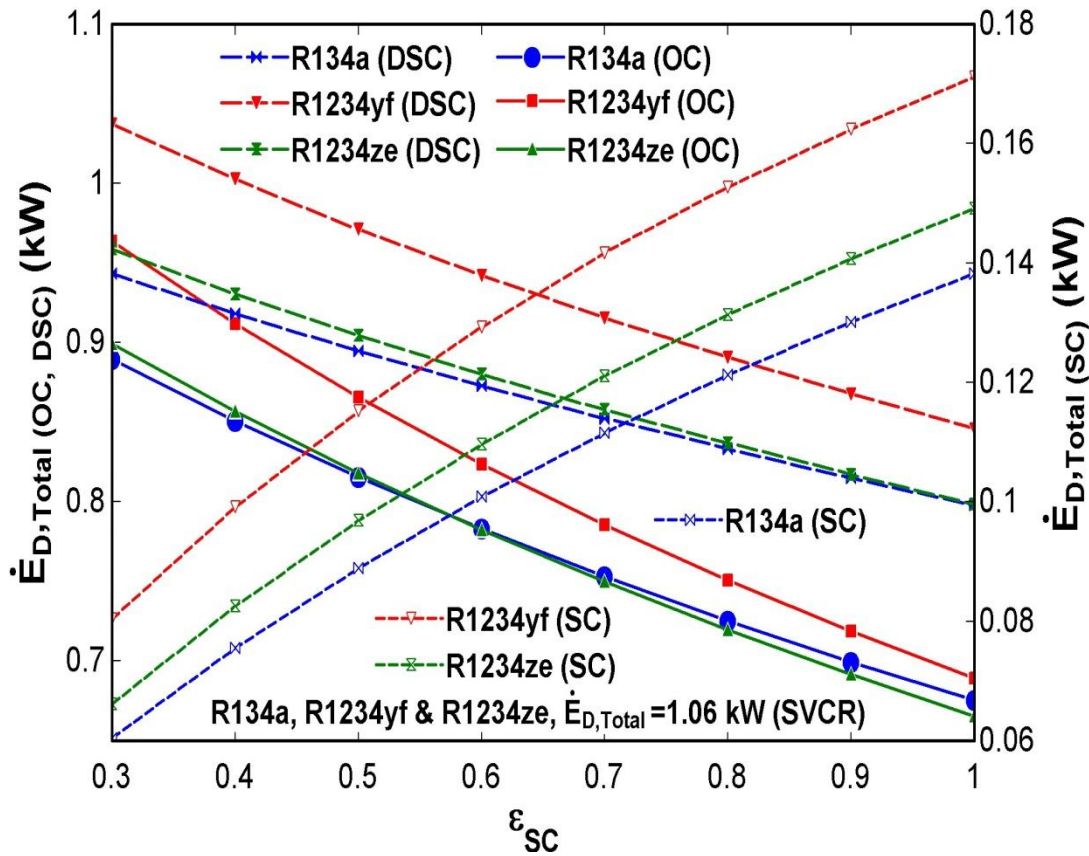


Fig. 4.25 Effect of effectiveness of subcooler (ϵ_{SC}) on $\dot{E}_{D, Total}$

Fig. 4.25 illustrates the effect of effectiveness of subcooler (ϵ_{SC}) on $\dot{E}_{D, Total}$. The value of $\dot{E}_{D, Total}$ decreases with increase in ϵ_{SC} for DSC and OC. However, the value of $\dot{E}_{D, Total}$ increases with increase in ϵ_{SC} for SC. $\dot{E}_{D, Total}$ remains constant for simple VCR cycle. As the exergy recovered from the system components increases with increase in ϵ_{SC} (Fig. 4.24). Therefore, the value of \dot{E}_D in each component of system decreases with increase in ϵ_{SC} which results decrease in $\dot{E}_{D, Total}$ with increase in ϵ_{SC} . However, the amount of heat transfer to the evaporator2 increases with increase in ϵ_{SC} as the degree of subcooling increases with increase in ϵ_{SC} (Fig. 4.21). It has been observed that the value of $\dot{E}_{D, Total}$ in DSC and OC is less than that of simple VCR cycle. The minimum and maximum value of $\dot{E}_{D, Total}$ is for R1234ze and R1234yf in DSC and OC. However, the minimum and maximum value of $\dot{E}_{D, Total}$ is for R134a and R1234yf in SC.

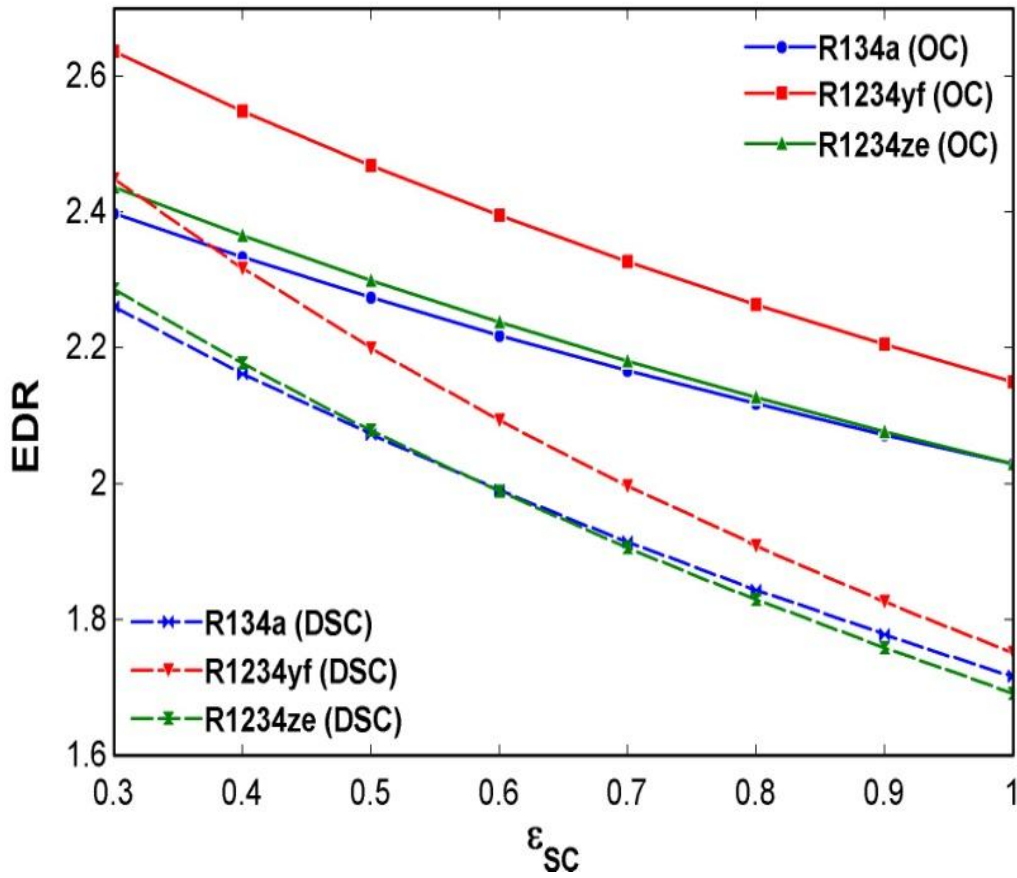


Fig. 4.26 Variation in exergy destruction ratio (EDR) with effectiveness of subcooler (ϵ_{SC})

Fig.4.26 illustrates the variation in exergy destruction ratio (EDR) with effectiveness of subcooler (ϵ_{SC}). The value of EDR in DSC and OC decreases with increase in ϵ_{SC} for refrigerants considered. EDR of DSC and OC are given by

$$\frac{\Sigma(\dot{E}_D)_{DSC}}{\left| \dot{Q}_{e,DSC} \left(1 - \frac{T_0}{T_{b,DSC}} \right) \right|} \quad (\text{Eq. 4.40}) \quad \text{and} \quad \frac{\Sigma(\dot{E}_D)_{OC}}{\left| \dot{Q}_{e,DSC} \left(1 - \frac{T_0}{T_{b,DSC}} \right) \right|} \quad (\text{Eq. 42}).$$

Which is directly proportional to the $\dot{E}_{D, Total}$ and inversely proportional to the $\left| \dot{Q}_{e,DSC} \left(1 - \frac{T_0}{T_{b,DSC}} \right) \right|$ and

the term $\left| \dot{Q}_{e,DSC} \left(1 - \frac{T_0}{T_{b,DSC}} \right) \right|$ remains constant and the value of $\dot{E}_{D, Total}$ decreases with increase in ϵ_{SC} . This results decrease in EDR with increase in ϵ_{SC} . It has been noticed that the minimum and maximum value of EDR is for R1234ze and R1234yf respectively.

4.4.1.6 EXERGETIC EFFICIENCY AND EXERGY DESTRUCTION RATE OF THE COMPONENTS OF SYSTEM

Exergetic efficiency (η_{ex}) and exergy destruction rate (\dot{E}_D) of components of system of simple and DSC VCR cycle have been depicted in Fig. 4.27 and 4.28.

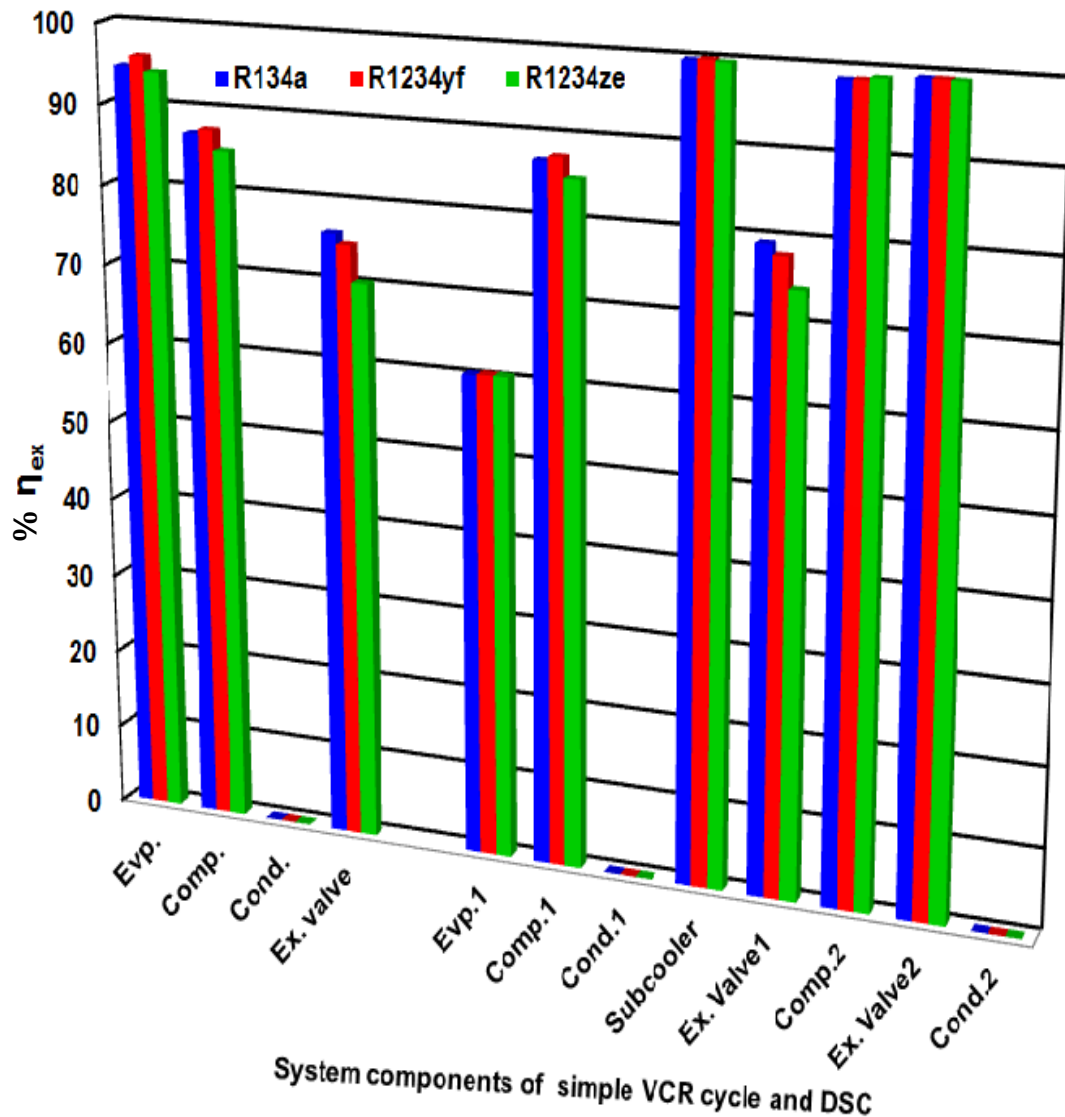


Fig. 4.27 Exergetic efficiency of system components of simple VCR cycle and DSC

Fig. 4.27 shows the exergetic efficiency (η_{ex}) of system components of simple and DSC VCR cycle. Evaporator and condenser of simple VCR cycle are the component of highest and lowest exergetic efficiency respectively. However, subcooler, condenser1,2 of are the site of highest and lowest exergetic efficiency of DSC VCR cycle. The exergetic efficiency of compressor2 and expansion valve2 lie within 99-100% for the considered refrigerants.

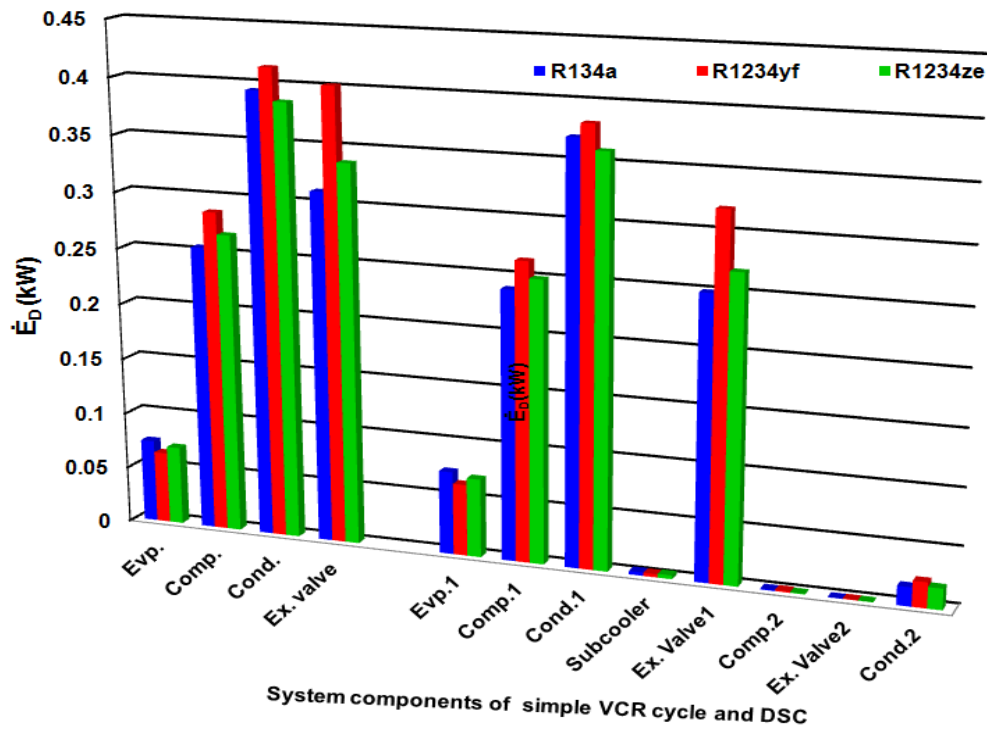


Fig. 4.28 Rate of destruction of exergy of the components of system in simple VCR system and DSC

Fig. 4.28 depicts the rate of destruction of exergy in components of system of simple VCR system and dedicated mechanically subcooled VCR system (DSC). Condenser is the site of SVCR and DSC where the maximum exergy destruction take place. However, evaporator is the place where minimum amount of exergy destruction occurs. In simple VCR system, expansion valve is the site where more exergy destruction occurs in comparison to compressor and evaporator. Similarly, in DSC, expansion valve1 is the second site of exergy destruction after condenser1. However, subcooler, compressor2 and expansion valve2 are the site where very less amount of exergy destruction takes place in comparison to other system components.

4.5 CONCLUSIONS

The current work presents the energy and exergy analysis of dedicated mechanically sub-cooled vapour compression refrigeration cycle (DSC). The comparison of DSC, overall cycle (OC), sub-cooler cycle (SC) and simple vapour compression refrigeration cycle (SVCR) has also been considered for R134a, R1234ya and R1234ze using a computer software based program in EES. The theoretical

performance analysis involves the variation of DOS, temperature of evaporator and x temperature of condenser to examine the performance parameters viz. compressor work, COP, η_{ex} and total \dot{E}_D and EDR. The main concluding points of the current work are as follows:

- The COP of dedicated mechanically sub-cooled VCR cycle (DSC) and overall cycle (OC) is higher than the simple VCR cycle.
- The optimum value of DOS lies between 20⁰C to 25⁰C for which \dot{W}_C , COP and η_{ex} are maximum in OC.
- The COP of OC improves while η_{ex} goes down with increase in evaporator temperature.
- The high condenser temperature reduces the performance (COP and η_{ex}) of the cycle.
- Higher condenser temperature promotes exergy destruction while exergy destruction reduces for lower values of evaporator temperature. The optimum value of DOS lies between 20⁰C to 25⁰C.
- Exergy destruction rate of system components of simple VCR cycle is higher than that of DSC.
- The performance (COP & η_{ex}) of DSC and OC improves with increase in subcooler effectiveness and isentropic efficiency of compressors.
- The higher values of subcooler effectiveness and isentropic efficiency of compressor reduce the the total exergy destruction rate and EDR.
- R1234ze performs better than that of R1234yf and competes with R134a. It can be a good alternate to R134a.
- Condenser1 is the site where the maximum amount of exergy destruction occurs in comparison to other system components.
- Subcooler, condenser2 and expansion valve2 are the components of DSC VCR cycle where maximum amount of exergy has been recovered.
- Subcooler of DSC VCR cycle is the component of highest exergetic efficiency.

Finally, it is inferred that the dedicated mechanically sub-cooled VCR cycle performs better than that of simple VCR cycle and the performance of HFO R1234ze is better than R1234yf. These systems can be used in frozen food, preservation and medical industries.

4.6 COMPARISON BETWEEN LVHE INCORPORATED VCR SYSTEM AND DEDICATED MECHANICALLY SUBCOOLED VCR SYSTEM

- The degree of superheating increases with increase in degree of subcooling of LVHE incorporated VCR system not in case of dedicated mechanically subcooled VCR system.
- Additional compressor work is not required in LVHE incorporated VCR system. However, additional compressor work of subcooler cycle has been given to subcool the refrigerant in dedicated mechanically subcooled VCR system.
- There is no optimum value of degree of subcooling (DOS) for LVHE incorporated VCR system. However, the optimum value of DOS lies between 20⁰C to 25⁰C for dedicated mechanically subcooled VCR system.
- R1234ze performs better than that of R1234yf and competes with R134a in both the systems.
- Evaporator is the component of highest exergetic efficiency of LVHE incorporated VCR system while the subcooler of DSC VCR cycle is the component of highest exergetic efficiency.

PERFORMANCE ANALYSIS (ENERGY AND EXERGY) OF EXPERIMENTAL VAPOUR COMPRESSION REFRIGERATION CYCLE

5.1 INTRODUCTION:

The demand of refrigeration and air-conditioning is going on increasing day by day. Environmental issues are major considerations along with energy consumption and cost effectiveness in the refrigeration and air-conditioning applications. A number of refrigeration and air-conditioning applications viz. automotive & super markets air-conditioning, walk-in coolers, residential refrigerators and chillers prefers low GWP refrigerants.

Hence, the investigation of thermodynamic performance and compatibility of alternative refrigerants in conventional refrigeration system (VCRS) is required for their implementation.

The current work focuses on thermodynamic (exergy & exergy) analysis of an experimental VCR system using alternated refrigerants R1234yf and R1234ze as replacement of R134a. The drop-in replacement of R134a can be executed for alternative refrigerants R1234yf and R1234ze in small power refrigeration system (Jankovic et al., 2015; Sanchez et al., 2017). The experimental observations have been notified on the experimental VCR setup using R134a and the refrigerants R1234yf and R1234ze have been analysed under similar assumptions and input conditions of R134a assuming the drop-in replacements of R134a in the experimental VCR setup.

The observations have been taken on the experimental set after attaining steady state of operating variable viz. refrigerant flow rate, temperature and pressure etc. The experimental results of the analysis using R134a, R1234yf and R1234ze have been compared to the theoretical analysis using same refrigerants. The performance parameters viz. COP, exergetic efficiency, exergy destruction rate of exergy and EDR have been calculated for experimental as well as theoretical analysis. The impact of operating variables viz. pressure ratio, temperature of evaporator and temperature of condenser on the performance parameters has been seen and noticed during parametric analysis.

5.2 DESCRIPTION OF SYSTEM

Fig. 5.1 and 5.2 depict the block and P-h diagrams of experimental VCR system. It comprises of an evaporator, a compressor, a condenser, a reservoir, a rotameter, seven operative gate valves, one solenoid valve, capillary tube, two energy meters, temperature sensors and a control panel. Control panel consist suction, delivery, expansion and condenser pressure gauge. Temperature sensors show the temperature of different state points.

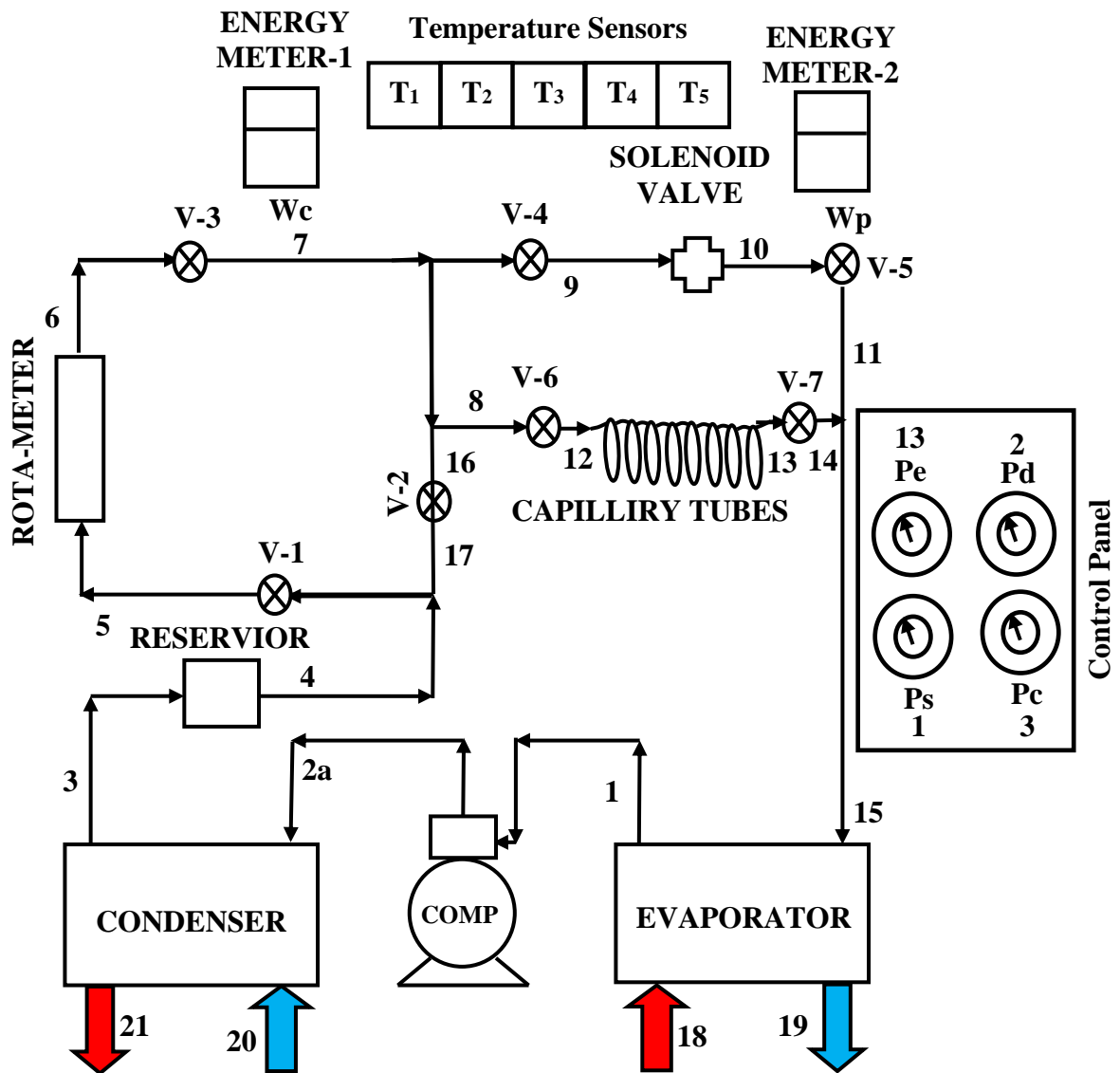


Fig. 5.1 Block diagram of experimental VCR unit

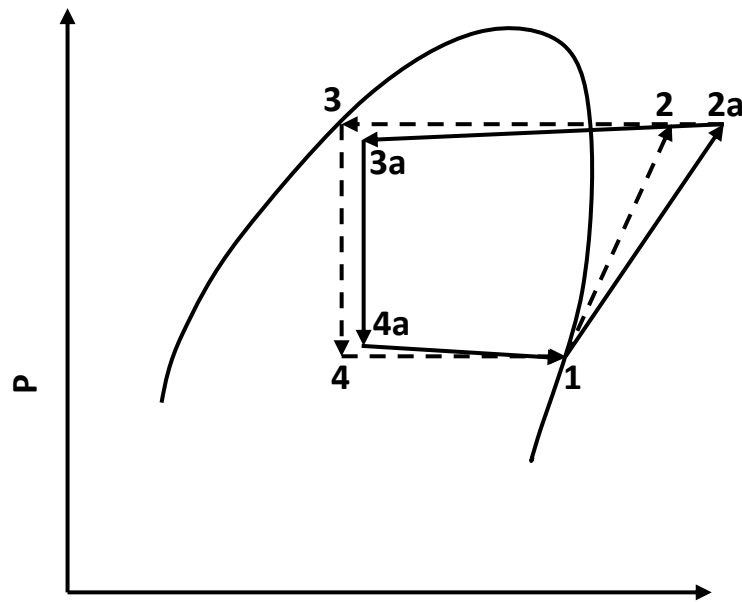


Fig. 5.2 P-h diagram of experimental VCR unit

The heat absorbed in the evaporator by the refrigerant transforms it in saturated vapour at state point 1. The refrigeration effect is obtained in the evaporator by entering the hot water at state point 18 and chilled water is taken out at state point 19. The refrigerating effect is used here to chill the hot water. The saturated vapour is compressed in compressor and leaving it at state point 2a. The high pressure and temperature refrigerant vapour enters in the condenser at state point 2a. The high temperature refrigerant vapour transforms in to liquid in the condenser at state point 3. A reservoir has been situated after the condenser to collect the refrigerant. The condensate refrigerant at high pressure can be expanded freely either by a solenoid valve or capillary tube. The low temperature vapour-liquid mixture of refrigerant enters in the evaporator.

In this work, experimental observations have been taken on an experimental set up of VCR system using HFC-R134a for its thermodynamic investigation. Under similar assumptions and input conditions of R134a, refrigerants R1234yf and R1234ze have been analysed assuming the drop-in replacements of R134a in experimental VCR system.

5.3 MATHEMATICAL FORMULATION

The current work presents the thermodynamic analysis of experimental VCR setup. The experimentation has been carried out on the VCR setup using R134a. Under similar assumptions and input conditions of R134a, refrigerants R1234yf and R1234ze have been analysed assuming the drop-in replacements of R134a. Various performance parameters have been computed using experimental observations in EES software. The experimental results has been represented in the form of graphs and steady state governing equations based on mass and energy conservation principles have been formulated for the thermodynamic modelling of complex system.

5.3.1 Energy analysis

The COP of VCR cycle is given by the equation (5.1)-(5.3).

$$\text{COP} = \frac{\dot{Q}_e}{\dot{W}_{\text{comp}}} \quad (5.1)$$

Where \dot{Q}_e is the net refrigeration effect produced and \dot{W}_{comp} is the actual work of the compressor.

$$\dot{Q}_e = \dot{m}_r (h_1 - h_{4a}) \quad (5.2)$$

$$\dot{W}_{\text{comp}} = \dot{m}_r (h_{2a} - h_1) \quad (5.3)$$

5.3.2 Exergy Analysis

In a refrigerating system during the flow of refrigerant, the exergy is defined as follows (Bejan et al., 1996):

$$\dot{E} = \dot{m}_r [(h - h_0) - T_0 (s - s_0)] \quad (5.4)$$

Where s_0 and h_0 are dead state entropy and enthalpy respectively.

Exergy destruction (\dot{E}_D) or internal exergy destruction losses which are caused by irreversibilities of the system is the algebraic sum of total exergy at the inlet and outlet of the system. General exergy balance is given by (Dincer and Kanoglu, 2010):

$$\dot{E}_D = \dot{E}_{\text{in}} - \dot{E}_{\text{out}} \quad (5.5)$$

Where \dot{E}_{in} is the input exergy, \dot{E}_D is the rate of destruction of exergy and \dot{E}_{out} is the output exergy of the system.

5.3.2.1 Exergy destruction (\dot{E}_D) in the components of experimental vapour compression refrigeration setup

The destruction of exergy and exergetic efficiency in the components of experimental VCR setup is given by the following equations:

Evaporator

$$\begin{aligned} (\dot{E}_D)_{evp} &= \dot{E}_{X_{4a}} + \dot{Q}_e \left(1 - \frac{T_0}{T_b}\right) - \dot{E}_{X_1} \\ &= \dot{m}_r(h_{4a} - T_0 s_{4a}) + \dot{Q}_e \left(1 - \frac{T_0}{T_b}\right) - \dot{m}_r(h_1 - T_0 s_1) \end{aligned} \quad (5.6)$$

Compressor

$$(\dot{E}_D)_{comp} = \dot{E}_{X_{1a}} + \dot{W}_{comp} - \dot{E}_{X_{2a}} = \dot{m}_r(h_{1a} - T_0 s_{1a}) + \dot{W}_{comp} - \dot{m}_r(h_{2a} - T_0 s_{2a}) \quad (5.7)$$

Condenser

$$(\dot{E}_D)_{cond} = \dot{E}_{X_{2a}} - \dot{E}_{X_{3a}} = \dot{m}_r(h_{2a} - T_0 s_{2a}) - \dot{m}_r(h_{3a} - T_0 s_{3a}) \quad (5.8)$$

Capillary tube

$$(\dot{E}_D)_{cpt} = \dot{E}_{X_{3a}} - \dot{E}_{X_{4a}} = \dot{m}_r(h_{3a} - T_0 s_{3a}) - \dot{m}_r(h_{4a} - T_0 s_{4a}) = \dot{m}_r T_0 (s_{4a} - s_{3a}) \quad (5.9)$$

5.3.2.2 Total exergy destruction (TEXD)

TEXD of the system is the sum of destruction of exergy in every component of the system.

The total exergy destruction in experimental VCR setup is given by:

$$\Sigma(\dot{E}_D) = (\dot{E}_D)_{evp} + (\dot{E}_D)_{comp} + (\dot{E}_D)_{cond} + (\dot{E}_D)_{cpt} \quad (5.10)$$

5.3.2.3 Exergetic efficiency (EXE)

Exergetic efficiency is an important parameter for evaluating performance (thermodynamic) of a system or a system component. In general exergetic efficiency is defined as (Dincer and Kanoglu, 2010):

$$\eta_{ex} = \frac{\Sigma \dot{E}_{out}}{\Sigma \dot{E}_{in}} = 1 - \frac{\Sigma \dot{E}_D}{\Sigma \dot{E}_{in}} \quad (5.11)$$

Where η_{ex} is the exergetic efficiency of the system. $\Sigma \dot{E}_{out}$, $\Sigma \dot{E}_{in}$ and $\Sigma \dot{E}_D$ are the total exergy recovered, supplied and destroyed respectively.

The exergetic efficiency of VCR system is defined as the ratio of the exergy of heat absorbed in the evaporator from the space to be cooled at temperature T_b to the actual compressor work input (\dot{W}_{comp}) (Arora and Kaushik, 2008).

$$\eta_{\text{ex}} = \frac{|\dot{Q}_e(1 - \frac{T_0}{T_b})|}{\dot{W}_{\text{comp}}} \quad (5.12)$$

Exergetic efficiency of each component of experimental vapour compression refrigeration cycle is given by the following equations:

Evaporator

$$\eta_{\text{ex, evp}} = 1 - \frac{(\dot{E}_D)_{\text{evp}}}{\dot{E}_{X_{4a}}} \quad (5.13)$$

Compressor

$$\eta_{\text{ex, comp}} = 1 - \frac{(\dot{E}_D)_{\text{comp}}}{\dot{W}_{\text{comp}}} \quad (5.14)$$

Condenser

$$\eta_{\text{ex, cond}} = 1 - \frac{(\dot{E}_D)_{\text{cond}}}{\dot{E}_{X_{2a}} - \dot{E}_{X_{3a}}} \quad (5.15)$$

Capillary tube

$$\eta_{\text{ex, cpt}} = \frac{\dot{E}_{X_{4a}}}{\dot{E}_{X_{3a}}} \quad (5.16)$$

5.3.2.4 Exergy destruction ratio (EDR)

The EDR is the total exergy destruction of the system divided by the exergy in the products (Arora and Kaushik, 2008) and is given by Eq. 5.17).

$$\text{EDR} = \frac{\dot{E}_{D, \text{total}}}{\dot{E}_P} = \frac{1}{\eta_{\text{ex}}} - 1 \quad (5.17)$$

The EDR of each component of experimental VCR setup is given by the following equations:

Evaporator

$$\text{EDR}_{\text{evp}} = \frac{(\dot{E}_D)_{\text{evp}}}{\dot{E}_{D, \text{total}}} \quad (5.18)$$

Compressor

$$\text{EDR}_{\text{comp}} = \frac{(\dot{E}_D)_{\text{comp}}}{\dot{E}_{D, \text{total}}} \quad (5.19)$$

Condenser

$$\text{EDR}_{\text{cond}} = \frac{(\dot{E}_D)_{\text{cond}}}{\dot{E}_{D, \text{total}}} \quad (5.20)$$

Capillary tube

$$EDR_{cpt} = \frac{(\dot{E}_D)_{cpt}}{\dot{E}_{D,total}} \quad (5.21)$$

5.3.2.5 Assumptions

Following assumption have been considered during theoretical analysis of VCR system.

- The steady state is considered for the operation of each component of the system.
- The refrigerant entering in the compressor is dry and saturated for simple VCR system (state points 1)..
- Heat losses in connected pipelines are neglected.
- The chemical, kinetic and potential exergies are neglected.

5.3.2.6 Experimental data

The following experimental data have been recoded as shown in Table 5.1.

Table 5.1 Experimental data recorded on experimental VCR set up

S. No.	Parameters	Values
1.	Electirc voltage	227 V
2.	Electric current	3.62 A
3.	Power factor	0.8
4.	Flow rate of refrigerant	33.5 LPM
5.	Isentropic efficiency of compressor	0.75
6.	Pump fraction	0.46 W
7.	Evaporator temperature	-5 ⁰ C
8.	Condenser temperature	48.5
9.	Pressure ratio	5.3

5.4. RESULTS AND DISCUSSION

In the current work, an experimental VCR setup has been analysed its performance (exergy & energy). The performance of R1234ze, R1234yf and R134a has been compared in the same experimental setup. The practical setup has the facility to measure the operating parameters viz. temperature,, pressure, flow rate of mass of

refrigerant and electricity consumed by compressor and pump etc. at each state point. The various performance parameters viz. COP, EXE, TEXD and EDR have been computed for different values of pressure ratio, temperature of evaporator and temperature of condenser using Engineering Equation Solver (EES) software (Klein and Alvarado, 2012).

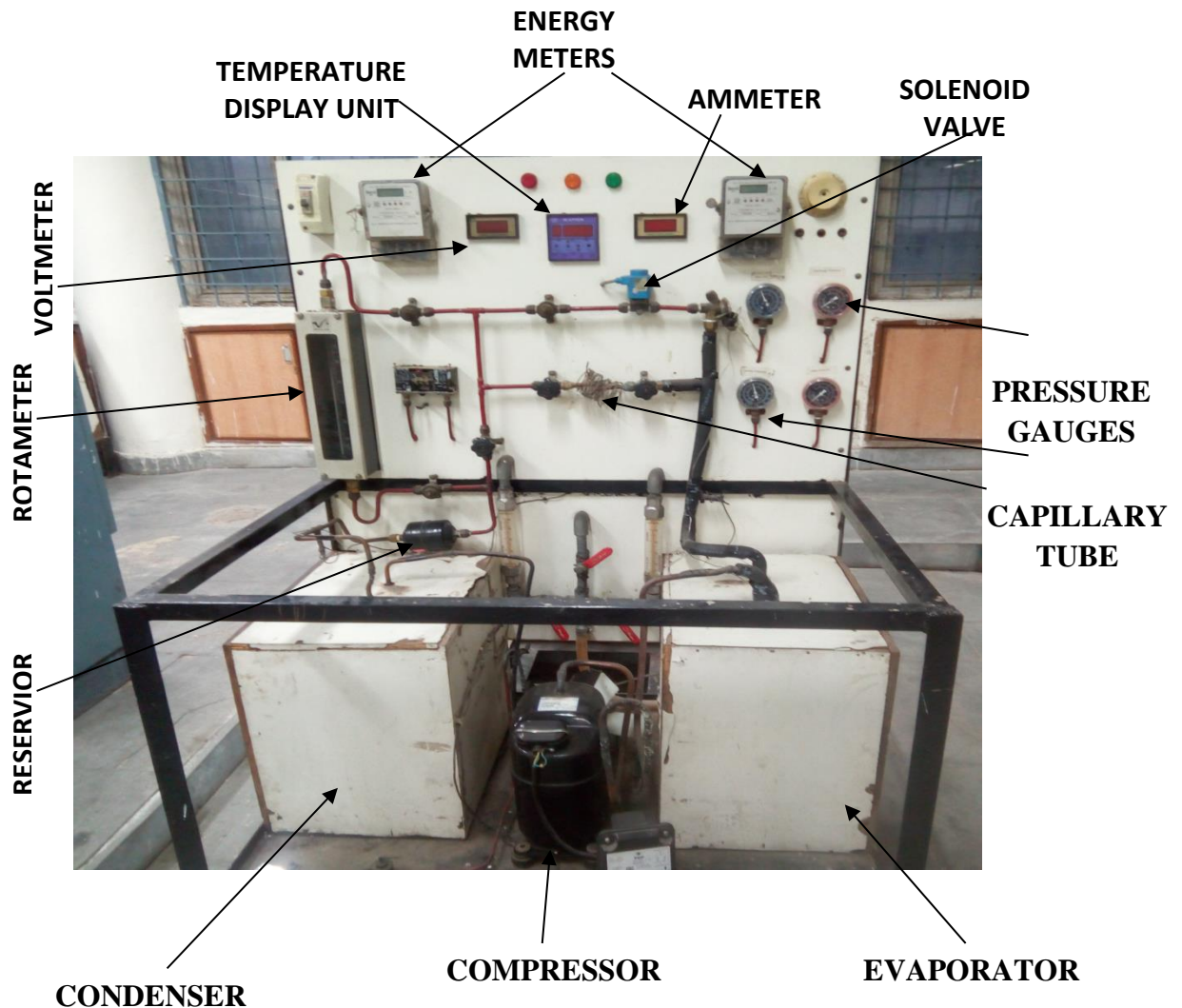


Fig. 5.3 Experimental setup of vapour compression refrigeration unit

5.4.1 Results of Energy, Exergy and Parametric Analysis

The various performance (exergy & energy) parameters have been computed in EES software using experimental data recorded and compared with theoretical results for refrigerants considered.

5.4.1.1 Effect of pressure ratio

The impact of pressure ratio (P_{ratio}) between evaporator and condenser on COP, EXE (η_{ex}), TEXD rate ($\dot{E}_{D,Total}$) and EDR has been depicted in Fig.5.4 to 5.8

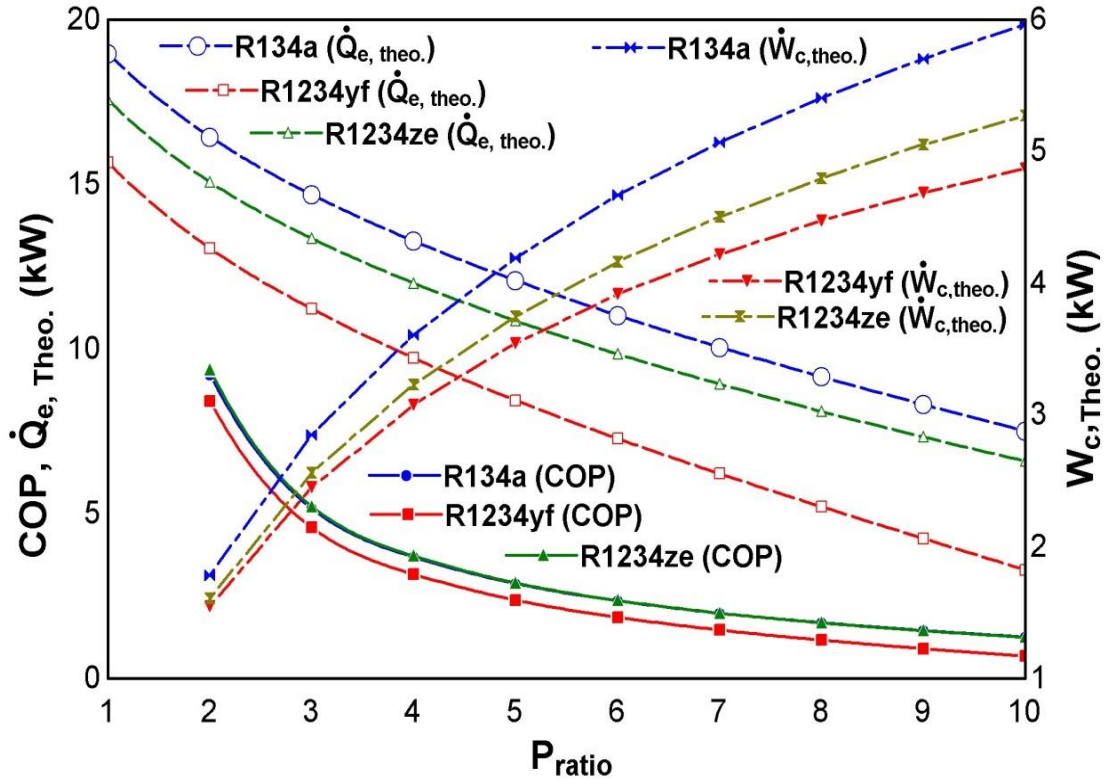


Fig. 5.4 Variation in theoretical refrigeration effect ($\dot{Q}_{e,Theo.}$), theoretical compressor work ($\dot{W}_{c,Theo.}$) and COP with pressure ratio (P_{ratio})

Fig. 5.4 illustrates the variation in pressure ratio (P_{ratio}) on theoretical refrigeration effect ($\dot{Q}_{e,Theo.}$), theoretical compressor work ($\dot{W}_{c,Theo.}$) and COP. The value of $\dot{Q}_{e,Theo.}$, COP decreases and $\dot{W}_{c,Theo.}$ increases with increase in pressure ratio. The compressor work is directly proportional to P_{ratio} ($\dot{W}_c = f(P_{ratio})$). The condenser temperature increases with increase in P_{ratio} for constant evaporator temperature of -5°C .

Fig. 5.5 depicts the impact of pressure ratio (P_{ratio}) on experimental values of refrigeration load ($\dot{Q}_{e,Exp.}$) and COP. The value of $\dot{Q}_{e,Exp.}$ and $\text{COP}_{Exp.}$ decreases with increase in the value of P_{ratio} as the compressor work increases with increase in P_{ratio} .

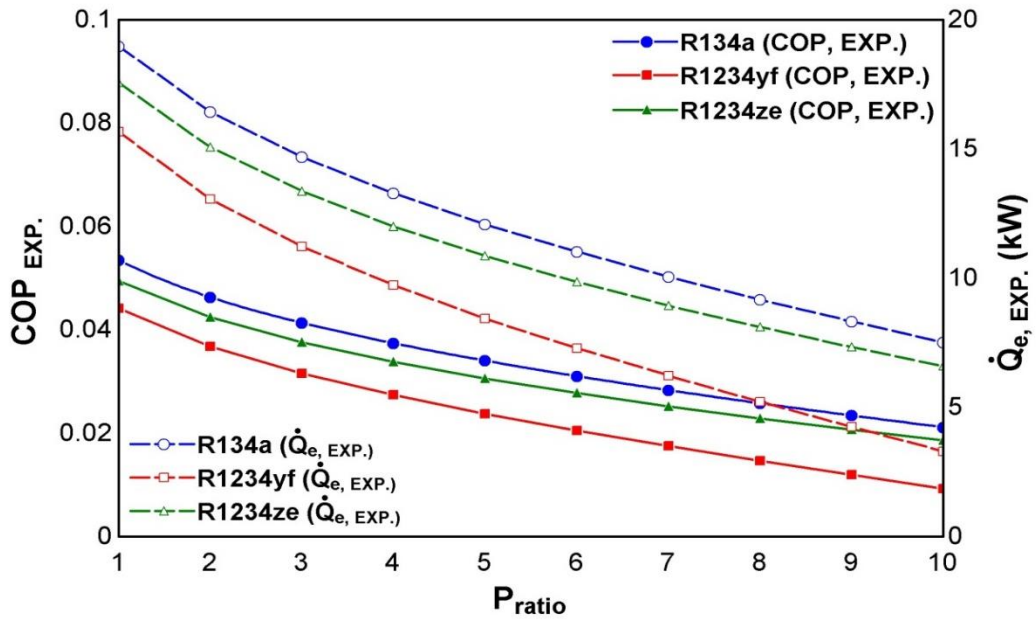


Fig. 5.5 Effect of pressure ratio (P_{ratio}) on experimental refrigeration effect ($\dot{Q}_{e,Exp.}$), and $COP_{Exp.}$.

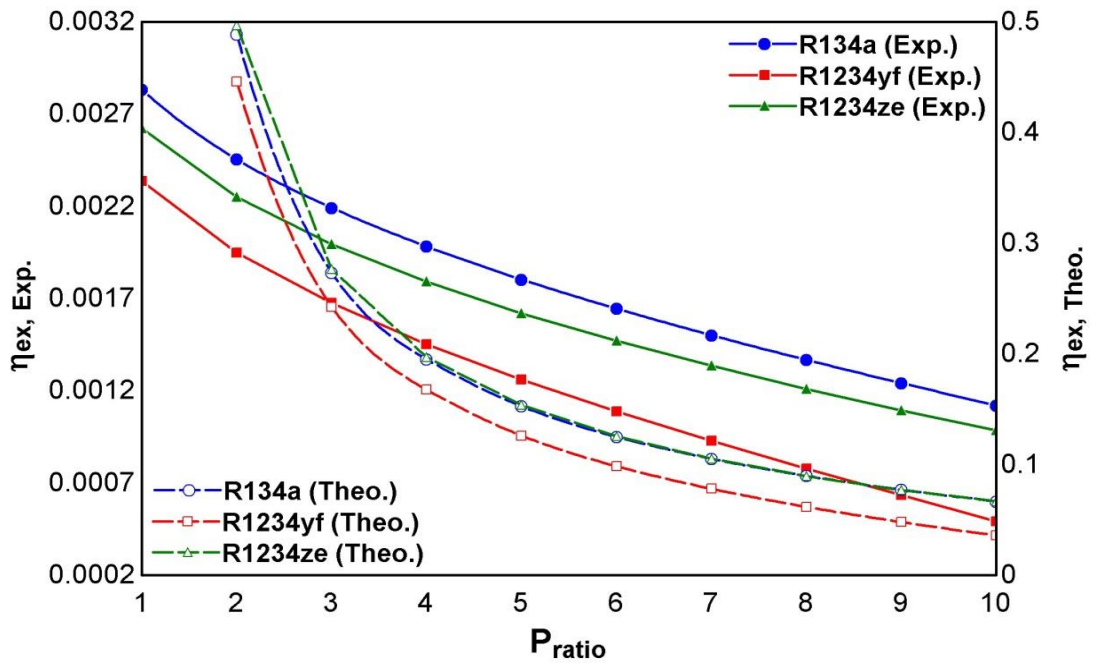


Fig. 5.6 Effect of pressure ratio (P_{ratio}) on theoretical and experimental exergetic efficiency ($\eta_{ex,Theo.}$, $\eta_{ex,Exp.}$)

The experimental value of COP lies between 0.02 and 0.1 for the refrigerants considered. The values of COP of R1234ze and R134a coincide with each other in theoretical analysis while experimental results show that values of COP for R1234ze are lower than that of R134a.

Fig. 5.6 shows the comparison of experimental and theoretical exergetic efficiency ($\eta_{ex,Exp.}, \eta_{ex,Theo.}$) with increase in P_{ratio} . The value of experimental and theoretical EXE decreases with increase in P_{ratio} . The value of refrigeration load decreases and compressor work increases with increase in pressure ratio. Hence the $\eta_{ex,Exp.}, \eta_{ex,Theo.}$ decreases with increase in pressure ratio. The values of $\eta_{ex,Theo.}$ for R1234ze and R134a coincide with each other in theoretical analysis while the values of $\eta_{ex,Exp.}$ for R1234ze are lower than that of R134a in experimental analysis.

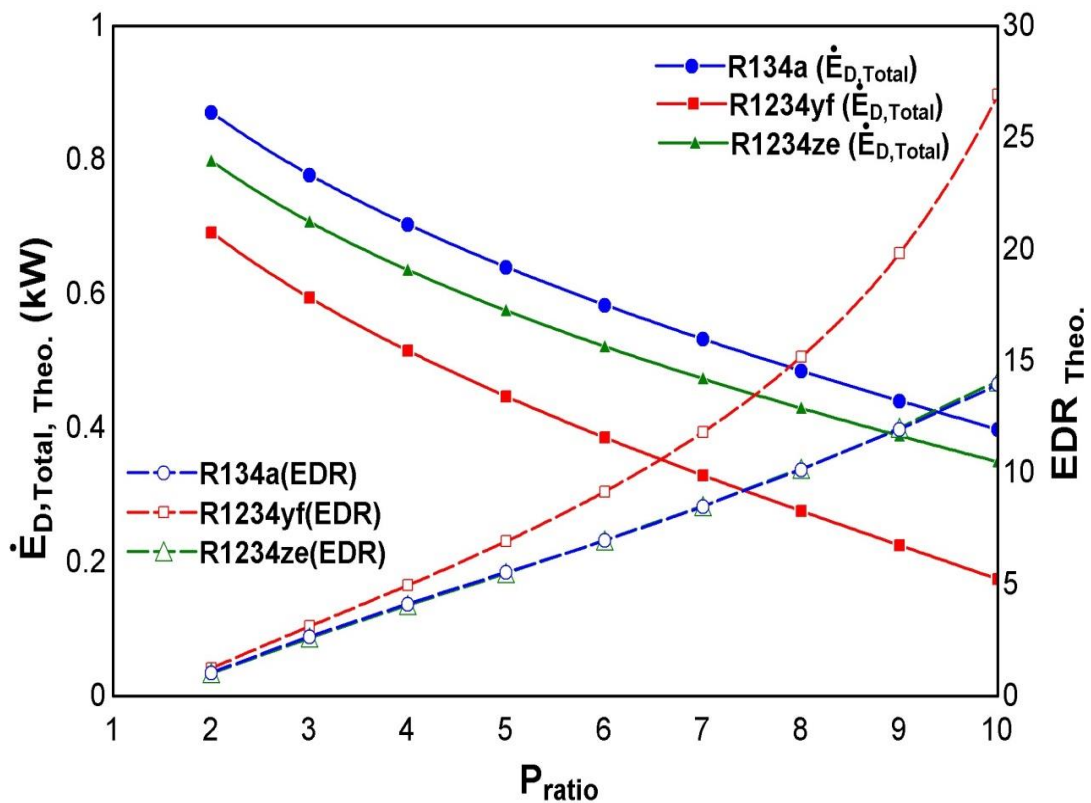


Fig. 5.7 Impact of pressure ratio (P_{ratio}) on theoretical TEXD rate ($\dot{E}_{D,Total,Theo.}$) and EDR (EDR_{Theo.})

Fig. 5.7 depicts the impact of P_{ratio} on theoretical TEXTD ($\dot{E}_{D,Total,Theo.}$) and EDR ($EDR_{Theo.}$). The value of $\dot{E}_{D,Total,Theo.}$ decreases and $EDR_{Theo.}$ increases with increase in P_{ratio} . The TEXTD rate is given by $\Sigma(\dot{E}_D) = (\dot{E}_D)_{evp} + (\dot{E}_D)_{comp} + (\dot{E}_D)_{cond} + (\dot{E}_D)_{cpt}$ and the \dot{E}_D in every component decreases with increase in pressure ratio. Consequently, the value of $EDR_{Theo.}$ increases as the $EDR_{Theo.}$ is given by $EDR = \frac{\dot{E}_{D,total}}{\dot{E}_P}$. It is observed that the value of $\dot{E}_{D,Total,Theo.}$ is maximum for R134a and minimum for R1234yf and $EDR_{Theo.}$ is maximum for and R1234yf and minimum for R134a.

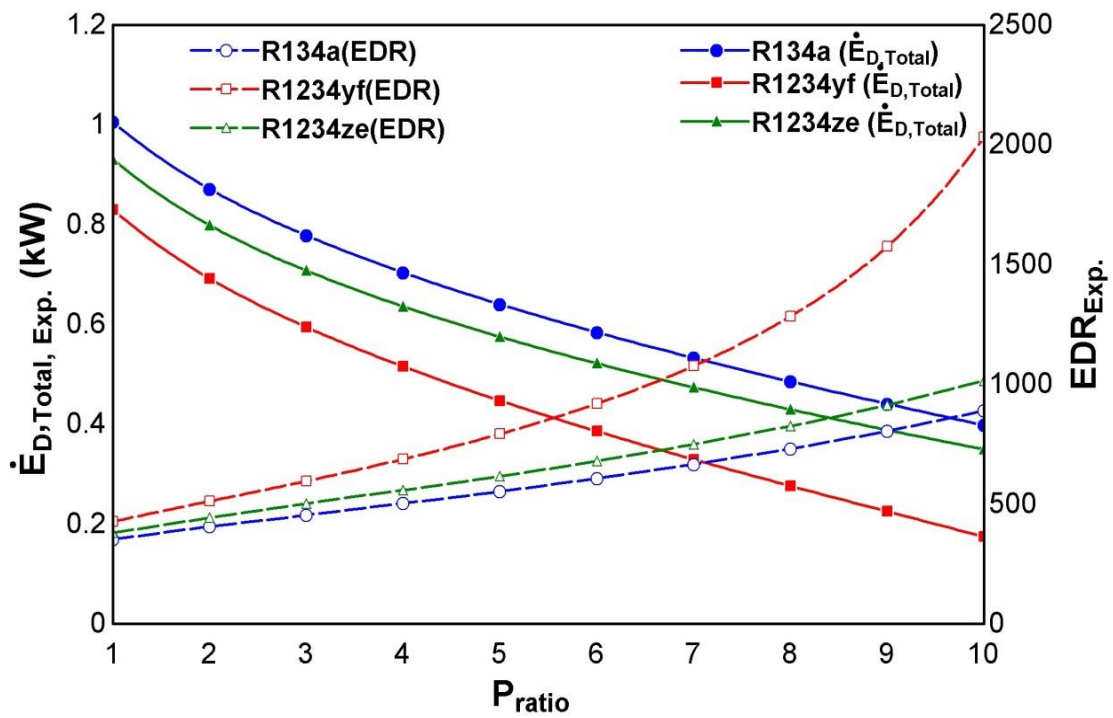


Fig. 5.8 Impact of pressure ratio (P_{ratio}) on experimental TEXTD ($\dot{E}_{D,Total,Exp.}$) and EDR ($EDR_{Exp.}$)

Fig. 5.8 illustrates the impact of P_{ratio} on experimental TEXTD rate ($\dot{E}_{D,Total,Exp.}$) and EDR ($EDR_{Exp.}$). The value of $\dot{E}_{D,Total,Exp.}$ decreases and $EDR_{Exp.}$ increases with increase in pressure ratio. The TEXTD rate is given by $\Sigma(\dot{E}_D) = (\dot{E}_D)_{evp} + (\dot{E}_D)_{comp} + (\dot{E}_D)_{cond} + (\dot{E}_D)_{cpt}$ and the \dot{E}_D in each component of the system decreases with increase in P_{ratio} . Consequently, the value of $EDR_{Exp.}$ increases as the $EDR_{Exp.}$ is given

by $EDR = \frac{\dot{E}_{D,total}}{\dot{E}_P}$. It has been observed that the value of $\dot{E}_{D,Total,Exp.}$ and $EDR_{Exp.}$ is maximum for R134a and R1234yf and minimum for R1234ze and R134a..

5.4.1.2 Effect of Evaporator Temperature

Impact of evaporator temperature (T_e) on COP, EXE (η_{ex}), TEXD ($\dot{E}_{D,Total}$) and EDR (EDR) has been illustrated in Fig.5.9 to 5.13.

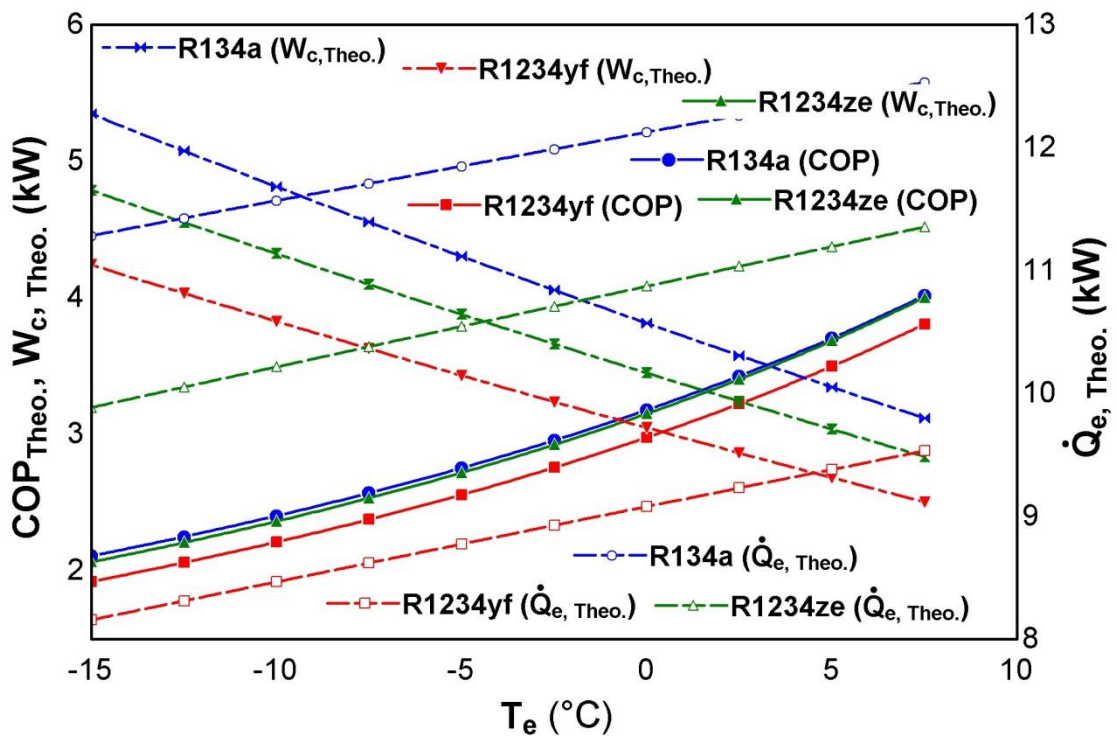


Fig. 5.9 Variation in refrigeration effect ($\dot{Q}_{e,Theo.}$), compressor work ($\dot{W}_{c,Theo.}$) and COP with temperature of evaporator (T_e) for theoretical VCR system

Fig. 5.9 and 5.10 illustrate the effect of evaporator temperature (T_e) on theoretical and experimental values of refrigeration effect ($\dot{Q}_{e,Theo.}, Q_{e,Exp.}$), and $COP_{Theo.}, COP_{Exp.}$. The value of $\dot{Q}_{e,Theo.}, Q_{e,Exp.}$ and $COP_{Theo.}, COP_{Exp.}$ increases with increase in temperature of evaporator. The value of compressor work decreases with increase in temperature of evaporator for theoretical VCR system (Fig. 5.9). Thus, the COP of the system increases with increase in temperature of evaporator.

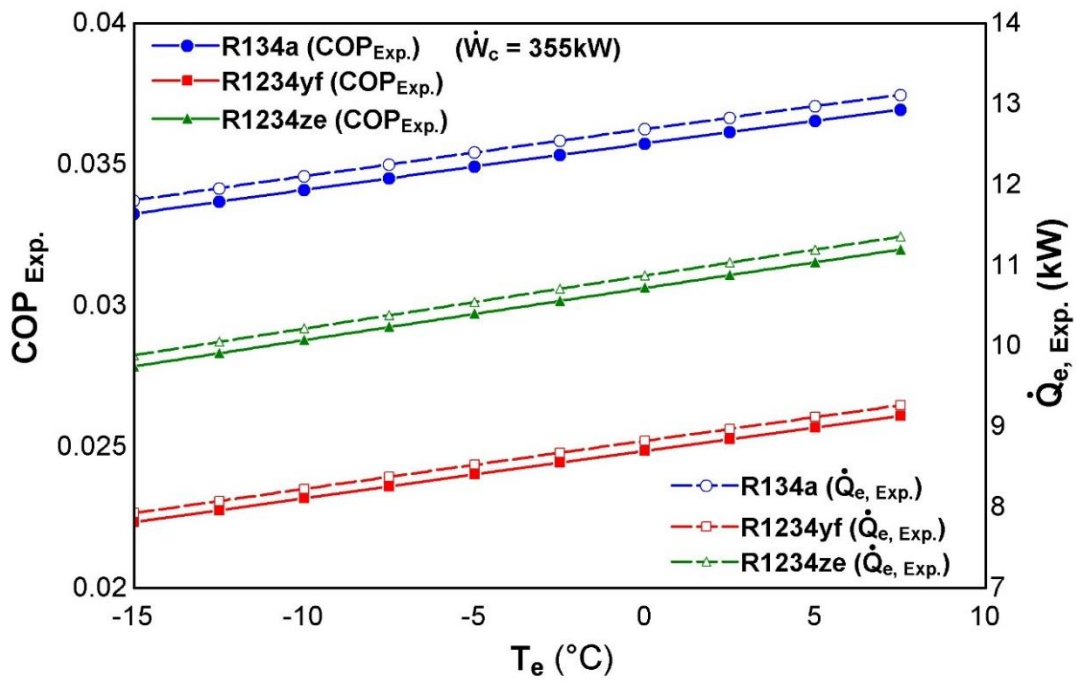


Fig. 5.10 Effect of evaporator temperature (T_e) on experimental refrigeration effect ($\dot{Q}_{e, Exp.}$), and $COP_{Exp.}$.

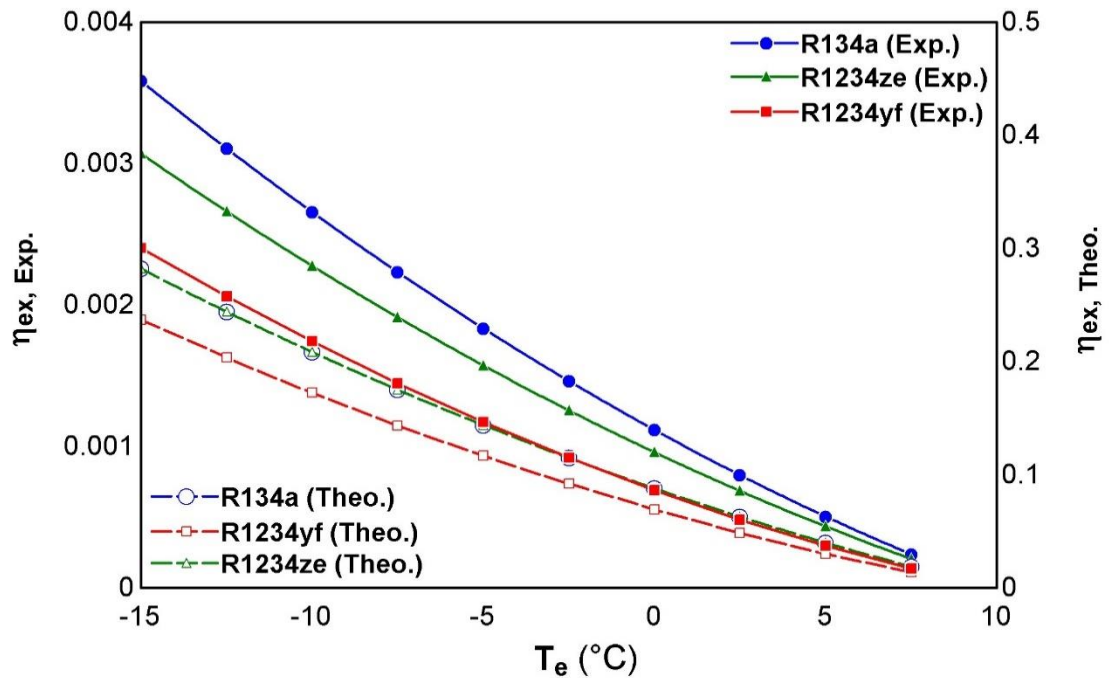


Fig. 5.11 Effect of evaporator temperature (T_e) on theoretical and experimental exergetic efficiency ($\eta_{ex, Theo.}, \eta_{ex, Exp.}$)

It has also been noticed that the values of $\dot{Q}_{e,Theo.}, Q_{e,Exp.}$ are maximum for R134a and minimum for R1234yf.

Fig. 5.11 depicts the impact of temperature of evaporator (T_e) on theoretical and experimental EXE ($\eta_{ex,Theo.}, \eta_{ex,Exp.}$). The value of $\eta_{ex,Theo.}, \eta_{ex,Exp.}$ decreases with increase in temperature of evaporator. The exergetic efficiency is given by $\eta_{ex} = \frac{|\dot{Q}_e(1 - \frac{T_0}{T_b})|}{\dot{W}_{comp}}$ in which, the value of $\frac{|\dot{Q}_e|}{\dot{W}_{comp}}$ i.e. COP increases, however, the value of term $(1 - \frac{T_0}{T_b})$ decreases with increase in evaporator temperature. Hence, the value of EXE decreases. It has been noticed that the value of $\eta_{ex,Theo.}, \eta_{ex,Exp.}$ are maximum for R134a and minimum for R1234yf.

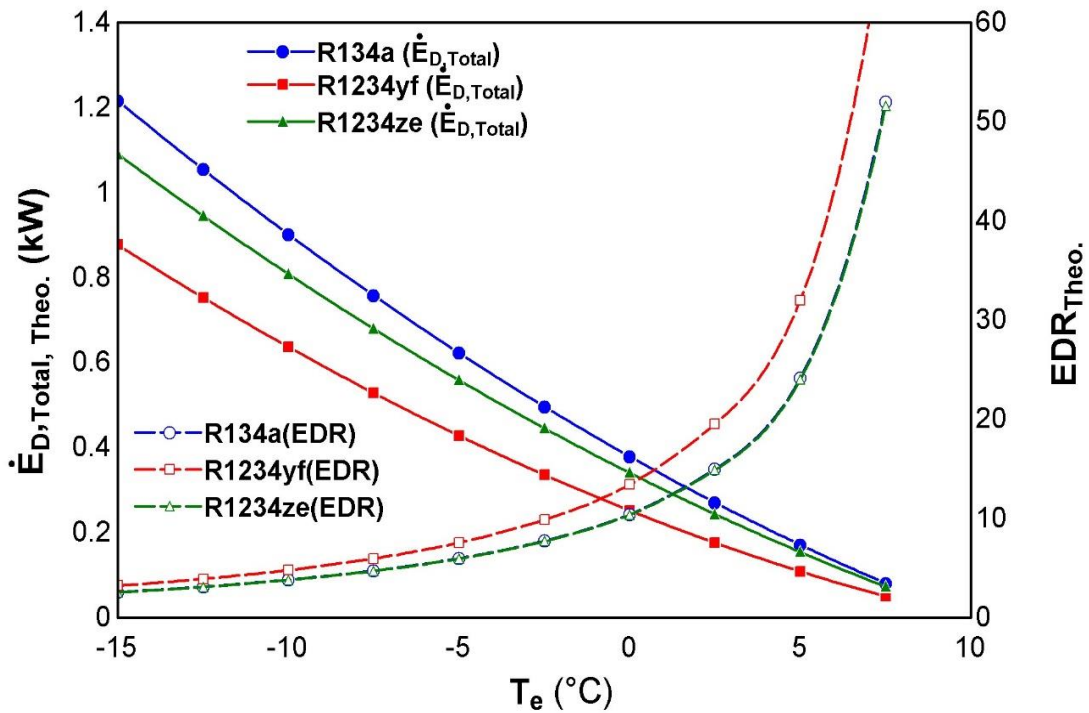


Fig. 5.12 Impact of temperature of evaporator (T_e) on TEXD rate ($\dot{E}_{D,Total,Theo.}$) and EDR ($EDR_{Theo.}$) for theoretical VCR setup

Fig. 5.12 and 5.13 depict the impact of temperature of evaporator (T_e) on theoretical and practical values of TEXD ($(\dot{E}_{D,Total,Theo.}, \dot{E}_{D,Total,Exp.})$) and EDR ($EDR_{Theo.}, EDR_{Exp.}$). The value of $\dot{E}_{D,Total,Theo.}$ increases and $\dot{E}_{D,Total,Exp.}$ decreases with increase in temperature of evaporator. However, the value of $EDR_{Theo.}, EDR_{Exp.}$

increases with increase in temperature of evaporator. It has been noticed that the $EDR_{Theo.}$ is maximum for R1234yf and minimum for R134a while $EDR_{Exp.}$ is maximum for R134a and minimum for R1234yf. $EDR_{Theo.}$, $EDR_{Exp.}$ are maximum for R1234yf and minimum for R134a.

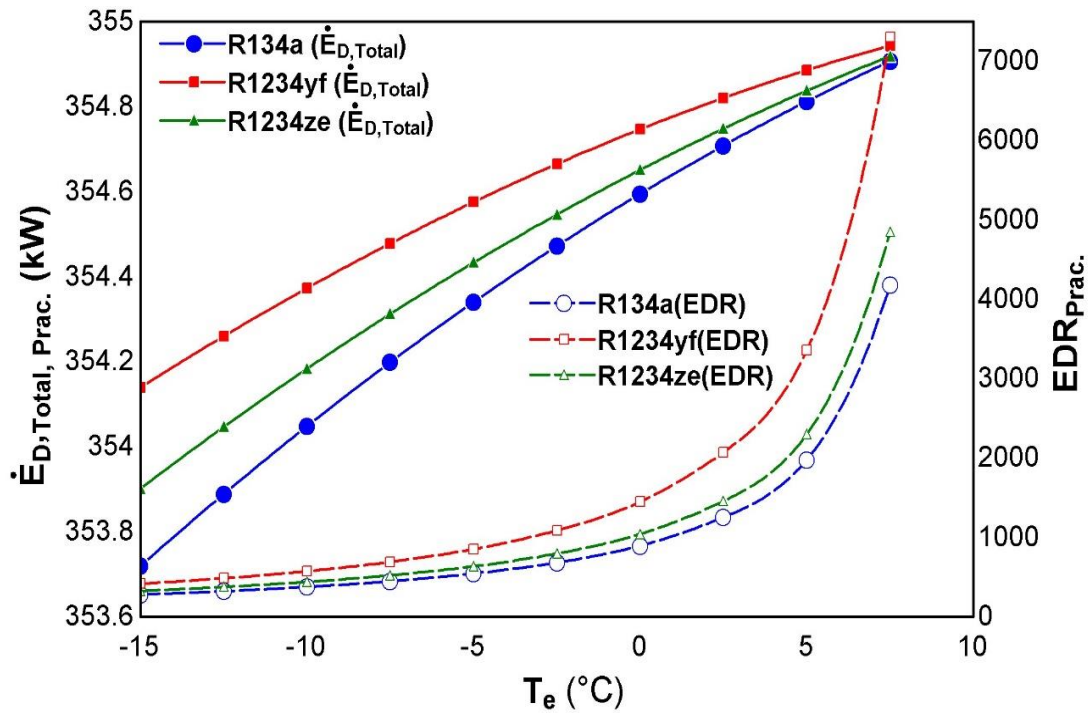


Fig. 5.13 Impact of temperature of evaporator (T_e) on TEXD rate ($\dot{E}_{D,Total,Prac}$) and EDR ($EDR_{Exp.}$) for experimental VCR setup

5.4.1.3 Effect of Condenser Temperature

Effect of temperature of condenser (T_c) on COP, EXE (η_{ex}), TEXD ($\dot{E}_{D,Total}$) and EDR has been illustrated in Fig.5.14 to 5.18.

Fig. 5.14 depicts that the value of $\dot{Q}_{e,Theo.}$ and COP decreases and $\dot{W}_{c,Theo.}$ increases with increase in temperature of condenser. As the gap between evaporator and condenser increases with increase in temperature of condenser, higher compressor work is required to achieve the high temperature of condenser. The refrigerating effect reduces due to higher temperature of saturated liquid refrigerant exiting from the condenser. Hence, the value of $\dot{Q}_{e,Theo.}$ decreases and $\dot{W}_{c,Theo.}$ increases with increase in temperature of condenser.

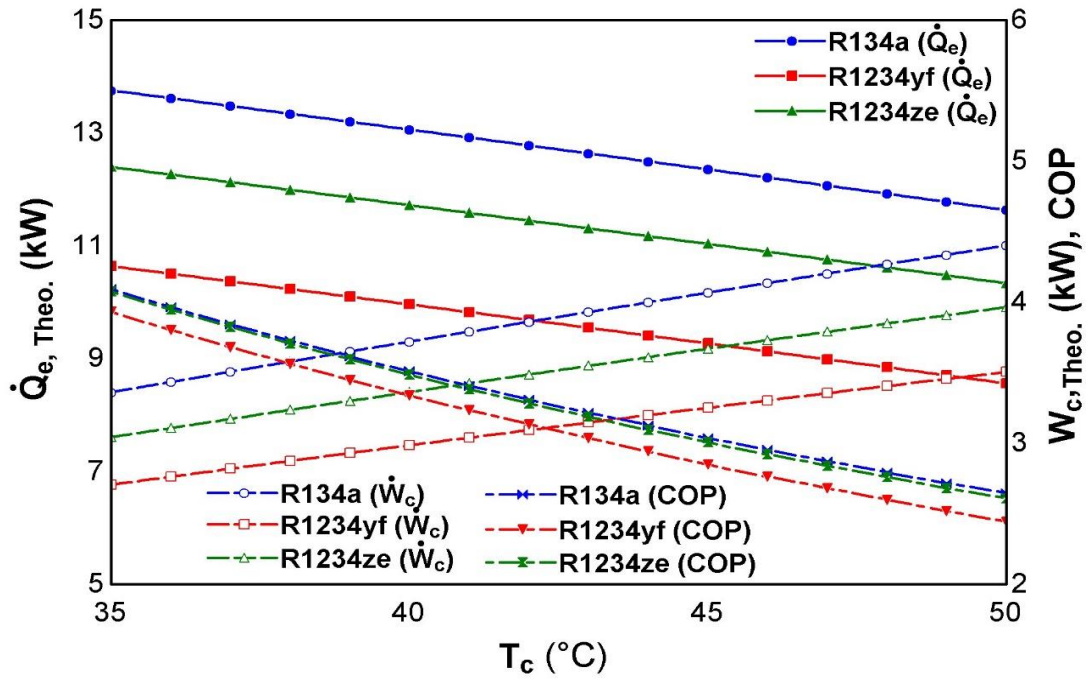


Fig. 5.14 Variation in refrigeration effect ($\dot{Q}_{e, Theo.}$), COP and compressor work ($\dot{W}_{c, Theo.}$) with condenser temperature (T_c) for theoretical VCR system

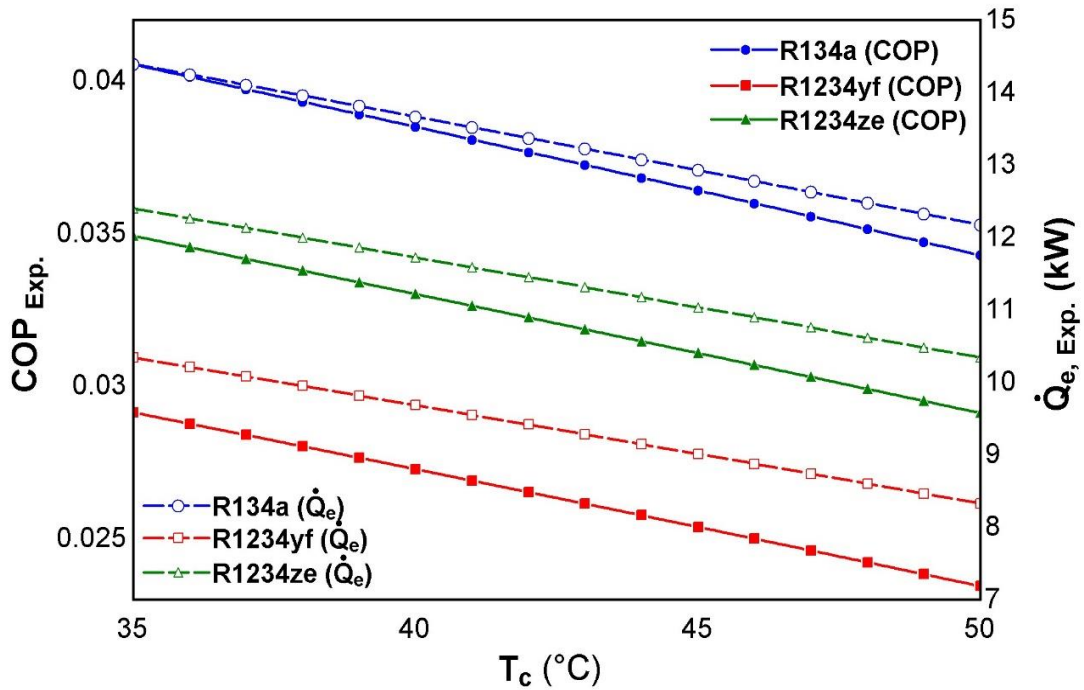


Fig. 5.15 Impact of temperature of condenser (T_c) on refrigeration effect ($\dot{Q}_{e, Exp.}$), and COP_{Exp.} For experimental VCR setup

Fig. 5.15 depicts the impact of temperature of condenser (T_c) on $\dot{Q}_{e,Exp.}$ and $COP_{Exp.}$. The value of $\dot{Q}_{e,Exp.}$ and $COP_{Exp.}$ decreases with increase in T_c . As the value of T_c increases, the temperature of saturation liquid refrigerant is higher and thus the refrigerating effect ($\dot{Q}_{e,Exp.}$) decreases. It has been noticed that the $\dot{Q}_{e,Exp.}$ and $COP_{Exp.}$ are maximum for R134a and minimum for R1234yf.

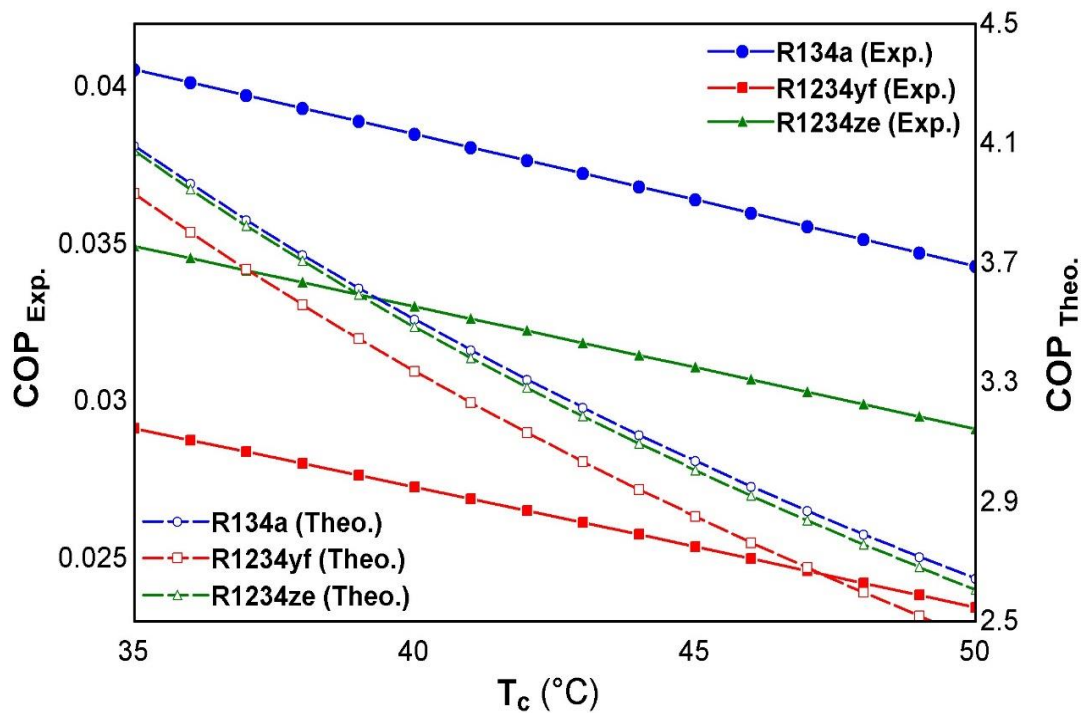


Fig. 5.16 Impact of temperature of condenser (T_c) on $COP_{Theo.}$ and $COP_{Exp.}$

Fig. 5.16 depicts the impact of temperature of condenser (T_c) on $COP_{Theo.}$ and $COP_{Exp.}$. The value of $COP_{Theo.}$ and $COP_{Exp.}$ decreases with increase in T_c . Refer to Fig. 5.14 the compressor work increases while the refrigeration load decreases with increase in T_c . It has been noticed that the value of COP is maximum for R134a and minimum for R1234yf in theoretical as well as experimental VCR set up. The value of COP for R1234ze lie between R134a and R1234yf in theoretical as well as experimental VCR setup. However, the values of COP for R1234ze is more close to R134a in theoretical VCR setup.

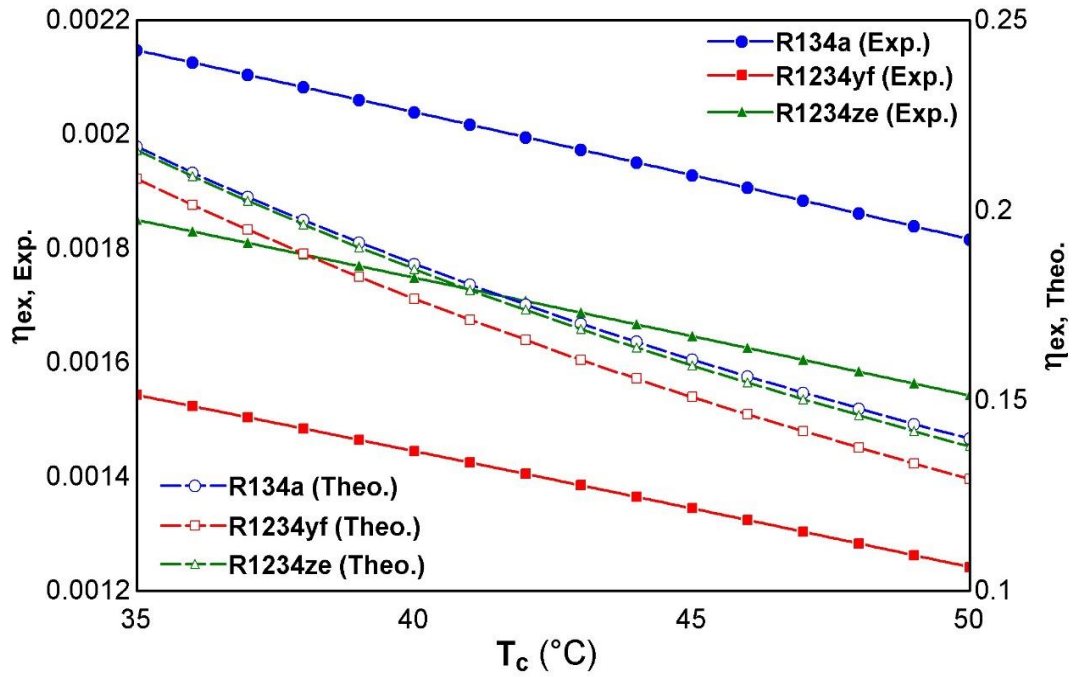
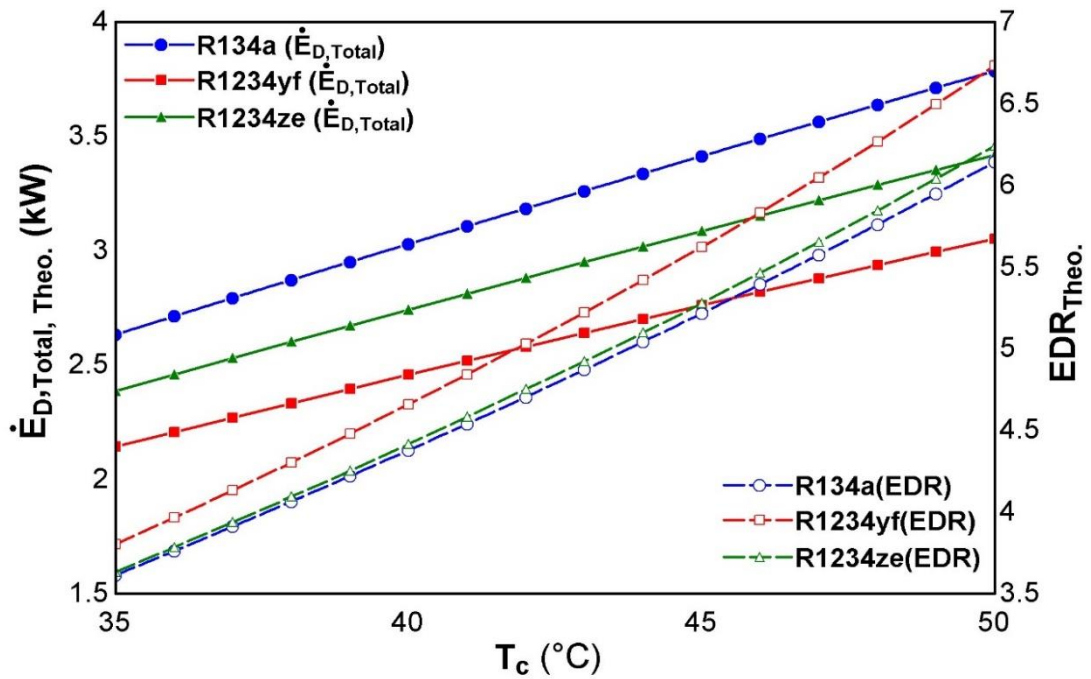


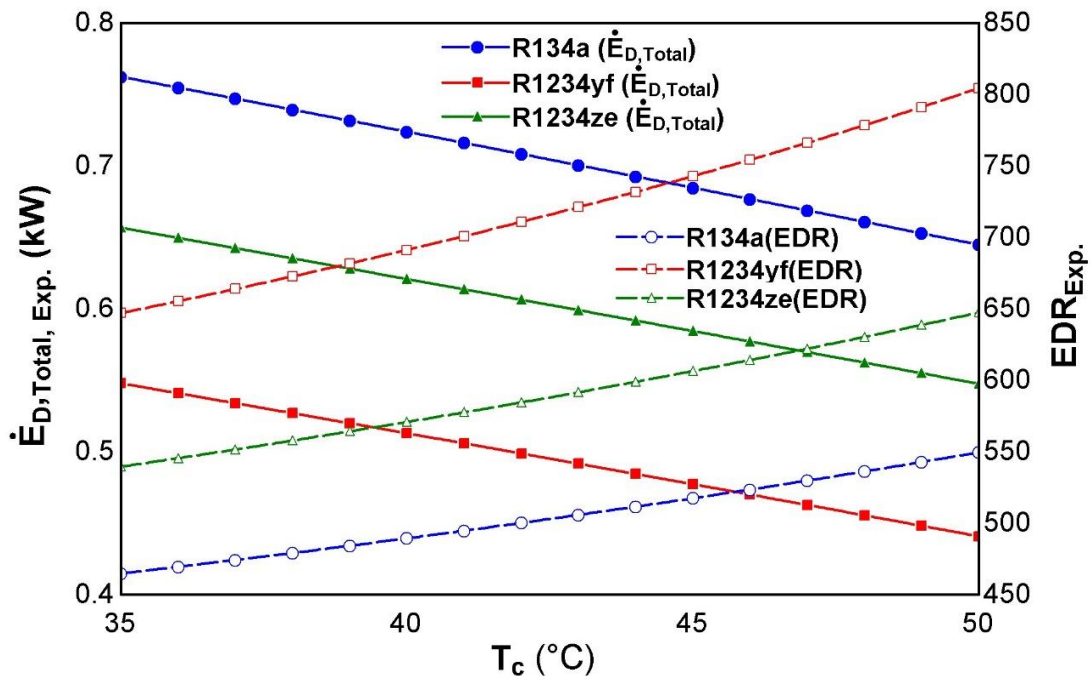
Fig. 5.17 Impact of temperature of condenser (T_c) on EXE ($\eta_{ex,Theo.}, \eta_{ex,Exp.}$) for theoretical and experimental VCR setup



5.18 Impact of T_c on TEXD rate ($\dot{E}_{D,Total,Theo.}$) and EDR ($EDR_{Theo.}$) for theoretical VCR setup

Fig. 5.17 illustrates the impact of T_c on theoretical and experimental EXE ($\eta_{ex,Theo.}, \eta_{ex,Exp.}$). The value of $\eta_{ex,Theo.}, \eta_{ex,Exp.}$ decreases with increase in condenser temperature. It has been noticed that the value of $\eta_{ex,Theo.}, \eta_{ex,Exp.}$ is maximum for R134a and minimum for R1234yf respectively.

Fig. 5.18 and 5.19 illustrate the impact of T_c on theoretical and experimental TEXD rate ($\dot{E}_{D,Total,Theo.}, \dot{E}_{D,Total,Exp.}$) and EDR ($EDR_{Theo.}, EDR_{Exp.}$). The value of $\dot{E}_{D,Total,Theo.}, EDR_{Theo.}$ and $EDR_{Exp.}$ increases and the value of $\dot{E}_{D,Total,Exp.}$ decreases with increase in T_c . It has been seen that $\dot{E}_{D,Total,Theo.}$ is maximum for R134a and minimum for R1234yf. $\dot{E}_{D,Total,Exp.}, EDR_{Theo.}$ and $EDR_{Exp.}$ are maximum for R1234yf



and minimum for R134a.

Fig. 5.19 Impact of T_c on TEXD rate ($\dot{E}_{D,Total,Exp.}$) and EDR ($EDR_{Exp.}$) for experimental VCR setup

5.5. CONCLUSIONS

In this work, the detailed energy and exergy analysis have been carried out for theoretical and experimental VCR setup. The comparison of two cycles is being summarized as follows:

- The COP of theoretical and experimental VCR cycles decreases with increase in pressure ratio and condenser temperature while increases with increase in temperature of evaporator.
- The percentage difference in COP and exergetic efficiency for experimental and theoretical systems are 97.33% and 94% respectively at pressure ratio 10 for R134a.
- The exergetic efficiency of theoretical and experimental VCR cycles decreases with increase in pressure ratio, temperature of evaporator and temperature of condenser.
- The total exergy destruction rate and exergy destruction ratio for theoretical and experimental VCR setup increases with increase in pressure ratio and temperature of condenser. However, experimental value of total exergy destruction rate decreases with increase in temperature of evaporator.
- The performance of R1234ze is closer to the R134a for theoretical as well as experimental VCR cycle.
- The % difference in the COP of R1234ze and R134a is 12.5% and 10% for experimental and theoretical VCR system respectively.
- Minor alternations are needed for drop-in replacement of R134a to the alternate R1234yf and R1234ze in the experimental setup.

**ENERGY AND EXERGY ANALYSIS OF VAPOUR
COMPRESSION-ABSORPTION (H₂O-LiBr) CASCADE
REFRIGERATION SYSTEM**

6.1 INTRODUCTION:

In the current scenario, the energy, exergy, economy, environment and safety strategies are the major issues which are being considered to evaluate the performance of refrigeration systems operating either at lower or very low evaporator temperatures. The low temperatures for cryogenics approaching 0 K, air conditioning around 0°C, industrial refrigeration are -35 to -50°C and its applications such as freeze drying, pharmaceuticals, chemical and petroleum industry use cascade refrigeration cycles (ASHRAE_R02_39SI.pdf). The demand of refrigeration at the low evaporation temperature is increasing which ranges from high heat flux electronics to rapid freezing, frozen food and cold storage (Chen et al., 2017; Eini et al., 2016; Tassou et al., 2010). Tassou et al. (2010) suggested that the refrigeration is a necessary part of the food chain and to slow down the physical, chemical and microbiological activities that cause deterioration in food, the food is frozen between -18 to -35°C. Generally, technologies of mechanical refrigeration are invariably employed in these processes which either contribute electricity consumption and environmental impact or low performance. These processes include vapour compression refrigeration, half, single, double and triple effect vapour absorption refrigeration. Although the performance of vapour compression refrigeration cycle supersedes the others yet its electricity consumption is higher.

Thus, the lower temperature production, reduction in high grade energy (electricity) and environmental safety are the significant challenges in the development of advanced refrigeration and air-conditioning systems.

The current work presents the absorption compression cascade refrigeration systems having triple, double, single and half effect VAR and simple VCR system. The evaporator of VAR system is coupled to condenser of VCR system through a cascade heat exchanger. Water-lithium bromide are proposed refrigerant-absorbent for VAR system and R1234yf for VCR system. The detailed parametric analysis followed to energy and exergy analysis has been carried out for the different configurations of absorption compression cascade refrigeration system (ACCRS). The effect of various operating

parameters viz. generator temperature, absorber temperature evaporator temperature has been investigated on performance parameters.

6.2 DESCRIPTION OF VAPOUR COMPRESSION-ABSORPTION (TRIPLE EFFECT SERIES FLOW H₂O-LiBr) CASCADE REFRIGERATION SYSTEM

Fig. 6.1 depicts the schematic diagram of absorption-compression cascade refrigeration system (ACCRS). It comprises of a vapour compression refrigeration (VCR) cycle and a triple effect H₂O/LiBr series flow vapour absorption refrigeration (TESFVAR) cycle. The vapour compression refrigeration system (VCRS) is in the low temperature section in which low temperature is achieved by using 1234yf as a refrigerant and triple effect H₂O-LiBr series flow vapour absorption refrigeration system (TESFVAR) is in the high temperature section having Lithium Bromide (LiBr) as an absorbent and water (H₂O) as a refrigerant.

The evaporator of vapour absorption refrigeration system (VAR) is coupled with the condenser of VCRS i.e. the two cycles are coupled by a heat exchanger which is designated as cascade heat exchanger (Che) in which evaporator of VAR absorbs the heat of the condenser of VCRS. The low temperature is obtained in the evaporator of the VCRS. The evaporator temperature of VCRS is lower than the VAR. This system can be used for various applications such as deep-freezers, chillers, biomedical applications, poultry industry etc.

The ACCRS comprises of an Evaporator, a Compressor, a Condenser and an Expansion valve in VCRS circuit along with an Evaporator, an Absorber, a Pump, three Solution heat exchanger (She 1, 2, 3), three Generators ('Hpg', 'Mpg' and 'Lpg') at high, medium and low pressures, one Condenser, three Refrigerant throttle valves (Rtv 1, 2, 3) and three Solution throttle valves (Stv 1, 2, 3). The condenser of VCRS is coupled to the TEFVAR in such a way that the heat dissipated by it is absorbed by the evaporator of TEFVAR. Thus the cascade system so obtained further produces cooling in the evaporator of VCRS. The TEFVAR is a four pressure system. The generator units are at high, medium and low pressures generate refrigerant vapour. The high pressure generator (Hpg) can be operated by the waste heat available from thermal power plant viz. steam turbine or gas turbine or an I.C. engine. The solar energy may also be used for the purpose. This energy is used in the generators (i.e. Hpg, Mpg &Lpg) to generate

refrigerant vapour. The COP of the TESFVARS is about three times that of a single effect system.

The absorber and evaporator of TESFVAR cycle operate at same lowest pressure. The strong solution is pumped from absorber to the high pressure generator through solution heat exchanger (She 1, 2 and 3) from state points 5-9. The refrigerant vapours is separated by high pressure generator at state point 19 which passes through medium pressure generator from state 19-20 and then from state 20-21 throttled to the condenser by refrigerant throttle valve 3 (Rtv3). The weak solution leaving Hpg form state 10-11 dissipates heat to the strong solution in the She3 and is throttled to medium pressure generator from state 11-12 by solution throttle valve 3 (Stv3). The refrigerant vapour generated in the Mpg is passed through low pressure generator from state 22-23 and after that it is throttled to the condenser at state 24 by Rtv 2. In this way, the solution flows in series through three generators and generates refrigerant vapour. Thus the system is known as triple effect H₂O-LiBr series flow vapour absorption refrigeration system (TESFVARS). The weak solution obtained from Mpg is passed through She 2 and dissipates heat to strong solution from state 13-14. It is throttled to Lpg from state 14-15 by Stv2. The refrigerant vapour obtained from the 'Lpg' is fed to the condenser. The refrigerant vapour from the condenser 2 is throttled to evaporator 2 from state 26-27 by Rtv 1. The refrigerating effect thus obtained in the evaporator, which is in the cascade heat exchanger (Che) from state 27-28 produces cascading effect in the 'Che'. Finally, the refrigerant vapour enters to the absorber. The weak solution from 'Lpg' enters to the She1 and dissipates heat to the strong solution from state 16-17. Finally, it is throttled to absorber by 'Stv' 1 from state 17-18. The cascade heat exchanger exchanges heat of condenser 1 i.e. \dot{Q}_{eVA} of VCR cycle with the evaporator 2 of VAR cycle. The refrigerant vapours of R1234yf at high pressure and temperature after compression from state 1-2 enters in the condenser1 at state point 2. These vapours dissipate heat \dot{Q}_{eVA} to the evaporator 2 in the Che from states 2-3a and gets transform in to subcooled liquid. Further, from state 3-3a, the subcooling of liquid refrigerant occurs. The subcooled liquid refrigerant is throttled to evaporator 1 at low temperature and pressure from state 3a-4 by expansion valve. Finally, the low temperature vapours of refrigerants produces cooling effect in the evaporator 1 from state 4-1.

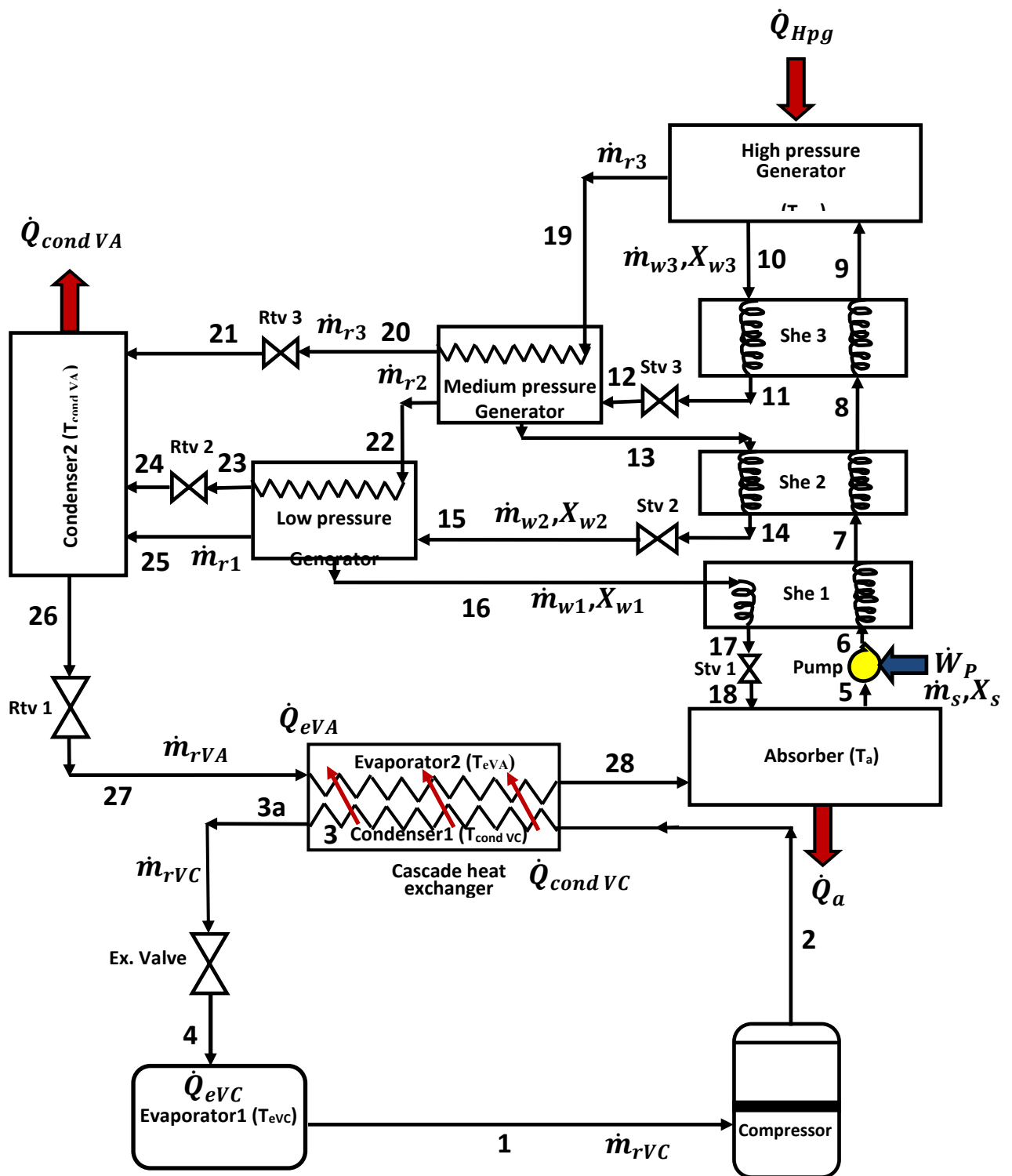


Figure 6.1 Schematic diagram of absorption-compression (triple effect H₂O-LiBr series flow) cascade refrigeration system (ACCRS)

6.3 MATHEMATICAL MODELLING

6.3.1. Assumptions

The following assumptions have been considered to formulate steady flow governing equations accounting the features of compression-absorption triple effect series flow cascade refrigeration system except where the variation of physical parameters involved.

- The state of refrigerant is dry and saturated at the entry of compressor at (state point 1).
- The state of refrigerant at the exit of condenser of VCRS is saturated subcooled liquid at state point 3a.
- Subcooling in the condenser 1 of VCR is from state 3-3a.
- The expansion or throttling in the expansion valve, solution throttle valve and refrigerant throttle valve is isoenthalpic.
- Difference between the temperature of space to be cooled and temperature of evaporator 1 ($\Delta T = T_b - T_{eVC}$) is 10°C .
- The approach temperature or overlap temperature between evaporator 2 and condenser 1 in the cascade heat exchanger ($T_{ov} = T_{cond VC} - T_{eVA}$) is 5°C .
- Isentropic efficiency of compressor (η_c) is 80%
- The heat losses and pressure losses from the system and system components are negligible. The whole system operates in steady state condition.
- The refrigerant of vapour compression cycle is R1234yf and the refrigerant and absorbent of triple effect series flow vapour absorption cycle are water (H_2O) and Lithium Bromide (LiBr).
- The reference values of entropy (s_0) and enthalpy (h_0) are considered at ambient or dead state conditions ($T_0 = 25^{\circ}\text{C}$, $P_0 = 101.325\text{kPa}$).
- The refrigerant vapour leaving the generator(s) ('Hpg', 'Mpg' and 'Lpg') is superheated vapour at the generator temperature..
- Heat exchanger (s) effectiveness (ϵ_{she1} , ϵ_{she2} , ϵ_{she3}) is 0.7.
- The temperature of condenser 2 and absorber are equal.

6.3.2. Energy analysis

The following equations (6.1)-(6.3) express applications of the first law based principles.

$$\sum \dot{m}_i - \sum \dot{m}_o = 0 \quad (6.1)$$

$$\sum \dot{m}_i \dot{X}_i - \sum \dot{m}_o \dot{X}_o = 0 \quad (6.2)$$

$$\sum \dot{Q} - \sum \dot{W} = \sum \dot{m}_o h_o - \sum \dot{m}_i h_i \quad (6.3)$$

Where \dot{m} , \dot{X} , \dot{W} and \dot{Q} are the rate of mass transfer, concentration of solution, work transfer and heat transfer crossing the system boundary respectively. A computer software based program in Engineering Equation Solver (EES)(Klein and Alvarado, 2012)has been developed to investigate system parameters viz. COP, exergetic efficiency, total exergy destruction and exergy destruction ratio (EDR) etc. The thermodynamic modeling has been divided in two sections energy and exergy analysis.

The energy performance, based on first law of absorption compression triple stage series flow cascade refrigeration cycle (ACCRC) is represented as coefficient of performance (COP):

$$COP = \frac{\dot{Q}_{eVC}}{\dot{Q}_{HPG} + \dot{W}_P + \dot{W}_C} \quad (6.4)$$

Where \dot{Q}_{eVC} and \dot{W}_C are the net refrigerating effect and rate of compressor work of VCRS and \dot{Q}_{HPG} and \dot{W}_P are the heat rate of high pressure generator and solution pump work rate of TESFVARs respectively.

6.3.3. Exergy analysis

The concept of exergy is derived from the second law of thermodynamics and the exergy is defined as the maximum useful work which can be extracted from a system as it reversibly comes into equilibrium with its environment or degree measure of usefulness, quality or an effective measure of the potential of substance to impact the environment (Arora and Kaushik, 2008; Bejan et al., 1996).

The total exergy (E) of a system is the sum of physical exergy (E^{PH}), kinetic exergy (E^{KN}), potential exergy (E^{PT}) and chemical exergy (E^{CH}) (Bejan et al., 1996).

$$E = (E^{PH}) + (E^{KN}) + (E^{PT}) + (E^{CH}) \quad (6.5)$$

For the refrigerant flowing in a refrigerating system, the exergy is defined as follows (Bejan et al., 1996):

$$\dot{E} = \dot{m}_r [(h - h_o) - T_o(s - s_o)] \quad (6.6)$$

where h_o and s_o are the enthalpy and entropy values of the refrigerant at dead state pressure P_o and temperature T_o .

Exergy destruction (\dot{E}_D) or internal exergy destruction losses which are caused by irreversibilities of the system is the algebraic sum of total exergy at the inlet and outlet of the system. General exergy balance is given by (Dincer and Kanoglu, 2010):

$$\dot{E}_D = \dot{E}_{in} - \dot{E}_{out} \quad (6.7)$$

Where \dot{E}_D is the exergy destruction rate and \dot{E}_{in} & \dot{E}_{out} are the total exergy at the inlet and outlet by work, mass and heat.

6.3.3.1 Total exergy destruction

Total exergy destruction of the system is the summation of exergy destruction in each system component.

The total exergy destruction in compression-absorption triple effect series flow cascade refrigeration system is given by:

$$\begin{aligned} \dot{E}_{D,total} = & \dot{E}_{D,eVC} + \dot{E}_{D,Comp} + \dot{E}_{D,Ex. valve} + \dot{E}_{D,Che} + \dot{E}_{D,Abs} + \dot{E}_{D,Pump} + \dot{E}_{D,She1} + \\ & \dot{E}_{D,She2} + \dot{E}_{D,She3} + \dot{E}_{D,Hpg} + \dot{E}_{D,Mpg} + \dot{E}_{D,Lpg} + \dot{E}_{D,Rtv1} + \dot{E}_{D,Rtv2} + \dot{E}_{D,Rtv3} + \\ & \dot{E}_{D,Stv1} + \dot{E}_{D,Stv2} + \dot{E}_{D,Stv3} (\dot{E}_D)_{Stv2} + \dot{E}_{D,cond2} \end{aligned} \quad (6.8)$$

6.3.3.2 Exergetic efficiency

Exergetic efficiency is an important parameter for evaluating thermodynamic performance of a system or a system component. In general exergetic efficiency is defined as (Bejan et al., 1996):

$$\eta_{ex} = \frac{\sum \dot{E}_{out}}{\sum \dot{E}_{in}} = 1 - \frac{\sum \dot{E}_D}{\sum \dot{E}_{in}} \quad (6.9)$$

Where η_{ex} is the exergetic efficiency of the cycle. $\sum \dot{E}_{out}$, $\sum \dot{E}_{in}$ and $\sum \dot{E}_D$ are the total exergy recovered, supplied and destructed respectively.

The exergetic efficiency of absorption-compression triple effect series flow cascade refrigeration system is given by:

$$\eta_{ex, CASCADE} = 1 - \frac{\sum(\dot{E}_D)}{\dot{Q}_{Hpg} \left[\left(1 - \frac{T_0}{T_{Hpg}} \right) \right] + \dot{W}_P + \dot{W}_c} = \frac{\dot{Q}_{eVC} \left[\left(1 - \frac{T_0}{T_b} \right) \right]}{\dot{Q}_{Hpg} \left[\left(1 - \frac{T_0}{T_{Hpg}} \right) \right] + \dot{W}_P + \dot{W}_c} \quad (6.10)$$

Where $\sum(\dot{E}_D)$, is the total exergy destruction rate of the cascade system in kW, \dot{Q}_{Hpg} and T_{Hpg} are the input heat in kW and temperature in °C of the high pressure generator and \dot{W}_P and \dot{W}_c are solution pump work and compressor work in kW respectively. \dot{Q}_{eVC} in kW is the rate of net refrigerating effect and T_b is the temperature

of space to be cooled in $^{\circ}\text{C}$ of VCRS respectively. T_0 is the ambient or dead state temperature in $^{\circ}\text{C}$.

6.3.3.3 Exergy destruction ratio (EDR)

The EDR is the total exergy destruction in the system to the exergy in the products (Arora and Kaushik, 2008) and is given by Eq. (6.11):

$$\text{EDR} = \frac{\dot{E}_{D,\text{total}}}{\dot{E}_P} = \frac{1}{\eta_{\text{ex}}} - 1 \quad (6.11)$$

The exergy destruction ratio is the rate of exergy destruction in a system component ($\dot{E}_{D,i}$) to the exergy recover rate of the fuel provided to the overall system ($\dot{E}_{E,\text{total}}$) or the total exergy destruction rate within the system ($\dot{E}_{D,\text{total}}$) (Bejan et al., 1996).

$$\text{EDR} = \frac{\dot{E}_{D,i}}{\dot{E}_{E,\text{total}}} = \frac{\dot{E}_{D,i}}{\dot{E}_{D,\text{total}}} \quad (6.12)$$

The exergetic destruction ratio (EDR) absorption compression triple effect series flow cascade refrigeration system is given by:

$$\text{EDR}_{\text{CASCADE}} = \frac{\sum(\dot{E}_D)}{\dot{Q}_{\text{eVC}} \left[\left(1 - \frac{T_0}{T_b} \right) \right]} \quad (6.13)$$

Where $\sum(\dot{E}_D)$ is the rate of total exergy destruction of the cascade system in kW, \dot{Q}_{eVC} in kW is the rate of net refrigerating effect of vapour compression refrigeration system, T_b in $^{\circ}\text{C}$ is the temperature of space to be cooled and T_0 is the ambient or dead state temperature in $^{\circ}\text{C}$ respectively.

The mass, energy and exergy balances relations of each component of compression-absorption triple effect series flow refrigeration system based on conservation principles are shown in Table 6.1.

Table 6.1 Mass balance, Energy balance and Exergy balance relations in individual component of compression-absorption (triple effect H₂O/LiBr series flow) cascade refrigeration system

S. No.	Components	Energy parameters	
		Mass balance	Energy balance
1.	Evaporator 1	\dot{m}_{rVC}	$\dot{Q}_{\text{eVC}} = \dot{m}_{\text{rVC}}(h_1 - h_4)$
2.	Compressor	\dot{m}_{rVC}	$\dot{W}_c = \dot{m}_{\text{rVC}}(h_2 - h_1)$
3.	Condenser 1	\dot{m}_{rVC}	$\dot{Q}_{\text{condVC}} = \dot{m}_{\text{rVC}}(h_2 - h_{3a}) = \dot{m}_{\text{rVA}}(h_{28} - h_{27})$ $= \dot{Q}_{\text{eVA}}$

4.	Expansion valve	\dot{m}_{rVC}	$\dot{m}_{rVC}h_{3a} = \dot{m}_{rVC}h_4$
5.	Cascade heat exchanger (Che)	$\dot{m}_{rVA}, \dot{m}_{rVC}$	$\dot{Q}_{condVC} = \dot{m}_{rVC}(h_2 - h_{3a}) = \dot{m}_{rVA}(h_{28} - h_{27}) = \dot{Q}_{eVA}$
6.	Evaporator 2	\dot{m}_{rVA}	$\dot{Q}_{eVA} = \dot{m}_{rVA}(h_{28} - h_{27}) = \dot{m}_{rVC}(h_2 - h_{3a}) = \dot{Q}_{condVC}$
7.	Absorber	$\dot{m}_s = \dot{m}_{rVA} + \dot{m}_{w1}$	$\dot{Q}_a = \dot{m}_{rVA}h_{28} + \dot{m}_{w1}h_{18} - \dot{m}_sh_5$
8.	Solution Pump	\dot{m}_s	$\dot{W}_P = \dot{m}_s(h_6 - h_5)$
9.	She 1	\dot{m}_s, \dot{m}_{w1}	$\dot{m}_{w1}(h_{16} - h_{17}) = \dot{m}_s(h_7 - h_6)$
10.	She 2	\dot{m}_s, \dot{m}_{w2}	$\dot{m}_{w2}(h_{13} - h_{14}) = \dot{m}_s(h_8 - h_7)$
11.	She 3	\dot{m}_s, \dot{m}_{w3}	$\dot{m}_{w3}(h_{10} - h_{11}) = \dot{m}_s(h_9 - h_8)$
12.	High pressure Generator	$\dot{m}_s = \dot{m}_{r3} + \dot{m}_{w3}$	$\dot{Q}_{Hpg} = \dot{m}_{r3}h_{19} + \dot{m}_{w3}h_{10} - \dot{m}_sh_9$
13.	Medium pressure Generator	$\dot{m}_{w3} = \dot{m}_{r2} + \dot{m}_{w2}$	$\dot{Q}_{Mpg} = \dot{m}_{r3}(h_{19} - h_{20}) = \dot{m}_{r2}h_{22} + \dot{m}_{w2}h_{13} - \dot{m}_{w3}h_{12}$
14.	Low pressure Generator	$\dot{m}_{w2} = \dot{m}_{r1} + \dot{m}_{w1}$	$\dot{Q}_{Lpg} = \dot{m}_{r2}(h_{22} - h_{23}) = \dot{m}_{r1}h_{25} + \dot{m}_{w1}h_{16} - \dot{m}_{w2}h_{15}$
15.	Rtv 1	\dot{m}_{rVA}	$\dot{m}_{rVA}h_{26} = \dot{m}_{rVA}h_{27}$
16.	Rtv 2	\dot{m}_{r2}	$\dot{m}_{r2}h_{23} = \dot{m}_{r2}h_{24}$
17.	Rtv 3	\dot{m}_{r3}	$\dot{m}_{r3}h_{20} = \dot{m}_{r3}h_{21}$
18.	Stv 1	\dot{m}_{w1}	$\dot{m}_{w1}h_{17} = \dot{m}_{w1}h_{18}$
19.	Stv 2	\dot{m}_{w2}	$\dot{m}_{w1}h_{14} = \dot{m}_{w2}h_{15}$
20.	Stv 3	\dot{m}_{w3}	$\dot{m}_{w3}h_{11} = \dot{m}_{w3}h_{12}$
21.	Condenser 2	\dot{m}_{rVA}	$\dot{Q}_{condVA} = \dot{m}_{r3}h_{21} + \dot{m}_{r2}h_{24} + \dot{m}_{r1}h_{25} - \dot{m}_{rVA}h_{26}$
Exergy parameters			
Exergy destruction (\dot{E}_D)		Exergy destruction ratio (EDR)	
$\dot{E}_{D,evc} = \dot{E}_{X_4} + \dot{Q}_{eVC} \left(1 - \frac{T_0}{T_b}\right) - \dot{E}_{X_1}$ $= \dot{m}_{rVC}(h_4 - T_0s_4) + \dot{Q}_{eVC} \left(1 - \frac{T_0}{T_b}\right) - \dot{m}_{rVC}(h_1 - T_0s_1)$		$EDR_{evc} = \frac{\dot{E}_{D,evc}}{\dot{E}_{D,total}}$	
$\dot{E}_{D,comp} = \dot{E}_{X_1} + \dot{W}_c - \dot{E}_{X_2}$ $= \dot{m}_{rVC}(h_1 - T_0s_1) + \dot{W}_c - \dot{m}_{rVC}(h_2 - T_0s_2)$		$EDR_c = \frac{\dot{E}_{D,comp}}{\dot{E}_{D,total}}$	

$\begin{aligned}\dot{E}_{D,\text{cond1}} &= \dot{E}_{X_2} - \dot{Q}_{\text{cond VC}} \left(1 - \frac{T_0}{T_{\text{condVC}}}\right) - \dot{E}_{X_{3a}} \\ &= \dot{m}_{\text{rVC}}(h_2 - T_0 s_2) \\ &\quad - \dot{Q}_{\text{cond VC}} \left(1 - \frac{T_0}{T_{\text{condVC}}}\right) \\ &\quad - \dot{m}_{\text{rVC}}(h_{3a} - T_0 s_{3a})\end{aligned}$	$\begin{aligned}EDR_{\text{cond VC}} &= \frac{\dot{E}_{D,\text{cond1}}}{\dot{E}_{D,\text{total}}}\end{aligned}$
$\begin{aligned}\dot{E}_{D,\text{Ex. valve}} &= \dot{E}_{X_{3a}} - \dot{E}_{X_4} \\ &= \dot{m}_{\text{rVC}}(h_{3a} - T_0 s_{3a}) - \dot{m}_{\text{rVC}}(h_4 - T_0 s_4)\end{aligned}$	$EDR_{\text{exp.valve}} = \frac{\dot{E}_{D,\text{Ex. valve}}}{\dot{E}_{D,\text{total}}}$
$\begin{aligned}\dot{E}_{D,\text{Che}} &= \dot{E}_{X_2} + \dot{E}_{X_{27}} - \dot{E}_{X_{3a}} - \dot{E}_{X_{28}} \\ &= \dot{m}_{\text{rVC}}(h_2 - T_0 s_2) + \dot{m}_{\text{rVA}}(h_{27} - T_0 s_{27}) \\ &\quad - \dot{m}_{\text{rVC}}(h_{3a} - T_0 s_{3a}) - \dot{m}_{\text{rVA}}(h_{28} - T_0 s_{28})\end{aligned}$	$EDR_{\text{Che}} = \frac{\dot{E}_{D,\text{Che}}}{\dot{E}_{D,\text{total}}}$
$\begin{aligned}\dot{E}_{D,\text{eVA}} &= \dot{E}_{X_{27}} + \dot{Q}_{\text{eVA}} \left(1 - \frac{T_0}{T_{\text{eVA}}}\right) - \dot{E}_{X_{28}} \\ &= \dot{m}_{\text{rVA}}(h_{27} - T_0 s_{27}) + \dot{Q}_{\text{eVA}} \left(1 - \frac{T_0}{T_{\text{eVA}}}\right) \\ &\quad - \dot{m}_{\text{rVA}}(h_{28} - T_0 s_{28})\end{aligned}$	$EDR_{\text{eVA}} = \frac{\dot{E}_{D,\text{eVA}}}{\dot{E}_{D,\text{total}}}$
$\begin{aligned}\dot{E}_{D,\text{Abs}} &= \dot{E}_{X_{18}} + \dot{E}_{X_{28}} - \dot{E}_{X_5} \\ &= \dot{m}_{\text{w1}}\{(h_{18} - h_0) - T_0(s_{18} - s_0)\} \\ &\quad + \dot{m}_{\text{rVA}}\{(h_{28} - h_0) - T_0(s_{28} - s_0)\} \\ &\quad - \dot{m}_s\{(h_5 - h_0) - T_0(s_5 - s_0)\}\end{aligned}$	$EDR_a = \frac{(\dot{E}_D)_a}{\dot{E}_{D,\text{total}}}$
$\dot{E}_{D,\text{Pump}} = \dot{E}_{X_5} - \dot{E}_{X_6} = \dot{m}_s(h_5 - T_0 s_5) - \dot{m}_s(h_6 - T_0 s_6)$	$EDR_p = \frac{(\dot{E}_D)_{\text{Pump}}}{\dot{E}_{D,\text{total}}}$
$\begin{aligned}\dot{E}_{D,\text{She1}} &= \dot{E}_{X_6} - \dot{E}_{X_7} + \dot{E}_{X_{16}} - \dot{E}_{X_{17}} = \dot{m}_s\{(h_6 - T_0 s_6) - \\ &\quad (h_7 - T_0 s_7)\} + \dot{m}_{\text{w1}}\{(h_{16} - T_0 s_{16}) - (h_{17} - T_0 s_{17})\}\end{aligned}$	$EDR_{\text{She1}} = \frac{\dot{E}_{D,\text{She1}}}{\dot{E}_{D,\text{total}}}$
$\begin{aligned}\dot{E}_{D,\text{She2}} &= \dot{E}_{X_7} - \dot{E}_8 + \dot{E}_{X_{13}} - \dot{E}_{X_{14}} = \dot{m}_s\{(h_7 - T_0 s_7) - \\ &\quad (h_8 - T_0 s_8)\} + \dot{m}_{\text{w2}}\{(h_{13} - T_0 s_{13}) - (h_{14} - T_0 s_{14})\}\end{aligned}$	$EDR_{\text{She2}} = \frac{\dot{E}_{D,\text{She2}}}{\dot{E}_{D,\text{total}}}$
$\begin{aligned}\dot{E}_{D,\text{she3}} &= \dot{E}_8 - \dot{E}_9 + \dot{E}_{X_{10}} - \dot{E}_{X_{11}} = \dot{m}_s\{(h_8 - T_0 s_8) - \\ &\quad (h_9 - T_0 s_9)\} + \dot{m}_{\text{w3}}\{(h_{10} - T_0 s_{10}) - (h_{11} - T_0 s_{11})\}\end{aligned}$	$EDR_{\text{She3}} = \frac{\dot{E}_{D,\text{she3}}}{\dot{E}_{D,\text{total}}}$
$\begin{aligned}\dot{E}_{D,\text{Hpg}} &= \dot{E}_9 + \dot{Q}_{\text{Hpg}} \left(1 - \frac{T_0}{T_{\text{Hpg}}}\right) - \dot{E}_{10} - \dot{E}_{X_{19}} \\ &= \dot{m}_s\{(h_9 - h_0) - T_0(s_9 - s_0)\} \\ &\quad + \dot{Q}_{\text{Hpg}} \left(1 - \frac{T_0}{T_{\text{Hpg}}}\right) \\ &\quad - \dot{m}_{\text{w3}}\{(h_{10} - h_0) - T_0(s_{10} - s_0)\} \\ &\quad - \dot{m}_{\text{r3}}\{(h_{19} - h_0) - T_0(s_{19} - s_0)\}\end{aligned}$	$EDR_{\text{Hpg}} = \frac{\dot{E}_{D,\text{Hpg}}}{\dot{E}_{D,\text{total}}}$
$\begin{aligned}\dot{E}_{D,\text{Mpg}} &= \dot{E}_{19} - \dot{E}_{20} + \dot{E}_{12} - \dot{E}_{13} - \dot{E}_{22} \\ &= \dot{m}_{\text{r3}}\{(h_{19} - T_0 s_{19}) - (h_{20} - T_0 s_{20})\} \\ &\quad + \dot{m}_{\text{w3}}\{(h_{12} - h_0) - T_0(s_{12} - s_0)\} \\ &\quad - \dot{m}_{\text{w2}}\{(h_{13} - h_0) - T_0(s_{13} - s_0)\} \\ &\quad - \dot{m}_{\text{r2}}\{(h_{22} - h_0) - T_0(s_{22} - s_0)\}\end{aligned}$	$EDR_{\text{Mpg}} = \frac{\dot{E}_{D,\text{Mpg}}}{\dot{E}_{D,\text{total}}}$

$\begin{aligned}\dot{E}_{D,Lpg} &= \dot{E}_{22} - \dot{E}_{23} + \dot{E}_{15} - \dot{E}_{16} - \dot{E}_{25} \\ &= \dot{m}_{r2}\{(h_{22} - T_0s_{22}) - (h_{23} - T_0s_{23})\} \\ &\quad + \dot{m}_{w2}\{(h_{15} - h_0) - T_0(s_{15} - s_0)\} \\ &\quad - \dot{m}_{w1}\{(h_{16} - h_0) - T_0(s_{16} - s_0)\} \\ &\quad - \dot{m}_{r1}\{(h_{25} - h_0) - T_0(s_{25} - s_0)\}\end{aligned}$	$EDR_{Lpg} = \frac{\dot{E}_{D,Lpg}}{\dot{E}_{D,total}}$
$\begin{aligned}\dot{E}_{D,Rtv1} &= \dot{E}_{26} - \dot{E}_{27} \\ &= \dot{m}_{rVA}\{(h_{26} - T_0s_{26}) - (h_{27} - T_0s_{27})\}\end{aligned}$	$EDR_{Rtv1} = \frac{\dot{E}_{D,Rtv1}}{\dot{E}_{D,total}}$
$\dot{E}_{D,Rtv2} = \dot{E}_{23} - \dot{E}_{24} = \dot{m}_{r2}\{(h_{23} - T_0s_{23}) - (h_{24} - T_0s_{24})\}$	$EDR_{Rtv2} = \frac{\dot{E}_{D,Rtv2}}{\dot{E}_{D,total}}$
$\dot{E}_{D,Rtv3} = \dot{E}_{20} - \dot{E}_{21} = \dot{m}_{r3}\{(h_{20} - T_0s_{20}) - (h_{21} - T_0s_{21})\}$	$EDR_{Rtv3} = \frac{\dot{E}_{D,Rtv3}}{\dot{E}_{D,total}}$
$\begin{aligned}\dot{E}_{D,Stv1} &= \dot{E}_{17} - \dot{E}_{18} \\ &= \dot{m}_{w1}\{(h_{17} - T_0s_{17}) - (h_{18} - T_0s_{18})\}\end{aligned}$	$EDR_{Stv1} = \frac{\dot{E}_{D,Stv1}}{\dot{E}_{D,total}}$
$\begin{aligned}\dot{E}_{D,Stv2} &= \dot{E}_{14} - \dot{E}_{15} \\ &= \dot{m}_{w2}\{(h_{14} - T_0s_{14}) - (h_{15} - T_0s_{15})\}\end{aligned}$	$EDR_{Stv2} = \frac{\dot{E}_{D,Stv2}}{\dot{E}_{D,total}}$
$\begin{aligned}\dot{E}_{D,Stv3} &= \dot{E}_{11} - \dot{E}_{12} \\ &= \dot{m}_{w3}\{(h_{11} - T_0s_{11}) - (h_{12} - T_0s_{12})\}\end{aligned}$	$EDR_{Stv3} = \frac{\dot{E}_{D,Stv3}}{\dot{E}_{D,total}}$
$\begin{aligned}\dot{E}_{D,cond2} &= \dot{E}_{21} + \dot{E}_{24} + \dot{E}_{25} - \dot{E}_{26} \\ &= \dot{m}_{r3}\{(h_{21} - h_0) - T_0(s_{21} - s_0)\} \\ &\quad + \dot{m}_{r2}\{(h_{24} - h_0) - T_0(s_{24} - s_0)\} \\ &\quad + \dot{m}_{r1}\{(h_{25} - h_0) - T_0(s_{25} - s_0)\} \\ &\quad - \dot{m}_{rVA}\{(h_{26} - h_0) - T_0(s_{26} - s_0)\}\end{aligned}$	$\begin{aligned}EDR_{cond VA} \\ &= \frac{\dot{E}_{D,cond2}}{\dot{E}_{D,total}}\end{aligned}$

6.3.4. Model validation

Model validation has been carried out on comparing the results of present work to the Arora et al. (2015) for the H₂O-LiBr TESFVAR cycle. Fig. 6.2, 6.3 and Table 6.2 shows comparison of the results of two studies for model validation. The corresponding values of COP and exergetic efficiency of VARS thus obtained merely lie within $\pm 3\%$ while compared to Arora et al. (2015) as shown in Fig. 6.2, 6.3 respectively. The COP and exergetic efficiency of the VARS are 1.456 and 10.82% in the current work and according to Arora et al. (2015), these were 1.456 and 11.17% at $T_a = T_{cond VA} = 37.8^\circ\text{C}$, $T_{Hpg} = 185^\circ\text{C}$, $\epsilon_{she(s)} = 0.7$ and $\dot{m}_{rVA} = 1\text{kg/s}$. The variation in the result is due to the inclusion of irreversibilities of pump work in the present model. The comparison of present work with Arora et al. (2015) for triple effect series flow vapour absorption refrigeration cycle (TESFVARC) shows that the results are close to each other and the values of heat rate (\dot{Q}_1) and work rate (\dot{W}_1) coincide to each other as shown in Table 6.2.

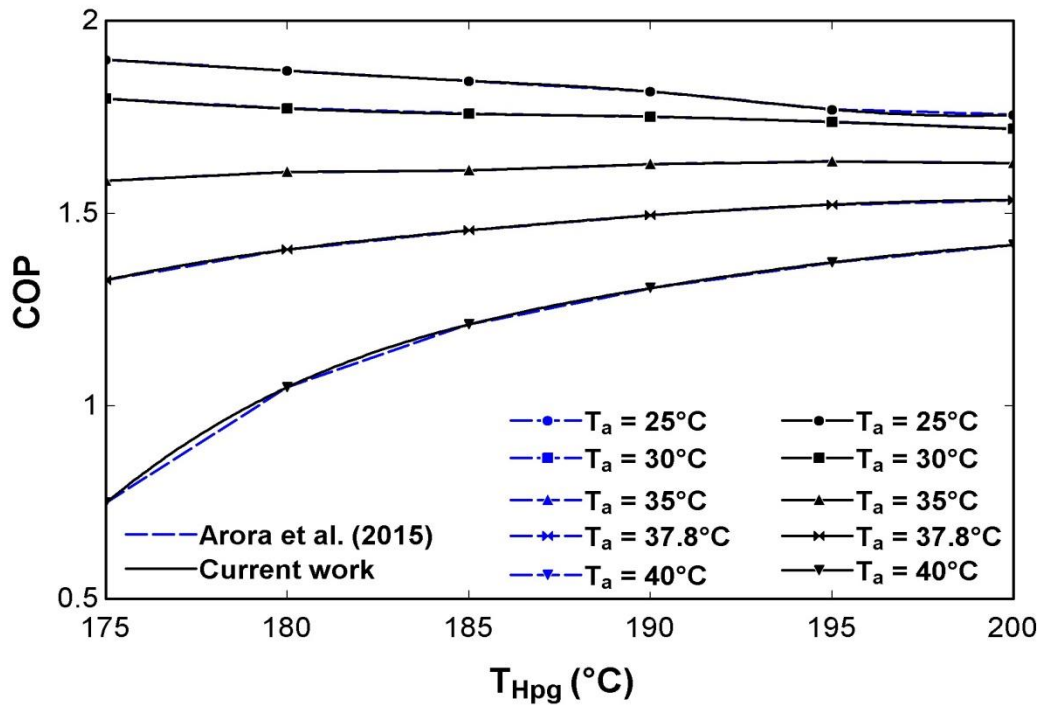


Figure 6.2 Variation of COP with THpg ($T_{eVA} = 7.20C$, $T_a = T_{cVA}$, $T_{eVC} = -400C$, $\epsilon_{she(s)} = 0.7$)

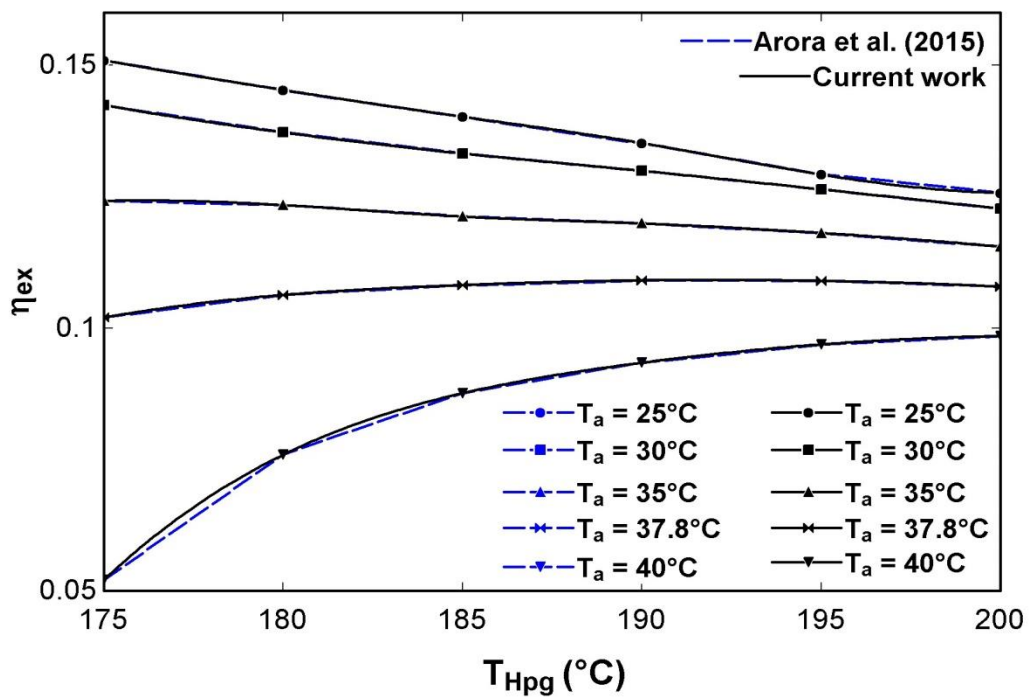


Figure 6.3 Variation in exergetic efficiency with THpg ($T_{eVA} = 7.20C$, $T_a = T_{cVA}$, $T_{eVC} = -400C$, $\epsilon_{she(s)} = 0.7$)

Table 6.2 Heat rate (\dot{Q}_i) or work rate (\dot{W}_i) of components of ACCRS. Comparison of present work with Arora et al. (2015) for H₂O-LiBr TESFVARs ($T_a = T_{cVA} = 37.8^\circ\text{C}$, $T_{Hpg} = 185^\circ\text{C}$, $\epsilon_{she(s)} = 0.7$ and $\dot{m}_{rVA} = 1\text{kg/s}$)

System components (i)	\dot{Q}_i or \dot{W}_i (kW)		
	Present work	Arora et al. (2015) (TESFVARs)	Difference (%)
Evaporator 1	1746	-	-
Compressor	240.6	-	-
Expansion valve	-	-	-
Cascade heat exchanger	2355	-	-
Absorber	-2991	-2991	0
Solution Pump	2.26	2.26	0
She 1	699.7	699.7	0
She 2	1117	1117	0
She 3	1394	1394	0
Hpg	1615	1615	0
Mpg	855.8	855.8	0
Lpg	754.8	754.8	0
Rtv 1	-	-	-
Rtv 2	-	-	-
Rtv 3	-	-	-
Stv 1	-	-	-
Stv 2	-	-	-
Stv 3	-	-	-
Condenser 2	-981.9	-981.9	0

6.3.5. Input Parameters

The present work has been assessed by the first and second laws of thermodynamics. The energy and exergy analysis of the absorption-compression triple effect series flow cascade refrigeration system evaluates the performance of combined system. The evaporator of vapour absorption system receives the heat of condenser of vapour compression system such that $\dot{Q}_{eVA} = \dot{Q}_{cond VC}$. The overlap temperature (T_{ov}) is

the difference between temperature of isobaric condensation in the condenser of VAR cycle and temperature of isobaric evaporation in the evaporator of TESFVAR cycle i.e. $T_{ov} = T_{cond VC} - T_{eVA}$ at the heat exchanger of the cascade system. The mean temperature of the heat exchange is T_m .

Table 6.3 Input parameters considered except where the variation of physical parameters involved (Arora et al., 2015)

S.No.	Input parameters	Values
1.	High pressure generator temperature (T_{Hpg})	185 ⁰ C
2.	Evaporator 2 temperature (T_{eVA})	7.2 ⁰ C
3.	Condenser 2 temperature ($T_{cond VA}$)]	37.8 ⁰ C
4.	Absorber temperature (T_a)	37.8 ⁰ C
5.	Mass flow rate of refrigerant (H ₂ O) in VARS (\dot{m}_{rVA})	1 kg/s
6.	Evaporator 1 temperature (T_{eVC})	-40 ⁰ C
7.	Degree of subcoolin($(\Delta T)_{sc}$)(3-3a)	5 ⁰ C
8.	Condenser 1 temperature ($T_{cond VC}$)	12.2 ⁰ C
9.	Ambient or dead state pressure (P_0) and temperature (T_0)	101.325kPa & 25 ⁰ C

6.4. RESULTS AND DISCUSSION

A computer software based code has been developed in Engineering Equation Solver (EES) software application for the model described in section 2.1 above, to evaluate the performance of absorption-compression (triple effect H₂O-LiBr series flow) cascade refrigeration cycle (ACCRC) on the basis of exergy and energy analysis. A vapour compression refrigeration (VCR) cycle having R1234yf refrigerant is coupled through cascade heat exchanger to triple effect series flow vapour absorption refrigeration cycle (VAR). The property codes for various properties are inbuilt in function directory of the EES and are called for computation of various properties such as specific enthalpy, specific entropy, specific volume, pressures and temperatures etc. The program validation has been done and the results lie within $\pm 3\%$ when compared to Arora et al. (2015) as shown in Fig. 6.2, 6.3 and Table 6.3 respectively.

6.4.1. Results of energy analysis

Table 6.4 The thermodynamic properties (temperature (T_k), pressure (P_k), concentration of solution (X_k), mass flow rate (\dot{m}_k), enthalpy (h_k) and entropy (s_k) of ACCRS at state points ($T_{eVA} = 7.2^0C$, $T_a = T_{cVA} = 37.8^0C$, $T_{Hpg} = 185^0C$, $T_{eVC} = -40^0C$, $\varepsilon_{she}(s) = 0.7$)

State Points (k)	T_k (°C)	P_k (kPa)	X_k (kg abs/kg sol)	m_k (kgs⁻¹)	h_k (kJkg⁻¹)	s_k (kJkg⁻¹K⁻¹)
1	-40	62.36	–	13.81	336.6	1.603
2	12.2	468.5	–	13.81	380.7	1.634
3	12.2	468.5	–	13.81	215.2	1.056
3a	7.2	468.5	–	13.81	210.1	1.033
4	-40	62.3	–	13.81	210.1	1.062
5	37.8	1.016	0.5542	12.567	91.88	0.2288
6	37.8	287.5	0.5542	12.567	92.06	0.2288
7	65.38	287.5	0.5542	12.567	147.7	0.4018
8	107.7	287.5	0.5542	12.567	236.7	0.6481
9	159.3	287.5	0.5542	12.567	347.6	0.9203
10	185	287.5	0.5542	12.19	403.6	1.018
11	131.2	287.5	0.5713	12.19	289.1	0.7535
12	131.2	53.67	0.5713	12.19	289.1	0.7539
13	132.1	53.67	0.5713	11.88	294.1	0.7399
14	85.74	53.67	0.5865	11.88	200	0.4941
15	85.74	6.558	0.5865	11.88	200	0.49419
16	83.11	6.558	0.5865	11.567	201.6	0.4679
17	51.56	6.558	0.6021	11.567	141.1	0.2901
18	51.56	1.016	0.6021	11.567	141.1	0.2901
19	185	287.5	0.6021	0.3096	2835	7.265
20	132.1	287.5	0	0.3096	555.4	1.657
21	37.8	6.558	0	0.3096	555.4	1.82
22	132.1	53.67	0	0.3149	2745	7.822
23	83.11	53.67	0	0.3149	348	1.112
24	37.8	6.558	0	0.3149	348	1.153
25	83.11	6.558	0	0.3755	2655	8.555
26	37.8	6.558	0	1	158.3	0.5428
27	7.2	1.016	0	1	158.3	0.5661
28	7.2	1.016	0	1	2514	8.968

6.4.2 Results of exergy analysis

Table 6.5 Exergy results of ACCRS. ($T_a = T_{cVA} = 37.8^{\circ}\text{C}$, $T_{Hpg} = 185^{\circ}\text{C}$, $\varepsilon_{she(s)} = 0.7$ and $\dot{m}_{rVA} = 1\text{kg/s}$)

System components (i)	$\dot{E}_{in,i}$ (kW)	$\dot{E}_{out,i}$ (kW)
Evaporator 1	-1469	-2347
Compressor	-1343	-1468
Expansion valve	-1349	-1349
Cascade heat exchanger	-1478	-1509
Absorber	471.2	297.4
Solution Pump	299.7	299.7
She 1	1018	982.1
She 2	1224	1171
She 3	1762	1706
Hpg	1484	1468
Mpg	1035	1026
Lpg	755.5	755.4
Rtv 1	-3.533	-10.47
Rtv 2	5.169	1.346
Rtv 3	23.06	4.811
Stv 1	785.6	784.3
Stv 2	625.9	625.6
Stv 3	631.2	631.2
Condenser 2	38.58	-3.533

6.4.3 Parametric Analysis

The performance of absorption-compression (triple effect H₂O-LiBr series flow) cascade refrigeration cycle (ACCRC) depends on various operating variables. The selection of operating variables plays significant role in the energy and exergy performance analysis of ACCRC. The effect of significant operating variables viz. high pressure generator temperature, absorber temperature and evaporator temperature of VCR cycle on thermodynamics and exergetic performance of ACCRC have been

explored. The only one variable has varied while others have been kept constant at their base value during the parametric analysis.

6.4.3.1. Effect of high pressure generator temperature

The effect of generator (T_{Hpg}) on various system and performance parameters i.e. mass flow rate of strong solution (\dot{m}_s), weak solution leaving HP generator (\dot{m}_{w3}), concentration of strong solution (X_s), weak solution leaving HP generator (X_{w3}), MP generator (X_{w2}) and LP generator (X_{w1}), difference of weak solution and strong solution concentration ($X_{w3} - X_s$), heat input to HP generator (\dot{Q}_{Hpg}), solution pump work (\dot{W}_P), solution circulation ratio (SCR), COP, exergetic efficiency (η_{ex}), total exergy destruction rate ($\dot{E}_{D, \text{total}}$) and exergy destruction ratio (EDR) is shown in figures 6.4 to 6.9.

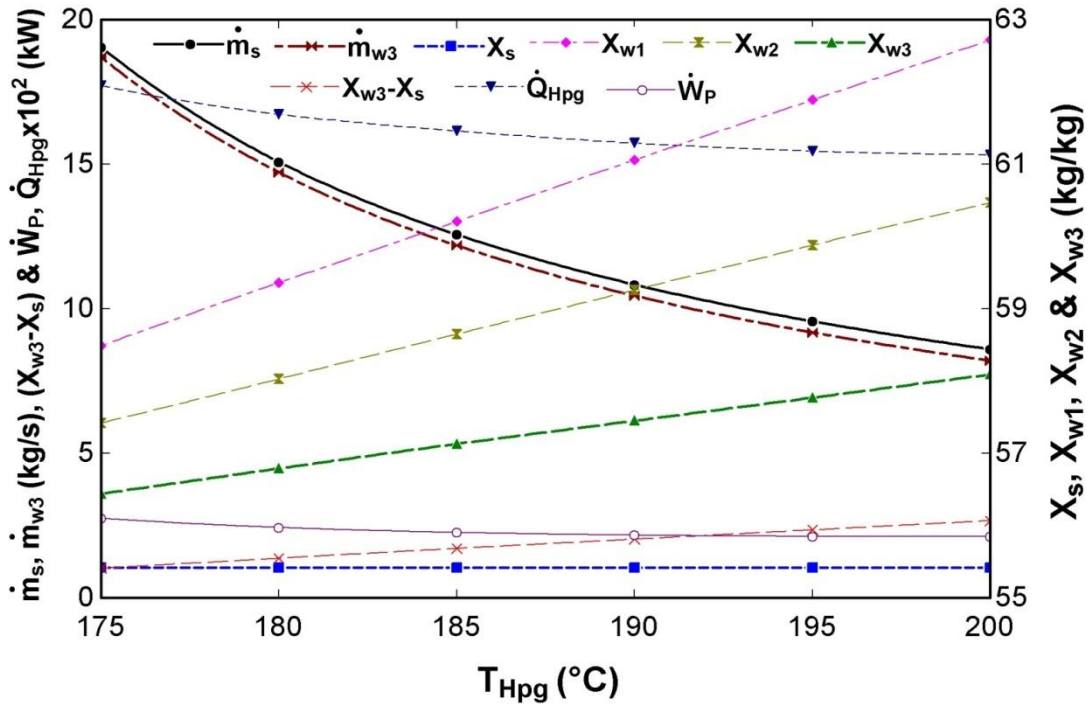


Figure 6.4 Effect of HP generator temperature (T_{Hpg}) on various parameters i.e. mass flow rate of strong solution (\dot{m}_s), weak solution left from HP generator (\dot{m}_{w3}), concentration of strong solution (X_s), weak solution left from HP generator (X_{w3}), MP generator (X_{w2}) and LP generator (X_{w1}), difference of weak solution and strong solution concentration ($X_{w3} - X_s$), heat input to HP generator (\dot{Q}_{Hpg}), solution pump work (\dot{W}_P) ($T_{\text{eVA}} = 7.2^\circ\text{C}$, $T_a = T_{\text{cVA}} = 37.8^\circ\text{C}$, $T_a = T_{\text{cVA}}$, $T_{\text{eVC}} = -40^\circ\text{C}$, $\varepsilon_{\text{she}}(s) = 0.7$)

Fig. 6.4 represents the effect of T_{Hpg} on strong solution concentration (X_s), concentration of weak solution leaving HP generator (X_{w3}), MP generator (X_{w2}), LP generator (X_{w1}), difference in X_{w3} and X_s i.e. ($X_{w3} - X_s$), mass flow rate of strong

solution (\dot{m}_s), weak solution leaving HP generator (\dot{m}_{w3}), heat input to HP generator (\dot{Q}_{HPg}) and solution pump work (\dot{W}_P).

The X_s remains constant and the values of X_{w3} , X_{w2} , X_{w1} and $(X_{w3} - X_s)$ increase with increase in HP generator temperature. The value of (X_s) does not change with increase in HP generator temperature because the strong solution concentration (X_s) depends upon absorber temperature (T_a) and pressure (P_a). Since the values of T_a and P_a are assumed constant, hence X_s remains constant. However, the values of X_{w3} , X_{w2} , X_{w1} and $(X_{w3} - X_s)$ increases with increase in HP generator temperature. This is due to the fact that at higher temperature and pressure, more refrigerant vapours are generated from the absorbent-refrigerant solution consequently, the amount of absorbent increases which increases the solution concentrations (X_{w3} , X_{w2} and X_{w1}). It has been observed that the rate of increase of $(X_{w3} - X_s)$ is more than the X_{w3} .

It can also be observed that the mass flow rate of strong solution (\dot{m}_s), weak solution leaving HP generator (\dot{m}_{w3}), heat input to HP generator (\dot{Q}_{HPg}) and solution pump work (\dot{W}_P) decreases with increase in HP generator temperature. The mass flow rate of strong solution is given by the relation $\dot{m}_s = \frac{X_{w3}}{X_{w3} - X_s} \times \dot{m}_{rVA}$. The mass flow rate of refrigerant $\dot{m}_{rVA} = 1$ kg/s (Table 2) which is constant and the rate of increase in $(X_{w3} - X_s)$ is more than the X_{w3} , thus \dot{m}_s decreases with increase in T_{HPg} . The conservation of mass-concentration is given by equation (6.2) (i.e. $\dot{m}_{w3} X_{w3} = \dot{m}_s X_s$) in which \dot{m}_s decreases, X_s remains constant and X_{w3} increases with increase in T_{HPg} results decrease in \dot{m}_{w3} . With the decrease in \dot{m}_s , the \dot{Q}_{HPg} and \dot{W}_P decrease with increase in HP generator temperature because \dot{Q}_{HPg} and \dot{W}_P both are directly proportional to \dot{m}_s .

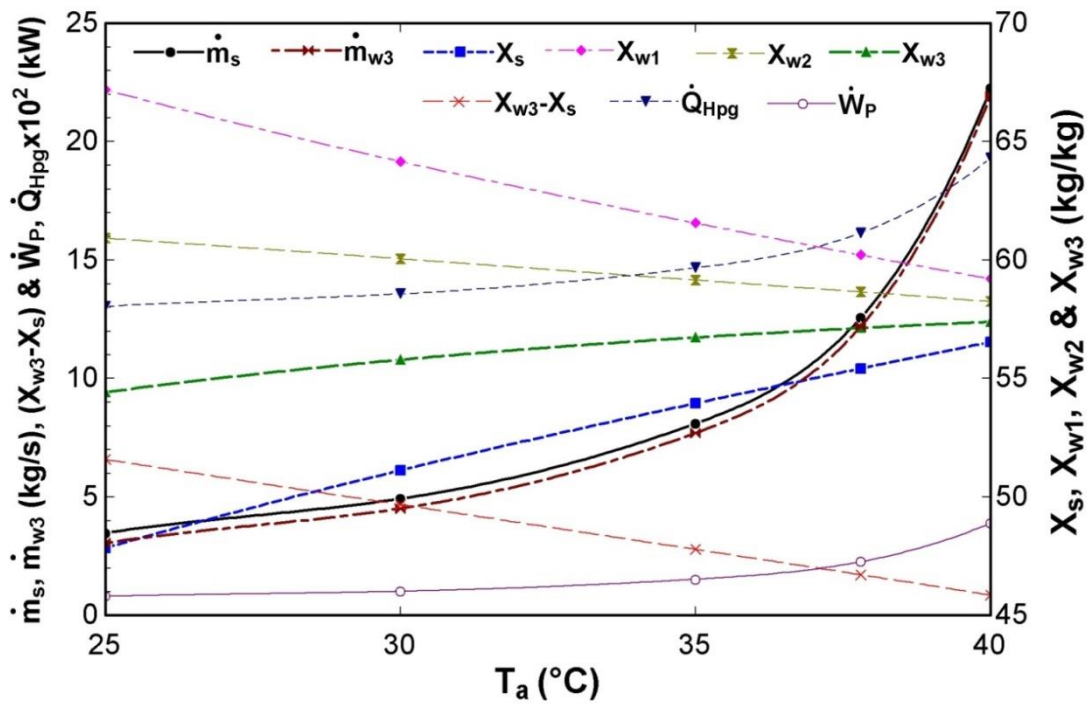


Figure 6.5 Effect of absorber temperature (T_a) on various parameters i.e. mass flow rate of strong solution (\dot{m}_s), weak solution left from HP generator (\dot{m}_{w3}), concentration of strong solution (X_s), weak solution left from HP generator (X_{w3}), MP generator (X_{w2}) and LP generator (X_{w1}), difference of weak solution and strong solution concentration ($X_{w3} - X_s$), heat input to HP generator (\dot{Q}_{Hpg}), solution pump work (\dot{W}_P) ($T_{cVA} = 7.2^0C$, $T_{Hpg} = 185^0C$, $T_a = T_{cVA}$, $T_{eVC} = -40^0C$, $\epsilon_{she(s)} = 0.7$)

Figure 6.5 illustrates that the strong solution concentration (X_s) and the concentration of weak solution leaving HP generator (X_{w3}) increases and the concentration of weak solution in MP generator (X_{w2}), LP generator (X_{w1}) and difference in X_{w3} and X_s i.e. ($X_{w3} - X_s$) decrease with increase in absorber temperature. It has been observed that the mass flow rate of strong solution (\dot{m}_s), weak solution left from HP generator (\dot{m}_{w3}), heat input to HP generator (\dot{Q}_{Hpg}) and solution pump work (\dot{W}_P) increase with increase in absorber temperature.

The values of X_s and X_{w3} increase with increase in absorber temperature as the solution concentration (X) is directly proportional to T (i.e. $X=f(T,P)$). It is the fact that at low pressure and high temperature, more amount of absorbent dissolves in the solution in the absorber. It can also be observed that the X_{w2} and X_{w1} decrease.

It has been observed that the value of X_{w3} increases and $(X_{w3} - X_s)$ decreases with increase in absorber temperature. Thus, the value of \dot{m}_s , which is given by the relation $\dot{m}_s = \frac{X_{w3}}{X_{w3} - X_s} \times \dot{m}_{rVA}$, increases with increase in absorber temperature consequently, the \dot{m}_{w3} , \dot{Q}_{HPg} and \dot{W}_p , which are directly proportional to \dot{m}_s increase with increase in absorber temperature.

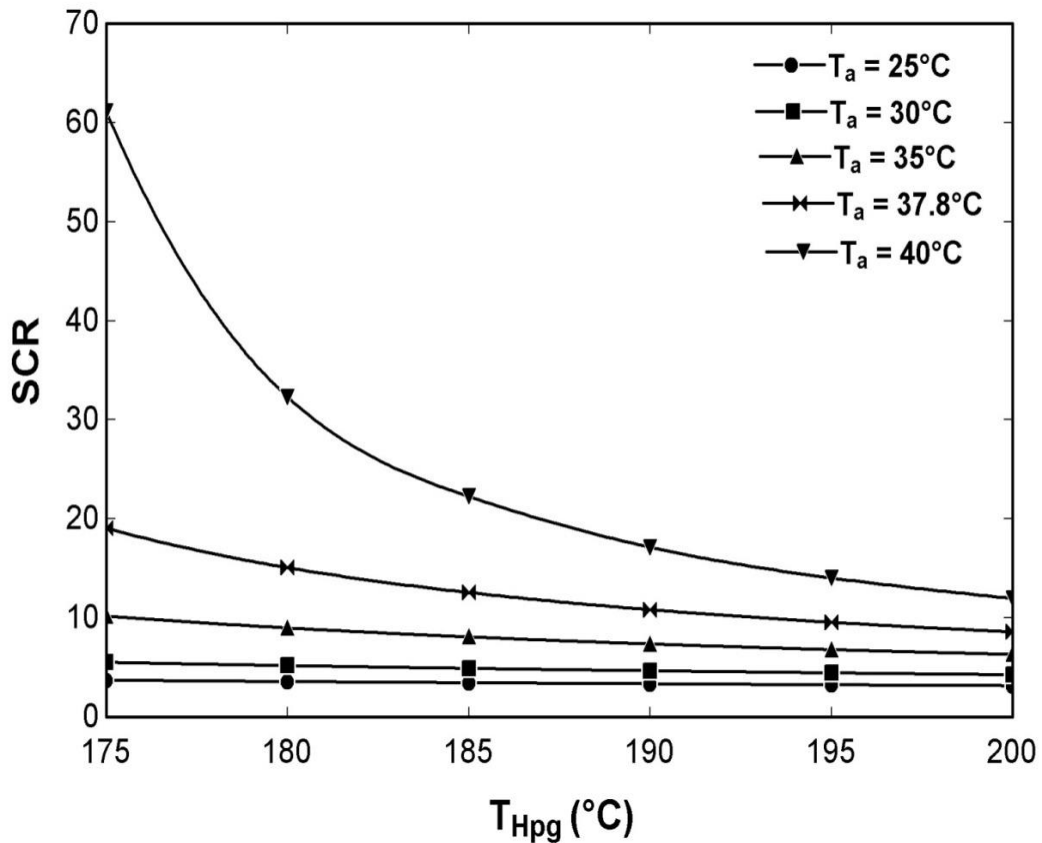


Figure 6.6 Variation of solution circulation ratio (SCR), with HP generator temperature (T_{HPg}) at different absorber temperatures ($T_{eVA} = 7.2^\circ\text{C}$, $T_a = T_{cVA}$, $T_{eVC} = -40^\circ\text{C}$, $\epsilon_{she}(s) = 0.7$)

Fig. 6.6 presents the variation in solution circulation ratio (SCR) with HP generator temperature (T_{HPg}) for different absorber temperatures of absorption compression cascade cycle (ACCRC). For a considered value of absorber temperature, the SCR decreases with increase in HP generator temperature. It has been observed that the SCR declines rapidly at the absorber temperatures above 37.8°C and 40°C . The value of X_s does not change whereas X_{w1} increases and the \dot{m}_s decreases with increase in HP generator as shown in Fig. 6.4.

Thus, the solution circulation ratio (i.e. $SCR = \frac{\text{Mass flow rate of strong solution}}{\text{Mass flow rate of refrigerant}} = \frac{\dot{m}_s}{\dot{m}_{rVA}}$) reduces with increase in HP generator temperature. It can also be observed that the SCR decreases slightly with increase in HP generator temperature at the absorber temperature below 37°C. It is noticed that the maximum and minimum values of SCR are 61.1 and 3.174 at 175°C, 40°C and 200°C, 25°C HP generator and absorber temperature respectively.

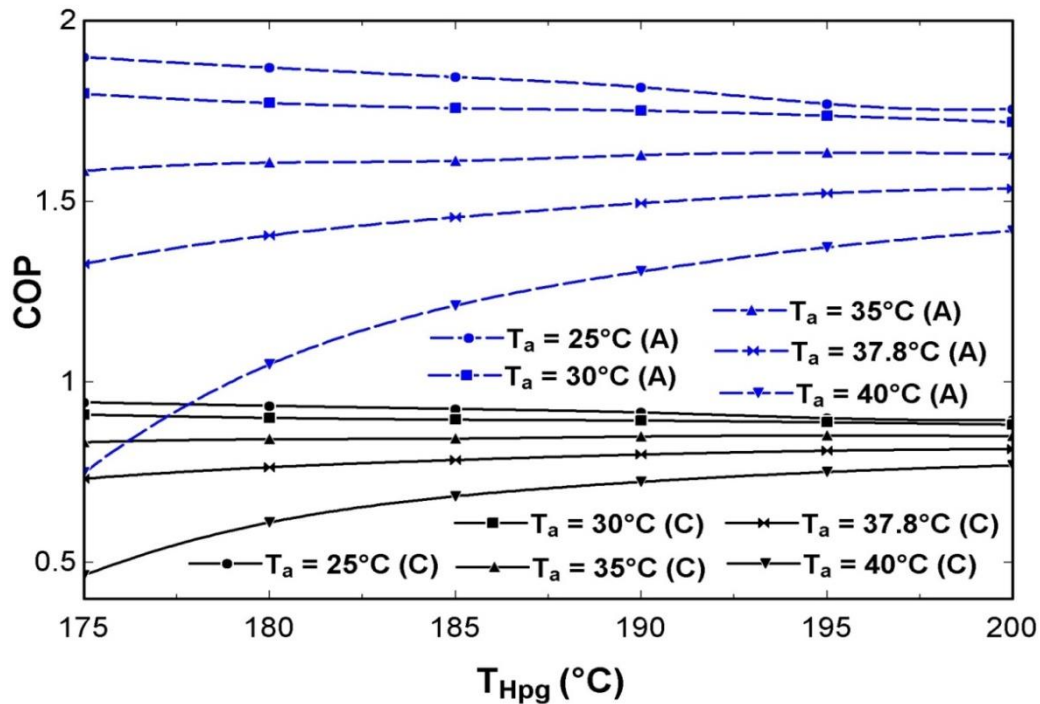


Figure 6.7 Variation of COP with HP generator temperature (T_{HPg}) at different absorber temperatures ($T_{eVA} = 7.2^\circ\text{C}$, $T_a = T_{cVA}$, $T_{eVC} = -40^\circ\text{C}$, $\epsilon_{she(s)} = 0.7$) *'A' stands for the triple effect series flow vapour absorption system and 'C' for absorption compression cascade system

Fig. 6.7 shows the effect of HP generator temperature (T_{HPg}) on COP at various absorber temperatures. The value of COP of absorption compression (triple effect $\text{H}_2\text{O}/\text{LiBr}$ series flow) cascade refrigeration cycle (ACCRC) increases with increase in HP generator temperature for absorber temperatures 37.8°C and 40°C. The COP of absorption compression cascade system is given by equation (6.4) which comprises of two factors, refrigerating effect (\dot{Q}_{eVC}) and input energy ($\dot{Q}_{HPg} + \dot{W}_P + \dot{W}_C$).

The pump work \dot{W}_P is negligible. It has been observed that the solution circulation ratio ($SCR = \frac{\dot{m}_s}{\dot{m}_{rVA}}$) decreases with increase in HP generator temperature as shown in Fig.

6.6. At absorber temperature of 40⁰C, with the increase in T_{HPg} , the rate of reduction of SCR is higher. At lower value of T_{HPg} i.e.175⁰C, this causes heat input to HP generator (\dot{Q}_{HPg}) to get enhanced as shown in Fig. 6.6. Since \dot{Q}_{HPg} is directly proportional to \dot{m}_s which is higher for higher SCR and with the increase in HP generator temperature, \dot{Q}_{HPg} decreases sharply. It is observed that with change in HP generator temperature, the \dot{Q}_{eVC} and \dot{W}_c remain constant. Hence the COP of the cascade system increases rapidly with the increase in HP generator temperature for absorber temperatures 40⁰C.

The COP of cascade system increases slightly at absorber temperature 37.8⁰C with the increase in HP generator temperature. The rate of reduction in SCR is lower with the increase in T_{HPg} . That is why the increase in COP is negligible. It can also be observed that the \dot{Q}_{HPg} increases with increase in HP generator temperature at absorber temperatures 25⁰C and 30⁰C which results decrease in the COP of cascade system with increase in HPgenerator temperature at absorber temperatures 25⁰C and 30⁰C. However, It is noticed that at absorber temperature 35⁰C, the \dot{Q}_{HPg} first decreases and then increases with the increase in HP generator temperature. Thus the COP of the cascade system first increases and then decreases with the increase in HP generator temperature. It is also noticed that the that the value of \dot{Q}_{eVA} decreases consequently \dot{Q}_{eVC} and \dot{W} decreases with increase in absorber temperature which causes decrease in the COP of cascade system with the increase in observer abosrber temperature. It can be observed that the COP of the absorption compression cascade system is lower than the VARS. The maximum and minimum values of COP observed are 0.944 and 0.4653 for ACCRS and 1.899 and 0.749 for VARS at 175⁰C of generator and 25⁰C and 40⁰C of absorber temperature respectively. The COP of the ACCR cycle increases with increase in T_{HPg} at absorber temperature more than 35⁰C. However the system COP is less than the TESFVAR cycle.

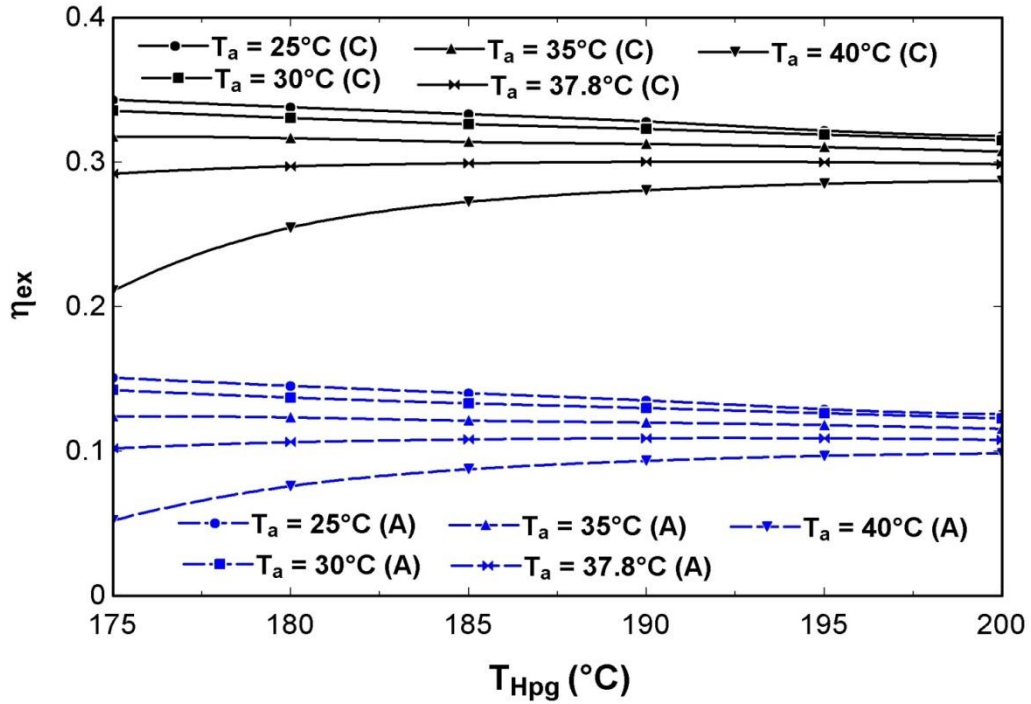


Figure 6.8 Variation of exergetic efficiency (η_{ex}) with HP generator temperature (T_{Hpg}) at different absorber temperatures ($T_{eVA} = 7.2^{\circ}\text{C}$, $T_a = T_{cVA}$, $T_{eVC} = -40^{\circ}\text{C}$, $\varepsilon_{she(s)} = 0.7$) *'A' stands for the triple effect series flow vapour absorption system and 'C' for absorption compression cascade system

Fig. 6.8 illustrates the effect of HP generator temperature (T_{Hpg}) on exergetic efficiency (η_{ex}) at various absorber temperatures (T_a). The exergetic efficiency of absorption compression cascade system (ACCRS) increases with increase in HP generator temperature for an absorber temperature of 40°C . The exergetic efficiency of cascade system is given by the equation (6.10) which depends on two factors, one is exergy output ($\dot{Q}_{eVC} \left| \left(1 - \frac{T_0}{T_b} \right) \right|$) and other is input exergy ($\dot{Q}_{Hpg} \left| \left(1 - \frac{T_0}{T_{Hpg}} \right) \right| + \dot{W}_P + \dot{W}_c$). It is observed that the pump work \dot{W}_P does not vary much with T_{Hpg} as shown in Fig 6.4 and there is no change in the values of \dot{Q}_{eVC} and \dot{W}_c with the change in T_{Hpg} . The term $\dot{Q}_{eVC} \left| \left(1 - \frac{T_0}{T_b} \right) \right|$ is constant with the change in Hp generator temperature as \dot{Q}_{eVC} remains constant and $\left| \left(1 - \frac{T_0}{T_b} \right) \right|$ is also constant. At an absorber temperature of 40°C , with the increase in HP generator temperature, the value of \dot{Q}_{Hpg} decreases as shown in Fig. 6.5 because \dot{Q}_{Hpg} is directly proportional to \dot{m}_s which is higher for higher SCR i.e

$\frac{\dot{m}_s}{\dot{m}_{rVA}}$ and the term $\left| \left(1 - \frac{T_0}{T_{HPg}} \right) \right|$ increases because T_{HPg} is greater than T_0 . Thus the exergetic efficiency of the absorption compression cascade system increases with increase in T_{HPg} at absorber temperature of 40°C .

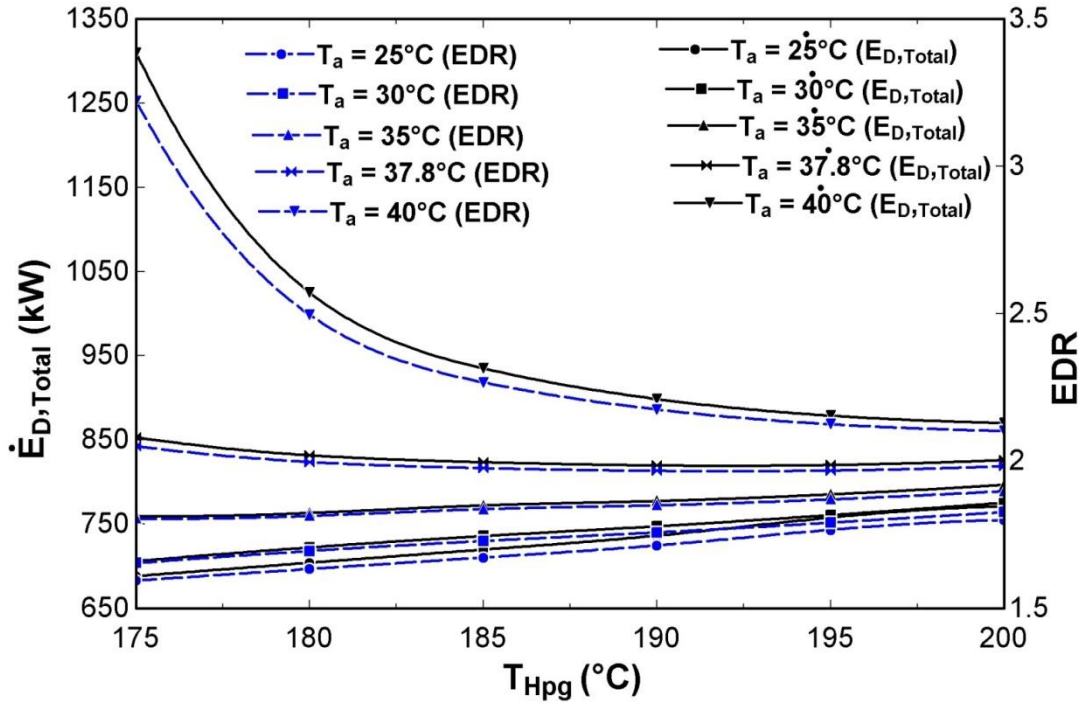


Figure 6.9 Variation of total exergy destruction ($\dot{E}_{D, total}$) and EDR with HP generator temperature (T_{HPg}) at different absorber temperatures ($T_{eVA} = 7.2^\circ\text{C}$, $T_a = T_{cVA}$, $T_{eVC} = -40^\circ\text{C}$, $\varepsilon_{she(s)} = 0.7$)

Fig. 6.9 presents the effect of HP generator temperature (T_{HPg}) on total exergy destruction rate ($\dot{E}_{D, total}$) and exergy destruction ratio (EDR) at various absorber temperatures of absorption compression cascade cycle. The $\dot{E}_{D, total}$ and EDR decreases with increase in HP generator temperature at absorber temperatures 37.8°C and 40°C . It has been observed that the total exergy destruction rate $\dot{E}_{D, total}$ of the cascade cycle increases with increase in HP generator temperature for absorber temperatures 25°C , 30°C and 35°C due to increase in irreversibility of system components at higher temperature. The increase in HP generator temperature reduces the SCR at absorber temperatures of 37.8°C and 40°C as shown in Fig. 6.6. Which reduces the exergy destruction rate of HP generator, absorber and condenser. Thus for the absorber temperature higher than the 35°C , total exergy destruction rate decreases with increase in HP generator temperature. EDR of absorption compression cascade cycle is given by

the Eq. 6.13 in which the term $\dot{Q}_{eVC} \left| \left(1 - \frac{T_0}{T_b} \right) \right|$ remains constant with the change in HP generator temperature. Consequently the EDR, which is the ratio of $\dot{E}_{D, total}$ and $\dot{Q}_{eVC} \left| \left(1 - \frac{T_0}{T_b} \right) \right|$, follows the same trend of $\dot{E}_{D, total}$ curve lines with the increase in HP generator at various absorber temperatures.

6.4.3.2. Effect of evaporator 1 temperature

The effect of evaporator1 temperature (T_{eVC}) on COP, exergetic efficiency (η_{ex}), total exergy destruction rate ($\dot{E}_{D, total}$) and exergy destruction ratio (EDR) has been shown in figures 6.11 to 6.13.

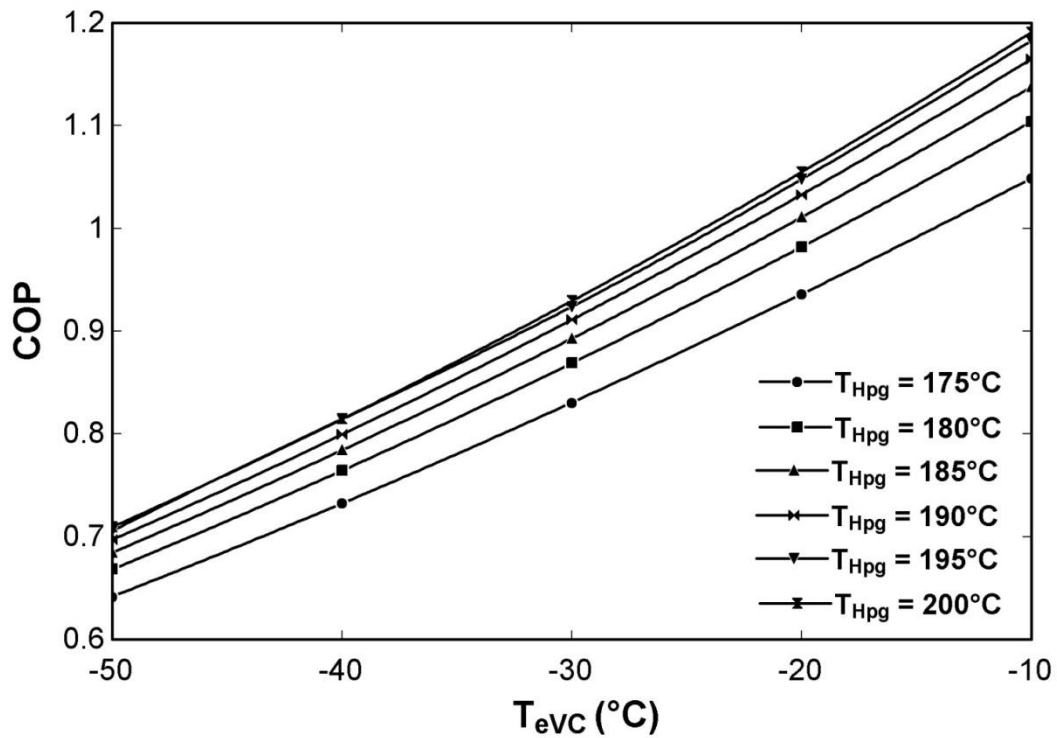


Figure 6.10 Effect of evaporator 1 temperature (T_{eVC}) on COP at different generator temperatures ($T_{eVA} = 7.2^\circ\text{C}$, $T_a = T_{cVA} = 37.8^\circ\text{C}$, $\epsilon_{she(s)} = 0.7$)

Fig. 6.10 shows the effect of evaporator1 temperature on COP at various generator temperatures. The COP of the ACCRC increases with increase in evaporator1 temperature. The COP of absorption compression cascade system is $\frac{\dot{Q}_{eVC}}{(\dot{Q}_{Hpg} + \dot{W}_P + \dot{W}_C)}$ (Eq. 6.4), in which the compressor work (\dot{W}_C) decreases and the specific refrigerating effect ($\frac{\dot{Q}_{eVC}}{\dot{m}_{rVC}}$) increases with increase in evaporator1 temperature (T_{eVC}) as observed for a VCR

cycle (Arora and Kaushik, 2008) Moreover, the \dot{W}_P is negligible and the variation in T_{eVC} does not change the value of \dot{Q}_{HPg} . Due to which, COP of the cascade system increases with increase in evaporator1 temperature (T_{eVC}). It has been observed that the COP of the cascade cycle is higher for higher HP generator temperature with increase in T_{eVC} . It is due to that the value of \dot{Q}_{HPg} decreases with increase in T_{HPg} (Fig. 6.5). The maximum and minimum values of COP observed are 1.191 and 0.6418 at 200°C and 175°C of generator and -10°C and -50°C of evaporator1 temperature respectively.

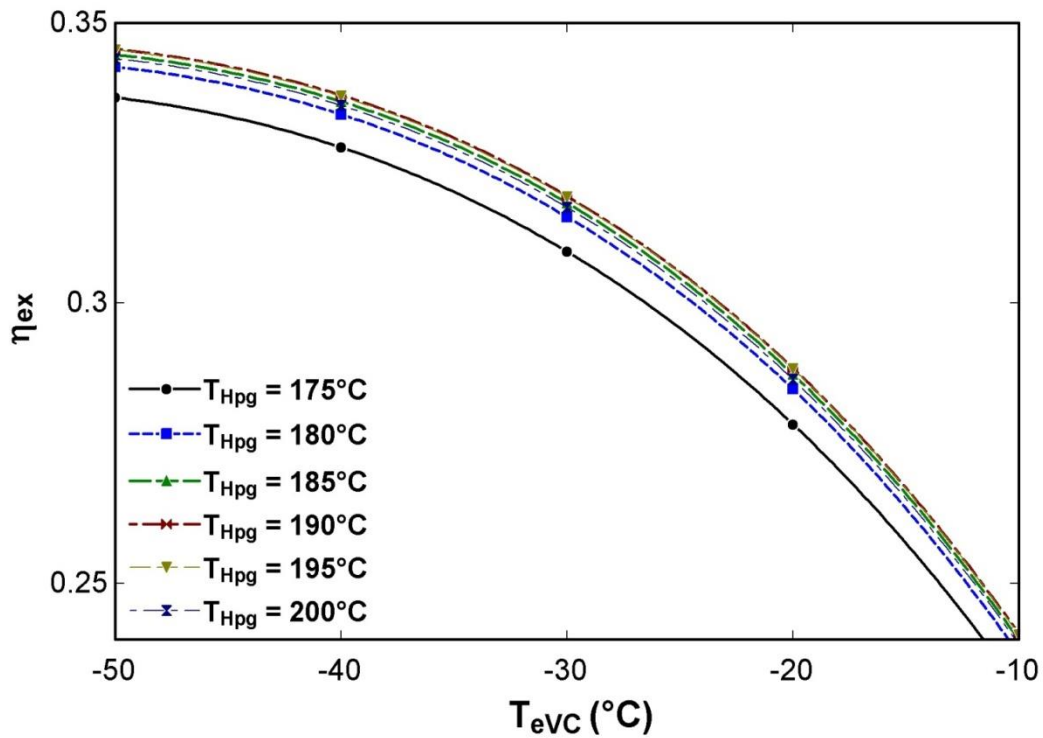


Figure 6.11 Effect of evaporator 1 temperature (T_{eVC}) on exergetic efficiency (η_{ex}) at different generator temperatures ($T_{eVA} = 7.2^\circ\text{C}$, $T_a = T_{cVA} = 37.8^\circ\text{C}$, $\varepsilon_{she(S)} = 0.7$)

Fig. 6.11 presents the effect of evaporator1 temperature (T_{eVC}) on exergetic efficiency (η_{ex}) at various generator temperatures. The exergetic efficiency of the ACCRC decreases with increase in T_{eVC} . The exergetic efficiency (η_{ex}) of the cascade

cycle is $\frac{\dot{Q}_{eVC} \left| \left(1 - \frac{T_0}{T_b} \right) \right|}{\dot{Q}_{HPg} \left| \left(1 - \frac{T_0}{T_{HPg}} \right) \right| + \dot{W}_P + \dot{W}_c}$ (Eq. 6.10) in which the term $\left| \left(1 - \frac{T_0}{T_b} \right) \right|$ decreases with

increase in T_{eVC} (Assumption (5), i.e. $(\Delta T = T_b - T_{eVC}) = 10^\circ\text{C}$) as the value of $T_b < T_0$. The

term $\left| \left(1 - \frac{T_0}{T_{HPg}} \right) \right|$ remains constant with the variation of T_{eVC} and refer to Fig. 6.10, it can

be concluded that the η_{ex} of the cascade cycle decreases with increase in T_{eVC} . Moreover,

it has been observed that the exergetic efficiency is higher for higher HP generator temperature with increase in T_{eVC} . Refer to Fig. 6.4, the value of \dot{Q}_{HPg} decreases and the term $\left(1 - \frac{T_0}{T_{HPg}}\right)$ increases (as $T_{HPg} > T_0$) with increase in T_{HPg} , the value of $\dot{Q}_{HPg} \times \left(1 - \frac{T_0}{T_{HPg}}\right)$ reduces and hence the η_{ex} is higher for higher T_{HPg} . Maximum and minimum values of η_{ex} observed are 0.3453 and 0.2314 at 190°C and 175°C of generator and -50°C and -10°C of evaporator1 temperature respectively.

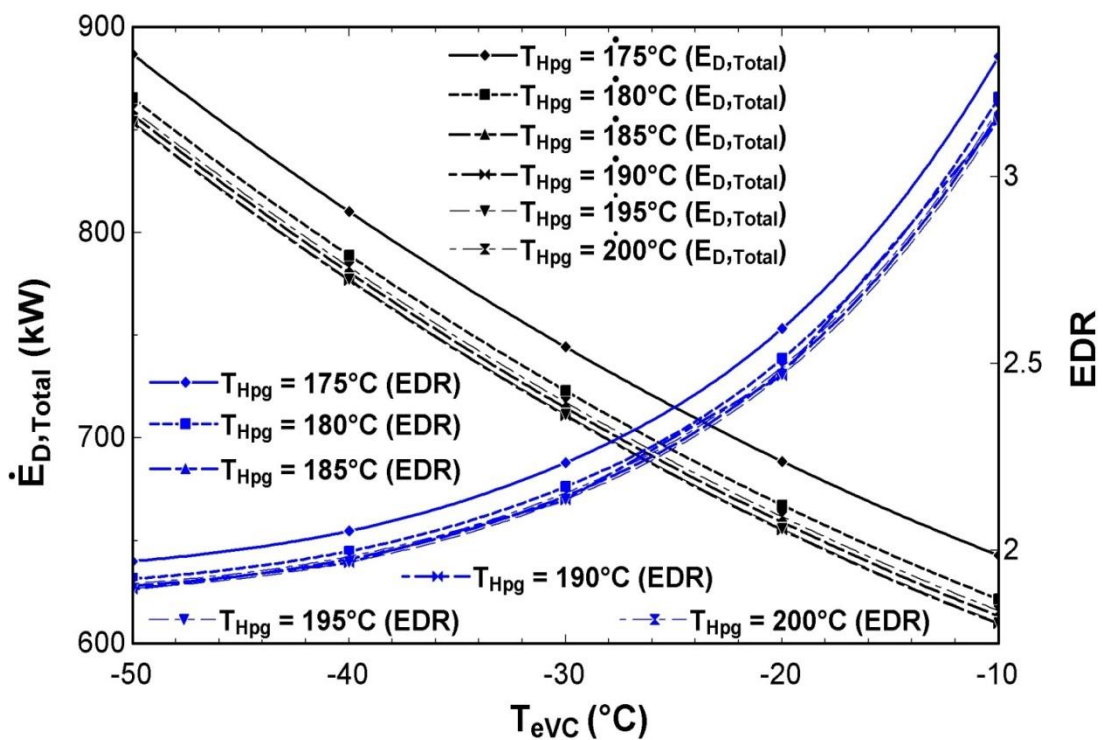


Figure 6.12 Variation of total exergy destruction rate ($\dot{E}_{D, total}$) and exergy destruction ratio (EDR) with evaporator 1 temperature (T_{eVC}) at different generator temperatures ($T_{eVA} = 7.2^\circ\text{C}$, $T_a = T_{cVA} = 37.8^\circ\text{C}$, $\varepsilon_{she(s)} = 0.7$)

Fig. 6.12 illustrates the effect of evaporator1 temperature (T_{eVC}) on total exergy destruction rate ($\dot{E}_{D, total}$) and exergy destruction ratio (EDR) at various generator temperatures. The $\dot{E}_{D, total}$ decreases and EDR increases with increase in evaporator 1 temperature. With the increase in T_{eVC} , the value of T_{eVC} approaches to ambient temperature T_0 . By which the exergy recovered is more than the exergy destroyed in various system components. Moreover, refer to Fig. 6.11, exergetic efficiency (η_{ex}) decreases with increase in T_{eVC} i.e. the rate of exergy recovered from the

system component decreases. Hence total exergy destruction rate ($\dot{E}_{D, total}$) decreases with the increase in T_{eVC} . It can be observed that the values of $\dot{E}_{D, total}$ and EDR are higher at lower generator temperatures with increase in T_{eVC} because the heat input to HP generator (\dot{Q}_{Hpg}) is more at low value of T_{Hpg} (Fig. 6.4). The maximum and minimum values of $\dot{E}_{D, total}$ observed are 886.7 kW and 609.6 kW at 175^oC and 190^oC of generator and -50^oC and -10^oC of evaporator1 temperature respectively.

6.4.3.3 Exergy destruction rate & EDR of system components

Fig. 6.13 & 6.14 illustrate the exergy destruction rate (\dot{E}_D) and percentage exergy destruction ratio (%EDR) of absorption compression cascade system components.

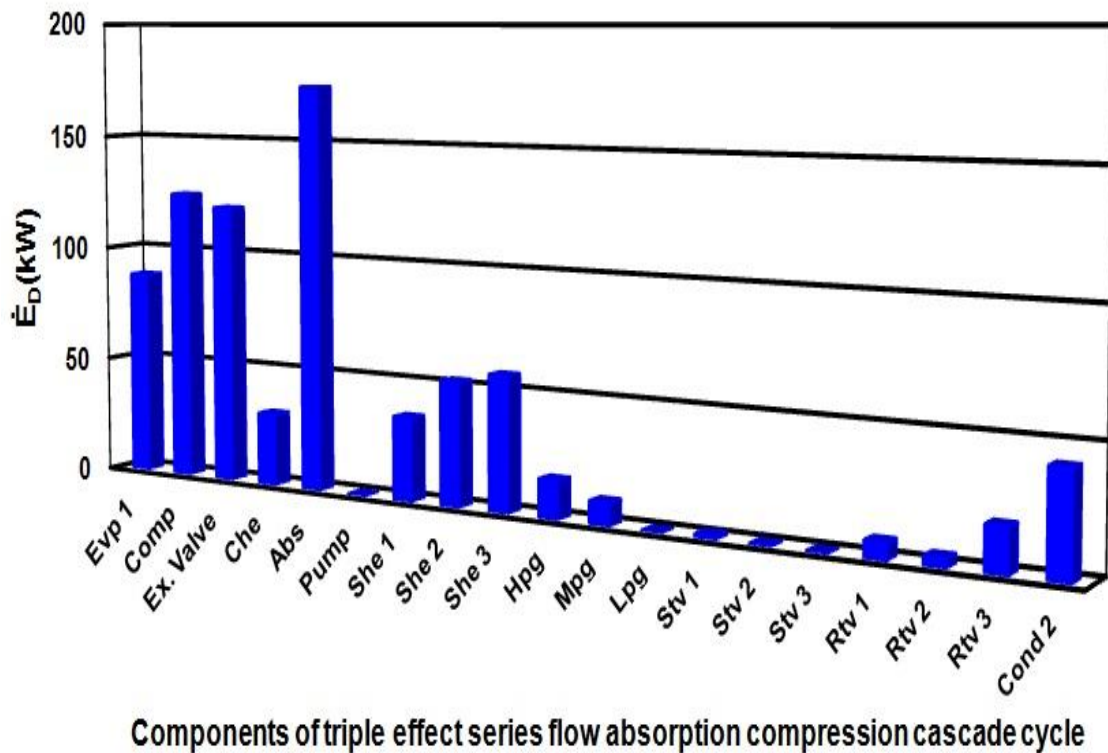


Figure 6.13 Exergy destruction rate (\dot{E}_D) in various components of ACCRC

Fig. 6.13 and 6.14 show the exergy destruction rate (\dot{E}_D) and exergy destruction ratio (%EDR) in various components of ACCRC. The values of \dot{E}_D and %EDR are highest in the absorber (Abs) and lowest in the solution pump. It is due to that the solution pump work is negligible and exergy recovered in the absorber is small. The compressor, expansion valve and evaporator 1 are also the next sites of higher exergy destruction after absorber. On the other hand, the low pressure generator (LPG) is the next site of lower exergy destruction after solution pump. It has been observed that the medium pressure

generator(Mpg), high pressure generator (Hpg), cascade heat exchanger, condenser 2, solution heat exchanges 1,2 & 3 (She 1,2 &3) are the sites where considerable amount of exergy has been recovered. . Compressor and evaporator 1 are also sensitive sites in which considerable amount of exergy destruction take place. However, cascade heat exchanger (Che) and condenser 2 recover handsome amount of exergy. Various refrigerant and solution vales have negligible exergy destruction.

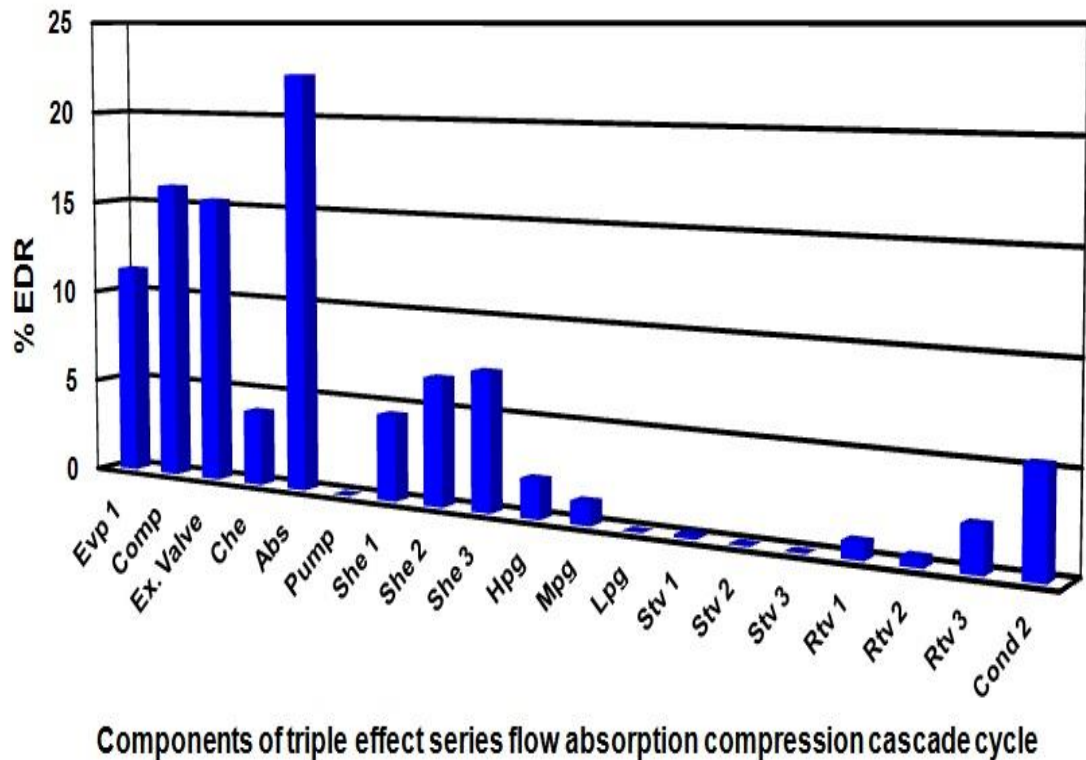


Figure 6.14 %Exergy destruction ratio(% EDR) of various components of ACCRC

6.5 CONCLUSIONS

- The electricity consumption of triple effect cascade system (ACCRS) is reduced by 45.84 % as compared to VCRS. Moreover the COP of the vapour compression circuit gets increased by 85.26% due to low electric power consumption. When compared to compression-absorption single and double effect cascade systems, the COP of triple effect cascade system lies between them.
- In addition, the triple recovery of waste heat or use of renewable source of heat reduces the system running cost as the waste heat is available at low cost and renewable energy is free of cost. However, the overall size of the system increases.

- The enhancement in the exergetic efficiency of VCR circuit of ACCRS is 85.28% and the reduction in total exergy destruction is 70.8%. It is also established that the exergetic efficiency of triple effect cascade system is highest in comparison to single and double effect cascade systems.
- The larger value of approach in the cascade heat exchanger reduces the COP and exergetic efficiency of the system.
- The increase in HP generator temperature increases the COP and exergetic efficiency of the system at absorber temperature 37.8^oC and 40^oC because of solution circulation ratio decreases. However, the total exergy destruction and exergy destruction ratio (EDR) decrease.
- The energetic (COP) and exergetic (η_{ex}) performance of the system fall with increase in absorber temperature due to increase in solution circulation ratio (SCR). The exergy destruction and exergy destruction ratio (EDR) register increment.
- The system COP increases and exergetic efficiency decreases with increase in evaporator 1 temperature for a range of generator temperature. Similarly, the exergy destruction (EDR) ratio increases and the total exergy destruction of the system decreases.
- The solution pump is the site of zero exergy destruction while absorber is the main component in which the exergy destruction is highest in comparison to other system components. After solution pump, lower pressure generator (LPG) recovers the major part of exergy.
- The use of R1234yf in low temperature VCR circuit of ACCRS establishes an eco-friendly agreement.

In the light of above discussion, it is inferred that the absorption compression (triple effect series flow) cascade system (ACCRS) is performing best among the systems considered. The electricity saver, cost effectiveness and eco-friendship are the unmatched features of the system associated to fulfil need of low cooling applications. However, the larger size of the system is manageable task.

6.6 DESCRIPTION OF VAPOUR COMPRESSION ABSORPTION (DOUBLE EFFECT SERIES FLOW H₂O-LiBr) CASCADE REFRIGERATION SYSTEM

Fig. 6.15 shows the schematic diagram of absorption-compression cascade refrigeration system (ACCRS). It comprises of a vapour compression refrigeration (VCR) cycle and a double effect H₂O-LiBr series flow vapour absorption refrigeration (DESFVAR) cycle. The vapour compression refrigeration system (VCRS) is in the low temperature section in which low temperature is achieved by using 1234yf as a refrigerant and double effect H₂O-LiBr series flow vapour absorption refrigeration system (DESFVARS) is in the high temperature section having Lithium Bromide (LiBr) as an absorbent and water (H₂O) as a refrigerant.

The evaporator of vapour absorption refrigeration system (VARS) is coupled with the condenser of VCRS i.e. the two cycles are coupled by a heat exchanger which is designated as cascade heat exchanger (Che) in which evaporator of VARS absorbs the heat of the condenser of VCRS. The low temperature is obtained in the evaporator of the VCRS. The evaporator temperature of VCRS is lower than the VARS. This system can be used for various applications such as food preservations, medicine preservations, cold storage and industrial refrigeration etc.

The ACCRS comprises of an Evaporator, a Compressor, a Condenser and an Expansion valve in VCRS circuit along with an Evaporator, an Absorber, a Pump, two Solution heat exchanger (She 1 & 2), two Generators ('Hpg' & 'Lpg') at high and low pressures, one Condenser, two Refrigerant throttle valves (Rtv 1 & 2) and two Solution throttle valves (Stv 1 & 2). The condenser of VCRS is coupled to the DESFVARS in such a way that the heat dissipated by it is absorbed by the evaporator of DESFVARS. Thus the cascade system so obtained further produces cooling in the evaporator of VCRS. The DESFVARS is a three pressure system. The generator units are at high and low pressures generate refrigerant vapour. The high pressure generator (Hpg) can be operated by the waste heat available from thermal power plant viz. steam turbine or gas turbine or an I.C. engine. The solar energy may also be used for the purpose. This energy is used in the generators (i.e. Hpg & Lpg) to generate refrigerant vapour. The COP of the DESFVARS is about two times that of a single effect system.

The absorber and evaporator of DESFVAR cycle operate at equal and lowest pressure of the cycle. The strong solution is pumped from absorber to the high pressure generator through solution heat exchanger (She 1 & 2) from state points 5-7 and 15. The refrigerant vapours is separated by high pressure generator (Generator1) at state point 19 which passes through the low pressure generator (Genertor2/Condenser3) from state point 19 to 20 and then it is throttled from state 20-21 to the condenser2 by refrigerant

throttle valve 1 (Rtv1). The weak solution leaving Hpg from state 16-17 dissipates heat to the strong solution in the She2 and then it is throttled to low pressure generator (Generator2/Condenser3) from state 17-18 by solution throttle valve 2 (Stv2). The refrigerant vapour generated in the Lpg (Generator2/Condenser3) is throttled to the condenser2 from state 20-21 by Rtv2. In this way, the solution flows in series through two generators and generates refrigerant vapour. Thus the system is termed as double effect H₂O-LiBr series flow vapour absorption refrigeration system (DESFVARs). The weak solution obtained from Lpg (Generator2/Condenser3) is passed through She 1 and dissipates heat to strong solution from state 8-9. From where, it is throttled to absorber from state 9-10 by Stv1. The refrigerant vapour obtained from the Lpg (Generator2/Condenser3) is fed to the condenser. The refrigerant vapour from the condenser 2 is throttled to evaporator2 from state 12-13 by Rtv 2. The refrigerating effect thus obtained in the evaporator2, which is in the cascade heat exchanger (Che) from state 12-14 produces cascading effect in the 'Che'. Finally, the refrigerant vapour enters to the absorber. The weak solution from Lpg (Generator2/Condenser3) enters to the She1 and dissipates heat to the strong solution from state 8-9. Finally, it is throttled to absorber by 'Stv' 1 from state 9-10. The cascade heat exchanger exchanges heat of condenser 1 i.e. \dot{Q}_{eVA} of VCR cycle with the evaporator 2 of VAR cycle. The refrigerant vapours of R1234yf at high pressure and temperature after compression from state 1-2 enters in the condenser1 at state point 2. These vapours dissipate heat \dot{Q}_{eVA} to the evaporator 2 in the Che from states 2-3a and gets transformed in to subcooled liquid. From state 3-3a, the subcooling of liquid refrigerant occurs. The subcooled liquid refrigerant is throttled to evaporator 1 at low temperature and pressure from state 3a-4 by expansion valve. Finally, the low temperature vapours of refrigerants produces cooling effect in the evaporator 1 from state 4-1.

The energy and exergy performance analysis of the absorption-compression (double effect) cascade refrigeration system (ACCRs) is presented by Colorado and Rivera (2015). The working fluids in the VAR system are H₂O-LiBr and in the VCR system is R134a. The waste heat available in the generator of VAR system reduces the electricity consumption of the VCR system for the same refrigeration load.

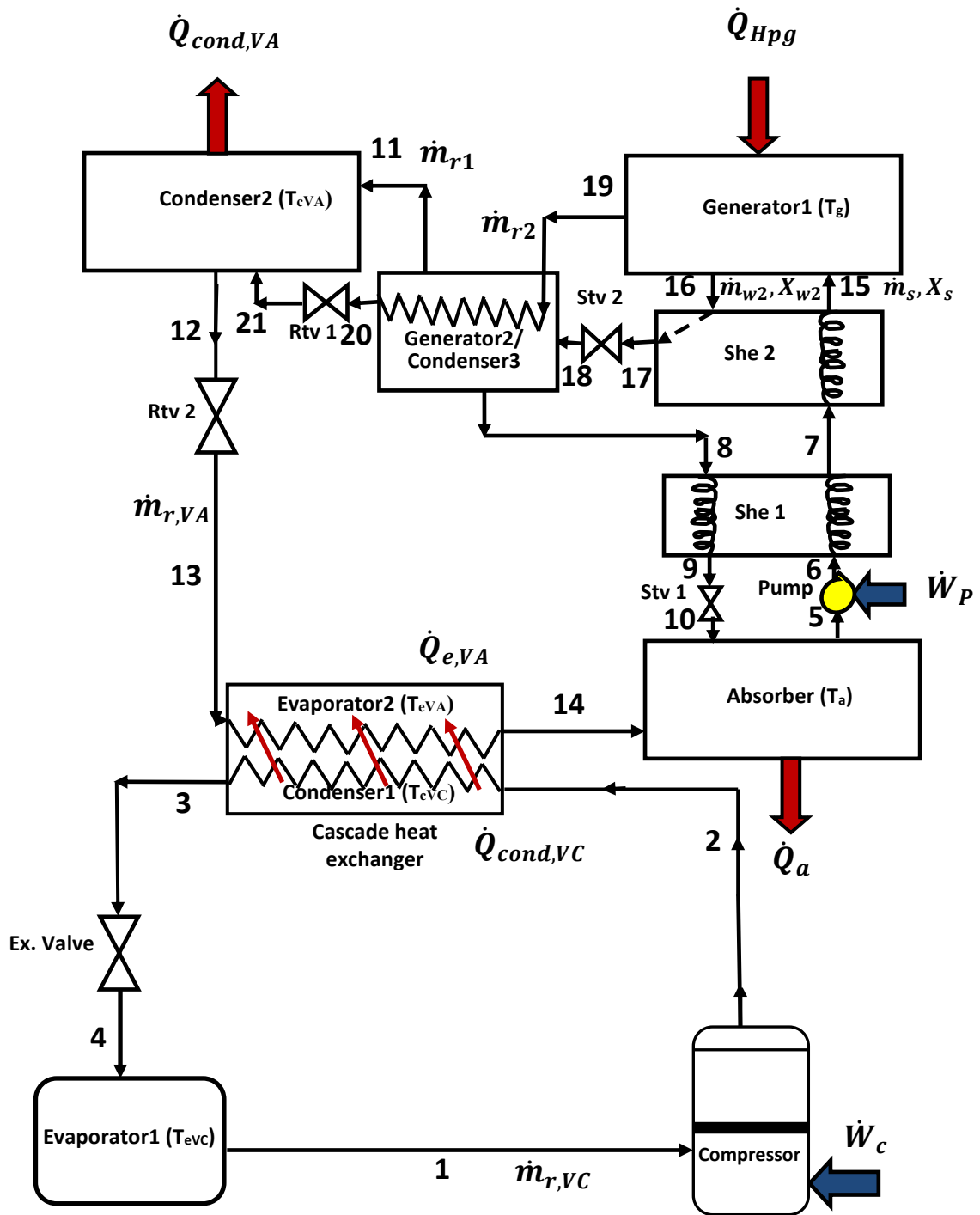


Figure 6.15 Schematic diagram of absorption-compression (double effect H₂O/LiBr series flow) cascade refrigeration system (ACCRS)

6.7 DESCRIPTION OF VAPOUR COMPRESSION ABSORPTION (SINGLE EFFECT H₂O-LiBr) CASCADE REFRIGERATION SYSTEM

Fig. 6.16 presents the schematic diagram of absorption (H₂O-LiBr single effect) - compression (R1234yf, R1234ze) cascade vapour refrigeration cycle (ACCVRC).

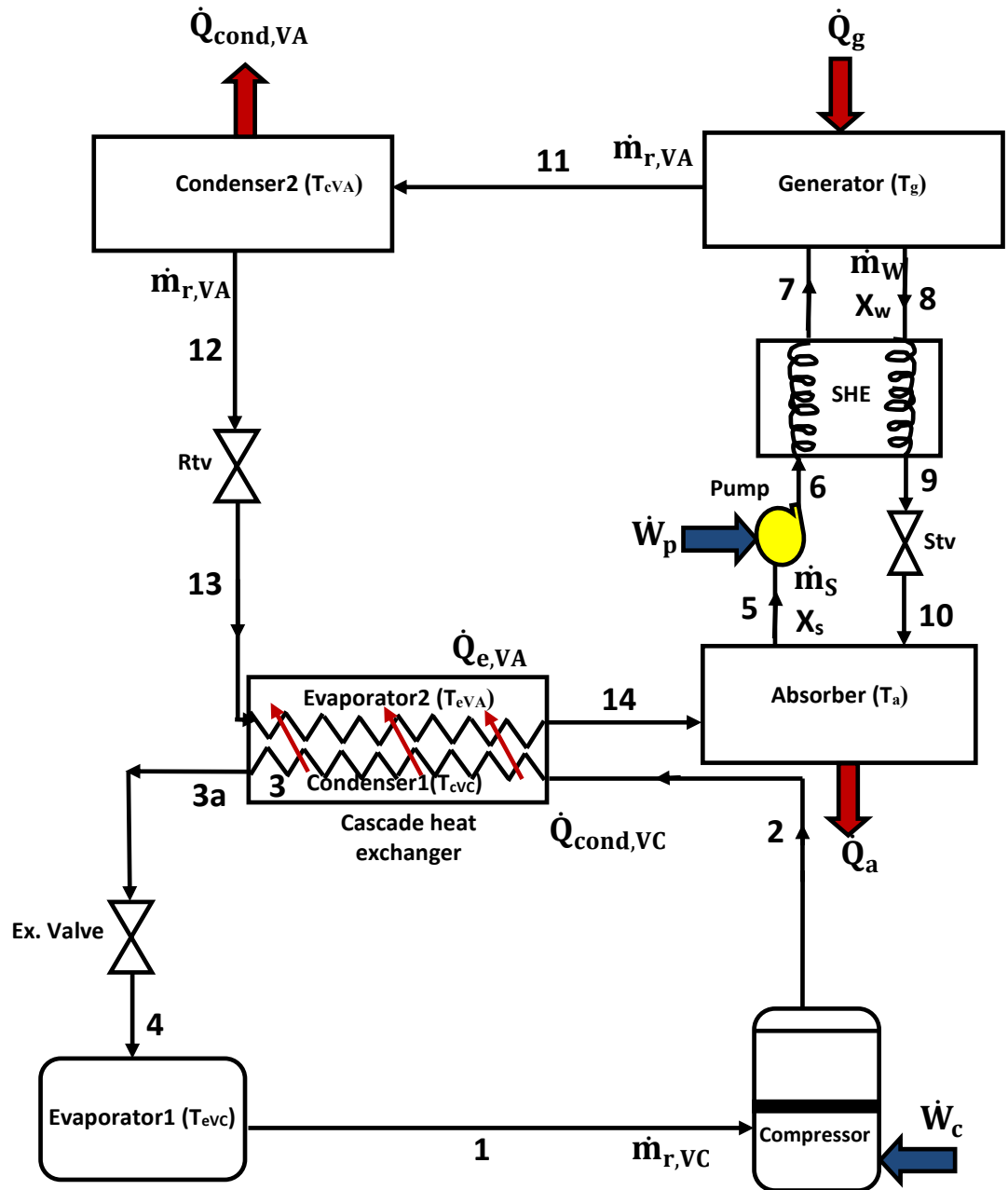


Figure 6.16 Schematic diagram of absorption-compression (single effect H₂O/LiBr series flow) cascade vapour refrigeration cycle (ACCVRC)

It comprises of single effect vapour absorption refrigeration (VAR) system using water as refrigerant and Lithium-Bromide absorbent and vapour compression refrigeration (VCR) system using R1234yf, R1234ze refrigerants. The single effect VAR is in comparative higher temperature section and cools the condensate of VAR section which is in lower temperature section. The evaporator of VAR cycle is coupled to the condenser of VCR cycle such that the net refrigeration is obtained in the evaporator of VCR cycle.

The VAR cycle comprises of an evaporator which serves as cascade heat exchanger, a generator, a condenser, an absorber, a solution pump, a solution heat exchanger, a solution throttle valve and a refrigerant throttle valve. VAR cycle comprises of an evaporator, a compressor, a condenser or cascade heat exchanger and a expansion valve.

The generator of VAR cycle receives low grade heat either from the exhaust of gas turbine cycle, steam turbine cycle (Rankine cycle) or solar collector. The refrigerant-absorbent solution gets separated in the generator and the saturated vapour of refrigerant leaving the generator and enters into the condenser at state point 11. The phase of refrigerant converts from saturated vapour to liquid in the condenser 2 and the liquid refrigerant leaving the condenser 2 at state point 12 is expanded by a refrigerant throttle valve (Rtv) at state point 13. The low temperature liquid-vapour mixture of refrigerant enters into the evaporator 2 of cascade heat exchanger (Che). The heat of condenser 1 is absorbed by the refrigerant of evaporator 2 such that $Q_{eVA} = Q_{eVC}$. The refrigerant vapour leaving the evaporator 2 enters the absorber at state point 14. The weak solution of H₂O and LiBr leaving the solution throttle valve (Stv) enters the absorber at state point 10. The strong solution of water and lithium bromide is pumped from absorber at state point 5 to solution heat exchanger (She) at state point 6 by a solution heat pump. The strong solution of refrigerant and absorbent solution receives heat from weak solution in the She and the strong solution leaving the She enters into the generator at state point 7. The weak solution of refrigerant and absorbent leaving the generator at state point 8 enters into the She at state point 9 and finally expanded to absorber at state point 10.

The liquid refrigerant (R1234yf or R1234ze) of condenser 1 which dissipates heat to the evaporator 2 in the cascade heat exchanger leaving the condenser 1 enters into the expansion valve at state point 3. The liquid refrigerant gets sub-cooled at state point 3. The sub-cooled liquid refrigerant is expanded from state 3 to state 4 by a expansion valve. The low temperature liquid vapour mixture of refrigerant (R1234yf or R1234ze) enters

into the evaporator1 and produces cooling effect. The liquid vapour refrigerant mixture receives heat and transformed into saturated vapour at state point 1. The saturated vapour refrigerant leaving the evaporator1 enters into the compressor at state point 1. The saturated vapour refrigerant is compressed from state 1 to 2 by a compressor and the high pressure and high temperature refrigerant vapour enters into the condenser1 at state point 2.

Thus the VAR and VCR coupled together through cascade heat exchanger by which the evaporator2 of VAR cycle absorbs the heat of condenser1 of VCR cycle and the net refrigeration is obtained in the evaporator1 of VCR cycle subsequently the low temperature is also achieved in the evaporator1 of VCR cycle.

6.8 MATHEMATICAL MODELLING

The current work presents the thermodynamic analysis of absorption (H₂O-LiBr single effect) -compression (R1234yf, R1234ze) integrated vapour refrigeration cycle (ACIVRC). The two cycles are coupled through the cascade heat exchanger (Che) in such a way that the net refrigeration is achieved in the evaporator1 of VCR cycle. The eco-sustainable HFOs (R1234yf and R1234ze) have been considered in VCR cycle. A computational code has been developed in the Engineering Equation Solver (EES) software (Klein and Alvarado, 2012). The first and second law based governing equations have been formulated using mass and energy conservations principles.

6.8.1 Assumptions

In order to model complex thermodynamic model of absorption (H₂O-LiBr single effect) -compression (R1234yf, R1234ze) integrated vapour refrigeration cycle, following assumptions have been considered except where variation of parameters involved.

- The state of refrigerant is dry and saturated at the entry of compressor at (state point 1).
- The state of refrigerant at the exit of condenser of VCR cycle is saturated subcooled liquid at state point 3.
- Subcooling of liquid refrigerant occurs from state point 3-3a.
- The expansion or throttling in the expansion valve, solution throttle valve and refrigerant throttle valve is isoenthalpic.

- Difference between the temperature of space to be cooled and temperature of evaporator 1 ($\Delta T = T_b - T_{eVC}$) is 10°C .
- The approach temperature or overlap temperature between evaporator 2 and condenser 1 in the cascade heat exchanger ($T_{ov} = T_{cVC} - T_{eVA}$) is 5°C .
- Isentropic efficiency of compressor (η_c) is 80%.
- The heat losses and pressure losses from the system and system components are negligible. The whole system operates in steady state condition.
- The reference values of entropy (s_0) and enthalpy (h_0) are considered at ambient or dead state conditions ($T_0 = 25^{\circ}\text{C}$, $P_0 = 101.325\text{kPa}$).
- The refrigerant vapour leaving the generator is superheated vapour at the generator temperature.
- Heat exchanger effectiveness is 0.7.

6.8.2 Energy analysis

The energy performance, based on first law of absorption ($\text{H}_2\text{O-LiBr}$ single effect) -compression (R1234yf, R1234ze) cascade vapour refrigeration cycle (ACCVRC) is represented as coefficient of performance (COP):

$$\text{COP}_{\text{ACCVRC}} = \frac{\dot{Q}_{eVC}}{\dot{Q}_g + \dot{W}_P + \dot{W}_c} \quad (6.14)$$

Where \dot{Q}_{eVC} and \dot{W}_c are the net refrigerating effect and rate of compressor work of VCRS and \dot{Q}_g and \dot{W}_P are the heat rate of generator and solution pump work rate of ACIVRS respectively.

6.8.3 Exergy analysis

6.8.3.1 Total exergy destruction

Total exergy destruction of the system is the summation of exergy destruction in each system component ($\dot{E}_{D,\text{total}}$).

The total exergy destruction in absorption ($\text{H}_2\text{O-LiBr}$ single effect) -compression (R1234yf, R1234ze) cascade vapour refrigeration system (ACCVRS) is given by:

$$\begin{aligned} \dot{E}_{D,\text{total}} = & \dot{E}_{D,e1} + \dot{E}_{D,C} + \dot{E}_{D,\text{Ex. valve}} + \dot{E}_{D,\text{Che}} + \dot{E}_{D,a} + \dot{E}_{D,P} + \dot{E}_{D,\text{She}} + \dot{E}_{D,g} + \\ & \dot{E}_{D,\text{Rtv}} + \dot{E}_{D,\text{Stv}} + \dot{E}_{D,\text{cond2}} \end{aligned} \quad (6.14a)$$

6.8.3.2 Exergetic efficiency

The exergetic efficiency of absorption (H₂O-LiBr single effect) -compression (R1234yf, R1234ze) cascade vapour refrigeration cycle (ACCVRC) is given by:

$$\eta_{ex, ACCVRC} = 1 - \frac{\Sigma(\dot{E}_D)}{\dot{Q}_g \left[\left(1 - \frac{T_0}{T_g} \right) + \dot{W}_p + \dot{W}_c \right]} = \frac{\dot{Q}_{e,VC} \left[\left(1 - \frac{T_0}{T_b} \right) \right]}{\dot{Q}_g \left[\left(1 - \frac{T_0}{T_g} \right) + \dot{W}_p + \dot{W}_c \right]} \quad (6.15)$$

Where $\Sigma(\dot{E}_D)$, is the total exergy destruction rate of the integrated system in kW, \dot{Q}_g and T_g are the input heat in kW and temperature in °C of the generator and \dot{W}_p and \dot{W}_c are solution pump work and compressor work in kW respectively. $\dot{Q}_{e,VC}$ in kW is the rate of net refrigerating effect and T_b is the temperature of space to be cooled in °C of VCRS respectively. T_0 is the ambient or dead state temperature in °C.

6.8.3.3 Exergy destruction ratio (EDR)

The exergetic destruction ratio (EDR) in absorption (H₂O-LiBr single effect) -compression (R1234yf, R1234ze) cascade vapour refrigeration cycle (ACCVRC) is given by:

$$EDR_{ACCVRC} = \frac{\Sigma(\dot{E}_D)}{\dot{Q}_{e,VC} \left[\left(1 - \frac{T_0}{T_b} \right) \right]} \quad (6.16)$$

Where $\Sigma(\dot{E}_D)$ is the rate of total exergy destruction of the absorption-compression integrated system in kW, $\dot{Q}_{e,VC}$ in kW is the rate of net refrigerating effect of vapour compression refrigeration system, T_b in °C is the temperature of space to be cooled and T_0 is the ambient or dead state temperature in °C respectively.

6.8.4 Input Parameters

Table 6.6 Input parameters considered except where the variation of physical parameters involved (Kaushik and Arora, 2009)

S.No.	Input parameters	Values
1.	generator temperature (T_g)	87.8°C
2.	Evaporator 2 temperature (T_{eVA})	7.2°C
3.	Condenser 2 temperature (T_{cVA})	37.8°C
4.	Absorber temperature (T_a)	37.8°C
5.	Mass flow rate of refrigerant (H ₂ O) in VARS (\dot{m}_{rVA})	1 kg/s
6.	Evaporator 1 temperature (T_{eVC})	-10°C
7.	Degree of subcooling ($(\Delta T)_{sc}$) (3-3a)	5°C

8.	Condenser 1 temperature (T_{cvc})	12.2 ⁰ C
9.	Ambient or dead state pressure (P_0) and temperature (T_0)	101.325kPa & 25 ⁰ C

6.9 RESULTS AND DISCUSSION

In the present work, energy and exergy analysis of absorption (H₂O-LiBr single effect) -compression (R1234yf, R1234ze) cascade vapour refrigeration system (ACCVRC) has been carried out involving control volume approach of each system component. A computer code has been formulated in the EES software (Klein and Alvarado, 2012) to compute the various performance parameters viz. COP, exergetic efficiency, total exergy destruction rate and exergy destruction ratio (EDR). The validation of results obtained has been carried out to compare these with Kaushik and Arora(2009). It has been observed that the variation in the results obtained and the results of Kaushik and Arora(2009) is within $\pm 1\%$ due to inclusion of solution pump work in the current analysis.

6.9.1 Results of Energy, Exergy and Parametric Analysis

Energy, exergy and parametric analysis of absorption compression (single effect H₂O-LiBr) cascade refrigeration system have been carried out and shows following results.

6.9.1.1 Effect of variation in effectiveness of solution heat exchanger

The effect of effectiveness of solution heat exchanger (ϵ_{She}) on performance parameters viz. COP_{ACCVRC}, exergetic efficiency ($\eta_{ex\ ACCVRC}$), total exergy destruction rate ($\dot{E}_{D, total, ACCVRC}$) and exergy destruction ratio (EDR_{ACCVRC}) has been shown in Fig. 6.17 and 6.18.

Fig. 6.17 shows the effect of effectiveness of solution heat exchanger (ϵ_{She}) on COP_{ACCVRC} and exergetic efficiency ($\eta_{ex\ ACCVRC}$). The value of COP_{ACCVRC} and $\eta_{ex\ ACCVRC}$ increases with increase in ϵ_{She} . The effectiveness of She is given by $\epsilon_{She} = \frac{T_7 - T_6}{T_8 - T_6}$. Thus the value of T_8 and \dot{Q}_8 decreases with increase in ϵ_{She} . The COP is given by the relation $\frac{\dot{Q}_{e, VC}}{\dot{Q}_g + W_P + W_c}$ (Eq.6.14), by which, the value of COP_{ACCVRC} increases with increase in ϵ_{She} .

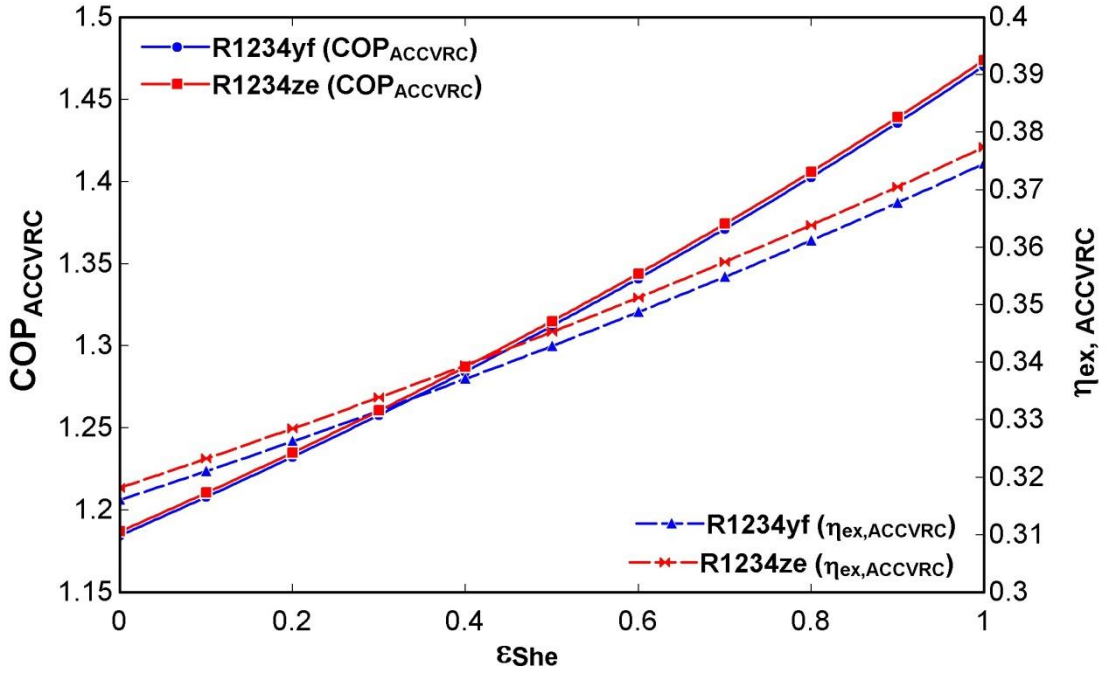


Figure 6.17 Variation in COP_{ACCVR} and exergetic efficiency ($\eta_{ex, ACCVR}$) with effectiveness of solution heat exchanger (ϵ_{She} .)

The exergetic efficiency of absorption (H₂O-LiBr single effect) -compression (R1234yf, R1234ze) cascade vapour refrigeration cycle (ACCVRC) is given by the

relation $\frac{\dot{Q}_{e,vc} \left| \left(1 - \frac{T_0}{T_b} \right) \right|}{\dot{Q}_g \left| \left(1 - \frac{T_0}{T_g} \right) \right| + \dot{W}_P + \dot{W}_c}$ (eq. (6.15)). The value of $\dot{Q}_{e,vc} \left| \left(1 - \frac{T_0}{T_b} \right) \right|$, \dot{W}_P and \dot{W}_c

remains unchanged and \dot{Q}_g decreases with increase in ϵ_{She} . Hence the value of $\eta_{ex, ACCVR}$ increases with increase in ϵ_{She} .

It has also been observed that the maximum value of COP_{ACCVR} and $\eta_{ex, ACCVR}$ are 1.474 and 0.3774 for R1234ze and the minimum value of COP_{ACCVR} and $\eta_{ex, ACCVR}$ are 1.185 and 0.3161 for R1234yf.

Fig. 6.18 illustrates the variation in total exergy destruction rate ($\dot{E}_{D, total, ACCVR}$) and exergy destruction ratio (EDR_{ACCVR}) with increase in ϵ_{She} . The value of $\dot{E}_{D, total, ACCVR}$ and EDR_{ACCVR} decreases with increase in ϵ_{She} . The relation for $\dot{E}_{D, total, ACCVR}$ is given by eq. (6.14a) which is the sum of exergy destruction rate of each system component. As the value of ϵ_{She} increases, the rate of exergy destruction in She and other system components decreases. Thus the value of $\dot{E}_{E, total, ACCVR}$ decreases with increase in ϵ_{She} .

The EDR_{Integ} is given by the relation $\frac{\Sigma(\dot{E}_D)}{\dot{Q}_{evc} \left| \left(1 - \frac{T_0}{T_b} \right) \right|}$ eq. (6.16) which is directly proportional to the $\dot{E}_{D,total,ACCVR}$ and the value of $\dot{Q}_{evc} \left| \left(1 - \frac{T_0}{T_b} \right) \right|$ remains constant with increase in ϵ_{She} . The EDR_{ACCVR} increases with increase in ϵ_{She} .

It is also observed that the minimum value of $\dot{E}_{D,total,ACCVR}$ and EDR_{ACCVR} are 430.9 kW and 1.649 for R1234ze and the maximum value of $\dot{E}_{D,total,ACCVR}$ and EDR_{ACCVR} are 564.5 and 2.164 for R1234yf.

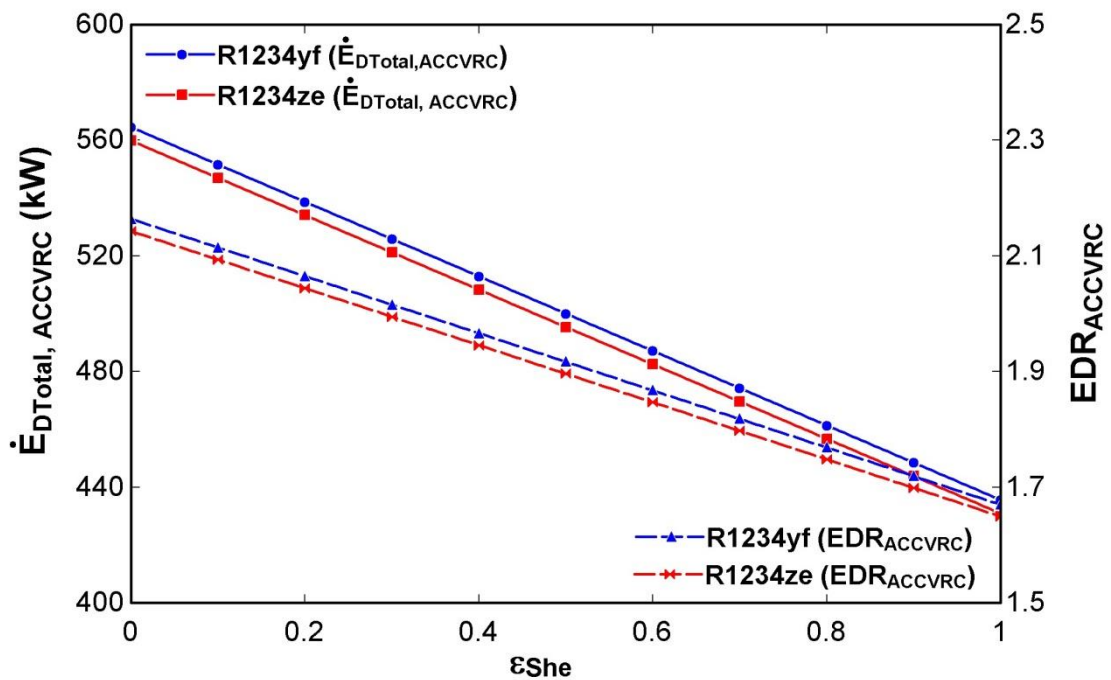


Figure 6.18 Variation in total exergy destruction rate ($\dot{E}_{E,total,ACCVR}$) and exergy destruction ratio (EDR_{ACCVR}) with effectiveness of solution heat exchanger (ϵ_{She} .)

6.9.1.2 Effect of variation in evaporator1 temperature

The effect of evaporator1 temperature (T_{evc}) on performance parameters viz. COP_{ACCVR} , exergetic efficiency ($\eta_{ex,ACCVR}$), total exergy destruction rate ($\dot{E}_{D,total,ACCVR}$) and exergy destruction ratio (EDR_{ACCVR}) has been illustrated in Fig. 6.19 and 6.20.

Fig. 6.19 depicts the variation in evaporator1 temperature ($T_{e,VC}$) on COP_{ACCVR} and exergetic efficiency ($\eta_{ex,ACCVR}$) of absorption (H_2O -LiBr single effect) -compression (R1234yf, R1234ze) cascade vapour refrigeration cycle (ACCVR) for R1234ze and R1234yf. The value of COP_{ACCVR} increases and $\eta_{ex,ACCVR}$ decreases with increase in evaporator1 temperature.

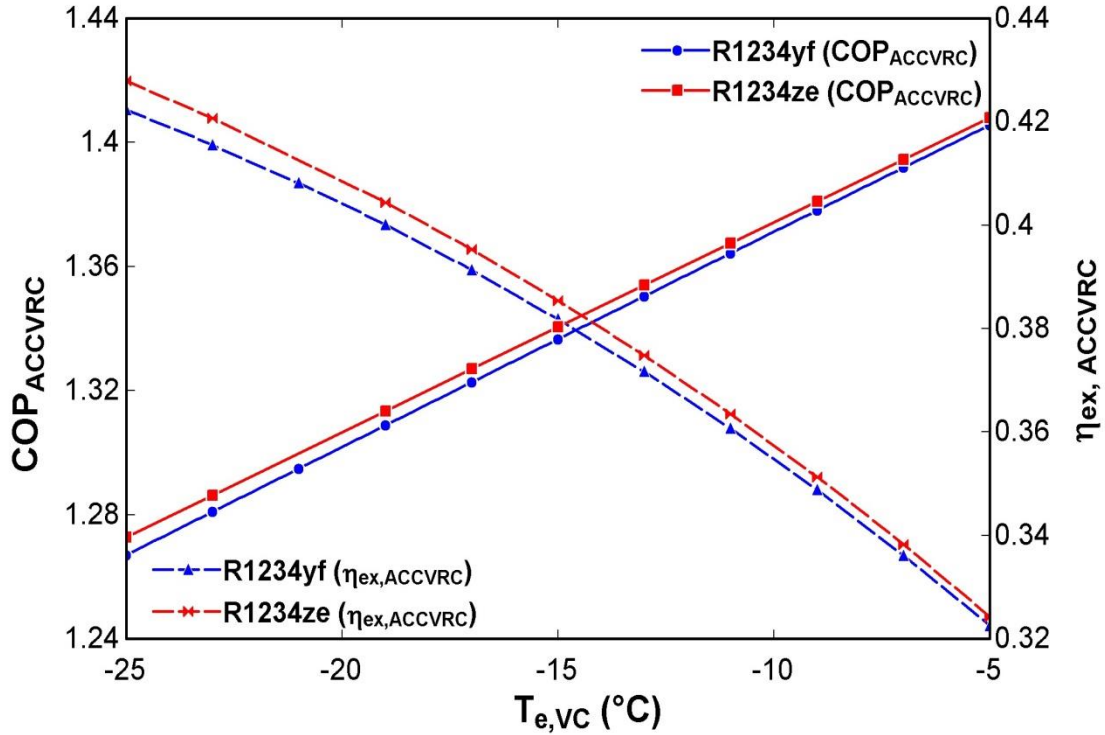


Figure 6.19 Effect of evaporator1 temperature ($T_{e,VC}$) on COP_{ACCVR} and exergetic efficiency ($\eta_{ex,ACCVR}$)

The COP_{ACCVR} is given by eq. (6.14) i.e. $\frac{\dot{Q}_{e,VC}}{\dot{Q}_g + \dot{W}_P + \dot{W}_c}$ in which the value of $\dot{Q}_{e,VC}$ increases and \dot{W}_c decreases with increase in $T_{e,VC}$. The terms \dot{Q}_g and \dot{W}_P remain constant with increase $T_{e,VC}$. Hence the value of COP_{ACCVR} increases with increase in $T_{e,VC}$.

Similarly, the exergetic efficiency is given by the relation $\frac{\dot{Q}_{e,VC} \left(1 - \frac{T_0}{T_b}\right)}{\dot{Q}_g \left(1 - \frac{T_0}{T_g}\right) + \dot{W}_P + \dot{W}_c}$ (Eq. 6.15) in which the term T_0 and T_g remains unaffected while T_b increases with increase in $T_{e,VC}$ ($T_b - T_{e,VC} = 10^\circ C$) by which the term $\left(1 - \frac{T_0}{T_b}\right)$ decreases. Consequently, the value of $\eta_{ex,ACCVR}$ decreases with increase in $T_{e,VC}$.

It has been observed that the the maximum value of COP_{ACCVR} and $\eta_{ex ACCVR}$ are 1.408 and 0.4279 for R1234ze and the minimum value of COP_{ACCVR} and $\eta_{ex ACCVR}$ are 1.267 and 0.3225 for R1234yf.

Fig. 6.20 depicts the effect of evaporator1 temperature ($T_{e,vc}$) on total exergy destruction rate ($\dot{E}_{D,total,ACCVR}$) and exergy destruction ratio (EDR_{ACCVR}). The value of $\dot{E}_{D,total,ACCVR}$ decreases and EDR_{ACCVR} increases with increase in $T_{e,vc}$ for R1234ze and R1234yf. The exergy destruction rate of each system component decreases with increase in $T_{e,vc}$ and the EDR_{ACCVR} is the sum of exergy destruction rate of all system components. Thus, the value of EDR_{ACCVR} increases with increase in $T_{e,vc}$.

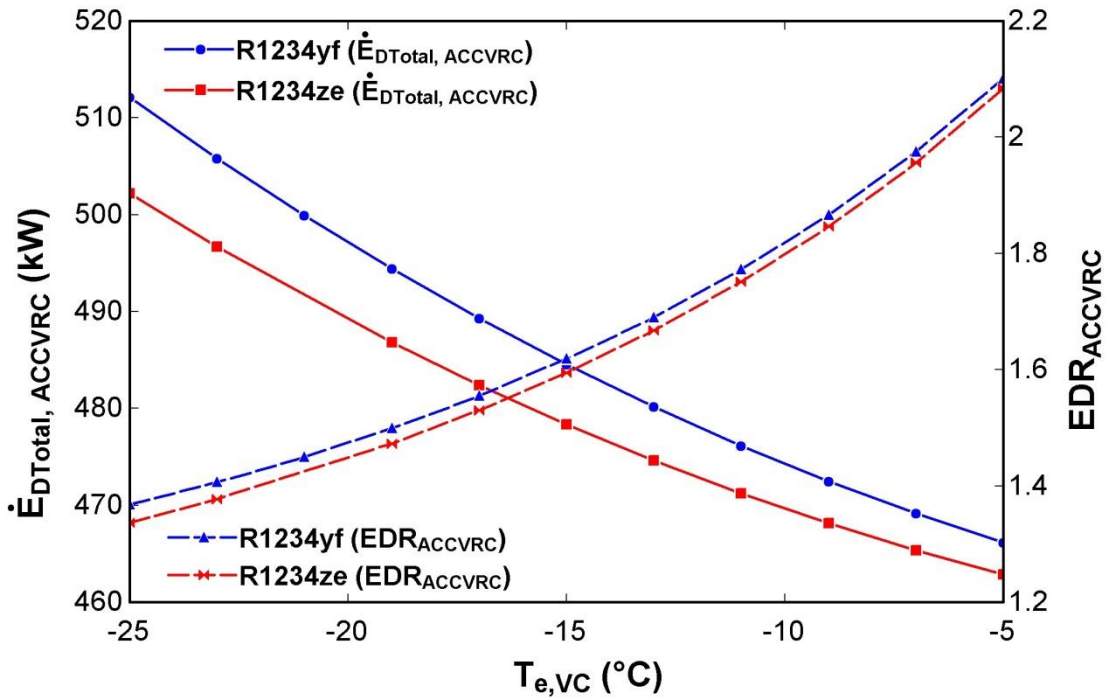


Figure 6.20 Variation in total exergy destruction rate ($\dot{E}_{E,total,ACCVR}$) and exergy destruction ratio (EDR_{ACCVR}) with evaporator1 temperature ($T_{e,vc}$)

$$EDR_{ACCVR} = \frac{\sum(\dot{E}_D)}{\dot{Q}_{e,vc} \left| \left(1 - \frac{T_0}{T_b} \right) \right|} \text{ (eq. (13)) in which } \dot{E}_{D,total,ACCVR}, \dot{Q}_{e,vc} \text{ increase and}$$

the term $\left| \left(1 - \frac{T_0}{T_b} \right) \right|$ decreases with increase in $T_{e,vc}$. Hence, the value of EDR_{ACCVR} increases with increase in $T_{e,vc}$.

It is observed that the the minimum value of $\dot{E}_{D,total,ACCVRC}$ and EDR_{ACCVRC} are 462.9 kW and 1.337 for R1234ze and the maximum value of $\dot{E}_{D,total,ACCVRC}$ and EDR_{ACCVRC} are 512.1 and 2.101 for R1234yf.

6.10 CONCLUSIONS

The current work presents the energy and exergy analysis of absorption (H₂O-LiBr single effect) -compression (R1234yf, R1234ze) integrated vapour refrigeration cycle (ACIVRC). A computer code has been developed to compute the effect of evaporator1 temperature and effectiveness of solution heat exchanger (She) on COP, exergy efficiency, total exergy destruction rate and exergy destruction ratio (EDR). The conclusions of the present analysis are as follows:

- The electricity consumption in ACCVRC cycle is reduces than that of conventional VCR cycle.
- The performance of VCR circuit of ACCVRC is better than that of simple vapour compression refrigeration cycle.
- The COP and exergetic efficiency of ACCVRC enhance with increase in effectiveness of solution heat exchanger.
- The COP of ACCVRC gets enhanced while exergetic efficiency gets declined with increase in evaporator1 temperature.
- The total exergy destruction rate and exergy destruction ratio (EDR) of ACCVRC get reduced with increase in effectiveness of solution heat exchanger while increase in evaporator1 temperature reduces total exergy destruction rate reduces and promotes EDR.
- The performance of R1234ze is better than that of R1234yf.

It is inferred from the above discussion that the absorption (H₂O-LiBr single effect)-compression (R1234yf, R1234ze) cascade vapour refrigeration cycle (ACCVRC) performs better than that of simple vapour compression refrigeration cycle and the use of HFOs establishes eco-friendship bond to the nature along with low temperature refrigeration applications.

6.11 DESCRIPTION OF VAPOUR COMPRESSION ABSORPTION (HALF EFFECT SERIES FLOW H₂O-LiBr) CASCADE REFRIGERATION SYSTEM

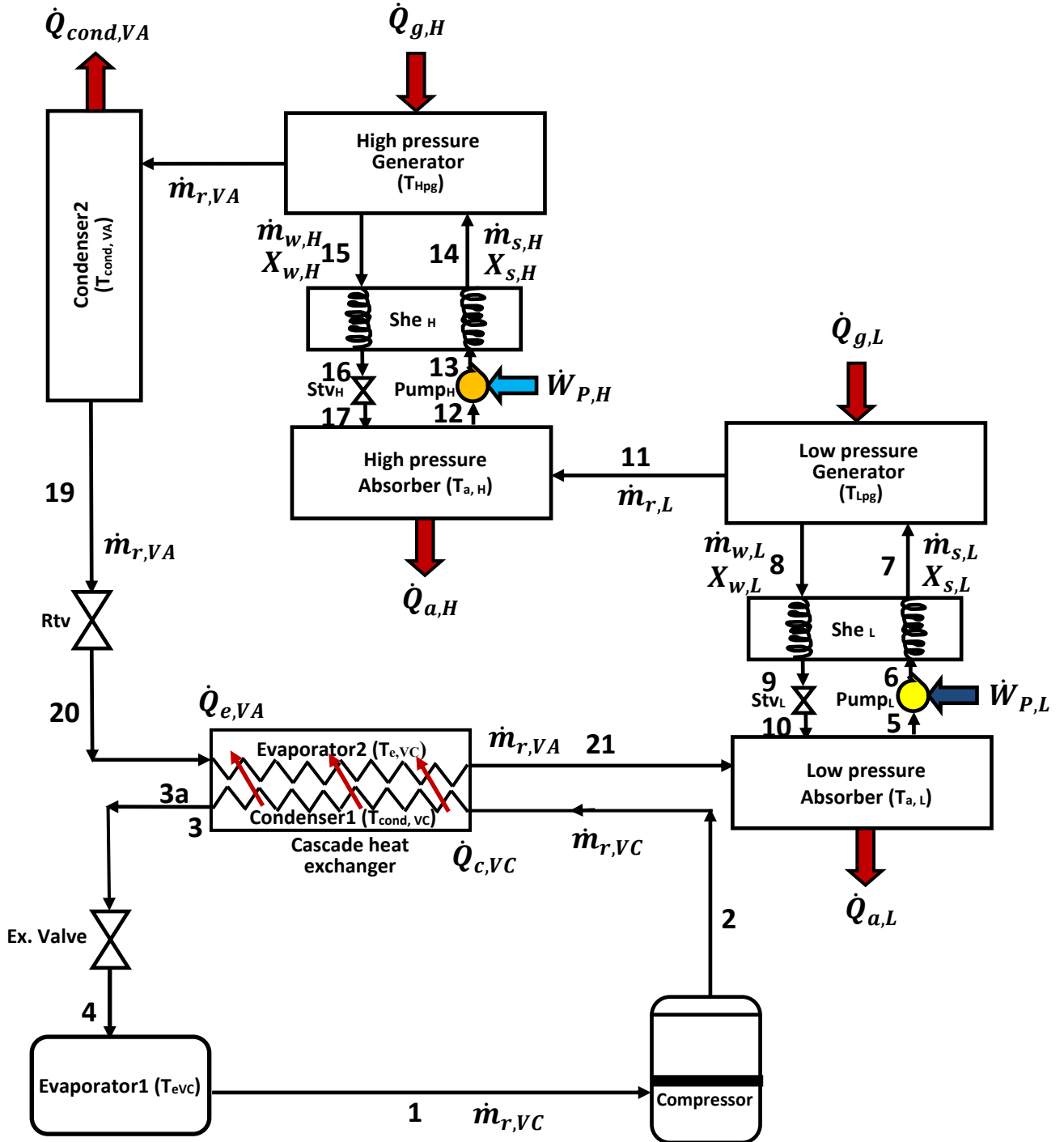


Figure 6.21 Schematic diagram of absorption-compression (half effect H₂O-LiBr series flow) cascade refrigeration system (ACCRS)

Fig. 6.21 depicts the schematic diagram of absorption compression (half effect H₂O-LiBr, R1234yf) cascade refrigeration system (ACCRS). It comprises of a half effect water lithium bromide vapour absorption refrigeration (VAR) system and a R1234yf vapour compression refrigeration (VCR) system. The higher temperature circuit of the ACCRS is a half effect H₂O-LiBr vapour absorption refrigeration system (HEVARs) having water as refrigerant and Lithium Bromide as an absorbent and the lower temperature circuit is a vapour compression refrigeration system (VCRS) where the low temperature is achieved using R1234 yf refrigerant.

The condenser of vapour compression refrigeration cycle is coupled to the evaporator of half effect vapour absorption refrigeration cycle via a heat changer which is termed as cascade heat exchanger (Che). Thus the two cycles are integrated through a cascade heat exchanger. The temperature difference between condenser1 and evaporator 2 is the overlap or approach temperature. The VAR cycle of ACCRS is using the low grade energy i.e. heat in LP and HP generator and the VCR cycle is using electric energy to run the compressor. The temperature of evaporator of VCR cycle is lower than that of VAR cycle. The low temperature is obtained in the evaporator of VCR cycle. This ACCR system can be used in various low temperature applications viz. frozen food, chemical separation reactions, preservation, semiconductor cooling, milk processing, freeze drying and medical diagnostic.

The ACCR system comprises of an evaporator (Evaporator2), a condenser (Condenser2), HP & LP absorbers, HP & LP generators, HP & LP solution heat exchangers (She_H&She_L), HP & LP solution pumps (Pump_H& Pump_L), HP and LP solution throttle valves (Stv_H& Stv_L) and a refrigerant throttle valve (Rtv) in VARS circuit and an evaporator (Evaporator1), a compressor, a condenser (Condenser1) and an expansion valve in VCRS circuit. The Condenser1 of VCRS is coupled to the Evaporator2 of VARS via a cascade heat exchanger (Che) as shown in Fig. 6.25. The heat dissipated by condenser1 ($\dot{Q}_{c, VC}$) is absorbed by evaporator2 ($\dot{Q}_{e, VA}$) such that the net cooling effect is obtained in the evaporator1 of VCRS. The ACCR is a five pressure system. The HP & LP generators generate high and low pressure refrigerant vapours at state points 18 and 11 respectively. The pressure of HP absorber is equal to the LP generator pressure ($P_{a,H} = P_{g,L}$). This pressure is the intermediate pressure of HEVARs. The evaporator2 and LP absorber are at same lowest pressure ($P_{e, VA} = P_{a,L}$). However, the condenser2 and HP generator are at same highest pressure ($P_{c, VA} = P_{g,H}$) of the VAR

system. The evaporator₁ and condenser₁ are at fourth & fifth stage of pressure of the ACCR system respectively. The low grade energy (heat) of Solar, waste heat of I.C. engine exhaust or exhaust of thermal power plant either gas turbine or steam turbine operated can be utilized in the HP and LP generators to operate the VAR cycle. The COP of the half effect VAR cycle is generally half of the single effect VAR cycle. Thus the system is known as half effect VAR system.

The strong solution of H₂O and LiBr is pumped from low pressure absorber to the LP generator via solution heat exchanger (She_L) from state points 5 to 7. The refrigerant vapours are separated by LP generator at state point 11 and the remaining weak solution of water and lithium bromide leaving the LP generator dissipates heat from state 8 to 9 in the She_L and is throttled back to the LP absorber from state conditions 9 to 10. The refrigerant vapours leaving the LP generator at state point 11 enter to the high pressure absorber. The strong solution thus obtained in HP absorber is pumped to the HP generator from state 12 to 14 via She_H. The refrigerant vapours are again separated by HP generator at state point 18 and the remaining weak solution leaving the HP generator dissipates heat in the She_H from state conditions 15 to 16 and is finally throttled to the HP absorber from state 16 to 17. The high temperature refrigerant vapours leaving the HP generator at state point 18 enter to the condenser. The condensed liquid refrigerant of high temperature is throttled to the evaporator₂ by refrigerant throttle valve (Rtv) from state 19 to 20 and is transformed into the low temperature-pressure liquid vapour refrigerant during the throttling process. The low temperature liquid vapour refrigerant present in the evaporator₂ receives the heat of condenser₁ inside the cascade heat exchanger from state 20 to 21. Thus the cascading effect is obtained in the Che. Finally, the refrigerant water vapours leaving the evaporator₂ enter into the LP absorber at state point 21. The heating load of condenser₁ $\dot{Q}_{e, VA}$ of VCR cycle is dissipated to the evaporator₂ of VAR cycle inside cascade heat exchanger. The refrigerant vapours of R1234yf at high pressure and temperature after compression from state 1-2 enter in the condenser₁ at state point 2. These vapours dissipate heat $\dot{Q}_{e, VA}$ to the evaporator 2 in the Che from states 2-3a and gets transformed into the subcooled liquid. Further, from state 3-3a, the subcooling of liquid refrigerant occurs. The subcooled liquid refrigerant is throttled to evaporator 1 at low temperature and pressure from state 3a-4 by expansion valve. Finally, the low temperature vapours of refrigerants produce cooling effect ($\dot{Q}_{e, VC}$) in the evaporator₁ from state 4-1.

6.12 THERMODYNAMIC AND MATHEMATICAL MODELLING

The present work carries out the energy and exergy analysis of absorption compression (half effect H₂O-LiBr) cascade refrigeration system (ACCRS). The low GWP and zero ODP HFO: R1234yf has been considered in the vapour compression section. Steady state governing equations of mass, energy and exergy conservation have been considered for the analysis. The principles of mass and material balance, energy balance and exergy balance have been applied to each system components. The control volume approach has been followed for heat transfer and work interaction of inlet and outlet streams of each system component. A computer program has been developed to compute the various performance parameters in the Engineering Equation Software (EES)(Klein and Alvarado, 2012). Various inbuilt thermodynamic properties of EES have been recalled in the subroutine program. Additionally, empirical relations for thermodynamic properties of LiBr and H₂O/LiBr mixture have been inserted in the EES library. The thermodynamic modelling has been categorized in to energy and exergy analysis.

6.12.1 Assumptions

The present work concerns the energy and exergy analysis of absorption compression half effect cascade refrigeration system. The system and system components have been analysed using principles of first and second law of thermodynamics. The formulation of steady state governing equations has been developed using control volume approach. The VCR and VAR cycles have been coupled through a cascade heat exchanger. In which, the condenser of VCR cycle rejects the heat to the evaporator of VAR cycle ($\dot{Q}_{c, VC} = \dot{Q}_{c, VA}$). The overlap temperature (T_{ov}) between condenser1 and evaporator2 is the difference between the temperature of isobaric condensation in the condenser of VCR cycle and temperature of isobaric evaporation in the evaporator of HEVAR cycle ($T_{ov} = T_{c, VC} - T_{e, VA}$). The mean temperature of cascade heat exchange is denoted as T_m and the pressure of HP and LP generators are denoted as $P_{g,H}$ and $P_{g,L}$.

In order to formulate the complex system modeling, the following assumptions have been considered for R1234yf VCR- H₂O/LiBr half effect VAR cascade cycle except where the variation of system parameters occurred (Arora et al., 2016; Arora, 2009; Arora and Kaushik, 2008).

- The approach temperature or overlap temperature between evaporator 2 and condenser 1 in the cascade heat exchanger ($T_{ov} = T_{cond, VC} - T_{e, VA}$) is 5.2°C .
- The pressure of LP generator and HP absorber are equal i.e. ($P_{g,L} = P_{a,H}$) and the optimum value of $P_{g,L}$ has been considered. The HP generator and condenser2 are at same pressure ($P_{cond,VA} = P_{g,H}$). Similarly, LP absorber and evaporator2 are at same pressure ($P_{e,VA} = P_{a,L}$) such that ($P_{e,VA} = P_{a,L}$) < ($P_{g,L} = P_{a,H}$) < ($P_{cond,VA} = P_{g,H}$).
- The state of refrigerant is dry and saturated at the entry of compressor at state point 1.
- The state of refrigerant at the exit of condenser of VCRS is saturated subcooled liquid at state point 3a. and the subcooling in the condenser1of VCR is from state 3 to 3a.
- Difference between the temperature of space to be cooled (T_b) and evaporator temperature ($T_{e, VC}$) i.e. ($\Delta T = T_b - T_{e, VC}$) is 10°C .
- The heat losses and pressure losses from the system and system components are negligible and the whole system assumed to operate in steady state condition.
- The reference values of entropy (s_0) and enthalpy (h_0) are at ambient or dead state conditions.
- The temperatures of HP & LP generator are assumed equal ($T_{HPg} = T_{LPg}$) and the temperature of HP, LP absorber and condenser2 are assumed same ($T_{a, H} = T_{a, L} = T_{cond, VA}$).

6.12.2 Energy analysis

The energy performance, based on first law of absorption compression (half effect $\text{H}_2\text{O}/\text{LiBr}$) cascade refrigeration cycle (ACCRC) is represented as coefficient of performance (COP):

$$\text{COP} = \frac{\dot{Q}_{e, VC}}{\dot{Q}_{HPg} + \dot{Q}_{LPg} + \dot{W}_{P, H} + \dot{W}_{P, L} + \dot{W}_c} \quad (6.17)$$

Where $\dot{Q}_{e, VC}$ and \dot{W}_c are the net refrigerating effect and rate of compressor work of VCRS in kW and \dot{Q}_{HPg} , \dot{Q}_{LPg} , $\dot{W}_{P, H}$ and $\dot{W}_{P, L}$ are the heat rate of HP & LP generator and solution pump work rate in kW of HEVARS respectively.

6.12.3 Exergy analysis

6.12.3.1 Total Exergy destruction (TEXD)

The total exergy destruction in compression-absorption half effect series flow H₂O-LiBr cascade refrigeration system is given by:

$$\begin{aligned} \dot{E}_{D, \text{ total}} = & (\dot{E}_D)_{e,VC} + (\dot{E}_D)_C + (\dot{E}_D)_{\text{Ex. valve}} + (\dot{E}_D)_{\text{Che}} + (\dot{E}_D)_{a, L} + (\dot{E}_D)_{\text{pump,L}} + \\ & (\dot{E}_D)_{\text{She, L}} + (\dot{E}_D)_{\text{Lpg}} + (\dot{E}_D)_{\text{Stv, L}} + (\dot{E}_D)_{a, H} + (\dot{E}_D)_{\text{pump,H}} + (\dot{E}_D)_{\text{She, H}} + \\ & (\dot{E}_D)_{\text{Hpg}} + (\dot{E}_D)_{\text{Stv, H}} + (\dot{E}_D)_{\text{cond,VA}} + (\dot{E}_D)_{\text{Rtv}} \end{aligned} \quad (6.18)$$

6.12.3.2 Exergetic efficiency (EXE)

The exergetic efficiency of absorption-compression half effect cascade refrigeration system can be expressed as:

$$\begin{aligned} \eta_{\text{ex, ACCRS}} = & 1 - \frac{\Sigma(\dot{E}_D)}{\dot{Q}_{\text{Hpg}} \left| \left(1 - \frac{T_0}{T_{\text{Hpg}}} \right) \right| + \dot{Q}_{\text{Lpg}} \left| \left(1 - \frac{T_0}{T_{\text{Lpg}}} \right) \right| + \dot{W}_{P, H} + \dot{W}_{P, L} + \dot{W}_c} \\ = & \frac{\dot{Q}_{e, \text{vc}} \left| \left(1 - \frac{T_0}{T_b} \right) \right|}{\dot{Q}_{\text{Hpg}} \left| \left(1 - \frac{T_0}{T_{\text{Hpg}}} \right) \right| + \dot{Q}_{\text{Lpg}} \left| \left(1 - \frac{T_0}{T_{\text{Lpg}}} \right) \right| + \dot{W}_{P, H} + \dot{W}_{P, L} + \dot{W}_c} \end{aligned} \quad (6.19)$$

Where $\Sigma(\dot{E}_D)$, is the total exergy destruction of the cascade system in kW, \dot{Q}_{Hpg} , \dot{Q}_{Lpg} , T_{Hpg} and T_{Lpg} are the input heat in kW and temperature in °C of the HP and LP generators respectively. $\dot{W}_{P, H}$, $\dot{W}_{P, L}$ and \dot{W}_c are HP & LP solution pump works and compressor work in kW respectively. $\dot{Q}_{e, \text{vc}}$ in kW is the rate of net refrigerating effect and T_b is the temperature of space to be cooled in °C of VCERS respectively. T_0 is the ambient or dead state temperature in °C.

6.12.3.3 Exergy destruction ratio (EDR)

The exergetic destruction ratio (EDR) of absorption-compression half effect cascade refrigeration system is expressed as:

$$\text{EDR}_{\text{ACCRS}} = \frac{\Sigma(\dot{E}_D)}{\dot{Q}_{e, \text{vc}} \left| \left(1 - \frac{T_0}{T_b} \right) \right|} = \frac{\dot{E}_{E, \text{total}}}{\dot{Q}_{e, \text{vc}} \left| \left(1 - \frac{T_0}{T_b} \right) \right|} \quad (6.20)$$

Where $\Sigma(\dot{E}_D)$, is the total exergy destruction of the cascade system in kW, $\dot{Q}_{e, \text{vc}}$ in kW is the rate of net refrigerating effect of vapour compression refrigeration system, T_b in °C is the temperature of space to be cooled and T_0 is the ambient or dead state temperature in °C respectively.

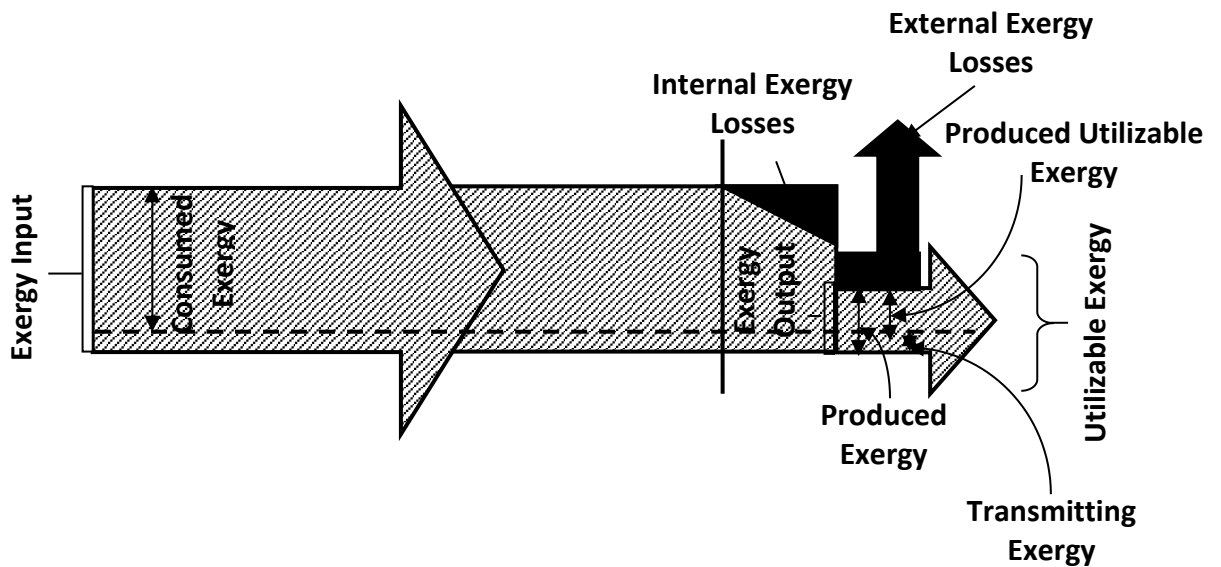


Figure 6.22 Pictorial representation of general exergy balance in a thermal system (Yataganbaba et al., 2015)

Fig. 6.22 shows the general exergy balance in a thermal system (Yataganbaba et al., 2015). The exergy input is equal to the sum of exergy consumed, exergy output and internal and external exergy losses.

The energy, exergy and mass balance formulation of each system component of compression-absorption half effect refrigeration system have been illustrated in Table 6.7.

Table 6.7 Energy, exergy and mass balance formulations of individual system component of absorption compression (half effect H₂O-LiBr) cascade refrigeration system

S. No.	Components	Mass balance	Energy balance
1.	Evaporator 1	$\dot{m}_{r,VC}$	$\dot{Q}_{e, VC} = \dot{m}_{r,VC}(h_1 - h_4)$
2.	Compressor	$\dot{m}_{r,VC}$	$\dot{W}_c = \dot{m}_{r,VC}(h_2 - h_1)$

3.	Condenser 1	$\dot{m}_{r,VC}$	$\dot{Q}_{cond, VC} = \dot{m}_{r,VC}(h_2 - h_{3a})$ $= \dot{m}_{r,VA}(h_{21} - h_{20})$ $= \dot{Q}_{e, VA}$
4.	Expansion valve	$\dot{m}_{r,VC}$	$\dot{m}_{r,VC}h_{3a} = \dot{m}_{r,VC}h_4$
5.	Cascade heat exchanger (Che)	$\dot{m}_{r,VA}$, $\dot{m}_{r,VC}$	$\dot{Q}_{cond, VC} = \dot{m}_{r,VC}(h_2 - h_{3a})$ $= \dot{m}_{r,VA}(h_{21} - h_{20})$ $= \dot{Q}_{e, VA}$
6.	Evaporator 2	$\dot{m}_{r,VA}$	$\dot{Q}_{e, VA} = \dot{m}_{r,VA}(h_{21} - h_{20})$ $= \dot{m}_{r,VC}(h_2 - h_{3a})$ $= \dot{Q}_{cond, VC}$
7.	Low pressure absorber	$\dot{m}_{s,L}$ $= \dot{m}_{r,VA}$ $+ \dot{m}_{w,L}$ or $\dot{m}_{s,L}$ $= \dot{m}_{r,L}$ $+ \dot{m}_{w,L}$	$\dot{Q}_{a, L} =$ $\dot{m}_{r,VA}h_{21} + \dot{m}_{w,L}h_{10} - \dot{m}_{s,L}h_5$
8.	Solution Pump _L	$\dot{m}_{s,L}$	$\dot{W}_{P,L} = \dot{m}_{s,L}(h_6 - h_5)$
9.	She _L	$\dot{m}_{s,L}$, $\dot{m}_{w,L}$	$\dot{m}_{w,L}(h_8 - h_9) = \dot{m}_{s,L}(h_7 - h_6)$
10.	Low pressure Generator	$\dot{m}_{s,L}$ $= \dot{m}_{w,L}$ $+ \dot{m}_{r,L}$ or $\dot{m}_{s,L}$ $= \dot{m}_{w,L}$ $+ \dot{m}_{r,VA}$	$\dot{Q}_{Lpg} = \dot{m}_{s,L}h_7 - \dot{m}_{w,L}h_8$ $- \dot{m}_{r,L}h_{11}$

11.	StvL	$\dot{m}_{w,L}$	$\dot{m}_{w,L}h_9 = \dot{m}_{w,L}h_{10}$
12.	High pressure absorber	$\dot{m}_{s,H}$ $= \dot{m}_{r,L}$ $+ \dot{m}_{w,H}$ Or $\dot{m}_{s,H}$ $= \dot{m}_{r,VA}$ $+ \dot{m}_{w,H}$	$\dot{Q}_{a, H} = \dot{m}_{r,L}h_{11} + \dot{m}_{w,H}h_{17} -$ $\dot{m}_{s,L}h_{12}$
13.	Solution Pump _H	$\dot{m}_{s,H}$	$\dot{W}_{P,H} = \dot{m}_{s,H}(h_{13} - h_{12})$
14.	She _H	$\dot{m}_{s,H}, \dot{m}_{w,H}$	$\dot{m}_{w,H}(h_{15} - h_{16}) = \dot{m}_{s,H}(h_{14} - h_{13})$
15.	High pressure Generator	$\dot{m}_{s,H}$ $= \dot{m}_{w,H}$ $+ \dot{m}_{r,VA}$	$\dot{Q}_{Hpg} = \dot{m}_{s,H}h_{14} - \dot{m}_{w,H}h_{15}$ $- \dot{m}_{r,VA}h_{18}$
16.	Stv _H	$\dot{m}_{w,H}$	$\dot{m}_{w,H}h_{16} = \dot{m}_{w,H}h_{17}$
17.	Condenser2	$\dot{m}_{r,VA}$	$\dot{Q}_{cond, VA} = \dot{m}_{r,VA}(h_{18}$ $- h_{19})$
18.	Rtv	$\dot{m}_{r,VA}$	$\dot{m}_{r,VA}h_{19} = \dot{m}_{r,VA}h_{20}$
S. No.	Exergy destruction (\dot{E}_D)		Exergy destruction ratio (EDR)
1.	$(\dot{E}_D)_{e,VC} = \dot{E}_{X_4} + \dot{Q}_{e, VC} \left(1 - \frac{T_0}{T_b}\right) - \dot{E}_{X_1}$ $= \dot{m}_{r,VC}(h_4 - T_0s_4)$ $+ \dot{Q}_{e, VC} \left(1 - \frac{T_0}{T_b}\right)$ $- \dot{m}_{r,VC}(h_1 - T_0s_1)$		$EDR_{e,VC} = \frac{(\dot{E}_D)_{e,VC}}{\dot{E}_{D,total}}$
2.	$(\dot{E}_D)_c = \dot{E}_{X_1} + \dot{W}_c - \dot{E}_{X_2}$ $= \dot{m}_{r,VC}(h_1 - T_0s_1) + \dot{W}_c$ $- \dot{m}_{r,VC}(h_2 - T_0s_2)$		$EDR_c = \frac{(\dot{E}_D)_c}{\dot{E}_{D,total}}$

3.	$ \begin{aligned} (\dot{E}_D)_{\text{cond,VC}} &= \dot{E}_{X_2} - \dot{E}_{X_{3a}} \\ &= \dot{m}_{r,VC}(h_2 - T_0s_2) \\ &\quad - \dot{m}_{r,VC}(h_{3a} - T_0s_{3a}) \end{aligned} $	$ \begin{aligned} EDR_{\text{cond,VC}} \\ &= \frac{(\dot{E}_D)_{\text{Cond,VC}}}{\dot{E}_{D,\text{total}}} \end{aligned} $
4.	$ \begin{aligned} (\dot{E}_D)_{\text{exp,valve}} &= \dot{E}_{X_{3a}} - \dot{E}_{X_4} \\ &= \dot{m}_{r,VC}(h_{3a} - T_0s_{3a}) \\ &\quad - \dot{m}_{r,VC}(h_4 - T_0s_4) \end{aligned} $	$ \begin{aligned} EDR_{\text{exp,valve}} \\ &= \frac{(\dot{E}_D)_{\text{exp,valve}}}{\dot{E}_{D,\text{total}}} \end{aligned} $
5.	$ \begin{aligned} (\dot{E}_D)_{\text{Che}} &= \dot{E}_{X_2} + \dot{E}_{X_{20}} + \dot{Q}_{e,VA} \left(1 - \frac{T_0}{T_{e,VC}}\right) \\ &\quad - \dot{E}_{X_{3a}} - \dot{E}_{X_{21}} \\ &= \dot{m}_{r,VC}(h_2 - T_0s_2) \\ &\quad + \dot{m}_{r,VA}(h_{20} - T_0s_{20}) \\ &\quad + \dot{Q}_{e,VA} \left(1 - \frac{T_0}{T_{e,VC}}\right) \\ &\quad - \dot{m}_{r,VC}(h_{3a} - T_0s_{3a}) \\ &\quad - \dot{m}_{r,VA}(h_{21} - T_0s_{21}) \end{aligned} $	$ EDR_{\text{Che}} = \frac{(\dot{E}_D)_{\text{Che}}}{\dot{E}_{D,\text{total}}} $
6.	$ \begin{aligned} (\dot{E}_D)_{e,VA} &= \dot{E}_{X_{20}} + \dot{Q}_{e,VA} \left(1 - \frac{T_0}{T_{e,VC}}\right) \\ &\quad - \dot{E}_{X_{21}} \\ &= \dot{m}_{r,VA}(h_{20} - T_0s_{20}) \\ &\quad + \dot{Q}_{e,VA} \left(1 - \frac{T_0}{T_{e,VC}}\right) \\ &\quad - \dot{m}_{r,VA}(h_{21} - T_0s_{21}) \end{aligned} $	$ EDR_{e,VA} = \frac{(\dot{E}_D)_{e,VA}}{\dot{E}_{D,\text{total}}} $
7.	$ \begin{aligned} (\dot{E}_D)_{a,L} &= \dot{E}_{X_{10}} + \dot{E}_{X_{21}} - \dot{E}_{X_5} \\ &= \dot{m}_{w,L}(h_{10} - T_0s_{10}) \\ &\quad + \dot{m}_{r,VA}\{(h_{21} - h_0) \\ &\quad - T_0(s_{21} - s_0)\} \\ &\quad - \dot{m}_s(h_5 - T_0s_5) \end{aligned} $	$ EDR_{a,L} = \frac{(\dot{E}_D)_a}{\dot{E}_{D,\text{total}}} $
8.	$ \begin{aligned} (\dot{E}_D)_{\text{Pump,L}} &= \dot{E}_{X_5} - \dot{E}_{X_6} \\ &= \dot{m}_{s,L}(h_5 - T_0s_5) \\ &\quad - \dot{m}_{s,L}(h_6 - T_0s_6) \end{aligned} $	$ EDR_{\text{Pump,L}} = \frac{(\dot{E}_D)_{\text{Pump,L}}}{\dot{E}_{D,\text{total}}} $
9.	$ \begin{aligned} (\dot{E}_D)_{\text{She,L}} &= \dot{E}_{X_6} - \dot{E}_{X_7} + \dot{E}_{X_8} - \dot{E}_{X_9} = \\ &\dot{m}_{s,L}\{(h_6 - T_0s_6) - (h_7 - \\ &T_0s_7)\} + \dot{m}_{w,L}\{(h_8 - T_0s_8) - (h_9 - T_0s_9)\} \end{aligned} $	$ EDR_{\text{She,L}} = \frac{(\dot{E}_D)_{\text{She,L}}}{\dot{E}_{D,\text{total}}} $

10.	$(\dot{E}_D)_{Lpg} = \dot{E}_{X_7} - \dot{E}_8 - \dot{E}_{X_{11}} = \dot{m}_{s,L}\{(h_7 - T_0s_7) - \dot{m}_{w,L}(h_8 - T_0s_8)\} + \dot{m}_{r,L}\{(h_{11} - h_0) - T_0(s_{11} - s_0)\}$	$EDR_{Lpg} = \frac{(\dot{E}_D)_{Lpg}}{\dot{E}_{D,total}}$
11.	$(\dot{E}_D)_{Stv,L} = \dot{E}_9 - \dot{E}_{10}$ $= \dot{m}_{w,L}\{(h_9 - T_0s_9) - (h_{10} - T_0s_{10})\}$	$EDR_{Stv,L} = \frac{(\dot{E}_D)_{Stv,L}}{\dot{E}_{D,total}}$
12.	$(\dot{E}_D)_{a,H} = \dot{E}_{X_{11}} + \dot{E}_{X_{17}} - \dot{E}_{X_{12}}$ $= \dot{m}_{r,L}\{(h_{11} - h_0) - T_0(s_{11} - s_0)\} + \dot{m}_{w,H}(h_{17} - T_0s_{17}) - \dot{m}_{s,H}(h_{12} - T_0s_{12})$	$EDR_{a,H} = \frac{(\dot{E}_D)_{a,H}}{\dot{E}_{D,total}}$
13.	$(\dot{E}_D)_{Pump,H} = \dot{E}_{X_{12}} - \dot{E}_{X_{13}}$ $= \dot{m}_{s,H}\{(h_{12} - T_0s_{12}) - (h_{13} - T_0s_{13})\}$	$EDR_{Pump,H} = \frac{(\dot{E}_D)_{Pump,H}}{\dot{E}_{D,total}}$
14.	$(\dot{E}_D)_{She,L} = \dot{E}_{X_{13}} - \dot{E}_{X_{14}} + \dot{E}_{X_{15}} - \dot{E}_{X_{16}} = \dot{m}_{s,H}\{(h_{13} - T_0s_{13}) - (h_{14} - T_0s_{14})\} + \dot{m}_{w,H}\{(h_{15} - T_0s_{15}) - (h_{16} - T_0s_{16})\}$	$EDR_{She,H} = \frac{(\dot{E}_D)_{She,H}}{\dot{E}_{D,total}}$
15.	$(\dot{E}_D)_{Hpg} = \dot{E}_{X_{14}} - \dot{E}_{15} - \dot{E}_{X_{18}} = \dot{m}_{s,H}\{(h_{14} - T_0s_{14}) - \dot{m}_{w,H}(h_{15} - T_0s_{15})\} + \dot{m}_{r,VA}\{(h_{18} - h_0) - T_0(s_{18} - s_0)\}$	$EDR_{Lpg} = \frac{(\dot{E}_D)_{Hpg}}{\dot{E}_{D,total}}$
16.	$(\dot{E}_D)_{Stv,H} = \dot{E}_{16} - \dot{E}_{17}$ $= \dot{m}_{w,H}\{(h_{16} - T_0s_{16}) - (h_{17} - T_0s_{17})\}$	$EDR_{Stv,H} = \frac{(\dot{E}_D)_{Stv,H}}{\dot{E}_{D,total}}$
17.	$(\dot{E}_D)_{cond,VA} = \dot{E}_{18} - \dot{E}_{19}$ $= \dot{m}_{r,VA}\{(h_{18} - T_0s_{18}) - (h_{19} - T_0s_{19})\}$	$EDR_{cond,VA} = \frac{(\dot{E}_D)_{cond,VA}}{\dot{E}_{D,total}}$
18.	$(\dot{E}_D)_{Rtv} = \dot{E}_{19} - \dot{E}_{20}$ $= \dot{m}_{r,VA}\{(h_{19} - T_0s_{19}) - (h_{20} - T_0s_{20})\}$	$EDR_{Rtv} = \frac{(\dot{E}_D)_{Rtv}}{\dot{E}_{D,total}}$

6.12.4 Model validation

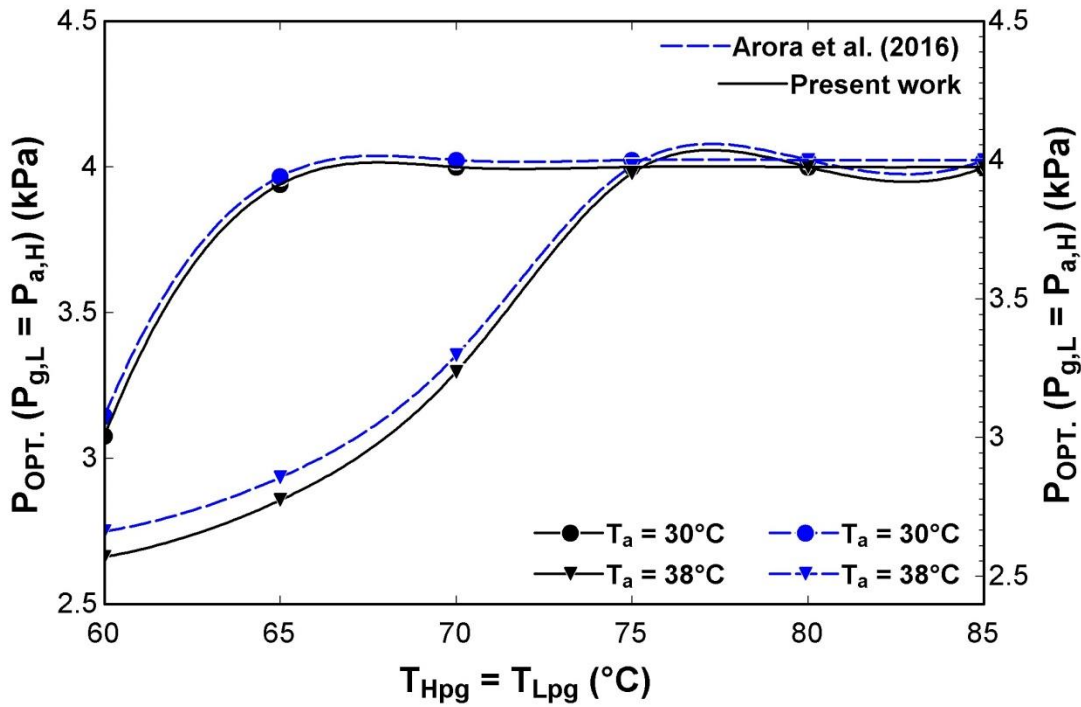


Figure 6.23 Variation in optimum pressure ($P_{OPT.}$) of LP generator with generator temperature (T_{Hpg} , T_{Lpg})

Model validation has been done on comparing the results of present work with the Arora et al.(2016) for half effect water lithium bromide vapour absorption system as shown in Fig. 6.23-6.25 and Table 6.8. Fig. 6.23-6.25 present the variation in optimum pressure ($P_{opt.}$) of HP & LP absorber, $COP_{MAX.}$ and maximum exergetic efficiency ($\eta_{ex}(MAX.)$) with generator temperature (T_{Hpg} , T_{Lpg}). Fig. 6.23 shows the effect of T_{Hpg} , T_{Lpg} on $P_{opt.}$ at 30°C and 38°C of absorber temperatures. At absorber temperature of 30°C , the value of $P_{opt.}$ first increases and then becomes constant with the increase in T_{Hpg} , T_{Lpg} . It is observed that the present work follows the Arora et al. (2016) for the variation in P_{opt} with increase in T_{Hpg} , T_{Lpg} .

Similarly, the variation in $COP_{MAX.}$ and ($\eta_{ex}(MAX.)$) with increase in T_{Hpg} , T_{Lpg} at various absorber temperatures have been shown in Fig. 6.24 and 6.25 respectively. The $COP_{MAX.}$ decreases at absorber temperatures 30 to 34°C while $COP_{MAX.}$ increases first and then decreases at absorber temperatures 36°C and 38°C with increase in T_{Hpg} , T_{Lpg} . The optimum generator temperature lies within 65 - 70°C . It is also observed that the $\eta_{ex}(MAX.)$ decreases with increase in T_{Hpg} , T_{Lpg} .

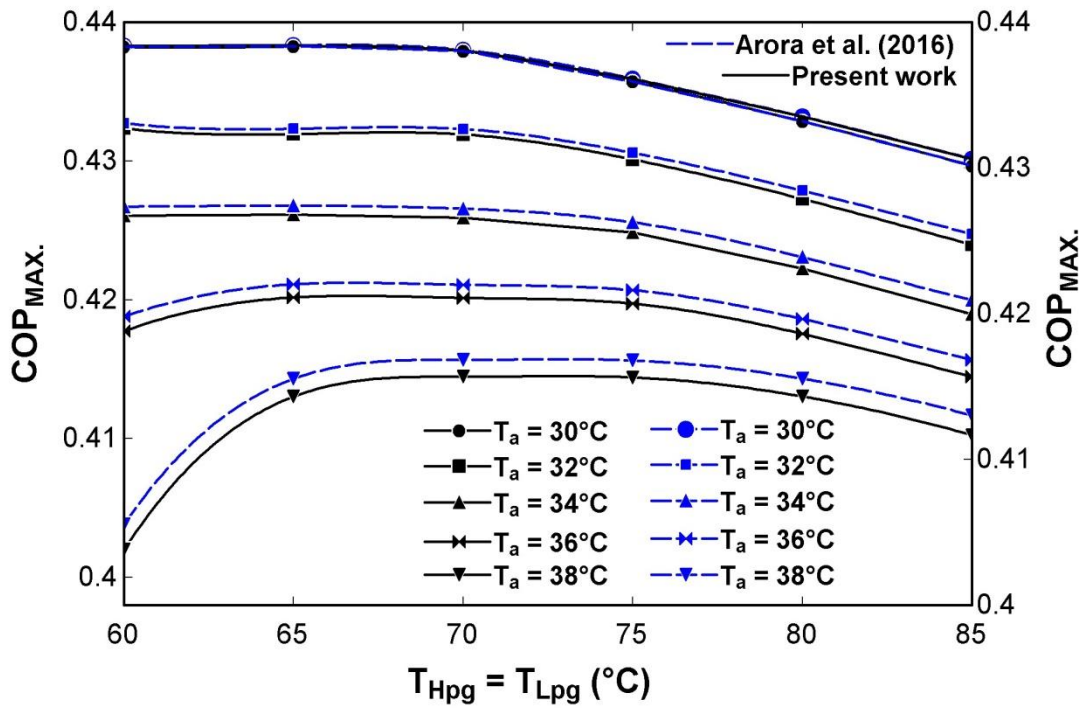


Figure 6.24 Effect of generator temperature (T_{Hpg} & T_{Lpg}) on maximum value of COP ($COP_{MAX.}$)

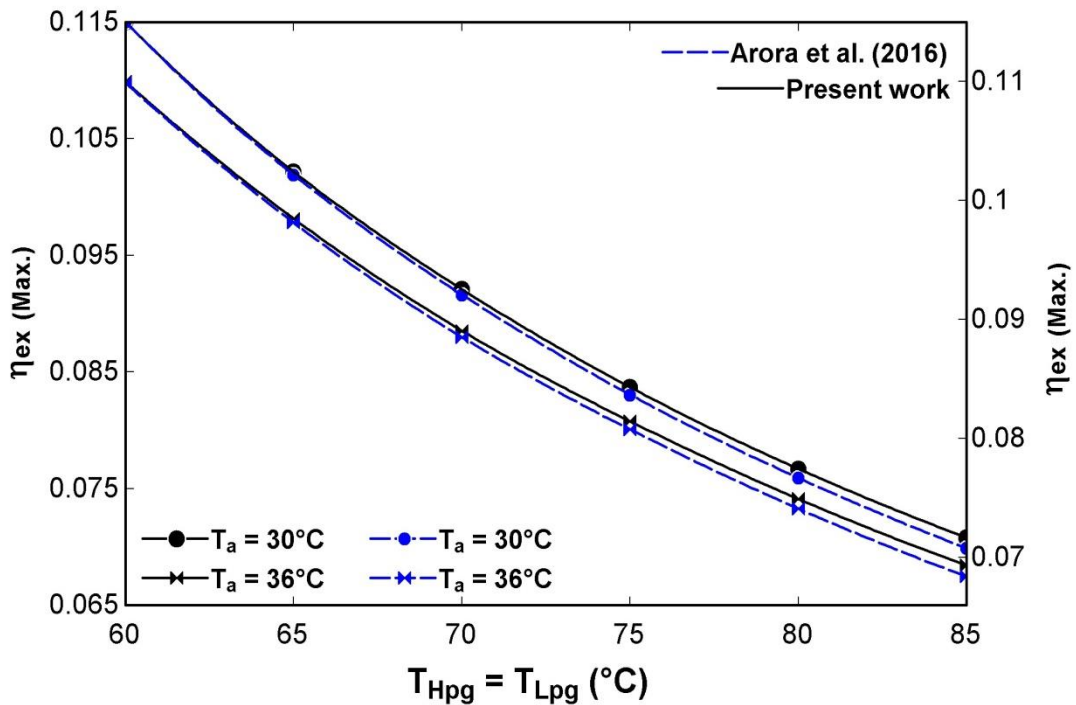


Figure 6.25 Variation in maximum thermal efficiency ($\eta_{ex}(MAX.)$) with generator temperature (T_{Hpg} , & T_{Lpg})

The values of COP_{MAX} and $\eta_{ex}(MAX.)$ for the present work are close to the Arora et al. (2016) for different absorber temperatures as shown in Fig. 6.24 and 6.25.

Table 6.8 Heat rate (\dot{Q}_i) or work rate (\dot{W}_i),) of components of ACCRS. Comparison of present work with Arora et al.(2016) for H₂O-LiBr HEVARS ($T_{e, VA} = 7, T_{a, L} = T_{a, H} = T_{cond, VA} = 37.8^{\circ}C$, $T_{Lpg} = T_{Hpg} = 67^{\circ}C$, $\epsilon_{She, L} = \epsilon_{She, H} = 0.7$, $\dot{m}_{r,VA}=1kg/s$ and $T_{e, VC} = -25^{\circ}C$)

System components (i)	\dot{Q}_i or \dot{W}_i (kW)		
	Present work ACCRS	(Arora et al., 2016) HEVARS	Difference (%)
Evaporator1	1936	-	-
Compressor	419.2	-	-
Expansion valve	-	-	-
Cascade heat exchanger	2355	-	-
Evaporator2	2355	2355	0
Low pressure Absorber	-2898	-2898	0
Solution Pump _L	0.01664	0.01664	0
She _L	472.7	472.7	0
Low pressure Generator	3010	3010	0
Stv _L	-	-	-
High pressure Absorber	-2654	-2654	0
Solution Pump _H	0.01397	0.01397	0
She _H	196	196	0
High pressure Generator	2653	2653	0
Stv _H	-	-	-
Condenser2	-2466	-2466	0
Rtv	-	-	-

The comparison of two works verified that the corresponding values of COP_{MAX} and $\eta_{ex}(MAX.)$ obtained by present work for VARS merely lie within $\pm 1\%$ while compared to Arora et al.(2016). The values of heat and work rate obtained by present work coincide to the values obtained by Arora et al.(2016) as shown in Table 6.8.

6.13 RESULTS AND DISCUSSION

A computer software based code has been compiled in Engineering Equation Solver (EES)(Klein and Alvarado, 2012) software application for the model described in section 6.11 above to evaluate the performance of absorption-compression (half effect H₂O-LiBr series flow) cascade refrigeration cycle (ACCRC) on the basis of exergy and energy analysis. A vapour compression refrigeration (VCR) cycle having R1234yf refrigerant is coupled through cascade heat exchanger to half effect series flow vapour absorption refrigeration (VAR) system. The property codes for various properties are inbuilt in function directory of the EES and are called for computation of various properties such as specific enthalpy, specific entropy, specific volume, pressures and temperatures etc. The program validation has been done and the results lie within $\pm 1\%$ when compared to Arora et al. (2016) as shown in Fig. 6.23-6.25 and Table 6.8 respectively.

6.13.1 Results of energy analysis

Table 6.9 The thermodynamic properties (temperature (T_j), pressure (P_j), concentration of solution (X_j), mass flow rate (\dot{m}_j), enthalpy (h_j) and entropy (s_j)) of ACCRS at state points ($T_{e,VA} = 7, T_{a,L} = T_{a,H} = T_{cond,VA} = 37.8^\circ\text{C}$, $T_{Lpg} = T_{Hpg} = 67^\circ\text{C}$, $\varepsilon_{She,L} = \varepsilon_{She,H} = 0.7$, $\dot{m}_{r,VA} = 1\text{kg/s}$ and $T_{e,VC} = -25^\circ\text{C}$)

State Points (j)	T_j ($^\circ\text{C}$)	P_j (kPa)	X_j (kg abs/kg sol)	\dot{m}_j (kgs^{-1})	h_j (kJkg^{-1})	s_j ($\text{kJkg}^{-1}\text{K}^{-1}$)
1	-25	122.9	-	14.17	346.7	1.598
2	12.2	468.5	-	14.17	376.3	1.618
3	12.2	468.5	-	14.17	215.2	1.056
3a	7.2	468.5	-	14.17	210.1	1.033
4	-25	122.9	-	14.17	210.1	1.049
5	37.8	1.002	0.5554	13.18	91.98	0.2281
6	37.8	3.0162	0.5554	13.18	114.4	0.2281
7	55.52	3.0162	0.5554	13.18	127.8	0.3403
8	67	3.0162	0.6010	12.18	169.9	0.3792
9	46.63	3.0162	0.6010	12.18	131.1	0.2616

10	37.8	1.002	0.6010	12.18	131.1	0.2616
11	67	3.0162	0	1	2625	8.827
12	37.8	3.0162	0.4294	5.505	77.76	0.3329
13	37.8	6.558	0.4294	5.505	82.69	0.3329
14	52.64	6.558	0.4294	5.505	113.4	0.4441
15	67	6.558	0.5247	4.505	144.8	0.4387
16	46.65	6.558	0.5247	4.505	101.3	0.3073
17	37.8	3.0162	0.5247	4.505	101.3	0.3073
18	67	6.558	0	1	2625	8.467
19	37.8	6.558	0	1	158.3	0.5428
20	7	1.002	0	1	158.3	0.5664
21	37.8	1.002	0	1	2513	8.973

6.13.2 Results of exergy analysis

Table 6.10 The input and output exergy in each system component of ACCRS ($T_{e,VA} = 7, T_{a,L} = T_{a,H} = T_{cond,VA} = 37.8^{\circ}\text{C}$, $T_{Lpg} = T_{Hpg} = 67^{\circ}\text{C}$, $\epsilon_{She,L} = \epsilon_{She,H} = 0.7$, $\dot{m}_{r,VA} = 1\text{kg/s}$ and $T_{e,VC} = -25^{\circ}\text{C}$)

System components (i)	$\dot{E}_{in,i}$ (kW)	$\dot{E}_{out,i}$ (kW)
Evaporator1	-1469	-2347
Compressor	-1343	-1468
Expansion valve	-1349	-1349
Cascade heat exchanger	-1478	-1509
Low pressure Absorber	471.2	297.4
Solution Pump _L	299.7	299.7
She _L	1018	982.1
Low pressure Generator	1224	1171
Stv _L	1762	1706
High pressure Absorber	1484	1468
Solution Pump _H	1035	1026
She _H	755.5	755.4
High pressure Generator	-3.533	-10.47

Stv _H	5.169	1.346
Condenser2	23.06	4.811
R _{tv}	785.6	784.3

6.13.3 Parametric analysis

The performance of absorption-compression (half effect H₂O-LiBr series flow) cascade refrigeration cycle (ACCRC) depends on various operating variables. The selection of operating variables plays significant role in the energy and exergy performance analysis of ACCRC. The effect of significant operating variables viz. high pressure generator temperature, absorber temperature and evaporator temperature of VCR cycle on thermodynamics and exergetic performance of ACCRC have been explored. The only one variable has varied while others have been kept constant at their base value during the parametric analysis.

6.13.3.1 Effect of generator temperature

The effect of generator temperature (T_{Hpg} , T_{Lpg}) on performance parameters viz. solution circulation ratio (SCR), coefficient of performance (COP), exergetic efficiency (η_{ex}), total exergy destruction rate ($\dot{E}_{D, \text{total}}$) and exergy destruction ratio (EDR) has been illustrated in Fig. 6.26-6.29 for various absorber temperatures.

Fig. 6.26 depicts the effect of generator temperature (T_{Hpg} , T_{Lpg}) on solution circulation ratio (SCR) at various absorber temperatures for absorption compression cascade refrigeration cycle. At a particular absorber temperature, the value of SCR decreases with increase in generator temperature. It is observed that the SCR decline rapidly at absorber temperatures 36⁰C, 37.8⁰C and 38⁰C. The SCR is equal to $\frac{\text{Mass flow rate of strong solution}}{\text{Mass flow rate of refrigerant}} = \frac{\dot{m}_s}{\dot{m}_{r,VA}}$ where \dot{m}_s and $\dot{m}_{r,VA}$ are mass flow rate of strong solution and refrigerant in kg/s respectively. SCR is the sum of LP circuit SCR (SCR_L) and HP circuit SCR (SCR_H). The value of \dot{m}_s decreases with increase in (T_{Hpg} , T_{Lpg}) and $\dot{m}_{r,VA} = 1 \text{ kg/s}$ (Table 2.) which is constant, thus the value of SCR decreases. This is because the solution concentration (X) is the function of absorber temperature (T) & pressure (P) and $\dot{m}_s = \frac{X_w}{X_w - X_s} \times \dot{m}_{r,VA}$.

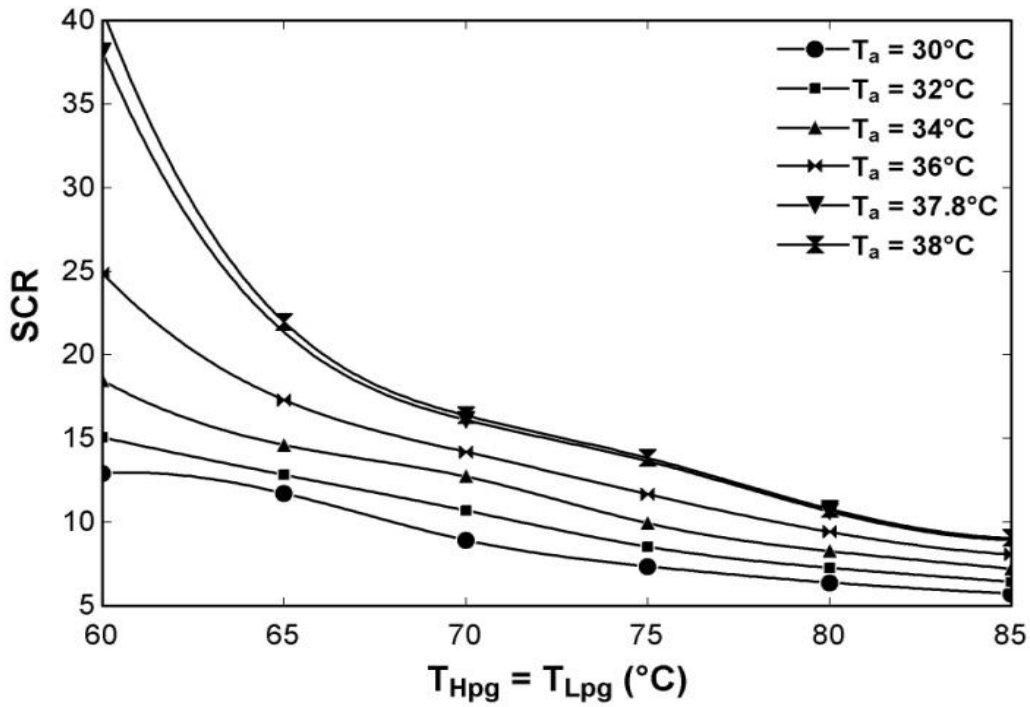


Figure 6.26 Variation in solution circulation ratio (SCR) with generator temperature (T_{Hpg} , T_{Lpg})

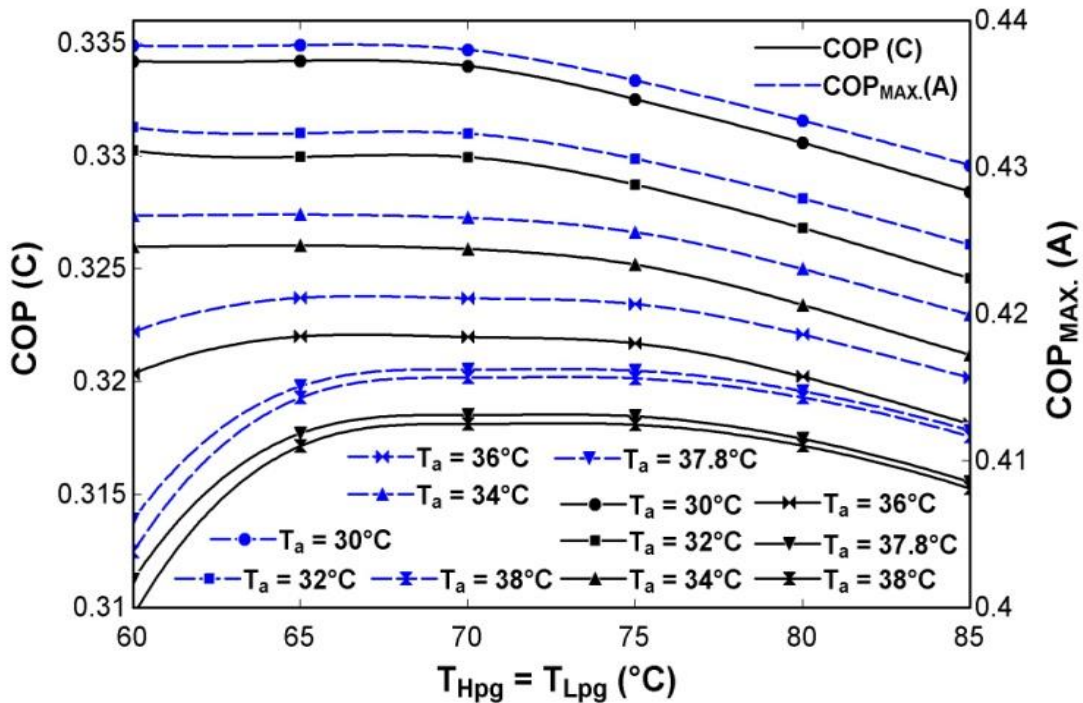


Figure 6.27 Effect of generator temperature (T_{Hpg} , T_{Lpg}) on COP

(A): Half effect H_2O -LiBr VAR cycle (HEVARC); (C): Absorption compression cascade refrigeration cycle (ACCRC)

The value of $(X_w - X_s)$ increases more than that of the weak solution concentration (X_w) with increases in (T_{Hpg}, T_{Lpg}) results decrease in \dot{m}_s . It has also been observed that the value of SCR decreases slightly with increase in (T_{Hpg}, T_{Lpg}) at absorber temperatures 30°C , 32°C and 34°C .

At a particular generator temperature, the value of SCR increases with increase in absorber temperature. The minimum and maximum values of SCR noticed correspond to $(T_{Hpg} = T_{Lpg} = 85^\circ\text{C}, T_{a,H} = T_{a,L} = T_{\text{cond,VA}} = 30^\circ\text{C})$ and $(T_{Hpg} = T_{Lpg} = 60^\circ\text{C}, T_{a,H} = T_{a,L} = T_{\text{cond,VA}} = 38^\circ\text{C})$ are 5.733 and 40.64.

Fig. 6.27 illustrates the variation of COP with generator temperature (T_{Hpg}, T_{Lpg}) at various absorber temperatures for absorption compression cascade refrigeration cycle (ACCRC). At absorber temperatures 30°C , 32°C and 34°C , the value of COP decreases with increase in generator temperature. According to Eq. (6.17), COP of ACCRC depends on $\dot{Q}_{e,vc}$ and $(\dot{Q}_{Hpg} + \dot{Q}_{Lpg} + \dot{W}_{P,H} + \dot{W}_{P,L} + \dot{W}_c)$. The values of $\dot{Q}_{e,vc}$ and \dot{W}_c remains constant with increase in generator temperature. The pump work $\dot{W}_{P,H}$ & $\dot{W}_{P,L}$ are negligible.

The value of $(\dot{Q}_{Hpg} + \dot{Q}_{Lpg})$ is so adjusted for the optimal value of LP generator pressure ($P_{g,L}$) at maximum COP that it increases at absorber temperatures 30°C , 32°C and 34°C and decreases at 36°C , 37.8°C and 38°C with increase in generator temperature. This is because the value of $(\dot{Q}_{Hpg} + \dot{Q}_{Lpg})$ is directly proportional to mass flow rate of strong solution (\dot{m}_s), \dot{m}_s is directly proportional to the SCR and the SCR is inversely proportional to (T_{Hpg}, T_{Lpg}) . At absorber temperatures 36°C , 37.8°C and 38°C , the value of COP increases first and then decreases slightly with increase in generator temperature. It is observed that the optimum value of generator temperature lies between 67 to 70°C for which the COP of ACCRC is maximum for various absorber temperatures. The maximum and minimum value of COP correspond to $(T_{Hpg} = T_{Lpg} = 60^\circ\text{C}, T_{a,H} = T_{a,L} = T_{\text{cond,VA}} = 30^\circ\text{C})$ and $(T_{Hpg} = T_{Lpg} = 60^\circ\text{C}, T_{a,H} = T_{a,L} = T_{\text{cond,VA}} = 38^\circ\text{C})$ are 0.3342 and 0.3284.

Fig. 6.28 illustrates the effect of generator temperature (T_{Hpg}, T_{Lpg}) on exergetic efficiency (η_{ex}) at different absorber temperatures. The exergetic efficiency of the ACCRC decreases with increase in generator temperature.

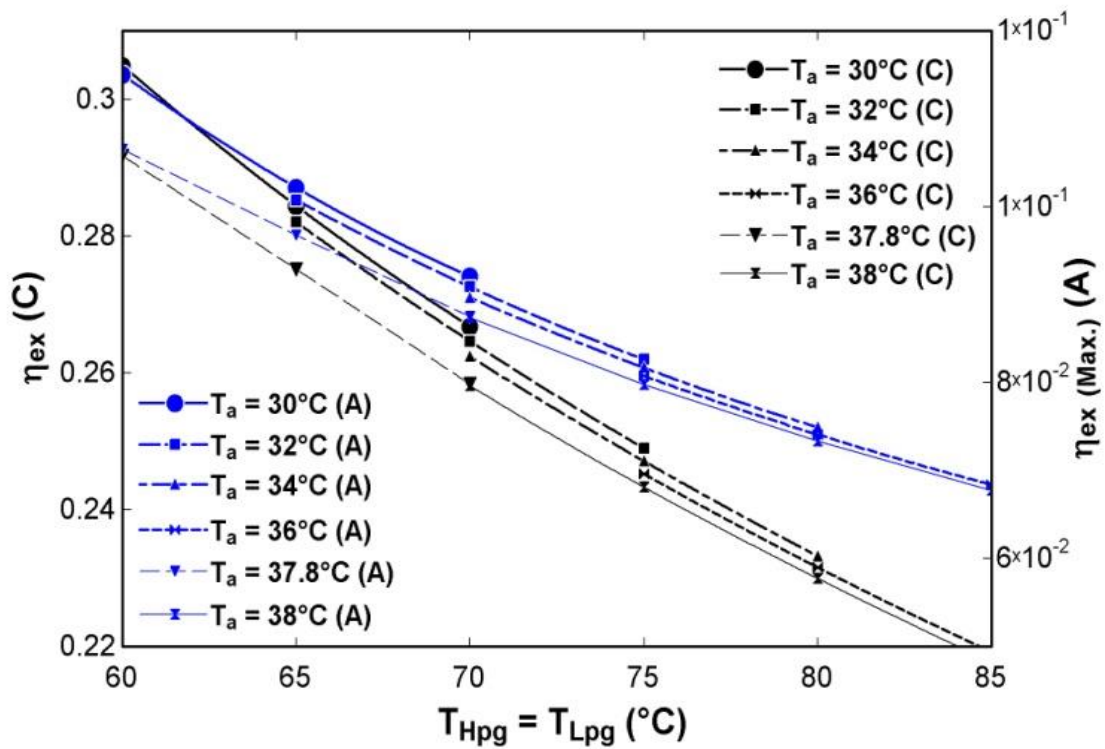


Figure 6.28 Effect of generator temperature (T_{Hpg} , T_{Lpg}) on exergetic efficiency (η_{ex})

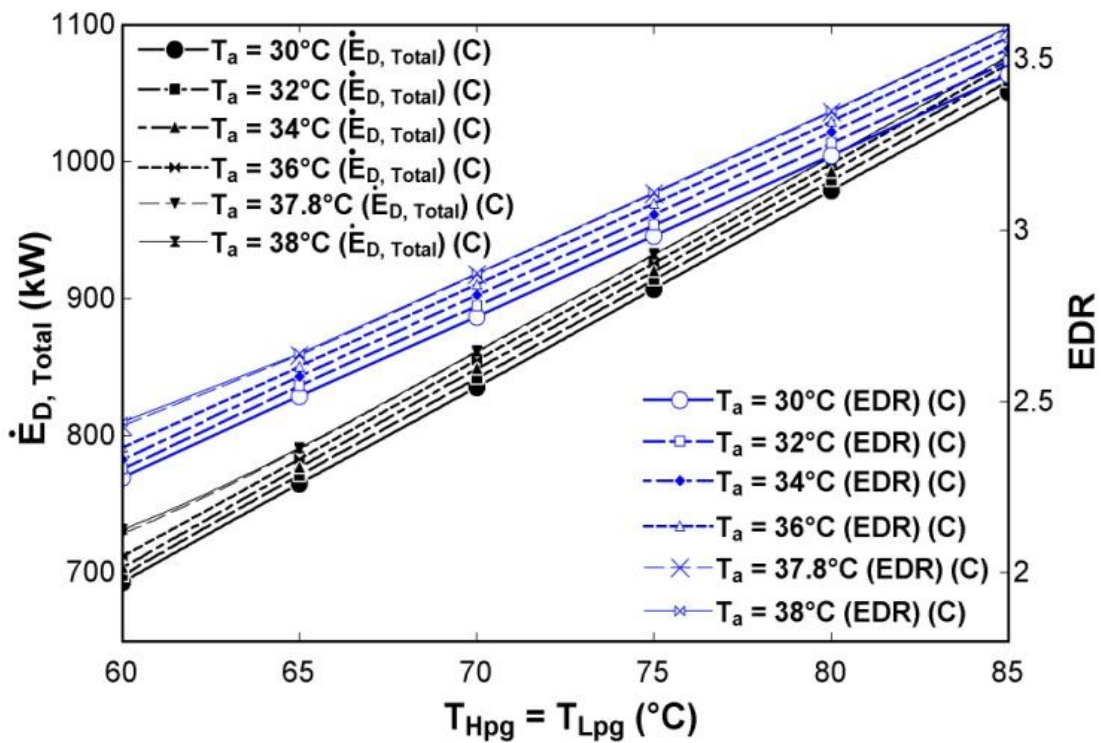


Figure 6.29 Variation in total exergy destruction ($\dot{E}_{D, total}$) and exergy destruction ratio (EDR) with (T_{Hpg} , T_{Lpg})

(A): Half effect H₂O/LiBr VAR cycle (HEVARC); (C): Absorption compression cascade refrigeration cycle (ACCRC)

According to Eq. (6.19), the value of η_{ex} depends on $\dot{Q}_{e, VC} \left| \left(1 - \frac{T_0}{T_b} \right) \right|$ and $\left(\dot{Q}_{HPg} \left| \left(1 - \frac{T_0}{T_{HPg}} \right) \right| + \dot{Q}_{LPg} \left| \left(1 - \frac{T_0}{T_{LPg}} \right) \right| + \dot{W}_{P, H} + \dot{W}_{P, L} + \dot{W}_C \right)$. The values of $\dot{Q}_{e, VC} \left| \left(1 - \frac{T_0}{T_b} \right) \right|$ and \dot{W}_C remains constant with increase in T_{HPg} , T_{LPg} . The pump work $\dot{W}_{P, H}$ & $\dot{W}_{P, L}$ are negligible. The values of $\left| \left(1 - \frac{T_0}{T_{HPg}} \right) \right|$ and $\left| \left(1 - \frac{T_0}{T_{LPg}} \right) \right|$ increases with increase in T_{HPg} , T_{LPg} . However, the values of \dot{Q}_{HPg} and \dot{Q}_{LPg} vary according to the optimal value of $P_{g,L}$ in order to maximize COP of HEVARC. Hence, the value of η_{ex} decreases with increase in T_{HPg} , T_{LPg} . It has been observed that at particular generator temperature, the value of η_{ex} decreases with increase in absorber temperature. The maximum and minimum values of η_{ex} correspond to ($T_{HPg} = T_{LPg} = 60^\circ\text{C}$, $T_{a, H} = T_{a, L} = T_{cond, VA} = 30^\circ\text{C}$) and ($T_{HPg} = T_{LPg} = 85^\circ\text{C}$, $T_{a, H} = T_{a, L} = T_{cond, VA} = 38^\circ\text{C}$) are 0.3342 and 0.3284.

Fig. 6.29 presents the variation in total exergy destruction rate ($\dot{E}_{D, total}$) and exergy destruction ratio (EDR) with generator temperature (T_{HPg} , T_{LPg}) for various evaporator temperatures. The $\dot{E}_{D, total}$ and EDR increase with increase in T_{HPg} , T_{LPg} . According to Eq.(6.18), $\dot{E}_{D, total}$ is the sum of \dot{E}_D of each system component. This is the fact that with the increase in generator temperature, the irreversibility of system components viz. LP and HP generators, condenser2, solution heat exchangers (She_L and She_H), refrigerant throttle valves (Rt_{VL} and Rt_{VH}) and LP & HP absorbers increases.

It is also been observed that for a particular generator temperature, the value of $\dot{E}_{D, total}$ and EDR increases with increase in absorber temperature. The irreversibility of system components also increases with increase in absorber temperature as the temperature of strong solution leaving the absorber increases. EDR is the ratio of $\dot{E}_{D, total}$ and $\dot{Q}_{e, VC} \left| \left(1 - \frac{T_0}{T_b} \right) \right|$ (Eq. 6.17). The values of $\dot{Q}_{e, VC}$, T_0 and T_b remain constant with increase in T_{HPg} , T_{LPg} . Thus the EDR follows the same trend of $\dot{E}_{D, total}$. The maximum and minimum values of $\dot{E}_{D, total}$ and EDR correspond to ($T_{HPg} = T_{LPg} = 85^\circ\text{C}$, $T_{a, H} = T_{a, L} = T_{cond, VA} = 38^\circ\text{C}$) and ($T_{HPg} = T_{LPg} = 60^\circ\text{C}$, $T_{a, H} = T_{a, L} = T_{cond, VA} = 30^\circ\text{C}$) are 1077 kW, 3.593 and 693.3 kW, 2.28.

6.13.3.2 Effect of evaporator temperature

The effect of evaporator1 temperature ($T_{e,vc}$) on performance parameters viz. coefficient of performance (COP), exergetic efficiency (η_{ex}), total exergy destruction rate ($\dot{E}_{D,total}$) and exergy destruction ratio (EDR) has been presented in Fig. 6.30-6.32 at various absorber temperatures.

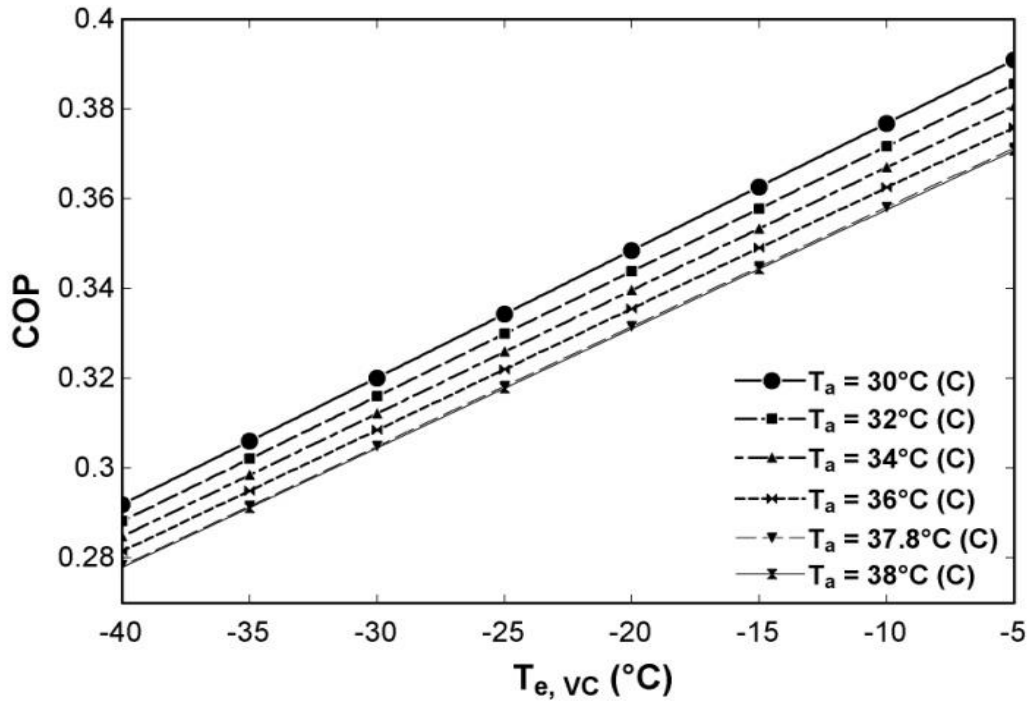


Figure 6.30 Effect of evaporator1 temperature ($T_{e,vc}$) on COP (C): Absorption compression cascade refrigeration cycle (ACCRC)

Fig. 6.30 depicts the variation in COP with evaporator1 temperature ($T_{e,vc}$) at various absorber temperatures. The COP of the absorption-compression (half effect H₂O-LiBr) cascade refrigeration cycle (ACCRC) increases with increase in evaporator1 temperature. According to the eq. (6.17), the COP of the ACCR cycle is

$$\frac{\dot{Q}_{e,vc}}{\dot{Q}_{HPg} + \dot{Q}_{LPg} + \dot{W}_{P,H} + \dot{W}_{P,L} + \dot{W}_c}$$
 in which the pump work ($\dot{W}_{P,H}$ & $\dot{W}_{P,L}$) are negligible. The

input heat to HP & LP generators (\dot{Q}_{HPg} & \dot{Q}_{LPg}) remain constant with increase in $T_{e,vc}$.

The compressor work (\dot{W}_c) decreases and specific refrigerating effect ($\frac{\dot{Q}_{e,vc}}{\dot{m}_{r,vc}}$) increases

with increase in evaporator temperature (Arora et al., 2009). Hence the COP of the cycle increases with increase in $T_{e,vc}$.

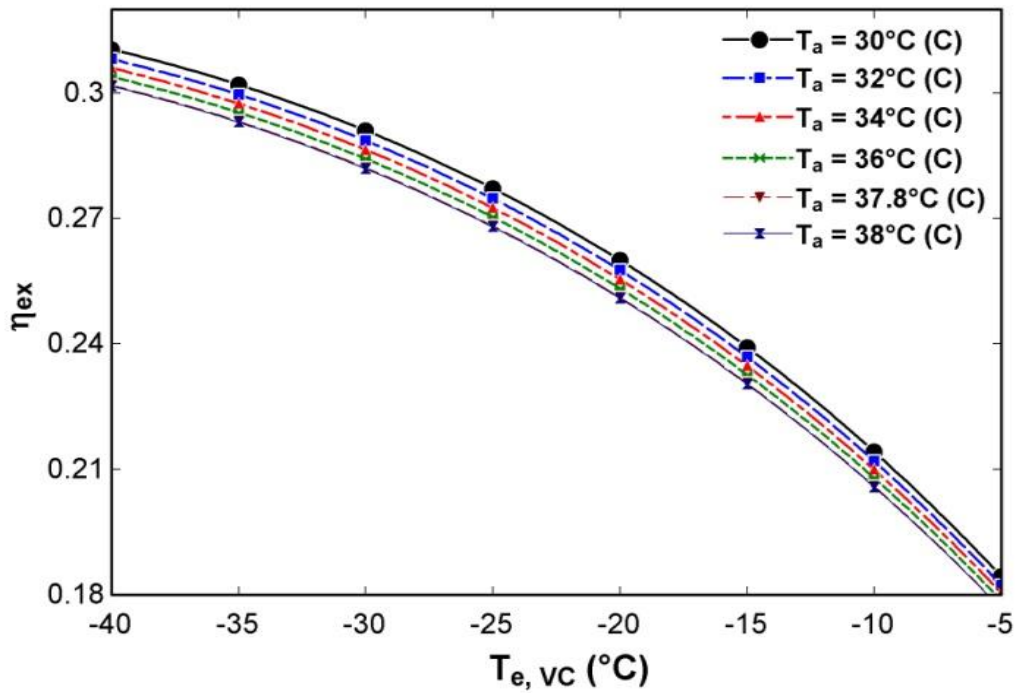


Figure 6.31 Variation in exergetic efficiency (η_{ex}) with evaporator1 temperature ($T_{e, vc}$) (C): Absorption compression cascade refrigeration cycle (ACCRC)

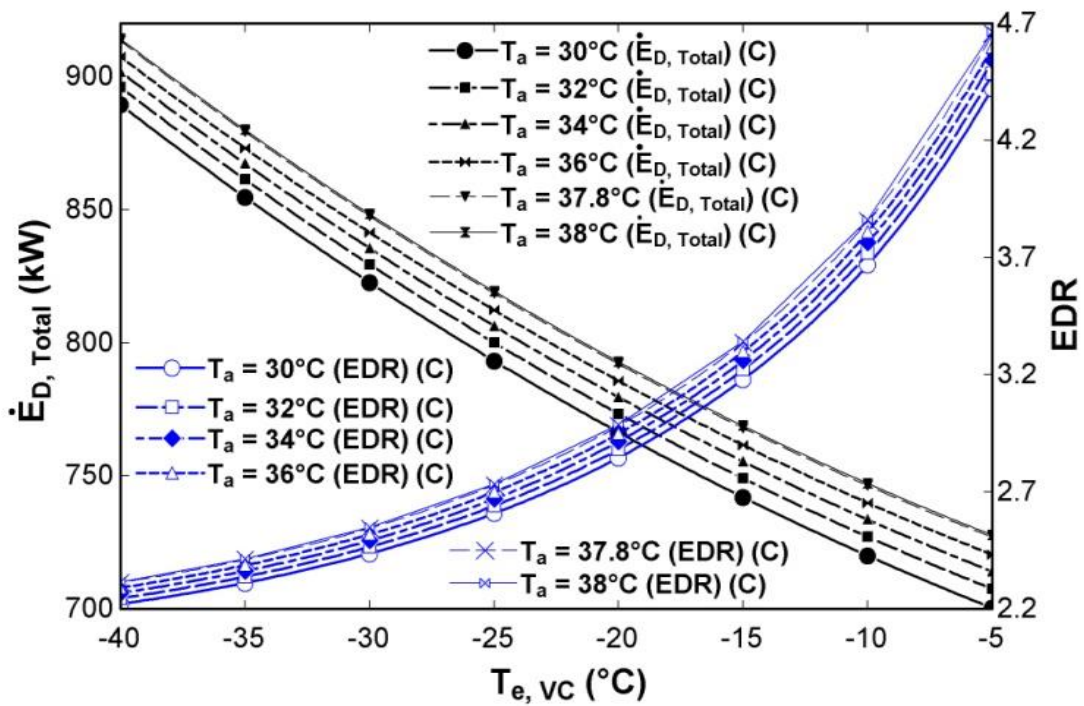


Figure 6.32 Effect of evaporator1 temperature on total exergy destruction rate ($\dot{E}_{D, total}$) and exergy destruction ratio (EDR)

It is observed that for a particular evaporator temperature, the COP of the cascade system decreases with increase in absorber temperature. The higher absorber temperatures are achieved due to higher values of heat input to the generators \dot{Q}_{HPg} & \dot{Q}_{LPg} results decrease in COP. The maximum and minimum values of COP correspond to ($T_{e, VC} = -5^{\circ}\text{C}$, $T_{a, H} = T_{a, L} = T_{cond, VA} = 30^{\circ}\text{C}$) and ($T_{e, VC} = -40^{\circ}\text{C}$, $T_{a, H} = T_{a, L} = T_{cond, VA} = 38^{\circ}\text{C}$) are 0.3903 and 0.278.

Fig. 6.31 illustrates the effect of evaporator1 temperature ($T_{e, VC}$) on exergetic efficiency (η_{ex}) for different absorber temperatures. The value of η_{ex} decreases with increase in evaporator1 temperature. The exergetic efficiency of ACCR system is the ratio of $\dot{Q}_{e, VC} \left| \left(1 - \frac{T_0}{T_b} \right) \right|$ and $\left\{ \dot{Q}_{HPg} \left| \left(1 - \frac{T_0}{T_{HPg}} \right) \right| + \dot{Q}_{LPg} \left| \left(1 - \frac{T_0}{T_{LPg}} \right) \right| + \dot{W}_{P, H} + \dot{W}_{P, L} + \dot{W}_c \right\}$ (Eq. 6.19) in which the values of $\dot{Q}_{e, VC}$ and $\left| \left(1 - \frac{T_0}{T_b} \right) \right|$ decrease with increase in evaporator1 temperature as $T_b = \Delta T + T_{e, VC}$ and $T_0 > T_b$. The value of $\dot{Q}_{HPg} \left| \left(1 - \frac{T_0}{T_{HPg}} \right) \right|$ remains constant with the variation in $T_{e, VC}$. The HP & LP pump work are negligible and the value of \dot{W}_c decreases with increase in $T_{e, VC}$. Thus, the value η_{ex} decreases with increase in $T_{e, VC}$.

It is observed that the value of η_{ex} decreases with increase in absorber temperature at a specific evaporator1 temperature. The value of SCR increases with increase in absorber temperature ($T_{a, L}$, $T_{a, H}$) (Fig. 6.26) by which the value of \dot{m}_s increases as $SCR = \frac{\dot{m}_s}{\dot{m}_{r, VA}}$ and the \dot{Q}_{HPg} and \dot{Q}_{LPg} get enhanced. However the terms \dot{W}_c , $\left| \left(1 - \frac{T_0}{T_b} \right) \right|$, $\left| \left(1 - \frac{T_0}{T_{HPg}} \right) \right|$ and $\left| \left(1 - \frac{T_0}{T_{LPg}} \right) \right|$ do not vary and the value of $\dot{Q}_{e, VC}$ decreases slightly with increase in $T_{a, L}$, $T_{a, H}$. Hence, η_{ex} decrease with increase in absorber temperature. The maximum and minimum values of η_{ex} correspond to ($T_{e, VC} = -40^{\circ}\text{C}$, $T_{a, H} = T_{a, L} = T_{cond, VA} = 30^{\circ}\text{C}$) and ($T_{e, VC} = -5^{\circ}\text{C}$, $T_{a, H} = T_{a, L} = T_{cond, VA} = 38^{\circ}\text{C}$) are 0.3104 and 0.1766.

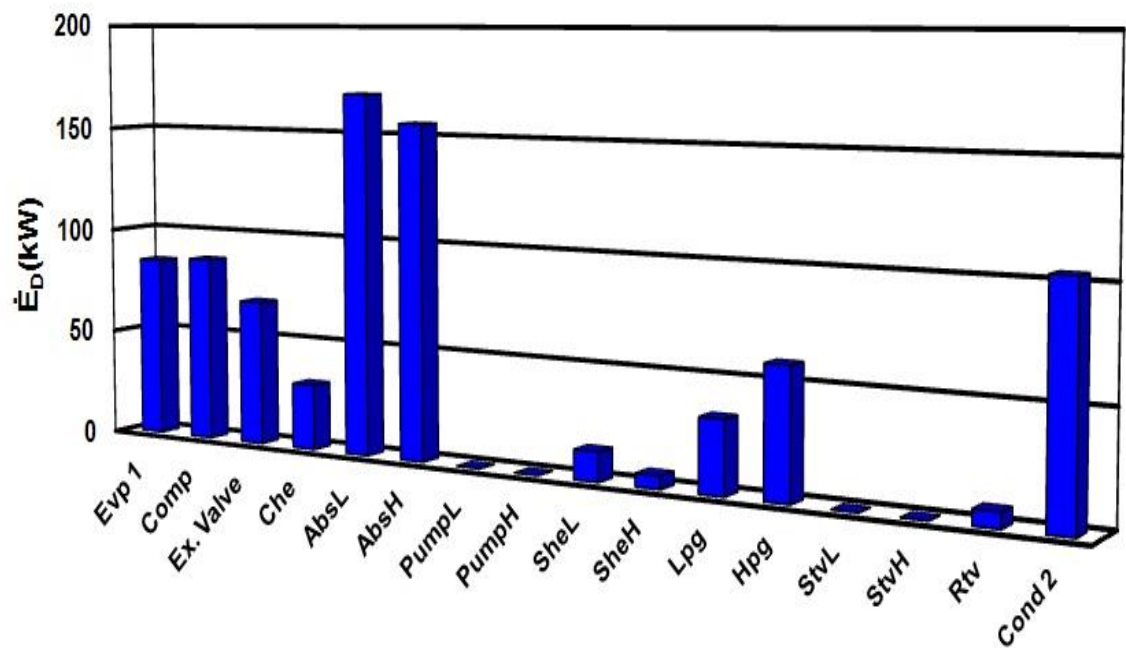
Fig. 6.32 illustrates variation in total exergy destruction rate ($\dot{E}_{D, total}$) and exergy destruction ratio (EDR) with evaporator1 temperature ($T_{e, VC}$). The $\dot{E}_{D, total}$ decreases and the EDR increases with increase in $T_{e, VC}$. As the value of $T_{e, VC}$ increases and approaches to ambient temperature T_0 , the exergy destruction in system component decreases. According to Eq. (6.18), $\dot{E}_{D, total}$ is proportional to the exergy destruction in each system component which results the decrease in $\dot{E}_{D, total}$ with increase in $T_{e, VC}$. The EDR is

given by Eq. (6.20), which is the ratio of $\dot{E}_{D, total}$ and $\dot{Q}_{e, VC} \left| \left(1 - \frac{T_0}{T_b} \right) \right|$. Fig. 6.31 shows that the exergy of products i.e $\dot{Q}_{e, VC} \left| \left(1 - \frac{T_0}{T_b} \right) \right|$ decreases with increase in $T_{e, VC}$. However, the decrease in $\dot{E}_{D, total}$ is more than the exergy of products. Hence the EDR increases with increase in evaporator temperature.

It is observed that for a particular value of $T_{e, VC}$, The value of $\dot{E}_{D, total}$ and EDR increases with increase in absorber temperature ($T_{a, H}$ & $T_{a, L}$). It is due to the fact that at higher temperature, the exergy destruction rate is higher.

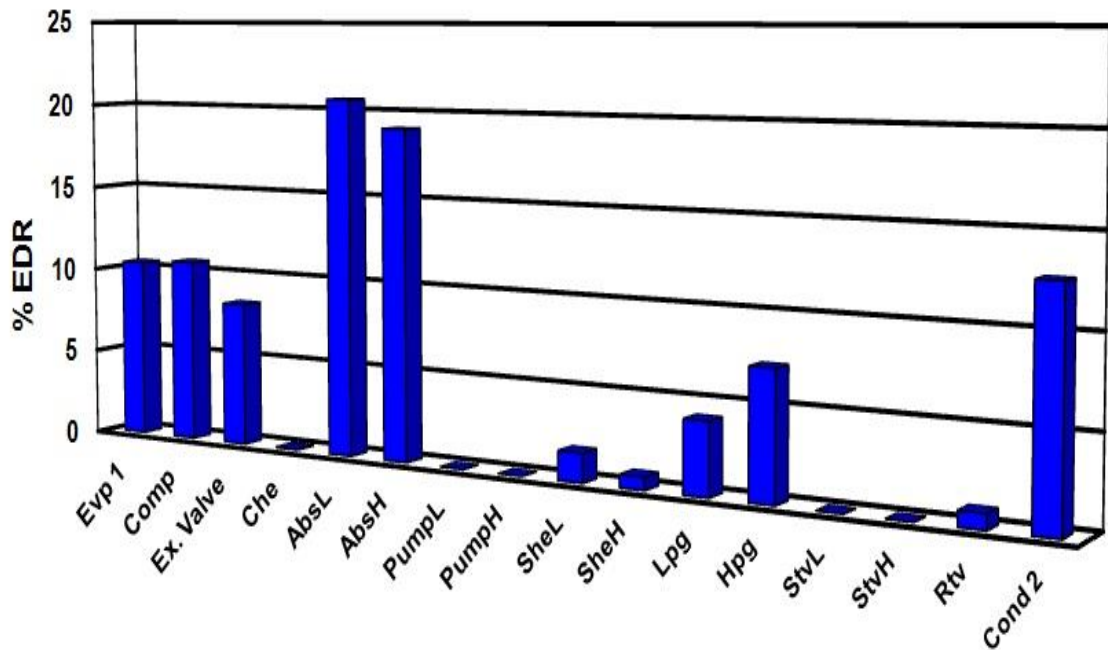
The minimum and maximum values of $\dot{E}_{D, total}$ correspond to ($T_{e, VC} = -5^{\circ}\text{C}$, $T_{a, H} = T_{a, L} = T_{cond, VA} = 30^{\circ}\text{C}$) and ($T_{e, VC} = -40^{\circ}\text{C}$, $T_{a, H} = T_{a, L} = T_{cond, VA} = 38^{\circ}\text{C}$) are 700.3 and 914.3. Similarly, for EDR correspond to ($T_{e, VC} = -40^{\circ}\text{C}$, $T_{a, H} = T_{a, L} = T_{cond, VA} = 30^{\circ}\text{C}$) and ($T_{e, VC} = -5^{\circ}\text{C}$, $T_{a, H} = T_{a, L} = T_{cond, VA} = 38^{\circ}\text{C}$) are 2.221 and 4.663.

6.13.3.3 Exergy destruction rate and EDR of system components



Components of half effect H₂O/LiBr absorption compression cascade refrigeration cycle

Figure 6.33 Exergy destruction rate (\dot{E}_D) of system components of ACCRS



Components of half effect H₂O/LiBr absorption compression cascade refrigeration cycle

Figure 6.34 Exergy destruction ratio (EDR) of system components of ACCRS

Fig. 6.33 and 6.34 depict the exergy destruction rate (\dot{E}_D) and EDR of system components. The LP absorber is the place where maximum amount of exergy destruction takes place than the other system components. The EDR for the LP absorber is more than 20%. Similarly, HP absorber, condenser2, evaporator1, compressor, expansion valve, HP, LP generators and cascade heat exchanger are the components in which considerable exergy destruction and EDR take place. HP pump is the system component with zero exergy destruction. The values of \dot{E}_D and EDR for LP pump, HP and LP solution heat exchanger are small and in increasing order.

6.14 CONCLUSIONS

Energy and exergy analysis have been presented to predict the performance of ACCRS using theoretical concepts of thermodynamics. In the present work, a half effect series flow H₂O-LiBr VAR cycle is coupled to the VCR cycle using refrigerant R1234yf through the cascade heat exchanger by the first time. The system has its utilities in low evaporation temperature ranging from semiconductor cooling, chemical separation to medical diagnostic. The feature to recover waste heat and utilization of renewable energy

source i.e. Solar makes it energy efficient and cost effective. Moreover, the use of refrigerant R1234yf in VCRS predicts eco-friendliness of the system. The effect of various operating parameters has been seen. A computer program has been formulated to investigate the different performance parameters viz. COP, exergetic efficiency (η_{ex}), total exergy destruction rate ($\dot{E}_{D, Total}$) and exergy destruction ratio (EDR) of the system. Component wise analysis has also been done to check the performance (i.e. exergy destruction rate and %EDR) of each component. A considerable range of parameters has been assumed viz. HP generator temperature (60-85⁰C), absorber temperature (30-38⁰C) and evaporator temperature (-40 to -5⁰C). The concluding remarks of the present communication are summarised below:

- The electricity consumption of half effect cascade refrigeration system (ACCRS) is reduced by 54.29 % as compared to VCRS. Moreover the COP of the vapour compression circuit gets increased by 118.7% due to low electric power consumption. However, while compared to compression-absorption single and double effect cascade refrigeration systems, the COP of half effect cascade system is observed lowest.
- In addition, the recovery of low temperature waste heat or use of renewable source of heat in Hpg and Lpg reduces the system running cost as the waste heat is available at low cost and renewable energy is free of cost. However, the overall size of the system increases.
- The enhancement in the exergetic efficiency of VCR circuit of ACCRS is 118.74% and the reduction in total exergy destruction is 80.66%. It is also established that the exergetic efficiency of half effect cascade system is lowest in comparison to single and double effect cascade refrigeration systems.
- The larger value of approach in the cascade heat exchanger reduces the COP and exergetic efficiency of the system.
- The increase in HP, LP generator temperature first increases slightly and then decreases the COP of the system at absorber temperature 37.8⁰C and 38⁰C because of solution circulation ratio decreases. The optimum value of HP, LP generator temperature observed lies within 65-75⁰C. The exergetic efficiency of the system decreases however, the total exergy destruction and exergy destruction ratio (EDR) increase.

- The energetic (COP) and exergetic (η_{ex}) performance of the system decline with increase in absorber temperature due to increase in solution circulation ratio (SCR). The exergy destruction and exergy destruction ratio (EDR) register increment.
- The system COP increases and exergetic efficiency decrease with increase in evaporator1 temperature for a range of LP, HP absorber temperature. Similarly, the exergy destruction (EDR) ratio increases and the total exergy destruction of the system decreases.
- The HP and LP solution pump are the site of zero exergy destruction while LP absorber is the main component in which the exergy destruction is highest in comparison to other system components. After solution pump,) HP and LP solution throttle valves recover the major part of exergy.
- The use of R1234yf in low temperature VCR circuit of ACCRS establishes an eco-loving agreement.

In the light of above conclusions, it is inferred that the absorption compression (half effect series flow) cascade system (ACCRS) is performing best among the systems considered. The electricity saver, cost effectiveness and eco-friendship are the attracting features of the system associated to fulfil need of low cooling applications. However, the larger size of the system is a manageable task.

6.15 PERFORMANCE COMPARISON OF COMPRESSION-ABSORPTION TRIPLE, DOUBLE, SINGLE AND HALF EFFECT (H₂O-LiBr) CASCADE REFRIGERATION SYSTEMS

Table 6.11 shows the energy and exergy performance comparison of absorption-compression (triple, double, single and half effect) cascade refrigeration systems. It also includes the performance comparison of triple, double, single and half effect vapour absorption refrigeration systems and vapour compression refrigeration cycle.

It has been observed that the COP and exergetic efficiency of single effect ACCRS are highest while for half effect ACCRS are lowest. The total exergy destruction is lowest for single effect ACCRS and highest for half effect ACCRS.

In the case of VAR system, the COP is highest for triple effect and lowest for half effect while exergetic efficiency is highest for double effect and lowest for half effect VAR system.

Table 6.11 Thermodynamic performance comparison of absorption-compression cascade, absorption and compression refrigeration cycles

Performance Parameters		Cascade				
		Triple effect series flow (H ₂ O-LiBr) absorption-compression (R1234yf) (ACCRS)	Double effect series flow (H ₂ O-LiBr) absorption-compression (R134a) (Colorado and Rivera, 2015)	Single effect (H ₂ O-LiBr) absorption-compression (R134a) (Colorado and Rivera, 2015)		Half effect (H ₂ O-LiBr) absorption-compression (R1234yf) (ACCRS)
(°C)	T _e	-40	-10	-10	-10	-25
	T _g	185	120	69	87.8	67
	T _a =T _c	37.8	35	-	37.8	37.8
(kg/s)	$\dot{m}_{r,VAR}$	1	0.025	-	25	1
(kW)	$\dot{Q}_{e,ACCR}$	1746	50	50	2149	1936
	$\dot{Q}_{e,VAR}$	2355.45	-	-	2355	2355
	$\dot{Q}_{e,VCRS}$	1746	-	-	2149	1936
	\dot{W}_P	2.26	-	-	0.03143	0.03061
	\dot{W}_C	609.2	9.10	9.10	206.1	419.2
Dimensionless	COP _{ACCRS}	0.7843	0.91	0.58	1.371	0.3183
	COP _{VAR}	1.456	1.29	0.78	0.7644	0.415875
	COP _{VCRS}	2.866	5.49	5.49	10.43	4.617
Dimensionless	$\eta_{ex, ACCRS}$	33.6%	28%	25.5%	35.49%	26.82%
	$\eta_{ex, VAR}$	11.17%	-	-	11.74%	9.286%
	$\eta_{ex, VCRS}$	64.83%	-	-	-	71.55%
(kW)	$\dot{E}_{D, total, ACCRS}$	780.5	-	-	474.3	818.5
	$\dot{E}_{D, total, VAR}$	566.3	-	-	-	634.3
	$\dot{E}_{D, total, VCRS}$	214.3	-	-	-	119.3
Performance Parameters		VAR				VCRS
		Triple effect series flow H ₂ O-LiBr (Arora et al., 2015)	Double effect series flow H ₂ O/LiBr (Kaushik and	Single effect H ₂ O-LiBr (Kaushik and Arora, 2009)	Half effect H ₂ O/LiBr (Arora, 2009)	R1234yf

		Arora, 2009)				
(°C)	T_e	7.2	7.2	7.2	7	-40
	T_g	185	140.6	87.8	65	-
	$T_a = T_c$	37.8	37.8	37.8	37.8	37.8
(kg/s)	\dot{m}_r	1	1	1	1	18.73
(kW)	$\dot{Q}_{e, VARS}$	2355.45	2355.45	2355.45	-	-
	$\dot{Q}_{e, VCRS}$	-	-	-	-	1746
	\dot{W}_P	2.26	0.3598	0.03143	-	-
	\dot{W}_C	-	-	-	-	1129
Dimensi onless	COP_{VARS}	1.456	1.26	0.7609	0.41	-
	COP_{VCRS}	-	-	-	-	1.547
Dimensi onless	$\eta_{ex, VARS}$	11.17%	12.3%	11.75%	9.5%	-
	$\eta_{ex, VCRS}$	-	-	-	-	34.99
(kW)	$\dot{E}_{D, total, VARS}$	502.98	277.284	250.967	-	-
	$\dot{E}_{D, total, VCRS}$	-	-	-	-	733.8

THE THERMODYNAMIC PERFORMANCE ANALYSIS OF TRIGENERATION SYSTEM (POWER, HEAT AND REFRIGERATION) FOR PERFORMANCE IMPROVEMENT USING RETROFITTED TECHNIQUES AND ALTERNATE REFRIGERANTS

7.1 INTRODUCTION:

The gas turbine based power plants contain a large amount of heat in the flue gases at high temperature. The waste heat available can be utilized to generate superheated steam to produce heating effect or it can be used in the steam turbine to produce electricity. A part of steam can also be utilized to improve the performance of the gas turbine power plant through retrofitted techniques. The waste heat after producing steam exits the heat recovery steam generator at the temperature higher than that of acid dew point temperature and can be further utilized to produce refrigeration through cascade refrigeration cycle. The purpose of the waste heat recovery is to reduce the cost and carbon emission. Simultaneously, power, heat and refrigeration can also be produced.

The present work describes the performance improvement of vapour compression absorption cascade refrigeration cycle powered by a small or mini gas turbine. The waste heat available in the flue gases of mini gas turbine is sufficient to run the low cooling capacity cascade refrigeration cycle for domestic purpose. In this way, the mini gas turbine generate power and hence electricity as well as refrigeration and air-condition. The electricity generated can run the compressor of the vapour compression cycle when the need of air-conditioning arises. These systems are very useful especially in remote areas.

Thermodynamic analysis of a tri-generation system (power, heat and refrigeration) for performance improvement using retrofitted techniques and alternative refrigerants (R1234yf and R1234ze) has also been carried out. The system comprises a gas turbine cycle, a steam turbine cycle, heat recovery steam generator (HRSG) and a cascade refrigeration cycle. The retrofitted techniques viz. inlet air cooling (IAC) and steam injection to gas turbine (STIG) have been considered to enhance the performance of gas turbine cycle. Various performance parameters viz. thermal efficiency, exergetic efficiency, COP, Overall cycle efficiency, exergy destruction rate and exergy

destruction ratio have been computed and the effect of ambient temperature and relative humidity have been observed on performance parameters. It has been observed that the retrofitted techniques improve the power output and exergetic efficiency of the gas turbine cycle. The waste heat recovered from the exhaust gases has been utilized in heat and refrigeration production.

7.2 DESCRIPTION OF VAPOUR COMPRESSION-ABSORPTION (H₂O-LiBr) CASCADE REFRIGERATION SYSTEM POWERED BYA MICRO-GAS TURBINE

The coupling of vapour compression and absorption refrigeration system can be powered by a small or mini or micro-gas turbine. The vapour absorption cycle is a single effect H₂O-LiBr cycle and the vapour compressor cycle uses R1234yf as refrigerant.

The evaporator of vapour absorption refrigeration system is coupled to the condenser of vapour compression refrigeration system. The coupling of two is designated as cascade heat exchanger. The heat rejected from the condenser of VCR cycle is taken by the evaporator of VAR cycle. The waste heat of micro-gas turbine has been utilized in the generator of the vapour absorption refrigeration system. The VAR system is a single effect water-lithium bromide vapour absorption refrigeration system.

The power is generated in the micro-gas turbine which can be used for electricity generation in remote area for domestic purpose. Simultaneously, waste heat is available for water heating in winters or the waste heat can be utilized for refrigeration or air-conditioning purpose through absorption-compression cascade refrigeration system (ACCRS)

The working of the system includes the ACCRS which has been described in detail in chapter 6. The micro-gas turbine is a natural gas based turbine which produces electricity and the produced electricity is used to run the compressor and pump of cascade refrigeration cycle. The rest of the electricity can be used for small domestic purposes such as lighting the electric LED bulb, to run the television, fan, mobile charging etc. Simultaneously, the waste heat of the MGT present in the flue gases can be used for heating purpose or refrigeration and air-conditioning purposes.

The micro-gas turbine is a Brayton cycle based turbo-generator which is compacted, small in size and high speed having power generation capacity of 30 to 200 kW. The electrical efficiency of the micro-gas turbine depends on its size ranging from 25 to 30% (Bruno et al., 2005).

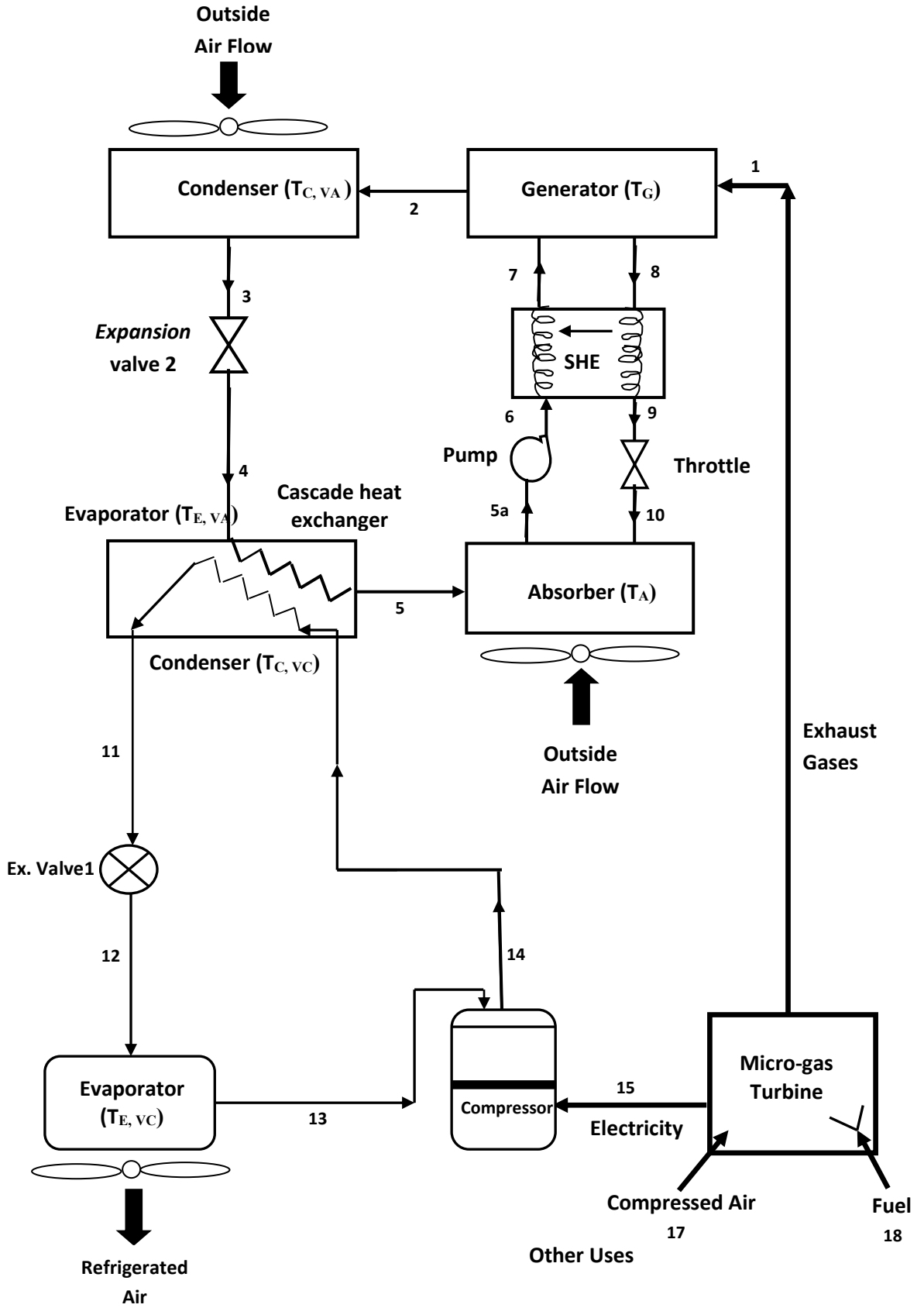


Fig. 7.1 Schematic diagram of micro-gas turbine based cascade refrigeration system

7.3 MATHEMATICAL FORMULATION

7.3.1 Assumptions

In order to model complex thermodynamic analysis of absorption (H₂O-LiBr single effect) -compression (R1234yf, R1234ze) cascade vapour refrigeration system energized by micro gas turbine, following assumptions have been considered except where variation of parameters involved.

- The state of refrigerant is dry and saturated at the entry of compressor at (state point 1).
- The state of refrigerant at the exit of condenser of VCR cycle is saturated subcooled liquid at state point 3.
- Subcooling of liquid refrigerant occurs from state point 3-3a.
- The expansion or throttling in the expansion valve, solution throttle valve and refrigerant throttle valve is isoenthalpic.
- Difference between the temperature of space to be cooled and temperature of evaporator 1 ($\Delta T = T_b - T_{eVC}$) is 10⁰C.
- The approach temperature or overlap temperature between evaporator 2 and condenser 1 in the cascade heat exchanger ($T_{ov} = T_{cVC} - T_{eVA}$) is 5⁰C.
- Isentropic efficiency of compressor (η_c) is 80%.
- The heat losses and pressure losses from the system and system components are negligible. The whole system operates in steady state condition.
- The reference values of entropy (s_0) and enthalpy (h_0) are considered at ambient or dead state conditions ($T_0 = 25^0\text{C}$, $P_0 = 101.325\text{kPa}$).
- The refrigerant vapour leaving the generator is superheated vapour at the generator temperature.
- Heat exchanger effectiveness is 0.7.
- The efficiency of micro gas turbine is formulated by relation: $\eta_{MGT} = 30.08 - (0.12 \times T_{Amb.})$. Where $T_{Amb.}$ is the ambient temperature.
- Waste heat of exhasut gases of micro gas turbine is given by the relation: $Q_{waste\ heat} = 667 - (667 \times \eta_{MGT}/100)$.
- The heat losses in the components have been considered negligible.
- The total amount of heat is supplied to the generator of cascade system.
- The electricity is supplied to the compressor of cascade system by the micro gas turbine.

The COP of vapour compression absorption cascade refrigeration system defined as:
$$\text{COP} = \frac{\dot{Q}_e}{\dot{W}_{\text{comp}} + \dot{W}_{\text{fan}} + \dot{W}_{\text{pump}}} \quad (7.1)$$

Where \dot{Q}_e is the net refrigeration effect produced, \dot{W}_{comp} is the actual work of the compressor, \dot{W}_{fan} is the amount of electricity provided to the fans and \dot{W}_{pump} is the pump work absorption refrigeration cycle.

The thermal efficiency of micro-gas turbine is the ratio of net power output to the heat energy supplied by the fuel to the turbine given by eq. (7.2).

$$\eta_{\text{Th}} = \frac{\dot{W}_{\text{MGT}}}{\dot{Q}_f} \quad (7.2)$$

Where \dot{W}_{MGT} is the power output and \dot{Q}_f is the amount of heat energy supplied to the micro-gas turbine by the fuel in kW.

The exergy efficiency of thermal system is defined as the ratio of net output energy available to the input energy.

$$\eta_{\text{ex}} = \frac{\sum \dot{E}_{\text{out}}}{\sum \dot{E}_{\text{in}}} = 1 - \frac{\sum \dot{E}_{\text{D}}}{\sum \dot{E}_{\text{in}}} \quad (7.3)$$

Where η_{ex} is the exergetic efficiency of the cycle. $\sum \dot{E}_{\text{out}}$, $\sum \dot{E}_{\text{in}}$ and $\sum \dot{E}_{\text{D}}$ are the total exergy recovered, supplied and destructed respectively.

The exergetic efficiency is the ratio of exergy in products to the exergy of fuel. The exergetic efficiency of vapour compression absorption cascade refrigeration system is defined as the ratio of the exergy of heat absorbed in the evaporator from the space to be cooled at temperature T_b to the actual compressor, fan and pump work input ($\dot{W}_{\text{comp}} + \dot{W}_{\text{fan}} + \dot{W}_{\text{pump}}$).

$$\eta_{\text{ex}} = \frac{\left| \dot{Q}_e \left(1 - \frac{T_0}{T_b} \right) \right|}{\dot{W}_{\text{comp}} + \dot{W}_{\text{fan}} + \dot{W}_{\text{pump}}} \quad (7.4)$$

$$\eta_{\text{ex}} = \text{COP} \times \left| \left(1 - \frac{T_0}{T_b} \right) \right| \quad (7.5)$$

where T_0 is the ambient or dead state temperature.

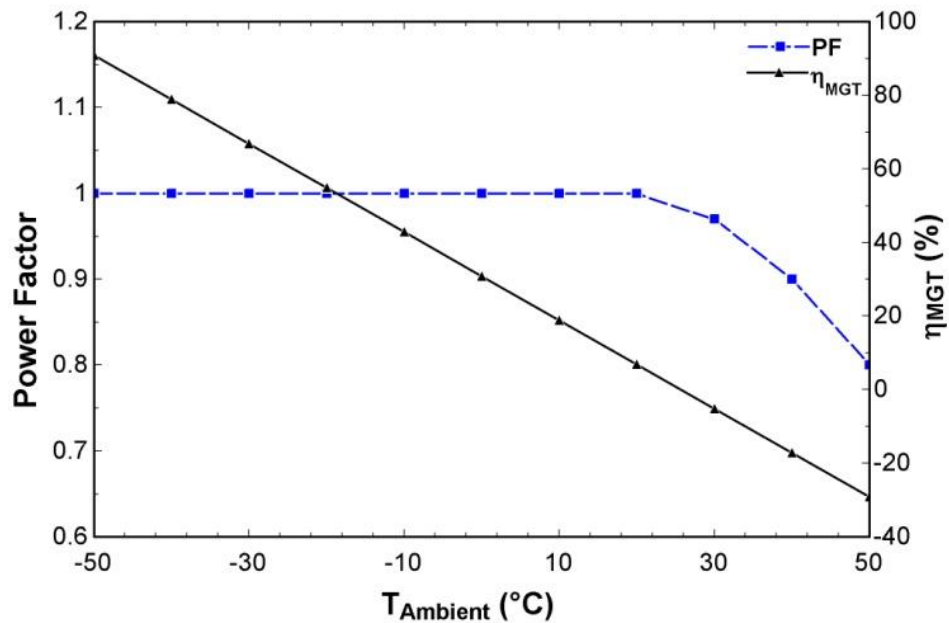


Fig. 7.2 Effect of ambient temperature on performance of micro-gas turbine (Hwang, 2004)

Fig. 7.2 shows the effect of ambient temperature on power factor and thermal efficiency of micro-gas turbine. The thermal efficiency of gas turbine, which is a micro type and given by the eq. 7.3 shows decrement with increase in ambient air temperature, however, the power factor remains constant up to 25°C and afterward decreases with increase in ambient temperature. The net power output of the gas turbine decreases with increase in ambient temperature. The power factor and thermal efficiency decide the performance of micro-gas turbine. The optimum condition can be obtained for the ambient temperature.

7.4 RESULTS AND DISCUSSION

Energy and exergy analysis of vapour compression absorption cascade refrigeration system has been carried out in the present work. A computational investigation has been done in Engineering Equation Solver (EES). Control volume approach has been assumed to frame the steady state governing equations for the each component of the system. The effect of various operating parameters viz. ambient

temperature, generator temperature and temperature of refrigerated air has been observed on COP and exergetic efficiency of cascade refrigeration system.

7.4.1 Effect of Ambient temperature

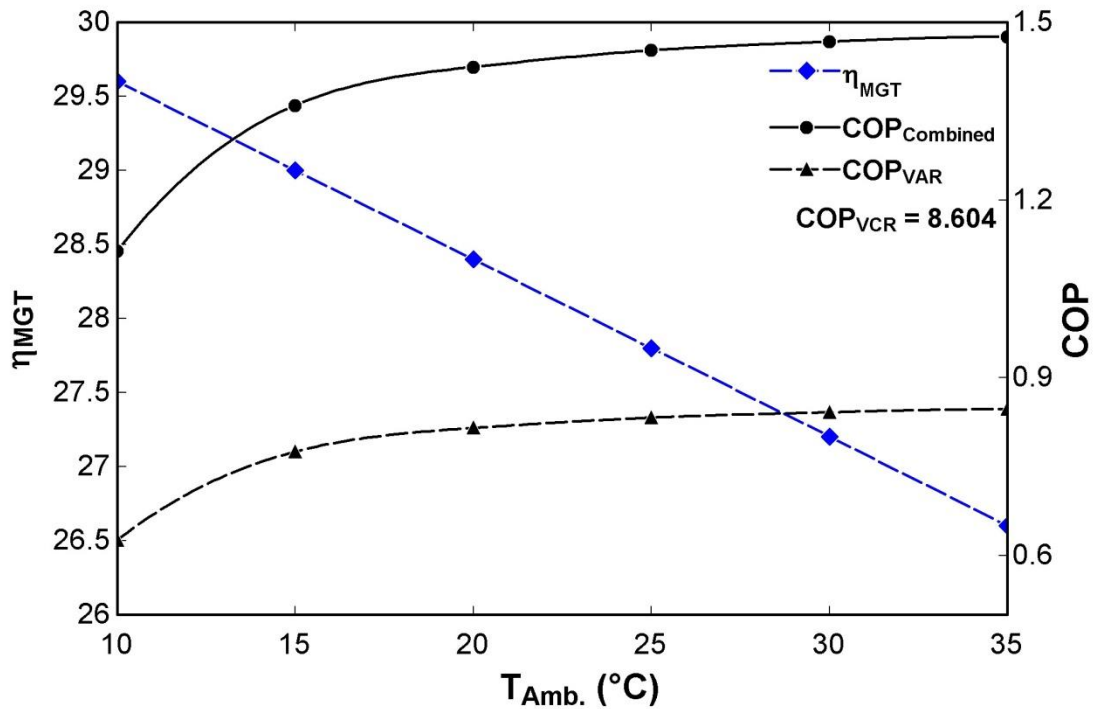


Fig. 7.3 Effect of ambient temperature on thermal efficiency of micro-gas turbine ($\eta_{ThermalMGT}$) and COP of the cascade refrigeration cycle

The variation in thermal efficiency of gas turbine (micro) and COP of the vapour compression absorption cascade refrigeration cycle has been shown in Fig. 7.3. As the temperature of ambient increases, the thermal efficiency of the gas turbine decreases (refer to Fig. 7.2). The net power output of the turbine decreases with increase in ambient temperature. The exhaust gases from turbine are at higher temperature and provides more heat to the generator of the vapour absorption cycle. However, the condenser temperature also increases with increase in ambient temperature. Thus the net refrigeration effect in the evaporator of vapour absorption refrigeration cycle increases and producing more cascading in the cascade heat exchangers. Consequently, the refrigeration effect in the evaporator of vapour compression refrigeration cycle enhances and hence the COP of cascade refrigeration cycle increases.

Moreover, the COP of cascade refrigeration system improves with increase in ambient temperature. Contrary, the COP of cascade refrigeration cycle and compression refrigeration cycle decreases with increase in ambient temperature due to more consumption of electricity in order to cool the outside air.

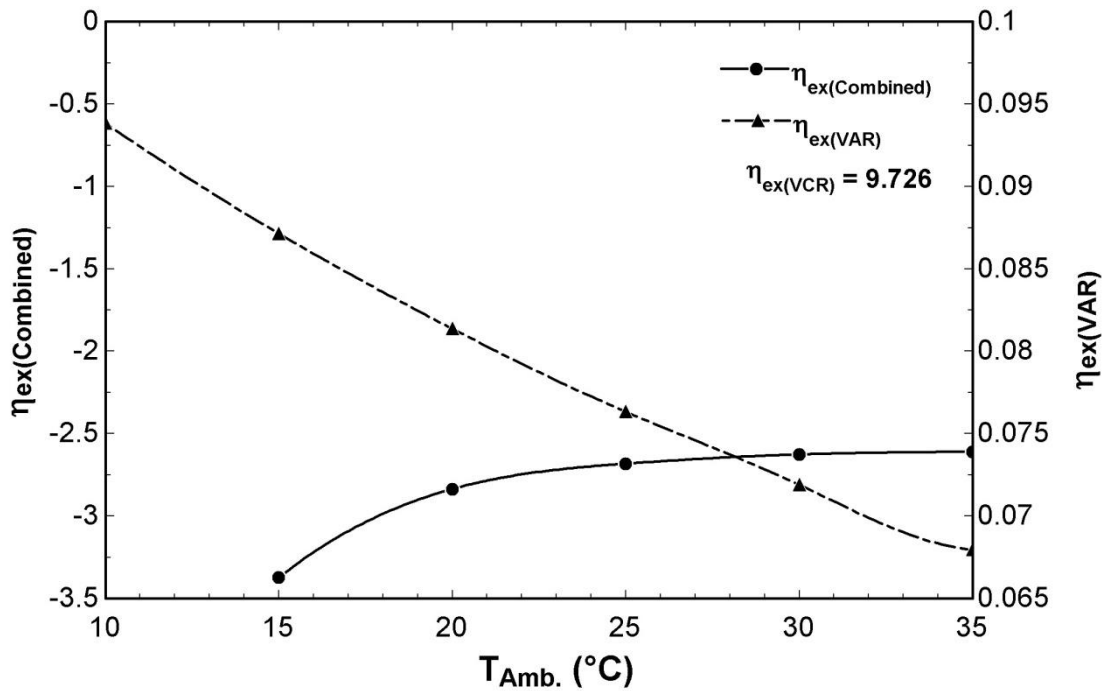


Fig. 7.4 Variation in exergetic efficiency of the cascade refrigeration cycle with ambient temperature

The variation in exergetic efficiency of vapour compression absorption cascade refrigeration system with increase in ambient temperature has been shown in Fig. 7.4. The exergetic efficiency of cascade system increases while vapour absorption system decreases with increase in ambient temperature. At high ambient temperature, the exergy recovered by the vapour absorption refrigeration cycle reduces and exergy efficiency of cascade cycle is given by $\eta_{ex} = COP \times \left| \left(1 - \frac{T_0}{T_b} \right) \right|$ in which the COP increases with increase in ambient temperature (refer Fig. 7.3) and the term $\left| \left(1 - \frac{T_0}{T_b} \right) \right|$ also increases with increase in ambient temperature for constant negative value of T_b . Hence the exergetic efficiency of the cascade cycle increase with increase in ambient temperature

7.4.2 Effect of Generator temperature

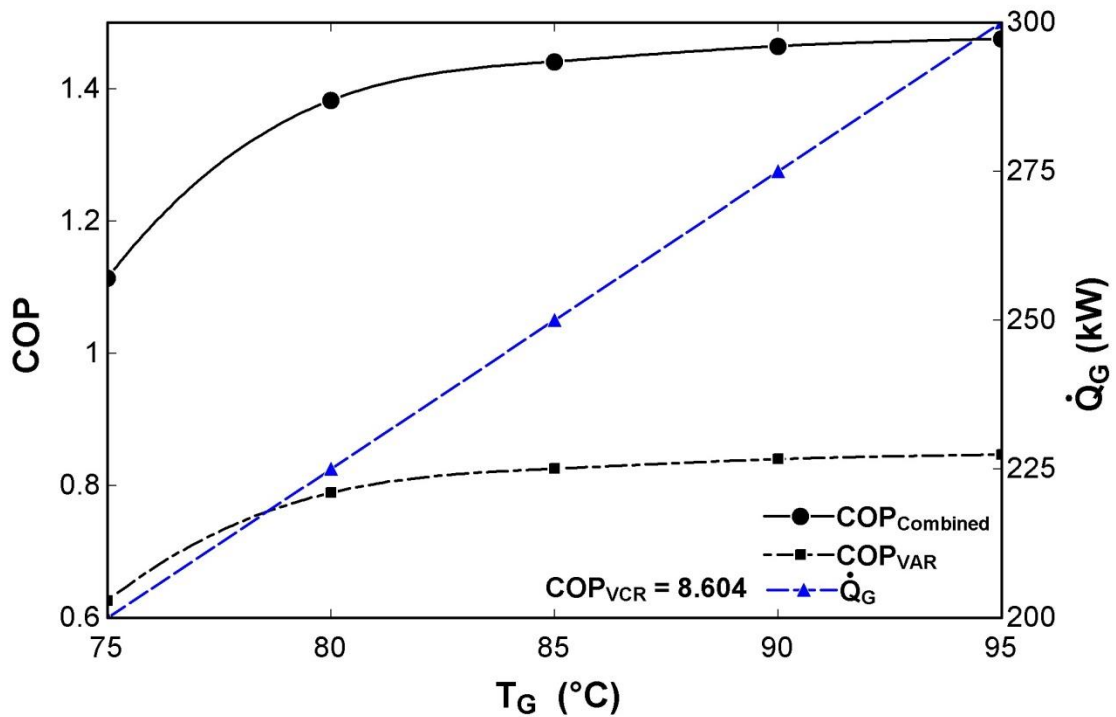


Fig. 7.5 Variation in COP and waste heat with generator temperature

Fig. 7.5 shows variation in COP and heat of generator provided by waste heat of gas turbine (micro) and COP. The process heat available in the flue gases of gas turbine (micro) decreases and the COP of vapour absorption, absorption compression cascade refrigeration system increases. It is established fact that the COP of cascade refrigeration system increase with increase in generator temperature. Hence, available waste heat at higher temperature increases the COP of cascade refrigeration system.

Fig. 7.6 shows the effect of generator temperature on exergetic efficiency of cascade refrigeration cycle. The exergetic efficiency of vapour absorption cycle decreases with increase in generator temperature while the exergetic efficiency of absorption compression cascade refrigeration cycle increases with increase in generator temperature. The exergetic efficiency is the function of COP as given by relation $\eta_{ex} = COP \times \left[\left(1 - \frac{T_0}{T_b} \right) \right]$. The value of COP increases with increase in generator temperature while the term $\left[\left(1 - \frac{T_0}{T_b} \right) \right]$ remains constant. Hence the exergetic efficiency of cascade refrigeration cycle increases with increase in generator temperature.

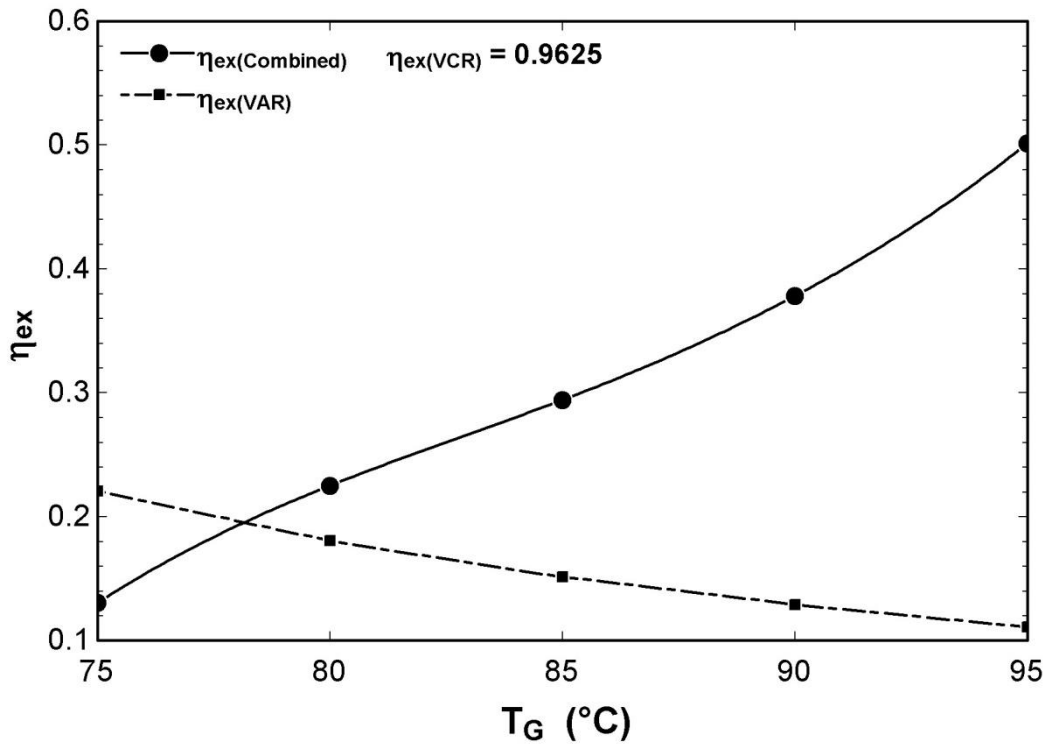


Fig. 7.6 Effect of generator temperature on exergetic efficiency

7.4.3 Effect of Refrigerated air temperature

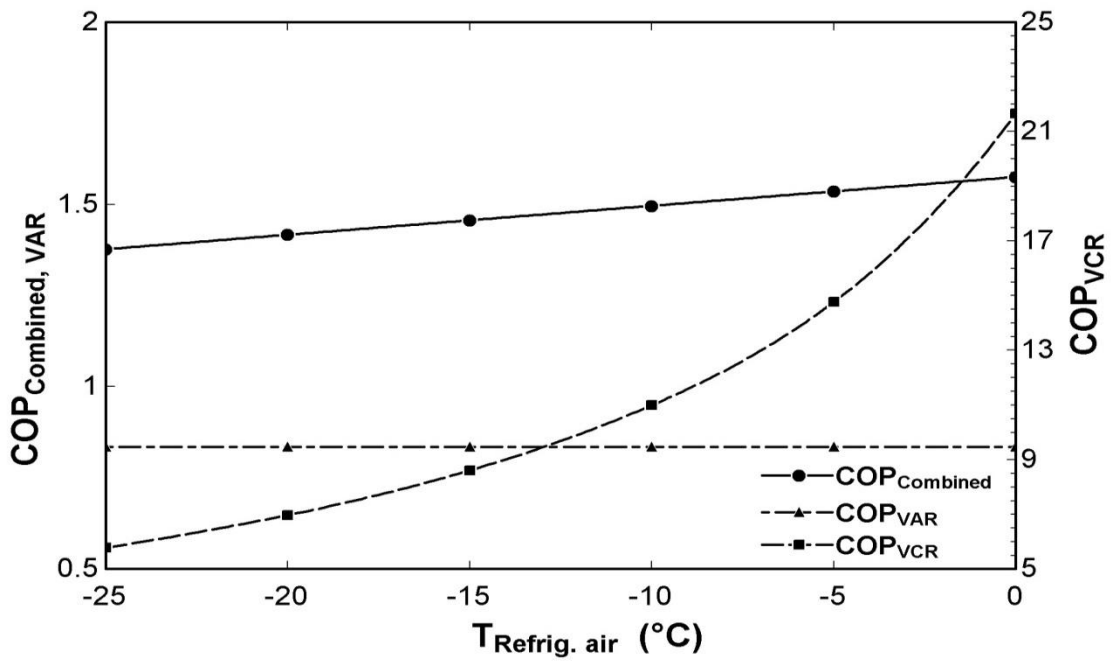


Fig. 7.7 Effect of refrigerated air temperature on COP

Fig. 7.7 shows the effect of refrigerated air temperature on the COP of absorption compression cascade refrigeration system. As the temperature of refrigerated air increases, the COP of vapour compression refrigeration cycle increase and the COP of vapour absorption cycle remains constant, consequently, the COP of absorption compression cascade refrigeration cycle increases with increase in refrigerated air temperature. The compressor work decreases with increase in refrigerated air temperature due to increase in evaporator temperature of vapour compressor cycle.

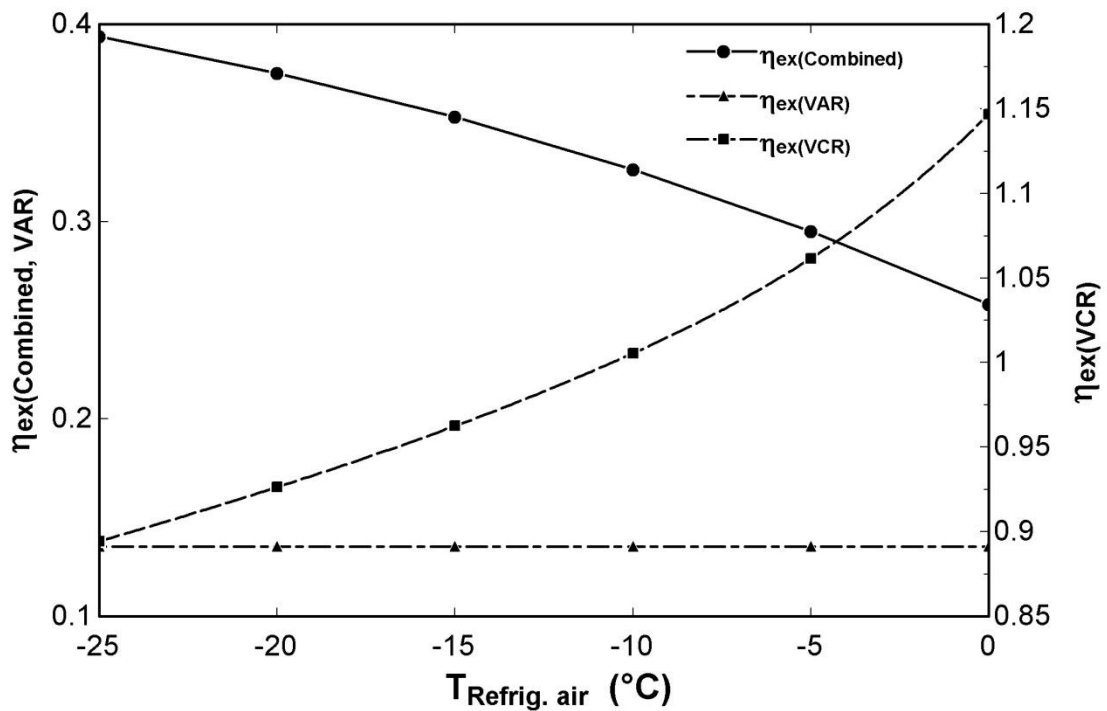


Fig. 7.8 Effect of refrigerated air temperature on exergetic efficiency

Fig. 7.8 shows the effect of refrigerated air temperature on exergetic efficiency of absorption compression cascade refrigeration cycle. The exergetic efficiency of vapour compression refrigeration cycle increases and vapour absorption cycle remains constant with increase in refrigerated air temperature, consequently the exergetic efficiency of absorption compression cascade refrigeration cycle decreases slightly.

7.5 CONCLUSIONS

In the present work, the performance of a compression absorption cascade refrigeration cycle has been explored which is powered by a gas turbine (micro). The vapour absorption cycle receives heat from the flue gases of the turbine while the

vapour compression cycle is electrified by the electricity generated by the turbine. The energy and exergy analysis of the thermal system has been carried out. The main conclusions of the analysis are summarized below:

- The energy (COP) and exergy (exergetic efficiency) performance of the cascade refrigeration cycle powered by gas turbine (micro) is better than that of conventional VCR and VAR cycles.
- Electricity consumption over the conventional vapour compression refrigeration cycle reduces for the constant refrigeration demand.
- The lower electricity consumption reduces the carbon emission as well running cost of the system and the use of R1234yf in the conventional vapour compression refrigeration cycle establishes eco-friendship.
- The use of waste heat improves overall efficiency of the thermal system.
- The proposed system is beneficial in remote areas.

7.6 DESCRIPTION OF A RETROFITTED TRI-GENERATION POWER PLANT

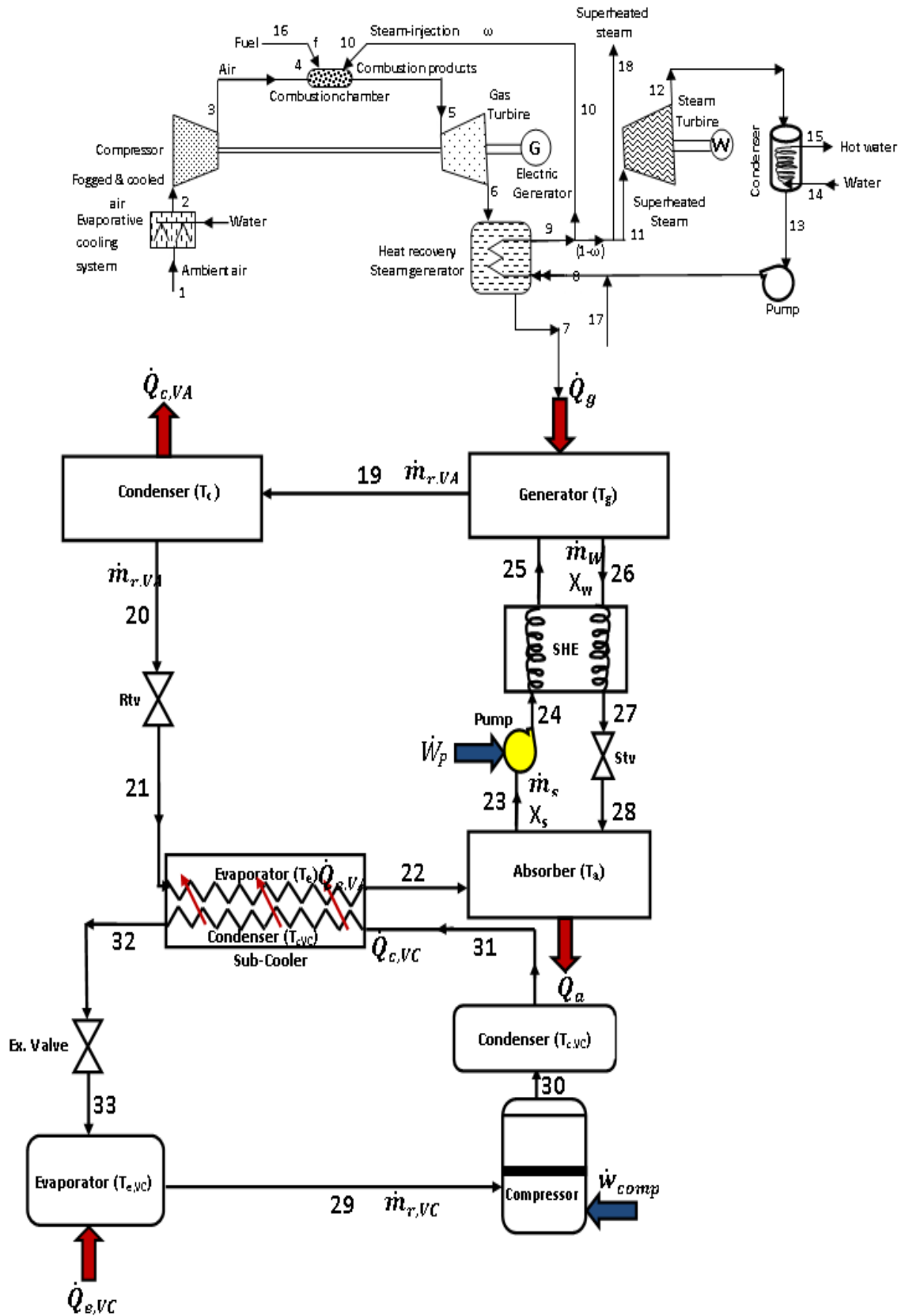


Fig. 7.9 Schematic diagram of a retrofitted tri-generation power system

Fig. 7.9 comprises of a retrofitted gas turbine power plant, a steam turbine based power system, a heat recovery steam generator and an absorption compression cascade refrigeration system. The retrofitted techniques used are evaporative cooling to inlet air of compressor (EVC) and steam injection to gas turbine (STIG). The cascade refrigeration system consists of simple VCR cycle using R1234yf and single effect H₂O/LiBr VAR cycle. The waste heat available in the flue gases of gas turbine is given to heat recovery steam generator. The superheated steam is generated in the HRSG. The fraction ω of the super-heated steam generated in HRSG is fed to the compressor and the $(1 - \omega)$ is available for heat generation or it can be utilized in the steam turbine to produce electricity. The flue gases, exit from the HRSG have the temperature about 140°C (which is below than acid dew point temperature). These flue gases can be utilized in the generator of absorption compression cascade refrigeration system for the production of refrigeration.

The system comprises a gas turbine cycle, a steam turbine cycle, heat recovery steam generator (HRSG) and a cascade refrigeration cycle. The retrofitted techniques viz. steam injection to gas turbine (STIG) and evaporative cooling (EVC) and have been considered to enhance the performance of gas turbine cycle. The injection ratio of the superheated steam varied from 0 to 0.2.

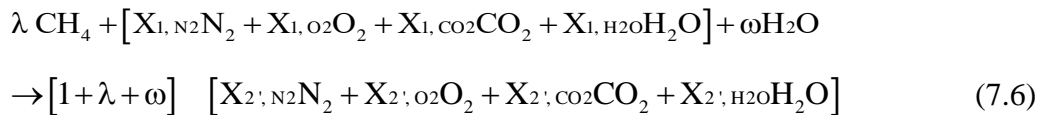
Simple cycle gas turbine system integrated with IAC and STIG features (Fig. 7.9) comprises a base unit that includes compressor, combustor, gas turbine and a generator. An HRSG was installed at downstream exit of turbine (state point 5) to recover heat from exhaust gases. Fraction of superheated steam generated from HRSG is used for STIG (state point 9) and remaining super heated steam is used for process application. An FCS is installed to cool ambient air (state point 1'). FCS uses very fine fog droplets of high pressure water injected through special atomizing nozzles located at discrete points across inlet duct at high pressure to create cooling effect. Amount of fog is to be monitored based on dry and wet bulb ambient conditions to achieve required cooling. A typical FCS consists of a high pressure pump skid connected for feeding to an array of manifolds located at a suitable place across compressor inlet duct. Manifolds have a requisite number of fog nozzles⁶, which inject very fine droplets of water into inlet air. Discharge through each nozzle is around 3 ml/s and produces 3 billion droplets per second. Fine fog evaporates very fast, thus dropping inlet air temperature.

7.7 Modeling of System

Assumptions considered for present study are as follows: i) Molar fraction ($N_2 = 0.78981$, $O_2 = 0.20989$, $CO_2 = 0.00031$ and $H_2O = 0$) is assumed of 1 mole of dry air; ii) Heat loss from combustion chamber is 2% of lower heating value of fuel (All other components operate without heat loss); iii) Fog cooling system has been maintained for 100% saturation of ambient air at wet bulb temperature of air; iv) pressure of water injected from nozzle into evaporative cooling chamber has been assumed 138 bar and converts into fog (fine droplets), absorbs latent heat of air through adiabatic mixing; and v) Combustion chamber has been maintained at constant temperature.

In addition, the assumptions of single effect H₂O-LiBr absorption-compression cascade refrigeration system mentioned in section 7.3.1 have also been considered.

A computer program has been developed in Engineering equations solver (EES) to formulate and simulate retrofitting techniques over simple gas turbine with a set of steady-state governing equations including mass, energy, entropy and exergy balances using control volume analysis sequentially for compressor, combustor, gas turbine and HRSG. Results of program were validated with available data⁶. After successful validation, EES program has been developed for analysis of IAC, STIG and integrated technologies retrofitted with simple gas turbine. For complete combustion of natural gas (methane) with steam injection in combustion chamber, chemical equation takes following form:



$$\text{Mole fraction of } N_2, X_{2,N_2} = \frac{X_{1,N_2}}{1 + \lambda + \omega} \quad (7.7)$$

$$\text{Mole fraction of } O_2, X_{2,O_2} = \frac{X_{1,O_2} - 2\lambda}{1 + \lambda + \omega} \quad (7.8)$$

$$\text{Mole fraction of } CO_2, X_{2,CO_2} = \frac{X_{1,CO_2} + \lambda}{1 + \lambda + \omega} \quad (7.9)$$

$$\text{Mole fraction of } H_2O, X_{2,H_2O} = \frac{X_{1,H_2O} + 2\lambda + \omega}{1 + \lambda + \omega} \quad (7.10)$$

where ω is steam injection ratio defined as ratio of mass of steam injected to mass of air supplied.

$$\omega = \dot{m}_s / \dot{m}_a, \quad \omega' = \dot{m}_s / \dot{m}_g, \quad \omega' = \omega / (1 + \lambda), \quad \omega'' = \frac{\dot{m}_s}{\dot{m}_f}, \quad \omega'' = \frac{\omega}{\lambda} \quad (7.11)$$

where ω' is ratio of mass of steam injected to mass of combustion gases formed and ω'' is ratio of mass of steam injected to mass of fuel supplied². Maximum amount of permitted STIG is 20% of mass flow rate of inlet air².

Heat transfer between exhaust gases and condensate water has been taken place in water heat recovery boiler where superheated steam is generated as $m_{\text{exh}}(h_6 - h_7) = m_w(h_{\text{sup}} - h_{\text{cond}})$, where m_{exh} and m_w are mass flow rate of exhaust gases of turbine and condensate water; h_6 , h_7 , h_{sup} and h_{cond} are enthalpies of exhaust gases at state 6 and 7, super-heated steam and condensate water. Also, $T_{\text{pp}} = T_{\text{sat}} + \Delta T_{\text{pp}}$ and $T_{\text{AP}} = T_{\text{sat}} - \Delta T_{\text{AP}}$, where T_{pp} , T_{sat} and T_{AP} are pinch point temperature, saturation temperature of water and approach point temperature, respectively. ΔT_{pp} is pinch-point difference and ΔT_{AP} is approach point difference at saturation temperature.

Temperature of air after fog cooling can be obtained from an energy balance on dry air, water spray and air-born water vapour before and after the system. Assuming adiabatic mixing, energy gained by sprayed water is balanced by energy lost by dry air, and original air-born mixture, after cooling such that $m_w(h_{v1} - h_{w1'}) = m_a(h_{a1'} - h_{a1}) + \omega_1 m_a(h_{v1'} - h_{v1})$, where m_w and $h_{w1'}$ are mass flow rate and enthalpy of cooling water, m_a is mass flow rate of dry air, $(h_{a1'} - h_{a1})$ is enthalpy change of dry air, $(h_{v1'} - h_{v1})$ is enthalpy change of water vapour during cooling. Humidity ratio (ω_1) can be specified as $\omega_1 = \frac{0.622 P_{v1'}}{P_1 - P_{v1'}}$, where $P_{v1'}$ is partial pressure of water

vapour and P_1 is total atmospheric pressure. From conservation of mass, amount of water evaporated is equal to the mass of water vapour at point 1 minus water vapour originally in air at point 1' as $\Delta m_w = (\omega_1 - \omega_1') m_a$, where ω_1 is humidity ratio of air after cooling. Partial pressure of water vapour (P_v) can be found from respective relative humidity (RH) (ϕ) as $P_v = \phi P_{\text{sat}}$, where P_{sat} is saturation pressure of water vapour for corresponding temperature. Pressure loss in adiabatic mixing is neglected. Enthalpy, entropy, and exergy can be determined at each state point using mass and energy balances.

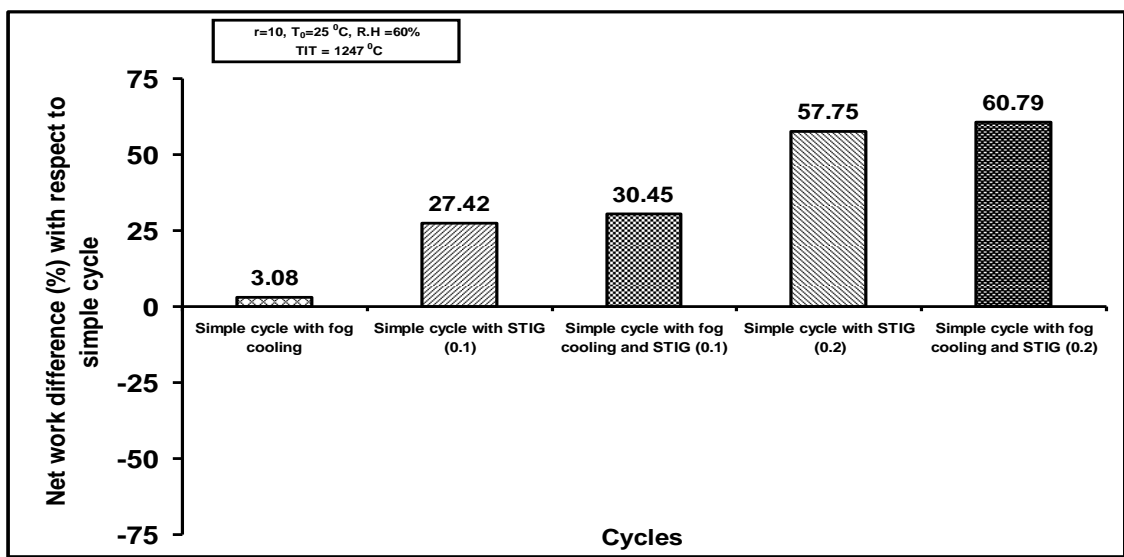


Fig. 7.10 Net power difference of retrofitted tri-generation power system with respect to simple gas turbine cycle

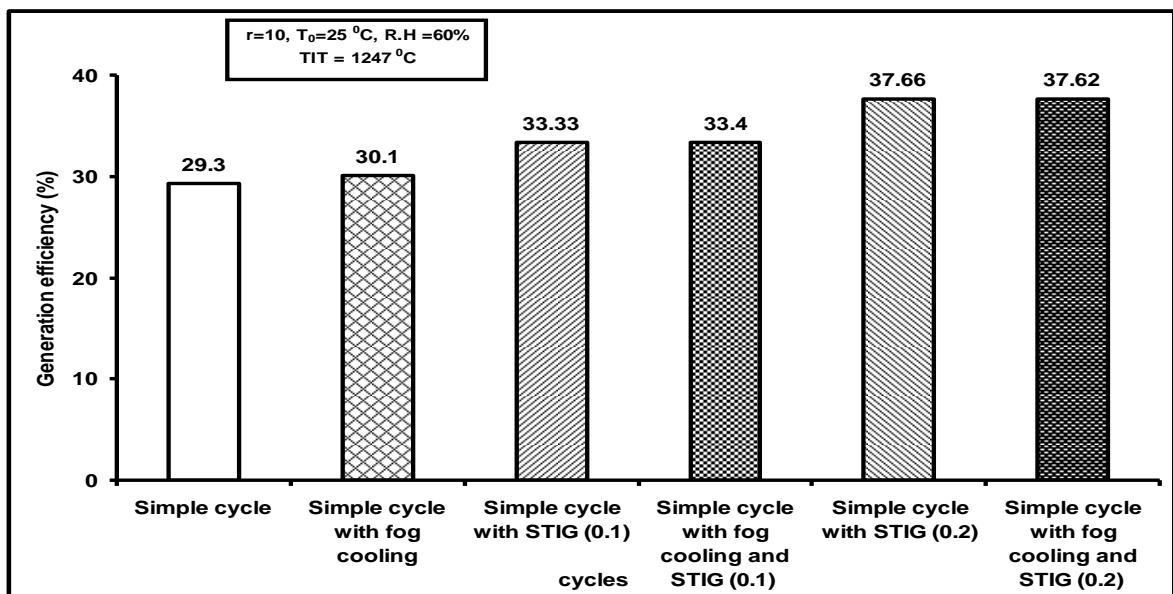


Fig. 7.11 Comparison of generation efficiency of various cycles using retrofitted techniques

Fig. 7.10 and 7.11 illustrate that the retrofitted technologies enhances the net power output and generation efficiency of the power plant as well as the waste heat of the exhaust gases increases the COP of the cascade refrigeration cycle.

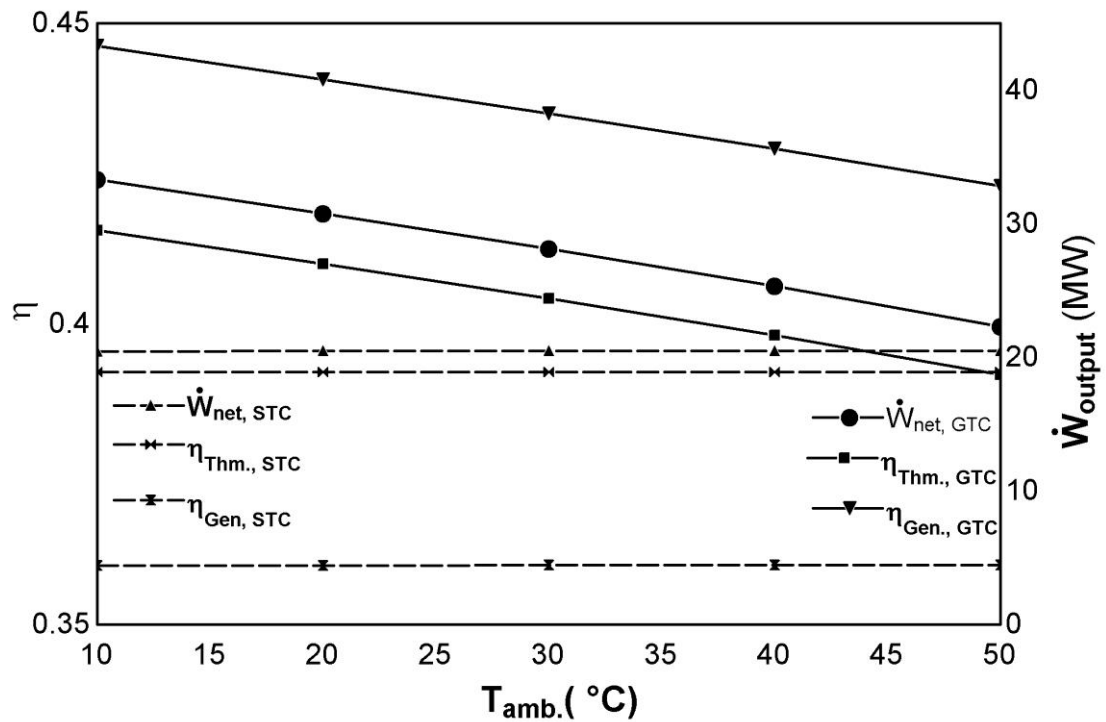


Fig. 7.12 Effect of ambient temperature on net power output, thermal efficiency and generation efficiency of gas turbine cycle and steam turbine cycle

Fig. 7.12 depicts the variation in net power output, thermal efficiency and generation efficiency of gas turbine cycle and steam turbine cycle with ambient temperature. The net power output, thermal efficiency and generation efficiency of gas turbine cycle decreases with increase in ambient temperature. However, net power output, thermal efficiency and generation efficiency of steam turbine cycle do not vary with ambient temperature. It has been observed that the values of net power output, thermal efficiency and generation efficiency of gas turbine cycle are more than that of steam turbine cycle.

Fig. 7.13 shows effect of ambient temperature on first law efficiency of gas turbine cycle and steam turbine cycle. The first law efficiency of gas turbine cycle increases and the first law efficiency of steam turbine cycle does not vary with increase in ambient temperature.

Fig. 7.14 shows effect of ambient temperature on second law efficiency of gas turbine cycle and steam turbine cycle. The second law efficiency of gas turbine cycle decreases with increase in ambient temperature. The second law efficiency of steam turbine cycle first decreases and then increases with increase in ambient temperature. The optimum value of ambient temperature lies between 35 to 40°C.

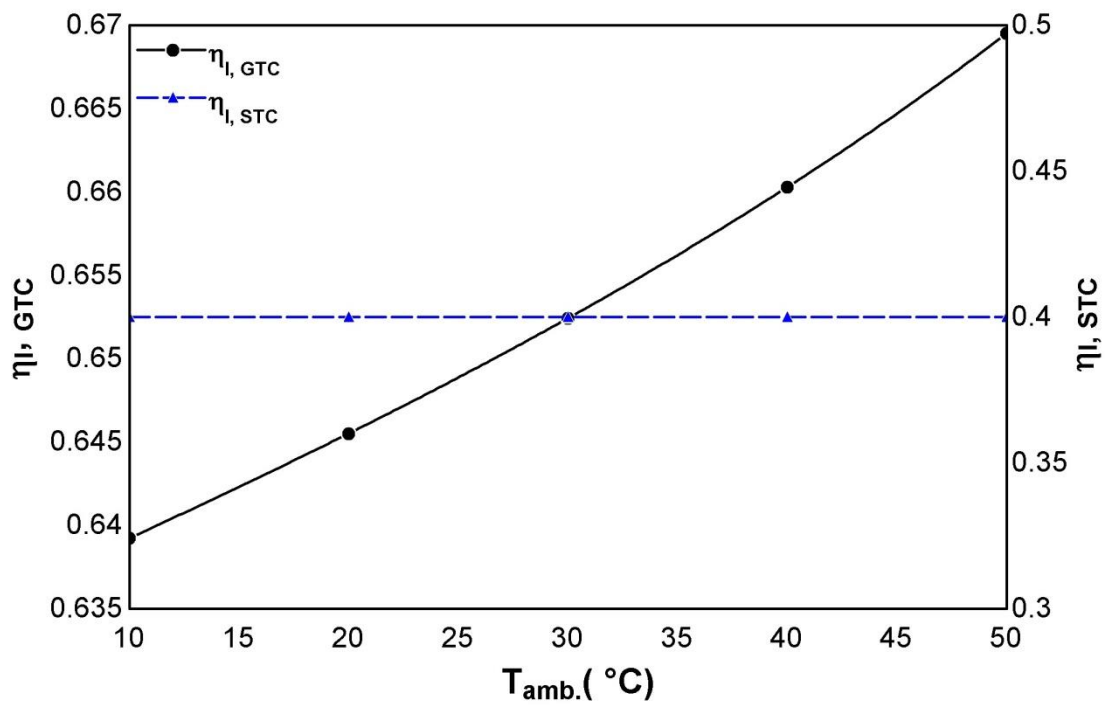


Fig. 7.13 Effect of ambient temperature on first law efficiency of gas turbine cycle and steam turbine cycle

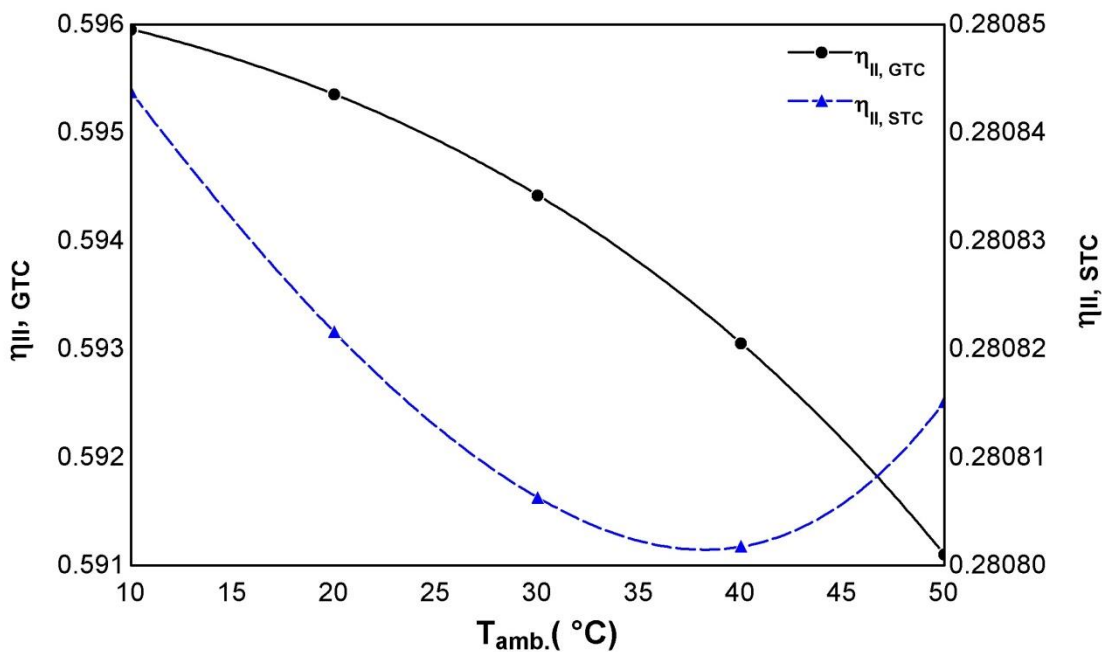


Fig. 7.14 Effect of ambient temperature on second law efficiency of gas turbine cycle and steam turbine cycle

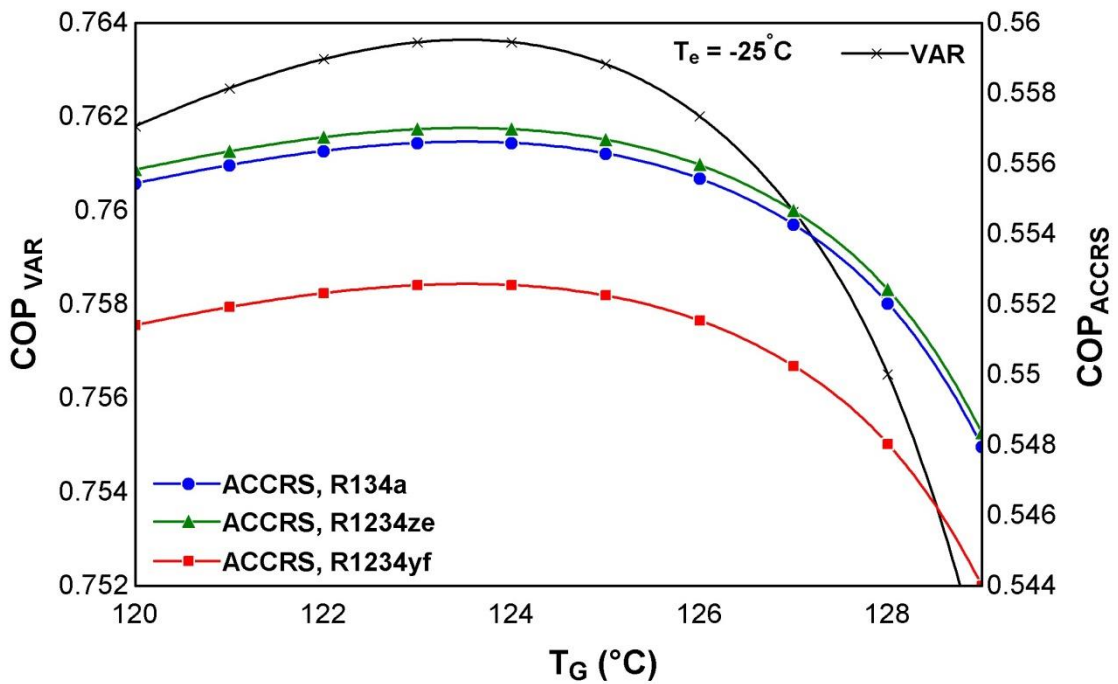


Fig. 7.15 Effect of generator temperature on COP of absorption-compression cascade refrigeration cycle

Fig. 7.15 shows the effect of generator temperature on COP of absorption-compression cascade refrigeration cycle. The COP of the VAR and absorption-compression cascade refrigeration cycles first increases and then decreases with increase in generator temperature.

7.8 CONCLUSIONS

The following conclusions of the analysis are summarized below:

- The use of retrofitted techniques enhances power output by 60.79% and generation efficiency by 28.4% of simple gas turbine cycle. However, the percentage of rejection of waste heat is 212.5 % of network output of simple cycle in the gas turbine power plant.
- The process heat of the thermal power plant decreases the net power output and generation efficiency of the tri-generation system enhances.
- The remaining heat of exhaust gases produces considerable refrigeration in the cascade refrigeration cycle.
- The net power output, thermal efficiency and generation efficiency of gas turbine cycle decreases with increase in ambient temperature.
- The optimum value of generator temperature lies between 122 to 126°C.

OVERALL CONCLUSIONS AND RECOMMENDATIONS

8.1 OVERALL CONCLUSIONS

The current work presents the energy and exergy analysis of thermal systems which includes LVHE associated VCR system, Dedicated mechanically subcooled VCR system, Experimental VCR setup for alternate refrigerants R1234yf and R1234ze. The different configurations of absorption compression cascade refrigeration systems in which VCR cycle having R1234yf is coupled to triple, double, single and half effect H₂O/LiBr VAR cycles have been investigated for performance improvement on the basis of energy and exergy principles. Additionally, tri-generation systems either micro-gas turbine or gas turbine and steam turbine based systems coupled to absorption compression cascade refrigeration cycle are also investigated for their performance improvement. The important conclusions of the present work are summarized below:

- HFO-R1234ze is the best among the refrigerants considered and can replace the traditional HFC-R134a with minor modifications in design. Although the performance of HFO-R1234yf is lower than that of HFC-R134a, having eco-loving characteristics and small deviation in the values of performance parameters, it can be a good alternative to HFC-134a.
- The energy performance of liquid vapour heat exchanger associated vapour compression refrigeration cycle is better than that of conventional vapour compression cycle.
- The energy and exergy performance of dedicated mechanically subcooled VCR cycle is better than that of conventional VCR cycle. R1234ze performs better than that of R1234yf and competes with R134a. It can be a good alternate to R134a.
- Subcooler of dedicated mechanically subcooled vapour compression cycle is the component of highest exergetic efficiency.
- The energy and exergy performance of R1234ze are closer to the R134a for theoretical as well as experimental VCR cycle. Minor alternations are needed for drop in replacement of R134a to the alternate R1234yf and R1234ze in the experimental setup..

- The electricity consumption of half and triple effect cascade refrigeration systems is reduced by 54.29 % and 45.84% than that of conventional vapour compression refrigeration cycle. For single and double effect cascade refrigeration system lies between half and triple effect which can be further reduced by optimization.
- Due to reduction in electricity consumption, enhancement in COP by 85.26% and 118.7% in triple and half effect cascade refrigeration systems reduces CO₂ emissions.
- The enhancement in the exergetic efficiency of VCR circuit of triple effect absorption compression cascade refrigeration is 85.28% and the reduction in total exergy destruction is 70.8% and in half effect absorption compression cascade refrigeration enhancement in the exergetic efficiency of VCR circuit is 118.74% and the reduction in total exergy destruction is 80.66%. It is also established that the exergetic efficiency of single effect cascade system is highest in comparison to single, double and half effect cascade refrigeration systems while, the total exergy destruction is lowest for half effect absorption compression cascade refrigeration system.
- The use of R1234yf in low temperature VCR circuit of triple, double, single and half effect absorption compression cascade refrigeration systems establishes an eco-friendly agreement.
- The electricity saver, cost effectiveness and eco-friendliness are the attracting features of the triple to half effect absorption compression cascade refrigeration systems associated to fulfil need of low cooling applications. However, the larger size of the systems is a manageable task.
- The C.O.P. and the exergetic efficiency of the absorption compression cascade refrigeration system of tri-generation power plant energized by micro-gas turbine are higher than that of conventional system for considerable range of ambient temperature.
- The use of waste heat available in the exhaust gases of micro-gas turbine of tri-generation power plant enhances the efficiency of overall system.
- The process heat of the thermal power plant decreases, the net power output and generation efficiency of the tri-generation system enhances. The remaining heat of exhaust gases produces considerable refrigeration in the cascade refrigeration

cycle. The retrofitted techniques improve the power output and generation efficiency of the tri-generation system.

Table 8.1 Comparison of considered systems

S. No.	Systems		Performance
1.	LVHE incorporated VCR system		Performs better for R134a and R1234ze
2.	Dedicated mechanically subcooled VCR system		Performs better for R134a and R1234ze
3.	Experimental VCR set up unit		Performs better for R134a and R1234ze
4	H ₂ O-LiBr absorption-compression cascade refrigeration system	Single effect	Single effect is having highest COP for R1234yf combination.
		Triple effect	
		Half effect	
5.	Trigeneration system	Energized by micro gas turbine	Shows higher performance than conventional power generation systems.
		Energized by gas turbine	

Hence, the modified systems and integrated systems perform better than that of conventional systems with replacement by alternative refrigerants.

8.2 RECOMMENDATIONS FOR FUTURE WORK

The following research work may be recommended as a follow up of the present work.

- Economic analysis of various refrigeration cycles and tri-generation power plants analyzed in the current work.
- Experimental investigations of various cascade refrigeration cycles analyzed in the present work as well as the use of alternate refrigerants (R1234yf and R1234ze) in the cascade cycles.
- Environmental analysis of various vapor compression and cascade refrigeration cycles analyzed in the present work.
- It would be beneficial for remote areas if proper commissioning of micro-gas turbine based tri-generation power plant is done and the generator of vapor absorption refrigeration system gets heat from Sun through flat plat solar collector.
- The modeling, strategies and correlations used in the thesis may be used to design and installed new thermal power plants and refrigeration plants.

REFERENCES

- Ahmadi, P., Dincer, I. and Rosen, M.A., 2013. Thermodynamic modeling and multi-objective evolutionary-based optimization of a new multigeneration energy system. *Energy Conversion and Management*, 76, pp.282-300.
- Ait-Ali, M.A., 1997. Optimum power boosting of gas turbine cycles with compressor inlet air refrigeration. *Journal of engineering for gas turbines and power*, 119(1), pp.124-130.
- Alexis, G.K., 2007. Performance parameters for the design of a combined refrigeration and electrical power cogeneration system. *International journal of refrigeration*, 30(6), pp.1097-1103.
- Al-Hawaj, O.M. and Hamad, A.M., 2007. A combined power cycle with absorption air conditioning. *Energy*, 32(6), pp.971-982.
- Álvarez, M.E., Esteve, X. and Bourouis, M., 2015. Performance analysis of a triple-effect absorption cooling cycle using aqueous (lithium, potassium, sodium) nitrate solution as a working pair. *Applied Thermal Engineering*, 79, pp.27-36.
- Ansari, N.A., Yadav, B. and Kumar, J., 2013. Theoretical exergy analysis of HFO-1234yf and HFO-1234ze as an alternative replacement of HFC-134a in simple vapour compression refrigeration system. *International Journal of Scientific and Engineering Research*, 4(8), pp.2229-5518.
- Arora, A. and Kaushik, S.C., 2008. Theoretical analysis of a vapour compression refrigeration system with R502, R404A and R507A. *International journal of refrigeration*, 31(6), pp.998-1005.
- Arora, A. and Kaushik, S.C., 2009. Theoretical analysis of LiBr/H₂O absorption refrigeration systems. *International Journal of Energy Research*, 33(15), pp.1321-1340.
- Arora, A., 2009. Energy and exergy analyses of compression, absorption, and combined cycle cooling systems (Ph. D. Thesis). *Centre for Energy Studies, IIT Delhi, India*.

- Arora, A., Arora, B.B. and Maji, S., 2012. *Energy and exergy analysis of engine exhaust driven vapour absorption refrigeration system* (No. 2012-28-0026). SAE Technical Paper.
- Arora, A., Arora, B.B., Pathak, B.D. and Sachdev, H.L., 2007. Exergy analysis of a vapour compression refrigeration system with R-22, R-407C and R-410A. *International journal of Exergy*, 4(4), p.441-454.
- Arora, A., Dixit, M. and Kaushik, S.C., 2016. Computation of optimum parameters of a half effect water lithium bromide vapour absorption refrigeration system. *Journal of Thermal Engineering*, 2(2), pp.683-692.
- Arora, A., Dixit, M. and Kaushik, S.C., 2016. Energy and exergy analysis of a double effect parallel flow LiBr/H₂O absorption refrigeration system. *Journal of Thermal Engineering*, 2(1), pp.541-549.
- Asdrubali, F. and Grignaffini, S., 2005. Experimental evaluation of the performances of a H₂O–LiBr absorption refrigerator under different service conditions. *International journal of refrigeration*, 28(4), pp.489-497.
- ASHRAE Standard 34: 2010. Designation and safety classification of refrigerants, *American society of heating ventilating and air-conditioning engineers, Atlanta, GA*.
- Ayala, R., Heard, C.L. and Holland, F.A., 1997. Ammonia/lithium nitrate absorption/compression refrigeration cycle. Part I. Simulation. *Applied Thermal Engineering*, 17(3), pp.223-233.
- Ayala, R., Heard, C.L. and Holland, F.A., 1998. Ammonia/lithium nitrate absorption/compression refrigeration cycle. Part II. Experimental. *Applied Thermal Engineering*, 18(8), pp.661-670.
- Azhar, M. and Siddiqui, M.A., 2019. Exergy analysis of single to triple effect lithium bromide-water vapour absorption cycles and optimization of the operating parameters. *Energy conversion and management*, 180, pp.1225-1246.
- Azzouzi, D., Kelkoul, M. and Amaryoucef, F., 2017. Parametric study of the wire-on-tube condenser subcooling effect on the performance of vapor compression refrigeration system. *Applied Thermal Engineering*, 122, pp.528-534.
- Bassily, A.M., 2004. Performance improvements of the intercooled reheat recuperated gas-turbine cycle using absorption inlet-cooling and evaporative after-cooling. *Applied Energy*, 77(3), pp.249-272.

- Bejan, A., Tsatsaronis, G., Moran, M. and Moran, M.J., 1996. *Thermal design and optimization*. John Wiley & Sons.
- Bellorio, M. and Pimenta, J., 2005, November. Theoretical analysis of air conditioning by evaporative cooling influence on gas turbine cycles performance. In *18th International Congress of Mechanical Engineering*.
- Bhargava, R. and Meher-Homji, C.B., 2002, January. Parametric analysis of existing gas turbines with inlet evaporative and overspray fogging. In *ASME Turbo Expo 2002: Power for Land, Sea, and Air* (pp. 387-401). American Society of Mechanical Engineers.
- Bilgen, E., 2000. Exergetic and engineering analyses of gas turbine based cogeneration systems. *Energy*, 25(12), pp.1215-1229.
- Bitzer Refrigerant Report 18, 2014, BITZER Khulmaschinenbau GmbH Eschenbrunnstr. 15//71065 Sindelfingen//Germany. <<http://www.bitzer.de>>
- Bouam, A., Aissani, S. and Kadi, R., 2008. Combustion chamber steam injection for gas turbine performance improvement during high ambient temperature operations. *Journal of Engineering for Gas Turbines and Power*, 130(4), p.041701-10.
- Bruno, J.C., Ortega-López, V. and Coronas, A., 2009. Integration of absorption cooling systems into micro gas turbine trigeneration systems using biogas: case study of a sewage treatment plant. *Applied energy*, 86(6), pp.837-847.
- Bruno, J.C., Valero, A. and Coronas, A., 2005. Performance analysis of combined microgas turbines and gas fired water/LiBr absorption chillers with post-combustion. *Applied Thermal Engineering*, 25(1), pp.87-99.
- Cabello, R., Sánchez, D., Llopis, R., Catalán, J., Nebot-Andrés, L. and Torrella, E., 2017. Energy evaluation of R152a as drop in replacement for R134a in cascade refrigeration plants. *Applied Thermal Engineering*, 110, pp.972-984.
- Cameretti, M.C. and Tuccillo, R., 2015. Combustion features of a bio-fuelled micro-gas turbine. *Applied Thermal Engineering*, 89, pp.280-290.
- Cecchinato, L., Corradi, M. and Minetto, S., 2010. Energy performance of supermarket refrigeration and air conditioning integrated systems. *Applied Thermal Engineering*, 30(14-15), pp.1946-1958.

- Cecchinato, L., Corradi, M. and Minetto, S., 2012. Energy performance of supermarket refrigeration and air conditioning integrated systems working with natural refrigerants. *Applied Thermal Engineering*, 48, pp.378-391.
- Centre for Energy Advancement through Technological Innovation (CEATI), 2010 *Refrigeration system energy efficiency reference guide*, <http://www.ceati.com/freepublications/7044_guide_web.pdf>.
- Chaker M., Meher-Homji C.B., Mee III T., 2004. Inlet fogging of gas turbine engines-PartII: fog droplet sizing analysis, nozzle types, measurement, and testing, *Journal of engineering for gas turbines and power*, pp.126/559.
- Chen, Y., Han, W. and Jin, H., 2017. Proposal and analysis of a novel heat-driven absorption–compression refrigeration system at low temperatures. *Applied energy*, 185, pp.2106-2116.
- Chinnappa, J.C.V., Crees, M.R., Murthy, S.S. and Srinivasan, K., 1993. Solar-assisted vapor compression/absorption cascaded air-conditioning systems. *Solar Energy*, 50(5), pp.453-458.
- Cimsit, C. and Ozturk, I.T., 2012. Analysis of compression–absorption cascade refrigeration cycles. *Applied Thermal Engineering*, 40, pp.311-317.
- Colorado, D. and Rivera, W., 2015. Performance comparison between a conventional vapor compression and compression-absorption single-stage and double-stage systems used for refrigeration. *Applied Thermal Engineering*, 87, pp.273-285.
- De Lucia, M., Lanfranchi, C. and Boggio, V., 1996. Benefits of compressor inlet air cooling for gas turbine cogeneration plants. *Journal of engineering for gas turbines and power*, 118(3), pp.598-603.
- de Sousa Teixeira, M. and Júnior, S.D.O., 2001. Thermo-economic evaluation of cogeneration systems for a chemical plant. *International Journal of Thermodynamics*, 4(3), pp.157-163.
- Dellenback, P.A., 2002. Improved gas turbine efficiency through alternative regenerator configuration. *Journal of Engineering for Gas Turbines and Power*, 124(3), pp.441-446.
- Dellenback, P.A., 2006. A reassessment of the alternative regeneration cycle. *Journal of engineering for gas turbines and power*, 128(4), pp.783-788.

- Devecioğlu, A.G. and Oruç, V., 2015. Characteristics of some new generation refrigerants with low GWP. *Energy Procedia*, 75, pp.1452-1457.
- Dincer, I. and Kanoglu, M., 2010. *Refrigeration systems and applications* (Vol. 2). New York: Wiley.
- Dixit, M., Arora, A. and Kaushik, S.C., 2016. Energy and exergy analysis of a waste heat driven cycle for triple effect refrigeration. *Journal of Thermal Engineering*, 2(5), pp.954-961.
- Dixit, M., Arora, A. and Kaushik, S.C., 2017. Thermodynamic and thermoeconomic analyses of two stage hybrid absorption compression refrigeration system. *Applied Thermal Engineering*, 113, pp.120-131.
- Dixit, M., Kaushik, S.C., Arora, A. 2017. Energy and exergy analysis of absorption-compression cascade refrigeration system. *Journal of Thermal Engineering*, 3(5), pp.1466-1477.
- Eini, S., Shahhosseini, H., Delgarm, N., Lee, M. and Bahadori, A., 2016. Multi-objective optimization of a cascade refrigeration system: exergetic, economic, environmental, and inherent safety analysis. *Applied Thermal Engineering*, 107, pp.804-817.
- El-Khattam, W. and Salama, M.M., 2004. Distributed generation technologies, definitions and benefits. *Electric power systems research*, 71(2), pp.119-128.
- Esen, H., Inalli, M. and Esen, M., 2006. Technoeconomic appraisal of a ground source heat pump system for a heating season in eastern Turkey. *Energy Conversion and Management*, 47(9-10), pp.1281-1297.
- Esen, H., Inalli, M., Esen, M. and Pihtili, K., 2007. Energy and exergy analysis of a ground-coupled heat pump system with two horizontal ground heat exchangers. *Building and environment*, 42(10), pp.3606-3615.
- Facchini, B., Fiaschi, D. and Manfrida, G., 1999, June. Exergy analysis of combined cycles using latest generation gas turbines. In *ASME 1999 International Gas Turbine and Aeroengine Congress and Exhibition* (pp. V003T02A003-V003T02A003). American Society of Mechanical Engineers.
- Facchini, B., Fiaschi, D. and Manfrida, G., 2000. Exergy analysis of combined cycles using latest generation gas turbines. *Journal of Engineering for Gas Turbines and Power*, 122(2), pp.233-238.

- Fang, Y., Croquer, S., Poncet, S., Aidoun, Z. and Bartosiewicz, Y., 2017. Drop-in replacement in a R134 ejector refrigeration cycle by HFO refrigerants. *international journal of refrigeration*, 77, pp.87-98.
- Fangtian, S. and Yitai, M., 2011. Thermodynamic analysis of transcritical CO₂ refrigeration cycle with an ejector. *Applied Thermal Engineering*, 31(6-7), pp.1184-1189.
- Farzaneh-Gord, M. and Deymi-Dashtebayaz, M., 2009. A new approach for enhancing performance of a gas turbine (case study: Khangiran refinery). *Applied Energy*, 86(12), pp.2750-2759.
- Garimella, S., Brown, A.M. and Nagavarapu, A.K., 2011. Waste heat driven absorption/vapor-compression cascade refrigeration system for megawatt scale, high-flux, low-temperature cooling. *International journal of refrigeration*, 34(8), pp.1776-1785.
- Gebreslassie, B.H., Medrano, M. and Boer, D., 2010. Exergy analysis of multi-effect water–LiBr absorption systems: from half to triple effect. *Renewable energy*, 35(8), pp.1773-1782.
- Gomri, R. and Hakimi, R., 2008. Second law analysis of double effect vapour absorption cooler system. *Energy conversion and management*, 49(11), pp.3343-3348.
- Han, W., Sun, L., Zheng, D., Jin, H., Ma, S. and Jing, X., 2013. New hybrid absorption–compression refrigeration system based on cascade use of mid-temperature waste heat. *Applied energy*, 106, pp.383-390.
- Ho, J.C., Chua, K.J. and Chou, S.K., 2004. Performance study of a microturbine system for cogeneration application. *Renewable Energy*, 29(7), pp.1121-1133.
- Honeywell, 2014. Solstice yf- a green solution to a global challenge, Cool for all concerned, <<http://www.honeywell-refrigerants.com/Europe> [assessed on 23.05.2018].
- Honeywell, 2015. Solstice ze Refrigerants (HFO-1234ze), Low GWP hydrofluoroolefins(HFO), The environmental alternative to traditional refrigerants <<http://www.honeywell-refrigerants.com>.
- Hwang, Y., 2004. Potential energy benefits of integrated refrigeration system with microturbine and absorption chiller. *International Journal of Refrigeration*, 27(8), pp.816-829.

- Invernizzi, C. and Iora, P., 2005. Heat recovery from a micro-gas turbine by vapour jet refrigeration systems. *Applied Thermal Engineering*, 25(8-9), pp.1233-1246.
- Jain, V., Kachhwaha, S.S. and Sachdeva, G., 2013. Thermodynamic performance analysis of a vapor compression–absorption cascaded refrigeration system. *Energy conversion and management*, 75, pp.685-700.
- Janković, Z., Atienza, J.S. and Suárez, J.A.M., 2015. Thermodynamic and heat transfer analyses for R1234yf and R1234ze (E) as drop-in replacements for R134a in a small power refrigerating system. *Applied Thermal Engineering*, 80, pp.42-54.
- Kachhhwaha S.S., Misra R.S., Saxena G., 2009. Thermodynamic analysis of single stage water/Lithium bromide vapour absorption refrigeration system, *National conference on refrigeration and Air Conditioning, IIT Madras, Chennai, India.*
- Kairouani, L. and Nehdi, E., 2006. Cooling performance and energy saving of a compression–absorption refrigeration system assisted by geothermal energy. *Applied thermal engineering*, 26(2-3), pp.288-294.
- Kaita, Y., 2001. Thermodynamic properties of lithium bromide–water solutions at high temperatures. *International Journal of refrigeration*, 24(5), pp.374-390.
- Kalla, S.K., Arora, B.B. and Usmani, J.A., 2018. Alternative refrigerants for HCFC 22—A REVIEW. *Journal of Thermal Engineering*, 4(3), pp.1998-2017.
- Kalla, S.K., Arora, B.B. and Usmani, J.A., 2018. Performance analysis of R22 and its substitutes in air conditioners. *Journal of Thermal Engineering*, 4(1), pp.1724-1736.
- Khaliq, A. and Choudhary, K., 2007. Combined first and second-law analysis of gas turbine cogeneration system with inlet air cooling and evaporative aftercooling of the compressor discharge. *Journal of Engineering for Gas Turbines and Power*, 129(4), pp.1004-1011.
- Khaliq, A. and Kaushik, S.C., 2004. Thermodynamic performance evaluation of combustion gas turbine cogeneration system with reheat. *Applied Thermal Engineering*, 24(13), pp.1785-1795.
- Khaliq, A. and Kumar, R., 2008. Thermodynamic performance assessment of gas turbine trigeneration system for combined heat cold and power production. *Journal of Engineering for Gas Turbines and Power*, 130(2), p.024501.

- Khaliq, A., 2009. Exergy analysis of gas turbine trigeneration system for combined production of power heat and refrigeration. *International Journal of Refrigeration*, 32(3), pp.534-545.
- Kilic, M. and Kaynakli, O., 2007. Second law-based thermodynamic analysis of water-lithium bromide absorption refrigeration system. *Energy*, 32(8), pp.1505-1512.
- Kim, K.H. and Perez-Blanco, H., 2007. Potential of regenerative gas-turbine systems with high fogging compression. *Applied Energy*, 84(1), pp.16-28.
- Klein, S.A., 2012. Engineering Equation Solver, FChart Software, Madison, WI. Version 9. 224-3D.
- Koeln, J.P. and Alleyne, A.G., 2013, October. Optimal subcooling in vapor compression systems via extremum seeking control. In *ASME 2013 Dynamic Systems and Control Conference* (pp. V001T13A005-V001T13A005). American Society of Mechanical Engineers.
- Koeln, J.P. and Alleyne, A.G., 2014. Optimal subcooling in vapor compression systems via extremum seeking control: Theory and experiments. *International Journal of Refrigeration*, 43, pp.14-25.
- Korakianitis T., Grantstrom J.P., Wassingbo P., 2005. Parametric Performance of Combined-Cogeneration Power Plants With Various Power and Efficiency Enhancements, *Engineering for gas turbine and Power*, Transaction of the ASME 128, pp. 65-72.
- Kotas, T. J., 1995. The exergy method of thermal plant analysis, Reprint ed., *Krieger Publishing Company, Krieger Drive, Malabar, Florida-32950*.
- Lanfranchi, C., 1996. Benefits of Compressor Inlet Air Cooling for Gas Turbine Cogeneration Plants.
- Lansing, F.L., 1976. Computer modeling of a single stage lithium bromide/water absorption refrigeration unit. *Jet Propulsion Laboratory, California Institute of Technology, Pasadena, CA, Deep Space Network Progress Report*, 42, pp.247-257.
- Lazzaretto, A. and Tsatsaronis, G., 2006. SPECO: a systematic and general methodology for calculating efficiencies and costs in thermal systems. *Energy*, 31(8-9), pp.1257-1289.
- Lazzaretto, A., Toffolo, A., Reini, M., Tacconi, R., Zaleta-Aguilar, A., Rangel-Hernandez, V. and Verda, V., 2006. Four approaches compared on the TADEUS

- (thermoeconomic approach to the diagnosis of energy utility systems) test case. *Energy*, 31(10-11), pp.1586-1613.
- Lemmon, E.W., McLinden, M.O. and Huber, M.L., 2010. REFPROP, Reference fluid thermodynamic and transport properties, NIST Standard Reference Database 23. V9., <http://www.nist.gov/srd/nist23.cfm>, National Institute of Standards and Technology, Gaithersburg, MD.
 - Llopis, R., Cabello, R., Sánchez, D. and Torrella, E., 2015. Energy improvements of CO₂ transcritical refrigeration cycles using dedicated mechanical subcooling. *International Journal of Refrigeration*, 55, pp.129-141.
 - Llopis, R., Sánchez, D., Sanz-Kock, C., Cabello, R. and Torrella, E., 2015. Energy and environmental comparison of two-stage solutions for commercial refrigeration at low temperature: Fluids and systems. *Applied Energy*, 138, pp.133-142.
 - Mafi, M., Naeynian, S.M. and Amidpour, M., 2009. Exergy analysis of multistage cascade low temperature refrigeration systems used in olefin plants. *International journal of refrigeration*, 32(2), pp.279-294.
 - Maryami, R. and Dehghan, A.A., 2017. An exergy based comparative study between LiBr/water absorption refrigeration systems from half effect to triple effect. *Applied Thermal Engineering*, 124, pp.103-123.
 - Maurizio, A. and Giovanni, C., 2015. Power reduction in vapour compression cooling cycles by power regeneration. *Energy Procedia*, 81, pp.1184-1197.
 - Messineo, A., 2012. R744-R717 cascade refrigeration system: performance evaluation compared with a HFC two-stage system. *Energy Procedia*, 14, pp.56-65.
 - Minciuc, E., Le Corre, O., Athanasovici, V., Tazerout, M. and Bitir, I., 2003. Thermodynamic analysis of tri-generation with absorption chilling machine. *Applied thermal engineering*, 23(11), pp.1391-1405.
 - Misra, R.D., Sahoo, P.K., Sahoo, S. and Gupta, A., 2003. Thermoeconomic optimization of a single effect water/LiBr vapour absorption refrigeration system. *International Journal of Refrigeration*, 26(2), pp.158-169.
 - Mosaffa, A.H., Farshi, L.G., Ferreira, C.I. and Rosen, M.A., 2016. Exergoeconomic and environmental analyses of CO₂/NH₃ cascade refrigeration systems equipped with different types of flash tank intercoolers. *Energy conversion and management*, 117, pp.442-453.

- Mostafavi, M., Alaktiwi, A. and Agnew, B., 1998. Thermodynamic analysis of combined open-cycle-twin-shaft gas turbine (Brayton cycle) and exhaust gas operated absorption refrigeration unit. *Applied Thermal Engineering*, 18(9-10), pp.847-856.
- Mota-Babiloni, A., Navarro-Esbrí, J., Barragán, Á., Molés, F. and Peris, B., 2014. Drop-in energy performance evaluation of R1234yf and R1234ze (E) in a vapor compression system as R134a replacements. *Applied Thermal Engineering*, 71(1), pp.259-265.
- Mota-Babiloni, A., Navarro-Esbri, J., Barragán-Cervera, Á., Molés, F., Peris, B. and Verdú, G., 2015. Commercial refrigeration—an overview of current status. *International journal of refrigeration*, 57, pp.186-196.
- Mota-Babiloni, A., Navarro-Esbrí, J., Barragán-Cervera, Á., Molés, F. and Peris, B., 2015. Experimental study of an R1234ze (E)/R134a mixture (R450A) as R134a replacement. *International journal of refrigeration*, 51, pp.52-58.
- Mota-Babiloni, A., Navarro-Esbrí, J., Barragán-Cervera, Á., Molés, F. and Peris, B., 2015. Analysis based on EU Regulation No 517/2014 of new HFC/HFO mixtures as alternatives of high GWP refrigerants in refrigeration and HVAC systems. *International journal of refrigeration*, 52, pp.21-31.
- Nishida, K., Takagi, T. and Kinoshita, S., 2005. Regenerative steam-injection gas-turbine systems. *Applied Energy*, 81(3), pp.231-246.
- Oh, S.D., Pang, H.S., Kim, S.M. and Kwak, H.Y., 1996. Exergy analysis for a gas turbine cogeneration system. *Journal of Engineering for Gas Turbines and Power*, 118(4), pp.782-791.
- Ondryas, I.S., Wilson, D.A., Kawamoto, M. and Haub, G.L., 1990, June. Options in gas turbine power augmentation using inlet air chilling. In *ASME 1990 International Gas Turbine and Aeroengine Congress and Exposition* (pp. V004T11A017-V004T11A017). American Society of Mechanical Engineers.
- Patek, J. and Klomfar, J., 2006. A computationally effective formulation of the thermodynamic properties of LiBr–H₂O solutions from 273 to 500 K over full composition range. *International Journal of Refrigeration*, 29(4), pp.566-578.
- Patek, J. and Klomfar, J., 2009. A simple formulation for thermodynamic properties of steam from 273 to 523 K, explicit in temperature and pressure. *International journal of refrigeration*, 32(5), pp.1123-1125.

- Pelster S., Favrat D., Von Spakovsky M.R., 2001. The thermo economic analysis and environomic modelling and optimization of the synthesis and operation of combined cycle with advanced options, *Engineering for gas turbine and Power*, Transaction of the ASME 123, pp.717-26.
- Pigani, L., Boscolo, M. and Pagan, N., 2016. Marine refrigeration plants for passenger ships: Low-GWP refrigerants and strategies to reduce environmental impact. *International Journal of Refrigeration*, 64, pp.80-92.
- Pilavachi, P.A., 2002. Mini-and micro-gas turbines for combined heat and power. *Applied thermal engineering*, 22(18), pp.2003-2014.
- Poachaiyapoom, A., Leardkun, R., Mounkong, J., Wongwises, S., 2019. Miniature vapour compression refrigeration system for electronics cooling, *Case studies in Thermal Engineering*, 13, 100365 (1-7).
- Pratihari, A.K., Kaushik, S.C. and Agarwal, R.S., 2010. Simulation of an ammonia–water compression–absorption refrigeration system for water chilling application. *International Journal of Refrigeration*, 33(7), pp.1386-1394.
- Qureshi, B.A. and Zubair, S.M., 2013. Mechanical sub-cooling vapor compression systems: Current status and future directions. *International Journal of Refrigeration*, 36(8), pp.2097-2110.
- Qureshi, B.A., Inam, M., Antar, M.A. and Zubair, S.M., 2013. Experimental energetic analysis of a vapor compression refrigeration system with dedicated mechanical sub-cooling. *Applied Energy*, 102, pp.1035-1041.
- Ravikumar, N. and Rama Krishna, K., 2006. Improved gas turbine efficiency using spray coolers and through Alternative regeneration configuration. In *ISHMT Heat & Mass Transfer Conf 2006* (pp. 1819-1824).
- Ravikumar, N. and Rama Krishna, K., 2006. Second law analysis of gas turbine power plant with alternative regeneration, In *ISHMT Heat & Mass Transfer Conf 2006* (pp. 1813-1818).
- Regulation, E.U., 2014. No 517/2014 of the European Parliament and the Council of 16 April 2014 on Fluorinated Greenhouse Gases and Repealing Regulation (EC) No 842/2006. 2014 [2016-05-15]. <http://eur-lex.europa.eu/legal-content/EN/TXT/PDF>.

- Şahin, A.Ş., 2011. Performance analysis of single-stage refrigeration system with internal heat exchanger using neural network and neuro-fuzzy. *Renewable energy*, 36(10), pp.2747-2752.
- Sahoo, P.K., 2008. Exergoeconomic analysis and optimization of a cogeneration system using evolutionary programming. *Applied thermal engineering*, 28(13), pp.1580-1588.
- Salvi, D. and Pierpaoli, P., 2002. Optimization of inlet air cooling systems for steam injected gas turbines. *International Journal of Thermal Sciences*, 41(9), pp.815-822.
- Sánchez, D., Cabello, R., Llopis, R., Arauzo, I., Catalán-Gil, J. and Torrella, E., 2017. Energy performance evaluation of R1234yf, R1234ze (E), R600a, R290 and R152a as low-GWP R134a alternatives. *International Journal of Refrigeration*, 74, pp.269-282.
- Sancho-Bastos, F. and Perez-Blanco, H., 2003, January. Cogeneration system simulation and control to meet simultaneous power, heating and cooling demands. In *ASME Turbo Expo 2003, collocated with the 2003 International Joint Power Generation Conference* (pp. 899-906). American Society of Mechanical Engineers.
- Schulz, M. and Kourkoulas, D., 2014. Regulation (EU) No 517/2014 of The European Parliament and of the council of 16 April 2014 on fluorinated greenhouse gases and repealing Regulation (EC) No 842/2006. *Off. J. Eur. Union*, 2014(517), p.L150.
- Sciubba, E., 2001. Beyond thermoeconomics? The concept of extended exergy accounting and its application to the analysis and design of thermal systems. *Exergy, an international journal*, 1(2), pp.68-84.
- Sethi, A., Becerra, E.V. and Motta, S.Y., 2016. Low GWP R134a replacements for small refrigeration (plug-in) applications. *international journal of refrigeration*, 66, pp.64-72.
- Shang, W. and Besant, R.W., 2006. Effects of manufacturing tolerances on regenerative exchanger number of transfer units and entropy generation. *Journal of engineering for gas turbines and power*, 128(3), pp.585-598.
- She, X., Yin, Y. and Zhang, X., 2014. A proposed subcooling method for vapor compression refrigeration cycle based on expansion power recovery. *International Journal of Refrigeration*, 43, pp.50-61.

- She, X., Yin, Y. and Zhang, X., 2014. Thermodynamic analysis of a novel energy-efficient refrigeration system subcooled by liquid desiccant dehumidification and evaporation. *Energy conversion and management*, 78, pp.286-296.
- Sinha R. and Bansode S., 2010. A thermodynamic analysis for gas turbine power optimization by fog cooling system, *20th national and 9th International ISHMT-ASME heat and mass transfer conference*.
- Srinivas, N. and Deb, K., 1994. Multiobjective optimization using nondominated sorting in genetic algorithms. *Evolutionary computation*, 2(3), pp.221-248.
- Srinivas, T., Gupta, A.V.S.S.K.S. and Reddy, B.V., 2008. Sensitivity analysis of STIG based combined cycle with dual pressure HRSG. *International journal of thermal sciences*, 47(9), pp.1226-1234.
- Staicovici, M.D.N., 2011. A method of improving the effectiveness of a mechanical vapour compression process and of its applications in refrigeration. *International Journal of Heat and Mass Transfer*, 54(9-10), pp.1752-1762.
- Sun, Z.G. and Guo, K.H., 2006. Cooling performance and energy saving of a compression-absorption refrigeration system driven by a gas engine. *International journal of energy research*, 30(13), pp.1109-1116.
- Sung, T., Lee, D., Kim, H.S. and Kim, J., 2014. Development of a novel meso-scale vapor compression refrigeration system (mVCRS). *Applied Thermal Engineering*, 66(1-2), pp.453-463.
- Talbi, M.M. and Agnew, B., 2000. Exergy analysis: an absorption refrigerator using lithium bromide and water as the working fluids. *Applied Thermal Engineering*, 20(7), pp.619-630.
- Taner, T. and Sivrioglu, M., 2015. Energy-exergy analysis and optimisation of a model sugar factory in Turkey. *Energy*, 93, pp.641-654.
- Taner, T. and Sivrioglu, M., 2017. A techno-economic & cost analysis of a turbine power plant: A case study for sugar plant. *Renewable and Sustainable Energy Reviews*, 78, pp.722-730.
- Taner, T., 2015. Optimisation processes of energy efficiency for a drying plant: A case of study for Turkey. *Applied Thermal Engineering*, 80, pp.247-260.

- Tassou, S.A., Lewis, J.S., Ge, Y.T., Hadawey, A. and Chaer, I., 2010. A review of emerging technologies for food refrigeration applications. *Applied Thermal Engineering*, 30(4), pp.263-276.
- Topal, H., Taner, T., Altıncı, Y. and Amirabedin, E., 2017. Application of trigeneration with direct co-combustion of poultry waste and coal: A case study in the poultry industry from Turkey. *Therm Sci*, pp.137-148.
- Topal, H., Taner, T., Naqvi, S.A.H., Altıncı, Y., Amirabedin, E. and Ozkaymak, M., 2017. Exergy analysis of a circulating fluidized bed power plant co-firing with olive pits: A case study of power plant in Turkey. *Energy*, 140, pp.40-46.
- Tsatsaronis, G., 2006. Application of thermoeconomics to the design and synthesis of energy plants. *Encyclopedia of Life Support Systems (EOLSS)*, Berlin, Germany.
- Turbine, S.C.G., 1990. Performance evaluation of selected combustion gas turbine cogeneration systems based on first and second-law analysis. *Journal of Engineering for Gas Turbines and Power*, 112, p.117.
- Valero, A., Correas, L., Zaleta, A., Lazzaretto, A., Verda, V., Reini, M. and Rangel, V., 2004. On the thermoeconomic approach to the diagnosis of energy system malfunctions: Part 1: the TADEUS problem. *Energy*, 29(12-15), pp.1875-1887.
- Vincent, C.E. and Heun, M.K., 2006. Thermoeconomic analysis & design of domestic refrigeration systems. In *Domestic use of energy conference*.
- Wang, F.J. and Chiou, J.S., 2004. Integration of steam injection and inlet air cooling for a gas turbine generation system. *Energy Conversion and Management*, 45(1), pp.15-26.
- Wang, F.J., Chiou, J.S. and Wu, P.C., 2007. Economic feasibility of waste heat to power conversion. *Applied Energy*, 84(4), pp.442-454.
- Wang, F.J., Chiou, J.S. and Wu, P.C., 2007. Economic feasibility of waste heat to power conversion. *Applied Energy*, 84(4), pp.442-454.
- Wang, J., Dai, Y., Gao, L. and Ma, S., 2009. A new combined cooling, heating and power system driven by solar energy. *Renewable Energy*, 34(12), pp.2780-2788.
- Wang, J., Zhao, P., Niu, X. and Dai, Y., 2012. Parametric analysis of a new combined cooling, heating and power system with transcritical CO₂ driven by solar energy. *Applied Energy*, 94, pp.58-64.

- Wang, L., Ma, A., Tan, Y., Cui, X. and Cui, H., 2012. Study on solar-assisted cascade refrigeration system. *Energy Procedia*, 16, pp.1503-1509.
- www.mandtsystems.com/documents/ASHRAE_R02_39SI.pdf [assessed on 23.05.2018].
- Xing, M., Yan, G. and Yu, J., 2015. Performance evaluation of an ejector subcooled vapor-compression refrigeration cycle. *Energy conversion and management*, 92, pp.431-436.
- Yadav J.P., 2005. Exergy analysis of novel gas/steam combined cycle gas turbines configuration, *ETME journal-MC*.
- Yadav, J.P. and Singh, O., 2006. Thermodynamic Evaluation of Influence of Different Coolants on the Performance of Simple Gas/Steam Combined Cycle Power Plants. *Journal of the Institution of Engineers(India), Part MC, Mechanical Engineering Division*, 87, p.28.
- Yang, M.H. and Yeh, R.H., 2015. Performance and exergy destruction analyses of optimal subcooling for vapor-compression refrigeration systems. *International Journal of Heat and Mass Transfer*, 87, pp.1-10.
- Yataganbaba, A., Kilicarslan, A. and Kurtbaş, İ., 2015. Exergy analysis of R1234yf and R1234ze as R134a replacements in a two evaporator vapour compression refrigeration system. *international journal of refrigeration*, 60, pp.26-37.
- Yokoyama, R. and Ito, K., 2006. Optimal design of gas turbine cogeneration plants in consideration of discreteness of equipment capabilities. *Journal of engineering for gas turbines and power*, 128(2), pp.336-343.
- Yu, J., Ren, Y., Chen, H. and Li, Y., 2007. Applying mechanical subcooling to ejector refrigeration cycle for improving the coefficient of performance. *Energy Conversion and Management*, 48(4), pp.1193-1199.
- Yumrutaş, R., Kunduz, M. and Kanoğlu, M., 2002. Exergy analysis of vapor compression refrigeration systems. *Exergy, An international journal*, 2(4), pp.266-272.
- Zaleta-Aguilar, A., Correas-Uson, L., Kubiak-Szyszk, J. and Sierra-Espinosa, F.Z., 2007. Concept on thermoeconomic evaluation of steam turbines. *Applied thermal engineering*, 27(2-3), pp.457-466.

- Zheng, N. and Zhao, L., 2015. The feasibility of using vapor expander to recover the expansion work in two-stage heat pumps with a large temperature lift. *International Journal of Refrigeration*, 56, pp.15-27.
- Zubair, S.M., 1999. Performance evaluation of vapour compression system. *International Journal of Refrigeration*, 22, pp.235-243.
- Zubair, S.M., 2000. Design and rating of an integrated mechanical-subcooling vapor-compression refrigeration system. *Energy Conversion and Management*, 41(11), pp.1201-1222.
- Zubair, S.M., Yaqub, M. and Khan, S.H., 1996. Second-law-based thermodynamic analysis of two-stage and mechanical-subcooling refrigeration cycles. *International Journal of Refrigeration*, 19(8), pp.506-516.

The work presented in the thesis has partially appeared as publications in International/National journals and conferences, as listed below:

1. Agarwal S., Arora A., Arora B. B., 2013. Performance and Exergetic analysis of a simple cycle gas turbine based power plant retrofitted with Inlet air Fog cooling (FCS) and Steam injection gas turbine (STIG). *International Journal of Higher Education and Research*, 2 (1), pp.16-44.
2. Agarwal S., Arora A., Arora B. B., Energy and Exergy investigations of R1234yf and R1234ze as R134a replacements in mechanically subcooled Vapour compression refrigeration cycle”, *Journal of Thermal Engineering* (Accepted, Nov. 2017).
3. Agarwal S., Arora A., Arora B. B., 2018. Thermodynamic Analysis of vapor-Absorption (H₂O- LiBr) Compression Combined refrigeration System Energized by A Micro Gas Turbine, *International Journal of Advance Research and Innovation*, 6(4), pp. 327-331
4. Agarwal, S., Arora, A. and Arora, B.B., 2019. Thermodynamic performance analysis of dedicated mechanically subcooled vapour compression refrigeration system. *Journal of Thermal Engineering*, 5(4), pp.222-236.
5. Agarwal, S., Arora, A. and Arora, B.B., 2019. Exergy Analysis of Dedicated Mechanically Subcooled Vapour Compression Refrigeration Cycle Using HFC-R134a, HFO-R1234ze and R1234yf. In *Advances in Energy and Built Environment* (pp. 23-42). Springer, Singapore.
6. Agarwal S., Arora A., Arora B. B., 2013. Parametric Analysis of a Simple Cycle Gas Turbine Based Power Plant through Integrated Retrofitting Techniques (Inlet Air Cooling and STIG), *ISTE, Delhi Section Convention, conference on Technological Universities and Institutions in New Knowledge Age: Future Perspectives and Action Plan, September 2013*.
7. Agarwal S., Arora A., Arora B. B., 2015. Thermodynamic Analysis of Vapour-absorption (H₂O- LiBr)-Compression Combined Refrigeration System Energized by Microgas-turbine, *International Conference of Advance Research and Innovation (ICARI, 2015)*.
8. Agarwal S., Arora A., Arora B. B., 2018. Exergy analysis of dedicated mechanically subcooled vapour compression refrigeration cycle using HFC-R134a, HFO- R1234ze and R1234yf, *TRACE conference, 2018*.
9. Agarwal S., Arora A., Arora B. B., 2018. Energy and Exergy analysis of absorption (H₂O-LiBr single effect) -compression (R1234yf, R1234ze) integrated vapour refrigeration cycle, *ICAPIE-2018*.
10. Agarwal S., Arora A., Arora B. B., 2019. Energy and Exergy Analysis of a Tri-generation (work, heat and refrigeration) Thermal System for Performance Improvement using Retrofitted Techniques and Alternative Refrigerants R1234ze and R1234yf in Cascade Refrigeration Cycle, *ICARI-2019*.
11. Agarwal S., Arora A., Arora B. B., 2019. Energy and Exergy analysis of vapour compression-triple effect absorption cascade refrigeration system, *Engineering Science and Technology, an International Journal* (available online), *Elsevier*.

ABOUT THE AUTHOR

Shyam Agarwal was born on July, 30 1977 in district Agra, Uttar Pradesh, India. He has completed his graduation in “Mechanical Engineering” from Institution of Engineers, India in the year 2006. He has passed Master in Engineering (Thermal Engineering) from Delhi College of Engineering, Delhi in 2011. He has been working in Mechanical Engineering Department of Delhi Technological University (Formerly, Delhi College of Engineering) Delhi since 2005.

His area of research includes Thermodynamics, Refrigeration and Air-conditioning, Fluid Mechanics and waste heat recovery. He is actively associated in research.